Magnetic Resonance Imaging to Assess Carotid-Brain Interactions in People with Stroke

Fraser Neil Sneden

BSc(Hons) Neurosciences, MSc(Res) Cognitive Neuroscience and Human Neuroimaging

Submitted in fulfilment of the requirements for the
Degree of PhD Cardiovascular Sciences

School of Cardiovascular and Metabolic Health
College of Medicine and Veterinary and Life Sciences
University of Glasgow

February 2024

Abstract

Carotid artery disease is a major risk factor for ischaemic stroke. It is associated with poorer functional outcomes, small vessel disease and may impact cognition. Allopurinol is a xanthine oxidase inhibitor that decreases serum uric acid levels. It is proposed that daily treatment of allopurinol may reduce oxidative stress and reduce carotid artery disease progression. The thesis aimed to address the relationship between carotid artery disease, brain imaging findings and cognitive function in people with ischaemic stroke. The thesis presents a systematic review of medical imaging studies investigating carotid artery disease and either brain imaging or cognitive function in ischaemic stroke (Chapter 3), before evaluating relationships between carotid artery disease and common vascular risk factors (Chapter 5) and brain structure, small vessel disease or post-stroke cognition (Chapter 6). Chapter 7 explored the potential treatment effects of longitudinal allopurinol on carotid artery disease and small vessel disease. Chapter 8 explored the use of a structural equation model in confirming the relationships between carotid artery disease, brain structure and post-stroke cognition.

Results from the systematic review I performed demonstrate that there is no overall standard for describing carotid artery disease. NASCET criteria are used to describe internal carotid artery stenosis, but often relationships between carotid structure and brain structure or cognition are under evaluated due to lack of reproducible standards in describing stroke populations. Moreover, univariate analysis between carotid artery measurements and common vascular risk factors found inconsistent relationships; no more than 3 common risk factors for stroke were related with a carotid artery measurement.

This thesis explored univariate and linear regression statistics for carotid artery disease and brain structure or cognition, finding a weak but positive relationship between common carotid intima-media thickness and WMH volume. Regression for common vascular risk factors found that age is a consistent covariant when evaluating the direction and strength of relationships between carotid structure and brain imaging findings. In a regression model, average vessel tortuosity was found to significantly relate to the WMH volume in the brain.

Described in the results from the longitudinal analyses, there was no significant difference between the treatment groups in the progression/regression of carotid artery stenosis, intima-media thickness, or vessel tortuosity. The data suggests that allopurinol does not influence carotid artery disease and may not act as a therapeutic agent for the reduction of stroke risk. WMH volume did not reduce significantly over the 2-year assessment period.

A structural equation modelling framework was proposed which aimed to describe carotid artery features and brain structure in separate variables. Though this framework did not reach significance, it is possible that more finetuning and exploratory analysis of vessel structure may provide a confirmatory model.

Overall, these data suggest that there should be more robust investigations into links between carotid artery disease and stroke, with attention to better reporting standards and greater longitudinal assessment.

Table of Contents

List of Tables

List of Figures

Acknowledgements

First, I give thanks to Dr David Alexander Dickie. You were my first supervisor in Glasgow. Though we are very different people (in personality and height), you always pushed me to go one step further. I give thanks to Professor Matthew Walters. You stepped in to assist in supervising at a time where I didn't know if I wanted to continue with my studies. You were always kind, and always unfailingly positive about the work that I was doing.

To Professor Jesse Dawson, I started out my PhD with such enthusiasm, but when Covid-19 lockdowns happened, I wholeheartedly admit that I changed. Yet you always remained rooted. You never showed anything other than positivity, and whilst there were times I considered leaving, you always reminded me of the good work I had done, and what I wanted to achieve. I couldn't always see the light at the end of the tunnel, but you were always there to guide me. Thank you.

To Rebecca Melville, somehow you finished a nursing degree during a global pandemic. You have consistently provided telephone support and reminded me of why I love research (and why I am glad I am not a nurse!)

Lastly, to my family, I couldn't have done this without you. My brother, Alisdair, might be over 100 miles away, and during most of 2020 unable to visit, but I know that if I truly needed it, would provide a sounding post for my frustrations. My parents, Kathryn and Robert Sneden, have been rocks in a few years that challenged us all. At times when I could barely function, you were always there when I needed you. You nodded along when I was rambling about arteries and statistics, even though I knew you it all meant nothing to you. You gave me space when I needed it; you gave me aid when I wanted it.

Thank you to you all. This has been the most trying experience of my life, and I could never have written this without your support.

Author’s Declaration

I declare the work of this PhD to be my own unless otherwise stated. This work has not been submitted for any other degree or professional qualification.

Fraser Neil Sneden

List of Abbreviations

ABPM	Ambulatory blood pressure management
ACA	Anterior cerebral artery
AChA	Anterior choroidal artery
AF	Atrial fibrillation
AGE	Advance glycation end products
ASL	Arterial spin labelling
ATP	Adenine triphosphate
BBB	Blood-brain barrier
CAS	Carotid artery stenosis
CCA	Common carotid artery
CEA	Carotid endarterectomy
CES-D	Centre for Epidemiologic Studies – Depression Scale
CI	Confidence interval
CMB	Cerebral microbleeds
CoW	Circle of Willis
CoWAT	Controlled Word Association Test
CSF	Cerebrospinal fluid
CT	Computed tomography
DSA	Digital subtraction angiography
DTI	Diffusion tensor imaging
DWI	Diffusion weighted imaging
ECA	External carotid artery
ECG	Electrocardiography
ECST	European Carotid Surgery Trial
eGFR	estimated Glomerular Filtration Rate
EICA	Extracranial internal carotid artery
FLAIR	Fluid attenuated inversion recovery
FOV	Field of view
HDL	High-density lipoprotein
HR	Hazard ratio
HVLT	Hopkins Verbal Learning Test
ICA	Internal carotid artery
IMP	Investigational medicinal product

IMT	Intima-media thickness
IQCODE	Informant Questionnaire for Cognitive Decline in the Elderly
LACI	Lacunar infarct
LDL	Low-density lipoprotein
MCA	Middle cerebral artery
MMSE	Mini Mental State Examination
MoCA	Montreal Cognitive Assessment
MR	Magnetic resonance
MRI	Magnetic resonance imaging
mRS	Modified Rankin Scale
MTL	Medial temporal lobe
NASCET	North American Symptomatic Carotid Endarterectomy Trial
NIHSS	National Institutes of Health Stroke Scale
NIP-Q	Neuropsychiatric Inventory Questionnaire Version
NO	Nitric oxide
OCSP	Oxford Community Stroke Project
OR	Odds ratio
PACI	Partial anterior circulation infarct
PD	Proton density imaging
POCI	Posterior circulation infarct
PSMD	Peak-width skeletonised mean diffusivity
PVS	Perivascular spaces
ROS	Reactive oxygen species
RR	Relative risk
SEM	Structural equation modelling
SHR	Spontaneously hypertensive rats
SIS	Stroke Impact Scale Short Form
SMC	Smooth muscle cell
SNR	Signal: noise
STRIVE	STandards for ReportIng Vascular changes on nEuroimaging
SVD	Small vessel disease
SWI	Susceptibility weighted imaging
T1	T1-weighted imaging
T2	T2-weighted imaging
TACI	Total anterior circulation infarct

TE	Echo time
TI	Inversion time
TIA	Transient ischaemic attack
TOAST	Trial of Org 10172 in Acute Stroke Treatment
TOF	Time of flight angiography
TR	Repetition time
US	Ultrasound
VCAM-1	Vascular adhesion molecule-1
VLDL	Very low-density lipoprotein
VMTK	Vascular modelling toolkit
WMH	White matter hyperintensities
XO	Xanthine oxidase

1 Motivation

With approximately 60,000 miles of arteries, veins and capillaries, the cardiovascular system is a highly complex organ system in the human body[1]. In comparison, the equatorial circumference of the Earth is 40,075km, or 24,901 miles[2]. This means that laid end-to-end, an individual's cardiovascular system is more than 2 times the Earth's circumference. The size and structure of this system has directed academic study for millennia, with many physicians and philosophers, including Herophilus and Galen believing the heart of the be the anatomical and spiritual centre of the human body. Over time, many philosophers added to the knowledge of the cardiovascular system, though are now considered to be incorrect. Galen's model of an open circulatory system, like in invertebrates, suggested that blood and oxygen dissipated at the end of the vessels as the tissues needed it. Additionally, it was the function of the liver to produce blood, which would simply ebb and flow through the arteries[3]. By 1628, William Harvey described the systemic circulation in *Exercitatio Anatomical de Motu Cordis et Sanguinis in Animalibus.* He demonstrated the functions of the cardiovascular system that we know to this day: the mechanical pump action of the heart, the circulatory system of blood through arteries and veins, and the functional connection with the lungs. This model has been studied ever since[3,4].

The complexity of the cardiovascular system is matched only with that of the brain, with 10^{11} neurons and 10^{15} connections[5]. The brain relies heavily on blood flow from the heart via the carotid and vertebral arteries. The brain is the most demanding organ structure in the body, requiring the most oxygen out of all the systems to function[6]. In the event of complete oxygen deprivation, this causes a cerebral infarction, or stroke.

As the global population increases, the incidence of various cardiovascular diseases rises as well. Stroke is an ever-increasing disease that effects millions of people each year. Therefore, there is an emphasis on the administration of preventive strategies to minimise the risk of secondary stroke, including medical management of the disease course. This work aims to investigate the relationship between carotid artery disease, brain structure, and cognition in people with ischaemic stroke. It aims to investigate the putative benefit of allopurinol induction in patients with carotid artery disease. It is hypothesised that:

1. Carotid artery disease will positively correlate with white matter hyperintensity (WMH) burden and cognitive function.
2. Longitudinally, participants who received alloupurinol will demonstrate slower progression in biomarkers of carotid artery disease – carotid artery stenosis and intima-media thickness – in comparison with the placebo group.

Chapter 2 will explain the theory behind ischaemic stroke, small vessel disease, carotid artery disease, medical imaging, and allopurinol treatment. Chapter 3 will describe a systematic review on carotid artery disease, brain structure and cognitive function in ischaemic stroke patients. Chapter 4 will illustrate the methods used in this work, including angiographic image analysis and validation of these techniques. Chapter 5 aims to clarify associations between carotid artery disease and common vascular risk factors. Chapter 6 will assess associations between carotid artery disease, brain structure and cognitive function in baseline data. Chapter 7 investigates the possible treatment effects of 2-year allopurinol treatment on carotid artery disease and brain structure in ischaemic stroke patients. Chapter 8 seeks to describe a structural equation modelling framework for carotid-brain interactions.

2 Introduction

2.1 Stroke

The brain requires an estimated 750ml/min of oxygenated blood, approximately 15% of cardiac output[7]. The cerebral arteries deliver oxygenated blood, glucose, and nutrients to the brain, with the venous drainage responsible for the removal of waste products such as carbon dioxide. The brain is vulnerable to a compromised blood supply, thus has developed mechanisms to combat this such as autoregulation of blood flow. Despite these safeguards, disruption to the autoregulatory mechanism may result in a stroke[8].

A stroke is defined as a syndrome of "rapidly developing clinical symptoms and/or signs of focal (or at times global) … loss of cerebral function, with symptoms lasting more than 24 hours with no apparent cause other than of vascular origin". Stroke symptoms include unilateral limb/facial weakness, speech disturbance and ataxia[9,10]. These symptoms can appear alone or combined and will occur in the contralateral side to the cerebral hemisphere affected[10]. A transient ischaemic attack (TIA) is a temporary episode of focal neurological symptoms that lasts less than 24 hours[9,10]. However, these definitions are thought of as outdated. It is noted that TIA, once thought to be imaging negative, may present lesions in approximately 66% patients[9].

Strokes can be classified as ischaemic or haemorrhagic. Most strokes are considered ischaemic caused by an occlusion of an artery. The remainder of strokes are typically caused by intracerebral or subarachnoid haemorrhage[9].

2.1.1 Stroke Burden and Recurrence

Stroke affects people of any age, though becomes increasingly prevalent in older individuals. Stroke burden is increasing worldwide, particularly in low- and middle-income countries[11]. Additionally, stroke incidence is increasing in younger individuals in

these poorer countries. By 2030, it is suggested that the global number of stroke survivors will surpass 70 million people[12]. Global stroke mortality is estimated at over 6 million people each year, as of 2019[13]. Stroke has a vast economic burden upon health services and patient families. In the UK this is tantamount of 5% of healthcare resources[14] and may cost over £7 billion pounds annually to the NHS and economy[15].

Stroke deaths vary by ethnic group, disproportionately affecting those from low- and middle-income countries[12]. Many non-Western countries, and Black and Asian countries experience higher incidence of stroke in comparison to Caucasian populations[12,16,17]. The Global Burden of Disease Study 2010 estimated that 68.6% of incident strokes and 70.9% stroke deaths can be attributed to low- and middle-income countries[12]. Furthermore, the incidence of cerebrovascular disease in many of these non-Western countries, such as China, is higher than that of coronary artery disease[18]. This is of particular importance as those who have had a stroke exhibit an increased risk of recurrence.

Many population-based studies investigate the long-term risk of stroke recurrence. A meta-analysis from 2011 of stroke risk identified 16 studies of note, with 13 describing cumulative risk of recurrence in 9115 survivors. They found that cumulative risk of stroke varied greatly across time points assessed with 11.1% (95% CI 9.0-13.3) at 1 year follow-up, increasing to 26.4% (95% CI 20.1-32.8) at 5-year follow-up. At a 10-year follow-up after first stroke, this figure increased to 39.2% (95% CI 27.2-51.2)[19]. It is noted that there are temporal reductions in stroke risk. Later studies published a smaller risk of stroke recurrence, potentially due to trends in improvement in secondary stroke management[19].

In Denmark, a comparison of ischaemic stroke risk found that the overall 1-year risk of recurrence was calculated at 3.9% (95% CI 3.8-4.0); 10-year risk was estimated at 13.3% (95% CI 13.0-13.5), respectively. Increasing age exhibited increased risk of recurrence, with participants within the 70-79 age bracket exhibiting the highest risk at 4.3% (95% CI 4.0-4.5) at 1 year follow-up; 15.0% (95% CI 14.5-15.5) after 10 years of initial stroke. Men demonstrated an increased risk of recurrence in comparison with women, with risk difference at 0.5% (95% CI 0.2-0.7) at 1-year after initial stroke. This

difference magnified throughout longitudinal follow-up, with 10-year risk difference estimated at 2.3% (95% CI 1.8-2.8). However, risk of recurrence decreased slightly when comparing between mild, moderate, and severe ischaemic stroke. In relation to mild stroke, the 10-year risk difference of moderate stroke was estimated at -2.8% (95% CI -3.5, -2.1%); for severe stroke this was calculated at -9.3% (95% CI -9.9%, -8.7%). This decreased risk of recurrence may be due to increased mortality associated with stroke severity[20]. Investigating mortality risk in this cohort found that the overall risk at 10 years after stroke was estimated at 56.2% (95% CI 55.8-56.6) for first stroke and 70.2% (95% CI 68.8-71.5%) for recurrent stroke[20]. These risk of recurrence data are at odds with the aforementioned meta-analysis. This variation may be due to many factors, including different methods of analysing survival data (Kaplan-Meier or Aalen-Johansen estimator), variation in population inclusion characteristics, and disparity in the description of recurrent stroke.

A diagnosis of a TIA is a risk factor for stroke recurrence. The risk of stroke after a TIA can be estimated at between 2 and 17% within the first 90 days of symptom onset. Among these patients, it is estimated what 20% develop a subsequent stroke, experience a heart attack, or die within 1 year. Mechanisms of recurrent stroke from TIA differ in progression: either the initial ischaemic episode progresses within the original territory, or a subsequent stroke occurs (either within the same vascular territory, or in a new location)[21].

2.1.2 Stroke Classification

The identification of the cause of ischaemic stroke is established through patient symptomatology and demographics, and the results of various examinations including brain and vascular imaging, echocardiograph (ECG) and blood tests. The Trial of Org 10172 in Acute Stroke Treatment (TOAST) aimed to classify and divide ischaemic stroke into categories based on the root cause[22]. The five core aetiological groupings are:

1. Large artery atherosclerosis
2. Cardioembolism

3. Small vessel occlusion
4. Stroke of other determined aetiology
5. Stroke of undetermined aetiology.

Large artery atherosclerosis is characterised by "significant stenosis" (>50%) or occlusion of a major artery, such as the internal carotid artery. Cardio-embolic strokes are caused by clots that occur from a cardiac source. Altered cardiac rhythms, for example atrial fibrillation (AF), may facilitate the formation of a cardio-embolic clot that blocks a cerebral artery[22]. Small vessel occlusions affect the small vessels in the brain, and display symptoms of lacunar syndromes e.g., pure motor hemiparesis or pure sensory stroke, or no cortical signs of stroke[22,23]. Stroke of other determined aetiology refers to patients with rare causes of stroke, including haematological disorders. Strokes that have an undetermined aetiology is described when a clinical examination remains inconclusive, potentially due to the identification of multiple causes of ischaemia[22].

Other schema for the classification of stroke exists. The Oxfordshire Community Stroke Project (OCSP) described four clinically distinct groups of patients with stroke (Figure 2.1). This stroke classification is based around the clinical symptoms, rather than cause. These are as follows:

1. Total anterior circulation infarcts (TACI)
2. Partial anterior circulation infarcts (PACI)
3. Posterior circulation infarcts (POCI)
4. Lacunar infarcts (LACI).

Total anterior circulation infarcts (TACI) present with signs of cortical dysfunction such as dysphasia and dyscalculia, but also display visual field defects and ipsilateral motor/sensory deficit in the face, arm, and leg. These infarcts are typically described as ischaemic lesions within both the superficial and deep territories of the middle cerebral artery (MCA). These infarcts are usually larger in volume than the other stroke subtypes [24]. Partial anterior circulation infarcts (PACI) symptoms are like the TACI classification but

are considered less numerous or more restricted in sensorimotor deficits e.g., motor deficit may be confined to part of a limb such as the hand. Like the clinical symptoms, the anatomical distribution of ischaemia is more restricted than TACI-based lesions. However, PACI lesions can be isolated further than its TACI counterpart. These lesions can exist within different cortical areas that are supplied by the middle and anterior cerebral arteries, resulting in a more heterogenous description of the clinical symptoms[24].

Posterior circulation infarcts (POCI) may present with visual field absences or cerebellar dysfunction such as ataxic hemiparesis that is not indicated in other syndromes. These infarcts are typically located in the brainstem, cerebellum, and occipital lobes[24]. Lacunar infarcts (LACI) do not exhibit any cognitive deficits such as visuospatial deficit or aphasia and are often described as sensorimotor strokes. Lacunar syndromes present with small infracts in the basal ganglia or pons[24].

Amaurosis fugax is considered a form of transient ischaemic attack, an episode of visual loss that may affect one or both eyes. Amaurosis fugax is commonly caused by ischaemia in the ipsilateral carotid artery[24].

Moreover, strokes can be classified by the severity of the impairment caused. The National Institutes of Health Stroke Scale (NIHSS) is a quantitative score of stroke severity ranging from 0 – 42, with 0 described as no evidence of stroke, and 42 the maximum score of severe strokes. Administration of the scale is separated into 11 areas including level of consciousness, motor function, sensory function, and speech. Each section of the scale is scored between a minimum of 0 and a maximum of 4 (some sections range 0-2 or 0-3)[25]. A comparison of the NIHSS and other neurological scales (Canadian Neurological Scale and Middle Cerebral Artery Neurological Score) to stroke prognosis was performed by Muir et al. in 1996. This study found that the accuracy of all 3 scales were high. The NIHSS performed best in logistic regression, with a predictive accuracy value of 0.83 (95% CI, 0.79-0.87). It was the most sensitive to a poor outcome (in care or dead) with a specificity of 0.90 (95% CI, 0.86-0.94)[26].

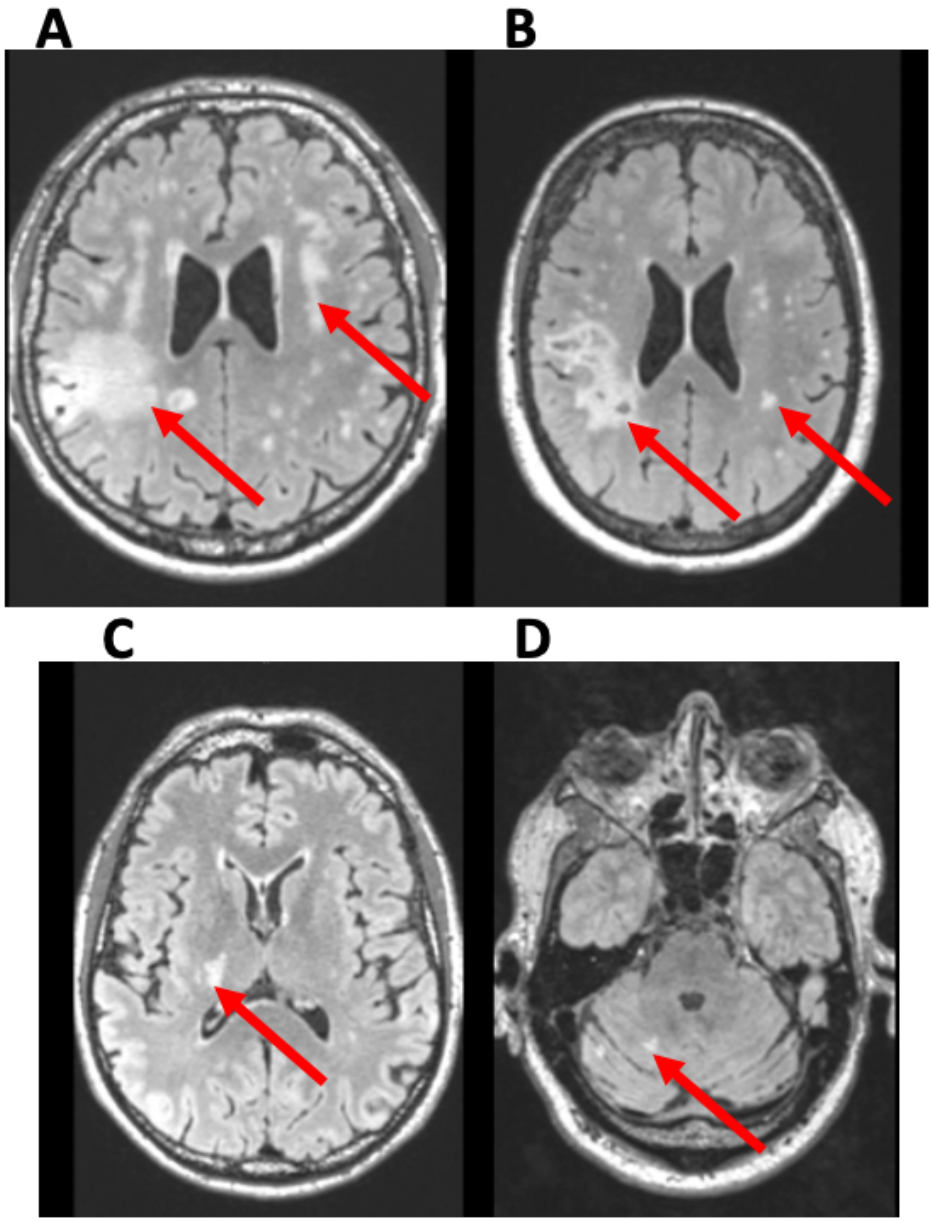

Figure 2.1: Radiological imaging of clinical stroke classifications according to the Oxfordshire Community Stroke Project. Typical lesions identified by red arrows. A: A large infarct in the right parietal lobe, multiple smaller lesions in both right and left hemispheres, diagnosed as total anterior circulation infarct (TACI). B: An infarct in the right parietal lobe, multiple smaller lesions in both right and left hemispheres, diagnosed as partial anterior circulation infarct (PACI). C: A right thalamic/internal capsule infarct, diagnosed as a lacunar infarct. D: A small right cerebella infarct, diagnosed as posterior circulation infarct (POCI). All images taken from the XILO-FIST patient cohort.

2.1.3 Small Vessel Disease

According to Wardlaw et al. (2013), cerebral small vessel disease (SVD) is a "term commonly used to describe a syndrome of clinical, cognitive, neuroimaging, and neuropathological findings thought to arise from disease affecting the perforating cerebral arterioles, capillaries, and venules, and the resulting brain damage in the cerebral white and deep grey matter"[27]. Radiological findings that are characteristic of SVD in the brain include:

1. White matter hyperintensities
2. Perivascular spaces
3. Lacunes
4. Cerebral microbleeds.

In 2013, STandards for ReportIng Vascular changes on nEuroimaging (STRIVE) recommendations were published which described the radiological assessments of SVD, seen below[28]. These recommendations (Figure 2.2) are commonly followed by various studies reporting putative links between SVD and many outcome measures, including our own in assessing white matter hyperintensities and carotid artery disease. However, the assessment of small vessels in the brain where this disease occurs is not entirely feasible given the current standard of imaging technology. Thus, studies into SVD are largely concerned around the quantification of their disruption upon normal functioning i.e., after stroke[27].

The pathogenic mechanisms involved in the development of SVD are poorly understood, though current data suggests endothelial dysfunction of these minor vessels plays a pivotal role. Impaired blood-brain barrier (BBB) functioning may allow the unregulated movement of harmful substances to the brain. This may promote the inhibition of waste clearance processes in the brain, triggering the manifestation of SVD[29,30].

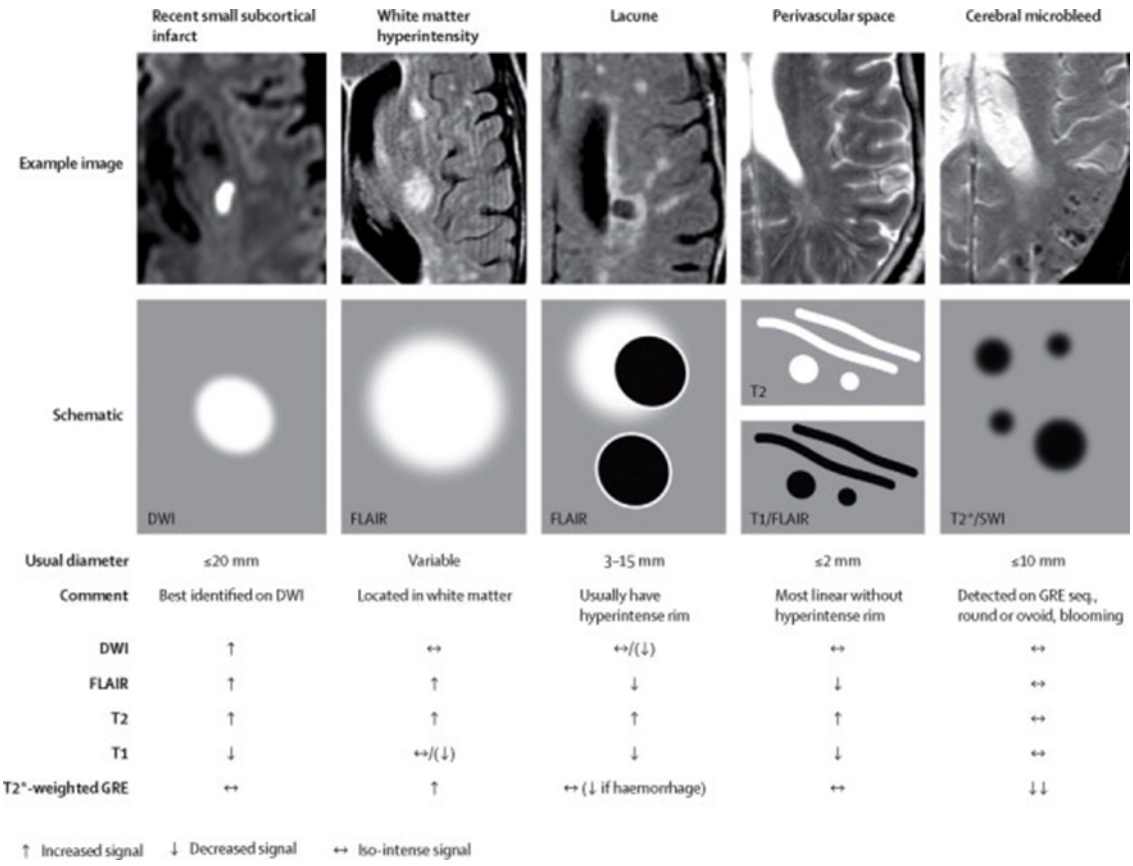

Figure 2.2: STRIVE recommendations for the evaluation of small vessel disease (SVD) using multimodal MRI. Example findings (upper), schematic representation (middle) and imaging characteristics (lower). Typical imaging features of small vessel disease include recent small subcortical infarct, white matter hyperintensity (WMH), lacune, perivascular spaces (PVS) and cerebral microbleeds (CMB). The arrows represent the signal intensity of lesions in each modality. An upwards arrow represents increased signal i.e., hyperintense to the background; a downwards arrow represents decreased signal i.e., hypointense to the background; an arrow pointing left/right represents isointense background signal[28].

White matter hyperintensities (WMH) were first discovered in computed tomography (CT) imaging as hypoattenuated areas. These lesions, of presumed vascular origin, are more easily identified in magnetic resonance imaging (MRI) due to their sensitivity in detecting changes in water content of tissue. WMH have distinct presentations, thus can be described as periventricular i.e., surround the fluid-filled lateral ventricles, or deep i.e., within subcortical white matter. WMH were overlooked due to subtle macroscopic changes that are only easily visible in advanced stages. They were previously dismissed as a consequence of "normal" ageing; however, the prevalence is

variable[31]. Additionally, these lesions increase with common vascular risk factors including hypertension, diabetes, and smoking. WMH are associated with infarct growth and poorer clinical outcomes in ischaemic stroke and have been identified as predictors of poor functional outcomes. The pathological understanding of WMH deposition is complex, owed to difficulties in image-matching with MRI, and limitations with sampling and tissue fixation, which alters the water content of the white matter tissue. WMH pathology has been related to demyelination of white matter tracts and loss of axons, which progress alongside white matter lesion growth. Proteins e.g., fibrinogens have been found to be deposited in perivascular tissue that are surrounded by these WMH. It is suggested that within these intracranial small vessels, wall thickening is caused by the movement of proteins from the plasma into the tissues. Other studies found the ratio of CSF:plasma albumin increases in patients with WMH, implying a role of oedema in the creation of WMH[31]. In a systematic review, WMH are associated with increased incident stroke risk (HR 3.3 95% CI 2.6-4.4)[32].

Perivascular spaces (PVS) are fluid-filled structures that surround the microvessels of the brain. These spaces are part of the lymphatic system, playing a key role in waste elimination. They are filled with interstitial fluid and are important in maintaining healthy brain functioning. They may appear linear if the image is in the same plane as the vessel or rounded when perpendicular to the plane. They have a small diameter (less than 3mm)[28]. In small vessel disease, PVS become dilated and visible on structural MRI sequences[30]. These PVS are found around arteries that supply certain brain structures, including the basal ganglia and centrum semiovale. Furthermore, PVS seem to be associated with ageing, hypertension and overall small vessel disease burden, key risk factors in stroke[33]. Data has suggested that PVS within the basal ganglia are associated with increased risk of recurrent ischaemic stroke, where the risk differs based on number of PVS. In a comparison with patients with 10 or less PVSs, risk was as follows: 11-20 PVS (HR 1.15, 95% CI 0.78-1.68); >20 PVS (HR 1.82, 95% CI 1.18-2.80, p=0.011). PVS within the centrum semiovale were not associated with recurrent stroke[34].

Lacunes are small ovoid, fluid-filled cavities that are consistent with a previous small subcortical infarct. Lacunes must be within the territory of a perforating artery[28]. Lacunar strokes are a type of ischaemic stroke where symptoms are related to these small

subcortical lesions[35]. Using imaging, lacunes have a similar presentation to both WMH and PVS. In comparison with PVS, lacunes are larger (greater than 3mm) whereas PVS may appear smaller or linear if imaged parallel to the perforating vessel. Distinguishing from WMH requires the use of apparent diffusion coefficient (ADC) imaging, a specific diffusion MRI sequence that would present a reduced signal in comparison to the white matter lesions[28,35]. Longitudinal follow-up (median 2.9 years) of patients found single asymptomatic lacunes exhibited an increased risk of recurrent ischaemic stroke (HR 1.53, 95% CI 0.67-3.49); multiple asymptomatic lacunes demonstrated additional risk (HR 2.52, 95% CI 1.25-5.09)[36].

Cerebral microbleeds (CMB) are small lesions that appear hypointense in some MRI sequences (T2* and susceptibility-weighted imaging). They are typically found at the border between cortical and subcortical structures, and around the brainstem and cerebellum[28]. Data concerning CMB and cognitive impairment recently describes a relationship between the presence of multiple lesions (>4) and cognitive decline. Lobar microbleeds were associated with a decline in executive function and memory processes; microbleeds in deep/infratentorial regions were associated with a decline in information processing speed and motor speed. Longitudinal follow-up demonstrated an increased risk of developing dementia (HR 2.02, 95% CI 1.25-3.24), including Alzheimer's disease, in participants with significant cerebral microbleeds[37]. A systematic review of cerebral microbleeds and stroke risk provided evidence of increased risk of ischaemic stroke recurrence in patients with CMBs (OR 1.55, 95% CI 1.12-2.13, $p<0.01$); the risk of intracerebral haemorrhage was found to be higher (OR 2.25, 95% CI 1.70-2.98, $p<0.01$)[38].

These inter-related lesions (PVS, WMH, lacunes and CMB) have variable patterns of progression and phenotype. They may promote lesion progression through different mechanisms (Figure 2.3). Furthermore, effects of all SVD markers are cumulative i.e., patients with multiple SVD features often have poorer cognitive function than those with a single SVD marker. This indicates that whilst there are different presentations of SVD, they are linked clinically and pathologically[31].

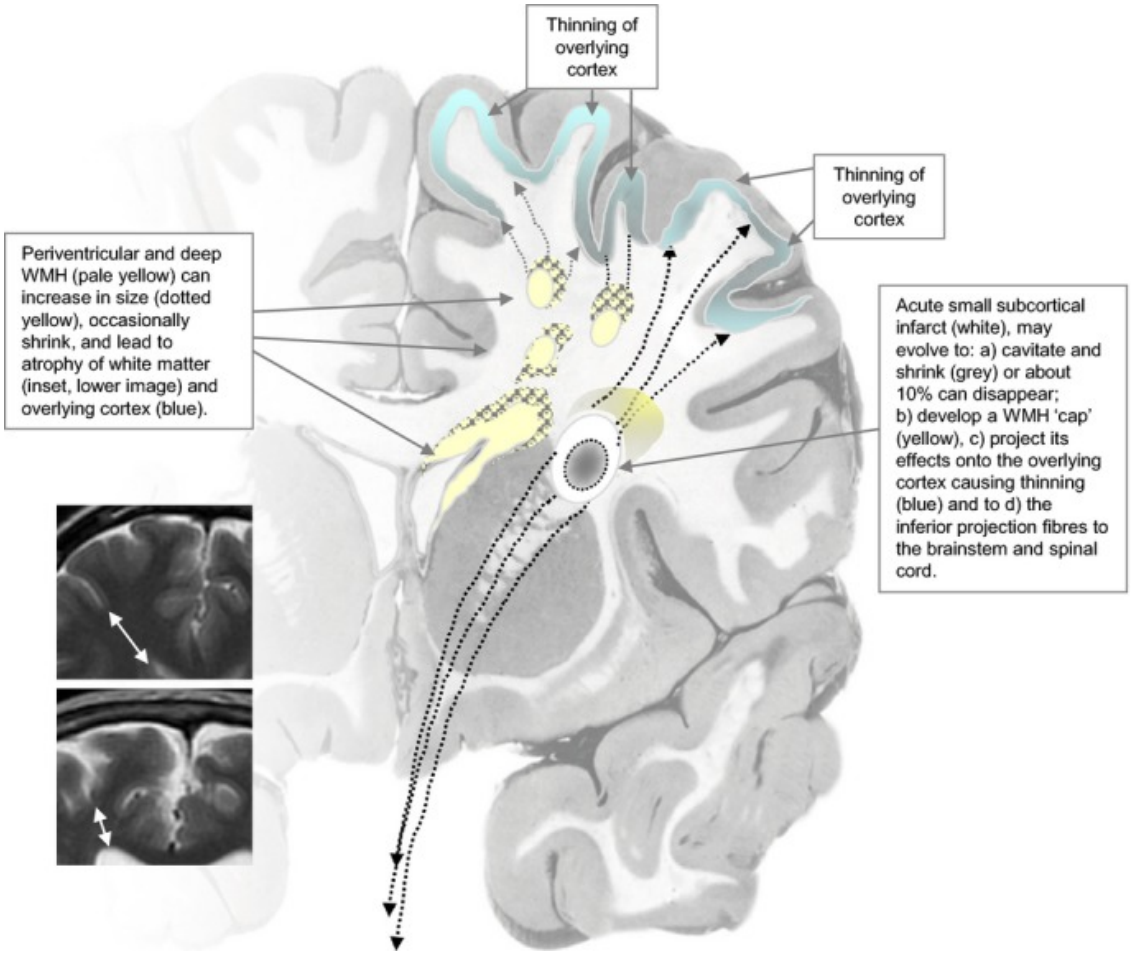

Figure 2.3: Mechanisms of white matter hyperintensity (WMH) progression in small vessel disease (SVD)[31].

2.1.4 Post-Stroke Cognition

Post-stroke cognitive impairment is identified in between 20-80% of stroke patients. The large variation in the prevalence of cognitive impairment is due to differences in diagnostic criteria, alongside population studied[39]. In a study of British stroke subjects, cognitive impairment was diagnosed by Mini-Mental State Examination (MMSE) in 24% stroke subjects in a 3-month follow-up period[40]. In a similar Dutch population, post-stroke cognitive impairment was diagnosed by MMSE in 70% first stroke subjects in a 6-month follow-up period. Furthermore, in this cohort, older age was the best predictor of subjects who would develop vascular cognitive impairment[41]. Estimates of post-stroke cognitive impairment have reached higher than this population, suggesting 96% stroke patients exhibit a form of cognitive dysfunction[39].

Many common vascular risk factors are thought to be associated with post-stroke cognitive impairment, including hypertension, diabetes, and history of previous stroke/TIA. In a study of 587 subjects, cardiovascular risk factors were found to explain over 60% of the variance in post-stroke cognitive impairment (R^2 = 62.10%) in a structural equation model. The study found evidence of prior stroke influencing cognitive function through an association with increased risk of incident dementia diagnosis (β = -0.39, 95% CI − 0.75 -− 0.13, p = 0.02). This relationship was not found in history of TIA. Atrial fibrillation was found to associate with higher stroke severity, and in turn poorer cognitive performance (β = -0.27, 95% CI − 0.49 - − 0.05, p = 0.02). Other vascular risk factors e.g., hypertension and diabetes did not reach a statistically significant threshold[42].

Post-stroke cognition can be affected by small vessel disease. In a longitudinal study, post-stroke cognitive impairment was defined as an MMSE score ≤26 and a total SVD burden calculated from the summation of the presence of SVD markers. Within this mild stroke cohort (451 subjects), SVD burden correlated with poorer MMSE performance (β = -0.37, p = 0.003). WMH load was the best predictor of poorer cognitive function (β = -0.25, p = 0.01)[43]. However, these findings are not always significant. In a study by Arba et al., 234 ischaemic stroke and TIA subjects were included in analysis investigating SVD and medial temporal lobe (MTL) atrophy, a marker of Alzheimer's disease. Moderate to severe lobe atrophy was identified in 104 (44%) participants. Whilst SVD markers were independently associated with MTL atrophy (p<0.001), only the lobe atrophy correlated with cognitive dysfunction (OR 1.94, 95% CI 1.28-2.94)[44].

Additional structural measures have been found to correlate with post-stroke cognitive impairment. In a recent study by Jochems et al., peak-width of skeletonised mean diffusivity (PSMD), a marker of white matter injury, was found to relate with poorer Montreal Cognitive Assessment (MoCA) performance at 1-year follow-up (β= −0.301, 95% CI −0.434−0.168; p < 0.001), and was more strongly associated than age and stroke severity[45]. These data suggests that white matter damage, regardless of whether SVD is included, could be a marker of post-stroke cognitive impairment. Limited evidence exists

in evaluating relationships between carotid artery disease and post-stroke cognitive impairment (see Chapter 3).

2.2 Neck Vasculature

The carotid arteries in the neck are the main arteries that supply oxygenated blood from the heart to the brain. They are divided into the common carotid artery (CCA), external carotid artery (ECA) and the internal carotid artery (ICA). The carotid arteries are protected by the carotid sheath. The carotid sheath is a layer of fibrous connective tissue in the neck that contains these arteries, the internal jugular vein, cranial nerves IX-XII, and lymph nodes (Figure 2.4)[46,47]. The function of the carotid sheath is to separate and protect these structures from damage. The carotid sheath is located posteriorly to the sternocleidomastoid muscle, extending from the base of the skull. The carotid sheath encapsulates the carotid canal and jugular fossa, two regions where the ICA and jugular vein pierce through the skull. The carotid sheath stretches downwards where it terminates at the aortic arch, merging with the axillary sheath at the level of the subclavian vein. The carotid sheath is divided into two portions, the suprahyoid and infrahyoid spaces. Between these spaces sits the bifurcation of the CCA into internal and external arteries[48].

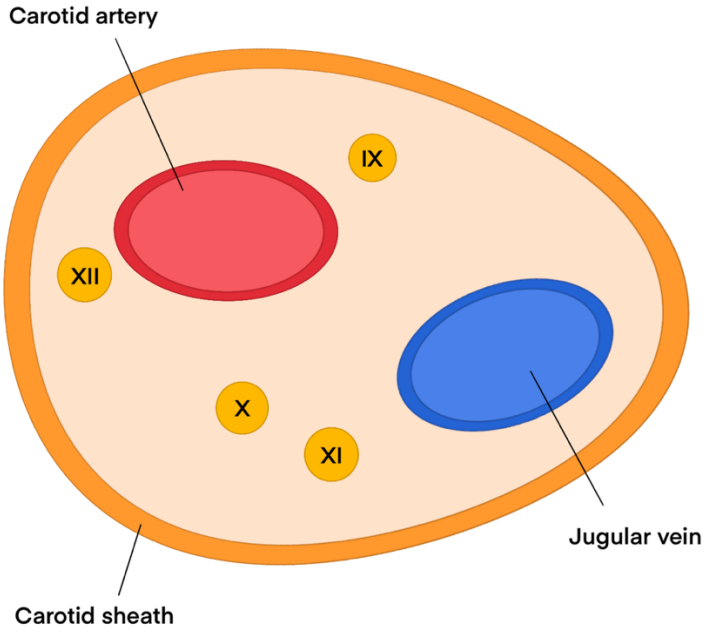

Figure 2.4: An axial representation of the carotid sheath in the neck, containing the common carotid artery (red), internal jugular vein (blue) and cranial nerves IX-XII (orange).

The origins of the common carotid artery are anatomically distinct on either side of the neck. The right CCA branches off the brachiocephalic artery behind the sternoclavicular joint. In comparison, the left CCA typically arises from the aortic arch, thus behind the mediastinum[46,49]. Anatomical variations in the origins of the CCA are well documented, but rare. The left CCA has been described as an additional branch of the brachiocephalic trunk in approximately 6% cases[50]. The CCA bifurcates into the ECA and ICA typically around C3-C4 of the cervical spine, near the upper border of the laryngeal cartilage[46,49]. However, this is prone to considerable variation. Most often, there is an asymmetry between the origins of the left and right ICA i.e., the carotid bifurcations are not level with each other and are unequal[46].

The ECA is one of two branches from the CCA. The ECA branches several times that supply many organs in the head and neck e.g., larynx and thyroid. It also supplies cranial nerves, facial bones and skull bones, and the dura matter. The ECA splits into many arteries, some of which branch afterwards. A main eight arteries are as follows,

terminating in the last two branches - the maxillary and superficial temporal arteries, seen in Figure 2.5:

- Superior thyroid artery
- Ascending pharyngeal artery
- Lingual artery
- Facial artery
- Occipital artery
- Posterior auricular artery
- Maxillary artery
- Superficial temporal artery[49,51].

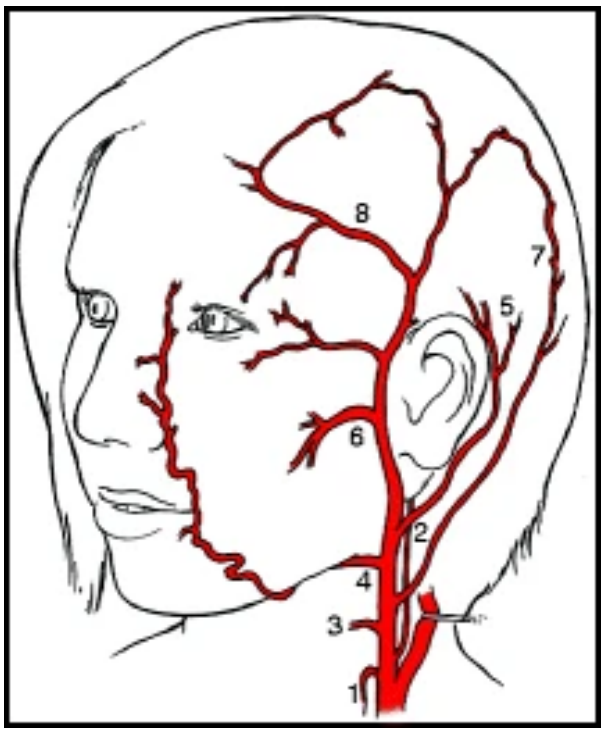

Figure 2.5: A schematic representation of the external carotid artery (ECA) and its major branches in numerical order as the artery rises superiorly through the neck and head. (1) superior thyroid artery; (2) ascending pharyngeal artery; (3) lingual artery; (4) facial artery; (5) posterior auricular artery; (6) internal maxillary artery; (7) occipital artery; (8) superficial temporal artery[51].

The ICA typically lies posterolateral to the ECA. The origin of the ICA is described as the carotid bulb or carotid sinus – an enlarged structure that lies distally to the carotid bifurcation. A classification system created by Bouthillier et al. (1996) is used to describe segments of the ICA as it rises through the neck and cranial vault[52]. This scale creates 7 distinct areas of the ICA based on its anatomy and the compartments that it travels through, seen in Figure 2.6.

The following terminology has been described by Bouthillier et al. (1996) as the ICA ascends superiorly from its most inferior portion:

- Cervical segment (C1)
- Petrous segment (C2)
    - Caroticotympanic artery
    - Vidian artery
- Lacerum segment (C3)
- Cavernous segment (C4)
    - Meningohypophyseal trunk
    - Inferolateral trunk
- Clinoid segment (C5)
- Ophthalmic segment (C6)
    - Ophthalmic artery
    - Superior hypophyseal trunk
- Communicating segment (C7)
    - Posterior communicating artery
    - Anterior choroidal artery (AChA)
    - Anterior cerebral artery (ACA)
    - Middle cerebral artery (MCA)[49,52].

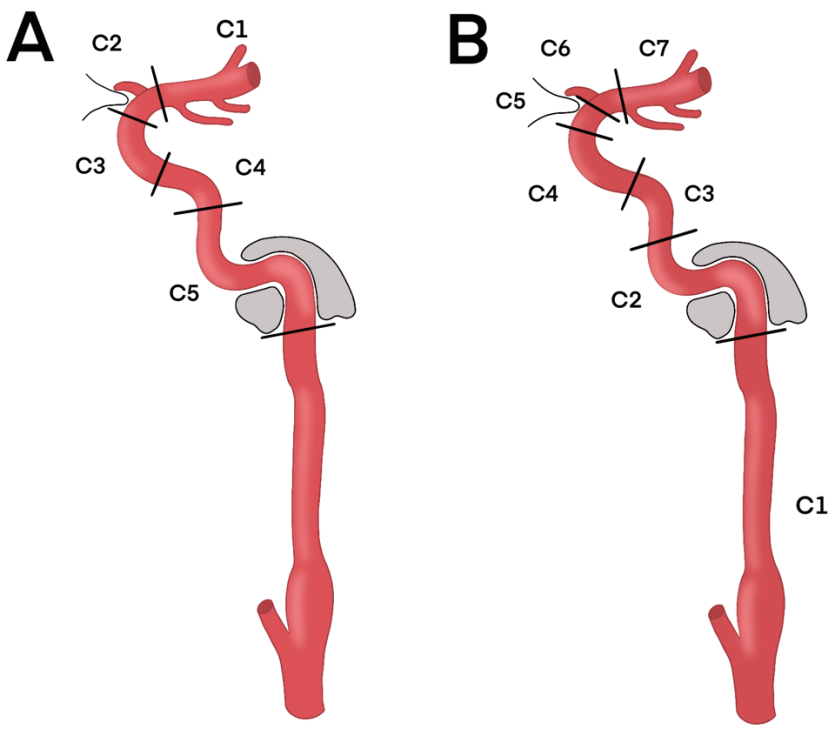

Figure 2.6: Comparison between the Fischer and Bouthillier classification systems for internal carotid artery structure. A: The Fischer system separates into 5 distinct areas (C1-C5) counting in a superior-inferior direction. B: The Bouthillier classification system splits the ICA into 7 distinct regions from the extracranial portion (C1) to the most superior segment (C7)[49,51,52].

Other anatomical classification systems exist for the carotid arteries. The work by Fischer et al. (1938) exists in opposition to the Bouthillier classification system (Figure 2.6). Fischer et al. (1938) describes segments of the carotid arteries based on the angiographic course of the ICA. However, this system only took intracranial ICA into consideration, omitting the extracranial ICA[52], thus undermining its importance. Gibo et al., (1981). Lasjaunias and Santoyo-Vasquez (1984) proposed a classification system based around the in-utero development of the carotid arteries, suggesting that all congenital structural abnormalities can be attributed to the embryological agenesis of the structure[53].

The cervical segment of the ICA is sometimes called the extracranial internal carotid artery (EICA). It describes the cervical (C1) portion of the ICA that extends from the carotid bifurcation to the carotid canal. The carotid artery terminates in the anterior and

middle cerebral arteries, which form part of the Circle of Willis (CoW). Therefore, the ICA are responsible for the anterior circulation in the brain[49].

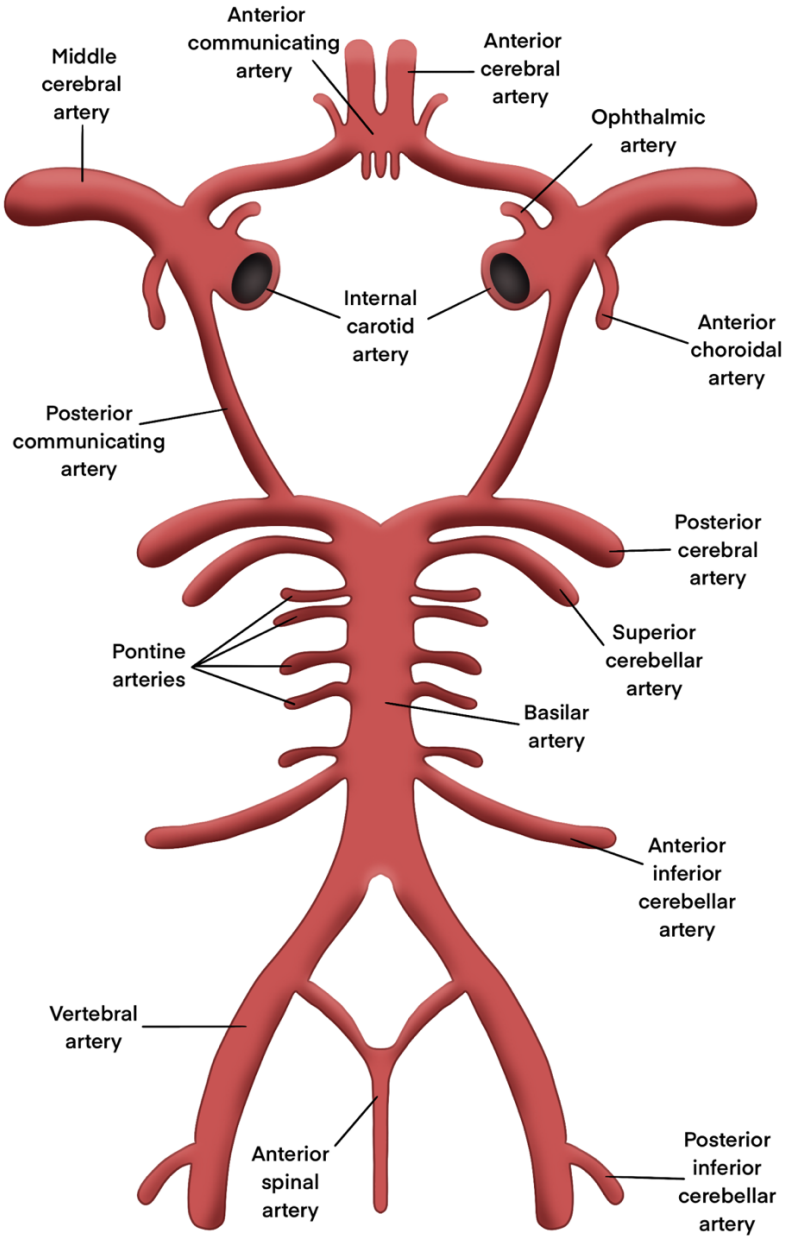

Figure 2.7: A schematic representation of the Circle of Willis. The paired internal carotid arteries join with the anterior communicating artery. These carotid arteries then develop into the middle cerebral arteries (MCA), providing the anterior circulation of the brain.

The vertebral arteries are two vessels that travel on either side of the spine and are responsible for the posterior circulation of the brain. They arise from the left and right subclavian arteries and enter the skull through the foramen magnum. The arteries then join to form the basilar artery[46].

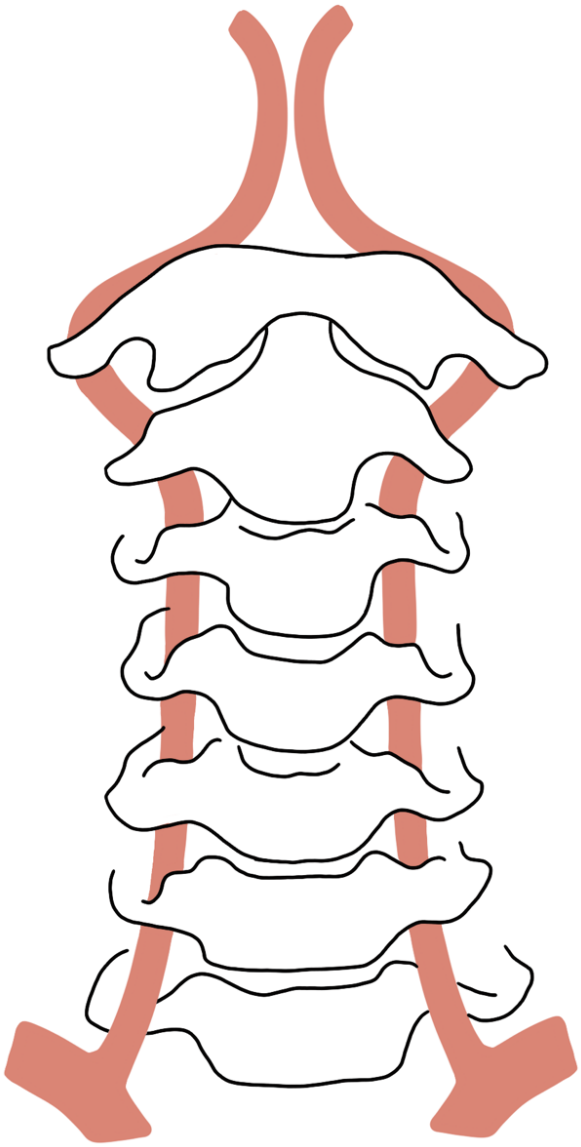

Figure 2.8: A schematic representation of the vertebral arteries (pink) as they rise superiorly through the spinal column from the subclavian arteries in the neck.

2.2.1 Vessel Wall Anatomy

The carotid arteries consist of three layers of tissue: tunica externa or tunica adventitia, tunica media, and tunica intima. The t. adventitia is the outermost layer of the artery. This layer consists of collagen and connective tissue that aid in anchoring the vessel to provide stability. The t. adventitia has elastic fibres that exist within the loose connective tissue that promote flexibility of the vessel, whilst maintaining the structure to prevent over-expansion due to blood pressure. Vessels can be described as elastic or muscular arteries based on the arrangement of the fibres within the t. adventitia. The carotid arteries are examples of elastic arteries[54]. The t. adventitia includes vaso vasorum that deliver oxygen and nutrients to the vessel; and nervi vasorum that small nerves piercing the arterial wall to allow the constriction and dilation of the blood vessel[55].

The tunica media is a layer of smooth muscle that aids the constriction and dilation of the artery. The t. media contains elastin fibres that provide elasticity and collagen that strengthens the artery. The complement of elastin fibres is such that the t. media is more flexible than the outer layer of the artery. Between the t. media and t. adventitia exist the external elastic lamina, which separates these two layers[55].

The tunica intima is the innermost layer of arteries. The t. media is lined by endothelial cells in muscular arteries, or epithelial cells in elastic arteries, which are in constant contact with the oxygenated blood. Between the t. intima and t. media exists the internal elastic lamina, separating these layers[55].

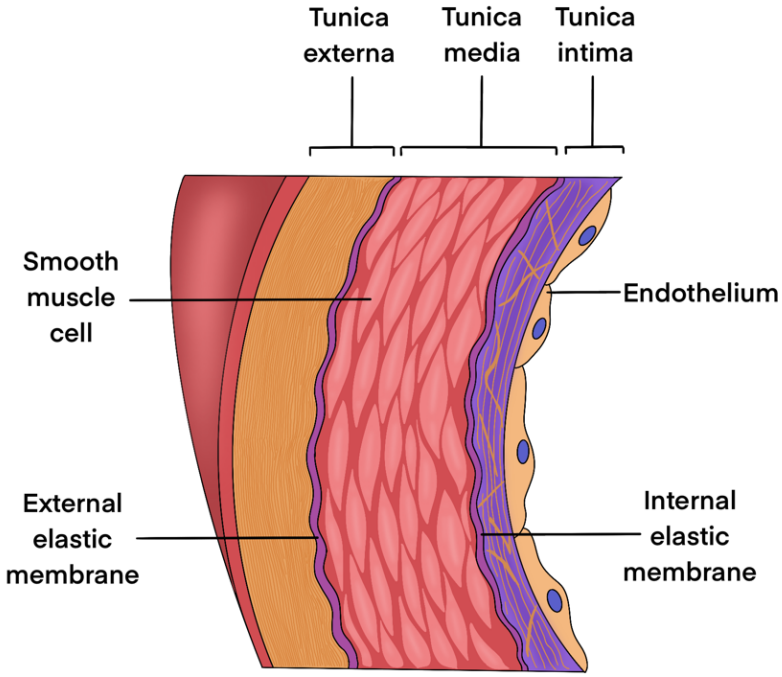

Figure 2.9: The different layers in the vessel wall. The tunica externa, tunica media, and tunica intima represent the outer, middle, and innermost layers. The layers are separated by elastic laminae.

2.2.2 Function of the Carotid Arteries

The carotid bulb, or carotid sinus is an important structure within the neck in terms of function. The carotid sinus is a “reflex” area of the carotid arteries and contains many baroreceptors that are sensitive to changes in blood pressure. These baroreceptors are innervated by the glossopharyngeal nerve – cranial nerve IX. The neurons as part of this nerve bundle project afferent signals to the solitary nucleus of the medulla[48,56]. Mechanical stretching of the carotid artery is a symptom of increased blood pressure. In response to an increase in blood pressure, the baroreceptors send signals to the brain, which in turn stimulates parasympathetic activity/ inhibits sympathetic activity, decreasing the heart rate and reducing blood pressure[56,57].

2.2.3 Carotid Artery Disease

Atherosclerosis is a chronic process of inflammation that causes the hardening of arteries. Initially, the endothelial monolayer lining the tunica intima exhibits structural alterations. In atherosclerosis, the endothelia express adhesion molecules e.g., vascular adhesion molecule-1 (VCAM-1), capturing white blood cells in response to certain stimuli such as hypertension and dyslipidaemia. The expression of these adhesive molecules is further enhanced by oxidative stress i.e., the presence of ROS such as O_2^-. In tandem, the endothelial permeability alters, promoting the movement and retention of lipid particles such as low-density lipoproteins (LDL) into the vascular wall. The leukocytes bind to the adhesion molecules and are internalised to the tunica intima with the aid of chemoattractant molecules, where they mature to macrophages. By endocytosis, lipid particles merge with the macrophages to create foam cells (Figure 2.10)[58–60].

Plaque formation involves the recruitment of smooth muscle cells (SMCs) from the tunica media to tunica intima, where these cells proliferate in response to signalling molecules. Once in the intimal layer, these SMCs produce molecules commonly found in the extracellular matrix i.e., they produce interstitial collagen and elastin that promotes the formation of a fibrous cap to cover the plaque. The cap covers an aggregation of foam cells, of which some may die releasing lipids. However, as these lipids and dead cells cannot clear normally, this creates a lipid-rich pool of cells known as the necrotic core of the plaque. A thrombus may form at the plaque site owing to a physical disruption i.e., fracture of the plaque cap. This fracture expresses procoagulant material that promotes the binding of blood compounds at the plaque site, forming a thrombus, and limiting blood flow (Figure 2.10)[58].

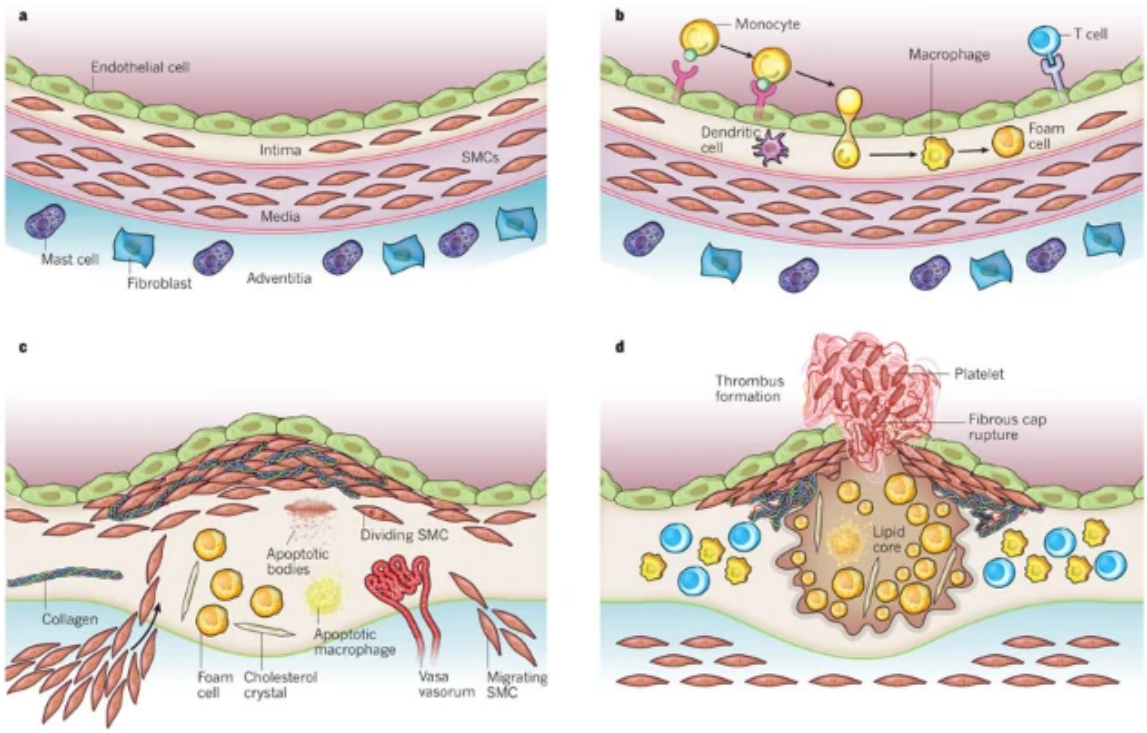

Figure 2.10: The different stages in the advancement of atherosclerosis. Panel A: The normal appearance of the arterial wall. The endothelial cells are a single layer that lie in contact with the blood. The intima layer is a thin layer of smooth muscle cells. The tunica intima contains more smooth muscle cells. The adventitia layer contains mast cells, fibroblasts and other structures that help promote vessel anchoring and structure. Panel B: The initial steps of plaque development include the production of adhesive cells to bind white blood cells, integration, and maturation of the monocytes into the intimal layer, and development of foam cells through the binding of lipid to macrophage. Panel C: The progression of the atherosclerotic lesion entails the movement of smooth muscle cells (SMCs) into the tunica intima, and the production of molecules such as collagen, forming a fibrous cap. Some cells may die, but due to improper clearance, form a lipid-rich necrotic core. Panel D: Thrombus formation is caused by the physical rupture of the plaque cap, allowing blood components to encounter pro-coagulant material[58].

Evidence suggests that impaired protective mechanisms against atherosclerotic deposition occurs at branching points of arteries. This may be reflective of different haemodynamics at the branching points of the arteries as well as distinctions in the development of these bifurcations. Normal laminar flow may promote a protective programme of gene expression. The presence of abnormal laminar shear stress at these points may relate to the reduction of local nitric oxide. The NO molecules exhibit anti-

inflammatory properties and may suppress the expression of VCAM-1. Additionally, disturbed laminar flow may increase the production of other adhesion molecules. The altered wall stress, by arterial SMCs, may promote the generation of molecules that bind and retain the lipoproteins. This facilitates their modification and promotes a local inflammatory response at arterial bifurcations. This may help to explain why plaques are more commonly seen at branching points in the arterial trees[58,61].

LDL, high density lipoproteins (HDL) and triglycerides are each independent predictors of atherosclerosis. Low concentrations of HDL are a strong predictor of atherosclerosis[58,59,61]. Conversely, HDL demonstrates preventive mechanisms of developing atherosclerosis. HDL may reverse cholesterol transport, and transfer antioxidant enzymes to neutralise inflammatory effects of lipids[58,61]. Despite these functions of HDL, trials manipulating HDL concentrations are yet find significant and conclusive benefits in reducing risk of cardiovascular events[58]. Data may suggest that the proportion of functional versus dysfunctional HDL may be important in the development of atherosclerosis, rather than the absolute concentrations[59]. Additionally, high levels of triglycerides are associated with low HDL and high concentrations of LDL particles[59].

Hypertension mediates atherosclerosis via the increase of oxidative stress through ROS, increasing the aggregation of cell adhesion molecules, and the production of cytokines. Evidence from spontaneously hypertensive rats (SHR) studies found that ROS production precedes that of hypertension, with O_2^- levels higher in SHR vasculature. Moreover, other markers of oxidative stress e.g., higher tissue concentrations of H_2O_2 and decreased antioxidant activity are seen in experimental hypertension, and hypertensive patients. Additionally, proinflammatory cytokines are increased in the plasma of hypertensive patients[60]. Previous studies have reported elevated concentrations of cell adhesion molecules such as VCAM-1 in hypertensive patients exhibiting increased IMT[60].

Hyperglycaemia associated with diabetes promotes atherosclerotic lesion progression. Hyperglycaemia can lead to the development of specific molecules known as advance glycation end products (AGE), that exhibit pro-inflammatory response by increasing the production of cytokines. Additionally, diabetes promotes oxidative stress by

ROS. Obesity predisposes to diabetes but exhibits atherogenic effects independent of insulin resistance. Elevated concentrations of free fatty acids from the viscera may stimulate very low-density lipoproteins (VLDL) by hepatocytes in the liver. VLDL can decrease concentrations of HDL by exchanging to VLDL, thus limiting atheroprotective effects[60,61].

Smoking cigarettes is a known contributor to carotid artery disease. Smoking increases the thickening of the artery wall and promotes the narrowing of the artery. Development of stenosis in smoking may be caused by increasing oxidative stress and expression of several inflammatory molecules. Smoking can produce ROS through tar, initiation of macrophages, xanthine oxidase activity and other substances. Cigarette smoke augments leukocyte activity to increase ROS production and contains peroxyl radicals damaging the endothelia. Smoking also reduces vitamin C and E antioxidant concentration and decreases the serum levels of HDL[60].

Outside of cardiovascular risk factors, mechanical forces may aid the promotion of atherogenesis. Three main fluid-based forces that alter blood flow are:

1. Wall shear stress
2. Hydrostatic pressure
3. Circumferential stretch.

These forces account for the deposition of atherosclerotic plaques at sites such as branches in an arterial tree. Wall shear stress is the force exerted on the endothelial monolayer by the direction of blood flow, seen in Figure 2.11. Hydrostatic pressure is the force exhibited by the blood in the vessels. Circumferential stretch is the change in the circumference of the vessel caused by pressure.[62,63]

A continuous exposure to shear stress is important for maintaining standard physiological function. Arteries that exhibit unidirectional laminar flow typically exist in antithrombotic and anticoagulative states. In vessel bifurcations such as within the carotid

arteries, the vessels are exposed to an oscillatory shear stress, and altering circumferential pressure. Low shear stress/changing shear stress caused by turbulent flow in these areas causes arteries to remodel themselves to preserve normal flow and luminal diameter. However, over time this remodelling causes the thickening of the intima layer, promoting atherogenesis at these sites. Moreover, disturbed flow i.e., flow splitting into multiple directions may increase the permeability of the endothelia and release pro-inflammatory compounds[62,63].

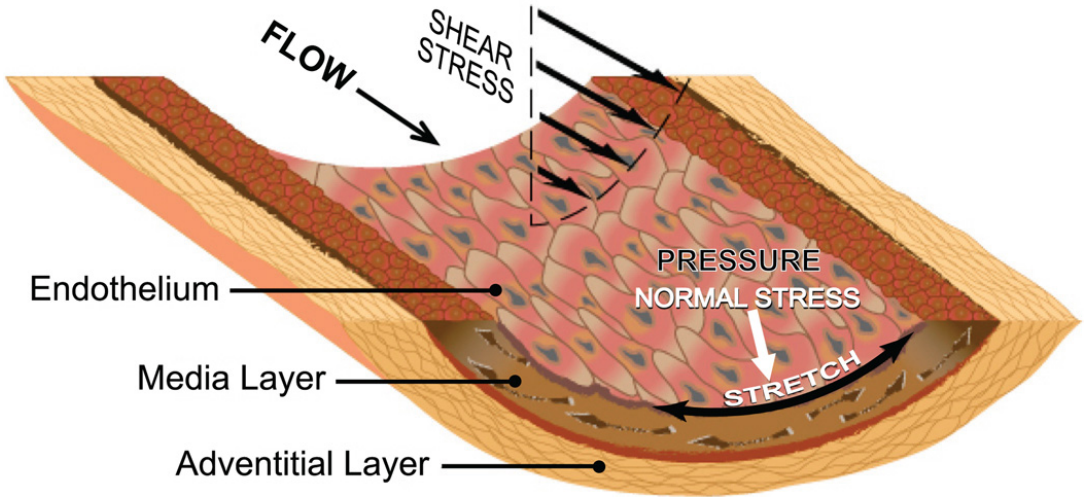

Figure 2.11: A schematic diagram of the mechanical forces in blood flow. Shear stress is parallel to the endothelial surface and moves along with blood flow; circumferential stretch is caused by the normal stress of the blood pressure (perpendicular to the wall)[63].

2.2.4 Measurements of Carotid Artery Disease

Carotid artery stenosis is currently the prime criterion for assessing the severity of carotid artery disease. Management of carotid disease is decided using the North American Symptomatic Carotid Endarterectomy Trial (NASCET) measurement criteria of stenosis. High degrees of carotid stenosis (70-99%) undergo the carotid endarterectomy (CEA) surgical procedure to repair the vessel[64].

The NASCET trial interned 1212 patients with carotid artery disease, randomised to endarterectomy (616 patients) or standard medical therapy (596 patients). CEA was found to significantly reduce the risk of stroke in patients with severe narrowing i.e., 70-99% stenosis[65,66]. The benefit of surgery was modest for moderate stenosis patients i.e., 50-69% with a cumulative five-year stroke risk of 15.7%, compared with 22.2% when treated medically ($p = 0.045$)[66]. Patients with <50% stenosis do not benefit from CEA; five year cumulative stroke risk is 14.9% for endarterectomy patients versus 18.7% for medical management ($p = 0.16$)[66]. Despite this, many strokes are caused by "subclinical" carotid artery stenosis.

A similar trial in Europe, the European Carotid Surgery Trial (ECST) demonstrated a different measurement of carotid stenosis, finding that 44% of the 3018 patients sampled displayed stenosis <30%[67]. In the UK, NASCET criteria are used to assess stenosis. These are a simpler indicator of stenosis, as it compares the maximum stenosed area to a non-stenosed portion more superior of the plaque. Comparatively, the ECST method estimates the diameter of the lumen within the stenosis, seen in Figure 2.12.

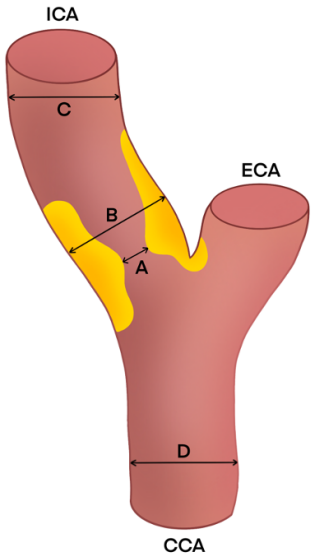

$$ECST = \left(\frac{B - A}{B}\right) \times 100$$

$$NASCET = \left(\frac{C - A}{C}\right) \times 100$$

$$Common\ carotid = \left(\frac{D - A}{D}\right) \times 100$$

Figure 2.12: The criteria for assessing carotid artery stenosis using the European Carotid Surgery Trial (ECST), North American Symptomatic Carotid Endarterectomy Trial (NASCET) and Common carotid artery measurements.

In the general population, subclinical carotid artery stenosis is common. The Cardiovascular Health Study assessed 5,201 participants aged ≥ 65 years old. CAS was detectable in 75% men and 62% women. Clinically significant stenosis i.e., ≥ 50% CAS was detected in 7% men and 5% women. Maximum stenosis increased with age, and was consistently greater in men than women[68]. A pooled meta-analysis of 4 population-based studies (23,706 participants) assessed outcomes of asymptomatic moderate (≥ 50%) and severe (≥ 70%) CAS stratified by age and sex. The prevalence of moderate and severe CAS is displayed in Figure 2.13[69]. In men, moderate CAS ranged from 0.5% (95% CI 0.3-1.1) below age 50 to 5.7% (95% CI 4.5-7.1) ages 80 and over. In comparison, women exhibited an age-matched prevalence of 0.3% (95% CI 0.1-0.6) to 4.5% (95% CI 2.8-6.8). The prevalence of severe CAS was lower in both men and women, reflecting that severe stenosis is more likely to be symptomatic i.e., a cause of recent stroke. The prevalence of severe asymptomatic CAS in men ranged from 0.1% (95% CI 0.0-0.4) below age 50 to 1.7% (95% CI 0.8-3.4) ages 80 and over. In women, the age-matched prevalence ranged from 0% (95% CI 0.0-0.2) to 0.9% (95% CI 0.4-2.4).

A

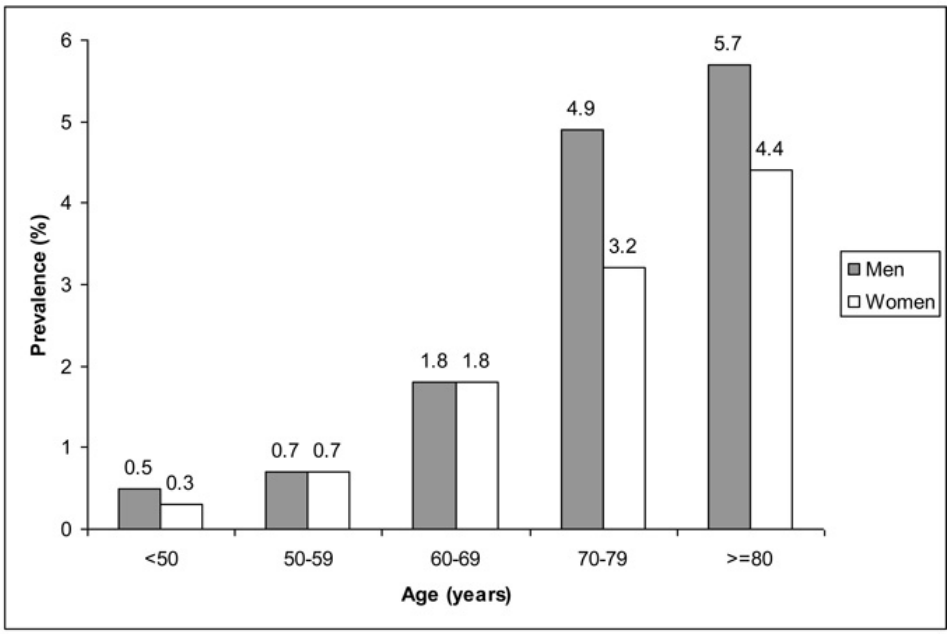

Adjusted for smoking, hypertension, hyperlipidemia and diabetes.

B

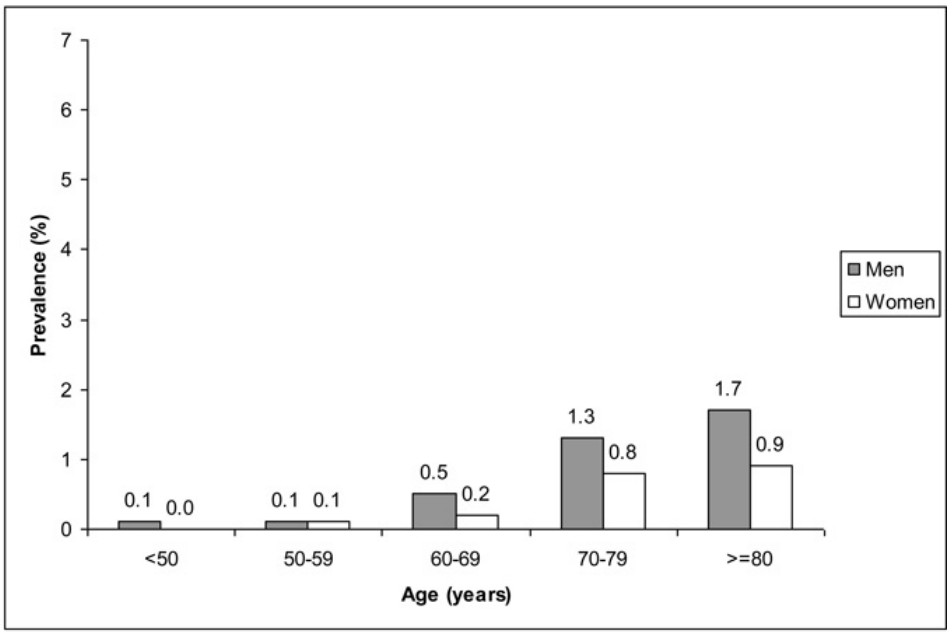

Adjusted for smoking, hypertension, hyperlipidemia and diabetes.

Figure 2.13: A meta-analysis of carotid artery stenosis (CAS) in the general population, separated by age and sex. A: The prevalence (%) of moderate (≥50%) CAS, adjusted for common cardiovascular risk factors. B: The prevalence (%) of severe (≥70%) CAS, adjusted for common cardiovascular risk factors[69].

Carotid artery plaques were originally classified into two main types: a fatty streak, containing foam and inflammatory cells, and the atheromatous plaque, containing the lipid-

rich necrotic core and fibrous cap. However, more recent classification systems have been developed, based on the histology of coronary artery plaques. This successive classification system, created by the American Heart Association (AHA) is as follows:

- Type I: initial lesion with foam cells
- Type II: fatty streak lesion, accumulation of intracellular lipid
- Type III: intermediate lesion, fatty streak with additional extracellular lipid aggregation
- Type IV: atheromatic lesion, core of extracellular lipid
- Type V: fibroatheroma lesion, lipid-rich core, fibrous cap, or mainly calcification
- Type VI: complicated lesion, surface defect and thrombus[70].

A systematic review and meta-analysis of MR-assessed carotid plaque features and stroke risk found that the presence of intraplaque haemorrhage (IPH), lipid-rich necrotic core (LRNC) and thinning fibrous cap were associated with increased risk of secondary stroke or TIA, independent of carotid stenosis. Though thinning/fibrous cap rupture displayed the highest hazard ratio (HR 5.93, 95% CI 2.65 – 13.29, p <0.01), the IPH (HR 4.59, 95% CI 2.92 – 7.24, p <0.01) and LNRC (HR 3.00, 95% CI 1.51 – 5.95, p = 0.002) each demonstrated pronounced hazard ratios. If described in rank order, it should be noted that the risk of stroke in relation to plaque elements is relative to that of plaque progression i.e., fibrous cap rupture has the most extreme hazard ratio, mirroring that it is the last stage in atherosclerotic development[71]. Additionally, a large histological study performed by Howard et al., found that stroke risk was significantly affected by plaque composition. These features (IPH, LRNC, fibrous cap, calcification etc.) are all associated with plaque instability. Whilst independently, these elements may not have exhibited any significant increases in stroke risk, together their contributions to plaque instability demonstrated an increase in both 1-year (OR 1.42, 95% CI 1.07 – 1.90, p = 0.02) and 5-year stroke risk (OR 1.40, 95% CI 1.05 – 1.87, p = 0.02)[72].

Intima-media thickness (IMT) is a measurement of arterial wall alteration. It is the thickness of the inner two layers of the vessel wall, and commonly assessed in relation to carotid artery disease. Measurements of IMT have great predictive value regarding cardiovascular risk and is thought to be related to increased risk of stroke[73]. Carotid IMT is

a measure of atherosclerosis and can be used to track the progression/regression of disease in the artery. IMT is commonly studied using ultrasound imaging, having first been conducted in the 1980s by Pignoli et al[74]. Carotid IMT is often measured at 3 distinct sites: the CCA (1 cm proximal to carotid bifurcation), the bifurcation and ICA. IMT measurements of the deeper wall are thought to be more reliant than the superficial vessel wall[75].

Stroke risk has been found to rise with increasing carotid IMT. In the Rotterdam study with a mean follow-up 2.7 years, risk of all (first or recurrent) stroke was found to increase per standard deviation (0.163mm) of common carotid IMT (OR 1.41, 95% CI 1.25-1.82). The risk of first stroke in these participants was found to increase per standard deviation of carotid IMT as well (OR 1.57, 95% CI 1.27-1.94)[76]. A population-based meta-analysis of 37,197 subjects found risk of cardiovascular events (including stroke and myocardial infarction) found the relative risk per IMT difference was RR 1.32 (95% CI 1.27-1.38) per increase in standard deviation for stroke patients in the common carotid artery. The risk of myocardial infarction was found to increase (RR 1.26, 95% CI 1.21-1.30). The meta-analysis described variation in the follow-up duration, as well as areas of IMT studied (CCA, ICA, combined CCA+ICA)[77]. However, more recent evidence from meta-analysis of 36,984 subjects found carotid IMT progression (mean follow-up 7 years) did not increase risk of cardiovascular events in the general population (HR 0.97, 95% CI 0.94-1.00)[78].

2.2.5 Vessel Tortuosity

Tortuous vessels are common anomalies seen in many species. Efficient transportation of blood is reliant upon vessel structure; straight arteries are effective in delivering blood to organs. A tortuous vessel is one that does not take a direct path to the organ of interest. This may occur due to abnormal embryological development or due to disease[79]. In some studies, vessel tortuosity is classified as a particular "type" e.g., curving, looping, etc (Figure 2.14)[79].

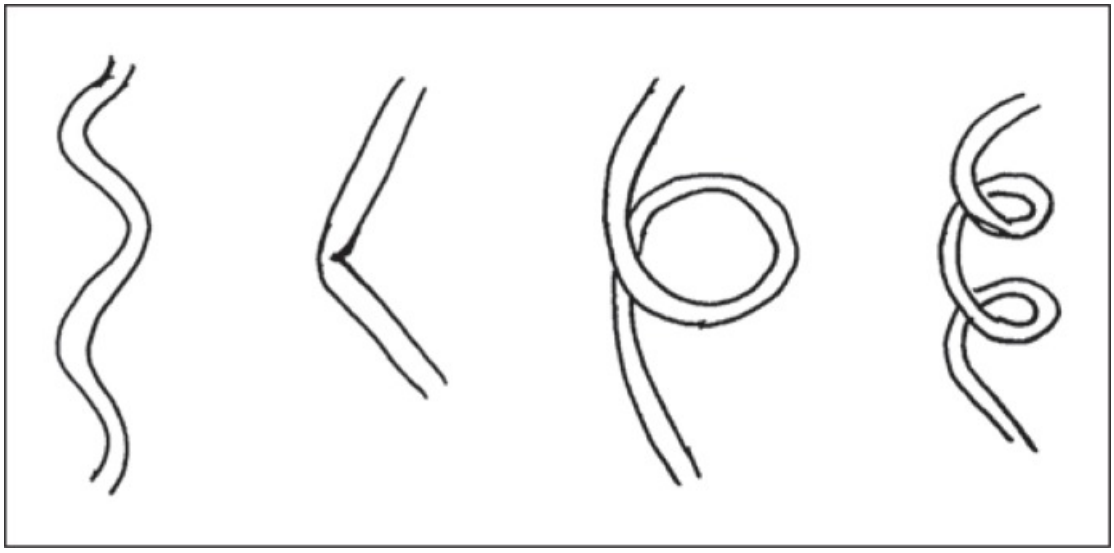

Figure 2.14: The descriptions of various phenotypes of tortuous vessels. In order (L-R): curving, kinking, looping and spiral twisting[79].

Previous studies have identified associations between large artery tortuosity (including the aorta and carotid arteries) and diseases including atherosclerosis, hypertension and normal ageing[79–81]. Carotid artery tortuosity is commonly asymptomatic; less than 20% patients present with symptoms attributable to vessel tortuosity e.g., dizziness and ischaemic stroke[81,82].

Vessel tortuosity can be calculated in multiple ways, commonly using an index value. Various tortuosity index calculations exist (Figure 2.15). The simplest formula is the ratio between the actual length and minimum length of the vessel. Alternatively, tortuosity can be calculated as the total curvature, normalised by vessel length, or ratio of wavelength versus amplitude[79].

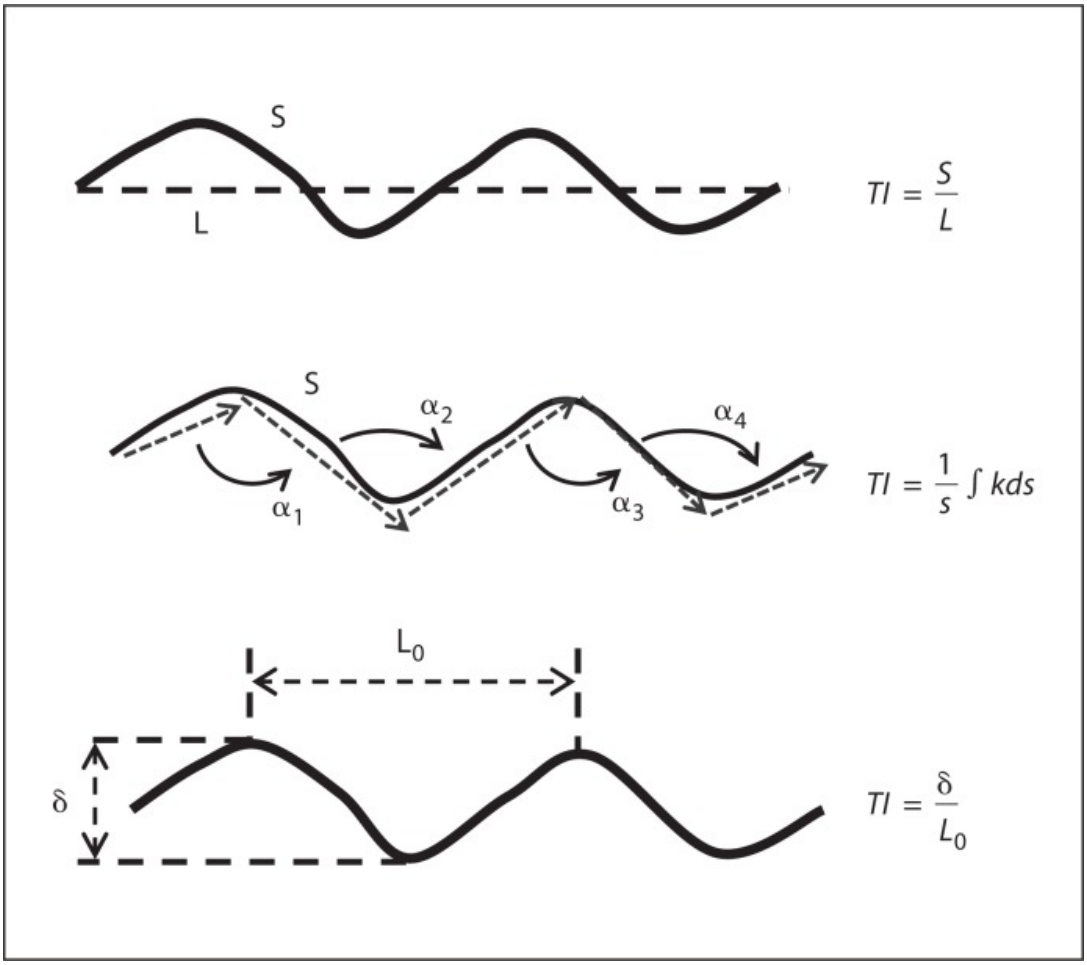

Figure 2.15: Different formulae to calculate a vessel tortuosity index value. The integral in the second formula is equal to the sum of the angles α_1-α_4[79].

A different protocol by Welby et al. describes carotid artery tortuosity in 3 types:

- Type 1: Loops defined as C- or S-shaped with 2 turns of angles ≤90^o
- Type 2: Coiling with complete 360^o turns
- Type 3: Kinking with 1 bend ≥ 90^o[82].

Tortuous vessels are commonly reported in elderly populations; they are rarely found in children. Carotid artery tortuosity has been associated with reduced lumen diameter; however, there are conflicting reports surrounding the correlation of atherosclerosis and vessel tortuosity. Additionally, degenerative arterial disease i.e., loss of elastin proteins is found to exist in tortuous vessels. Elastin insufficiency weakens the arterial walls, and elastin fragmentation is thought to cause vessel lengthening. These

mechanisms may lead to increased tortuosity, though associations between the two are unclear[79]. In "normal" arteries, significant axial tension maintains structural stability and prevents against the vessels becoming tortuous. Reduced axial tension is thought to associate with ageing[79]. Vessel tortuosity increases resistance to blood flow and alters lumen shear stress[79].

There are few studies that investigate carotid artery tortuosity and ischaemic stroke risk. A recent study by Saba et al. found a significant association between the tortuosity index of the ICA and CCA-ICA vessels with sides of stroke ($p<0.01$), though there seem to be no studies that investigate stroke risk with odds or hazard ratios at present[83] to the best of our knowledge. However, a different report by Abo Elfetouh et al. described morphological variations, including ICA tortuosity and kinking. These structural variations were not associated with increased risk of ischaemic stroke. This may be due to a small sample size; 11/102 participants exhibited a structural variation included for the study[84].

Despite evidence of structural changes causing vessel tortuosity, and links to clinical presentations, there is a limited understanding of the role of vessel tortuosity in ischaemic stroke. Evidence is limited by a lack of standardisation in calculating tortuosity indices, or visual classification of vessel shape.

2.3 Medical Imaging

Non-invasive imaging of the circulatory system plays a key role in the treatment and management of ischaemic stroke. Cross-sectional imaging techniques such as computed tomography (CT) and magnetic resonance imaging (MRI) offer anatomical visualisation with high spatial resolution. Techniques such as these allow for the discrimination between normal and pathological states using different contrast properties[85]. Imaging of arterial systems in the body can be done using different techniques, often dependent upon the artery in question. The following section will describe some of the techniques used to assess carotid artery disease: ultrasound, CT, MRI and digital subtraction angiography (DSA).

Medical imaging began in 1895, with Wilhelm Conrad Röntgen's discovery of the ionising radiation, X-ray. He found that invisible rays (later called Röntgen rays) penetrate certain tissues (such as skin) better than others (such as bone). His efforts in X-ray were rewarded with the first Nobel Prize in 1901[86]. By the 1970s, the advancement of CT allowed the acquisition of multiple slices (or tomographic images) of the body to be processed[86].

Assessment of vasculature using CT is known as CT angiography (CTA). Through the injection of a contrast bolus (iodine) into a blood vessel, images are created which display blood vessels as opaque and hyperintense. These images allow trained clinicians to discern vessel occlusions, plaques, and stenosis amongst other malformations[85]. In its infancy, radiodense contrast agents were injected directly into the artery studied. In the case of suspected stroke, this involved a "carotid puncture", requiring a needle thicker than a straw to inject the contrast agent. Further methodological developments included the catheterisation of guide wires from the groin to deliver contrast agent to the vessels of interest[86].

CTA is used widely in head and neck imaging due to the fast acquisition speed and high spatial resolution. It can be used to characterise plaque composition and is especially sensitive to calcifications within a plaque lesion[87]. Furthermore, CTA can be useful to detect plaque ulceration, showing higher sensitivity and specificity in comparison to surgical observation[88]. However, due to the image sensitivity to calcium, this may override other signals from the tissue i.e., detection of ulceration may prove inferior in the presence of a calcified plaque[89].

Despite these advantages, CTA uses ionising radiation (X-rays), and the use of contrast agents may not be suitable for patients who suffer with renal disease[90].

Ultrasound is a readily available technique developed that visualises *in vivo* vessels and atherosclerotic disease. Ultrasound uses sound waves to visualise arteries near the surface of the skin. This functions by delivering sound waves and reading the reflected signal[86]. B-mode ultrasound can be used to classify plaque type and location and assess the morphology[91]. Additionally, it is used to measure the intima-media thickness of the artery wall[92]. Atherosclerotic plaques can be described based on the signal observed by the ultrasound receiver. Lipid-rich plaques appear echolucent in an image, comparing with fibrous plaques which appear echogenic[93]. Colour-flow Doppler imaging combines the B-mode ultrasound with blood-flow velocity, measuring flow dynamics in the vessel lumen. This can be used to improve the estimation of vessel stenosis[94].

Downsides of ultrasound imaging include decreased sensitivity and specificity of diagnosis in comparison to other techniques such as DSA. Accuracy of ultrasound has been known to decrease due to increasing stenosis grades[95,96]. Additionally, the intra-observer variability of ultrasound may be insufficient for a diagnostic tool. However, these caveats are caused by imaging in a 2D plane. Ultrasound obtains a 2D plane of the vessel area, which may be inadequate for assessing vessels that are not parallel with the ultrasound probe, or tortuous arteries[97]. Thus, 3D imaging (CT/MRI) may be considered superior for their visualisation properties.

Magnetic resonance imaging (MRI) was also developed in the 1970s. In the beginning, these images were acquired in weak magnetic fields with low spatial resolution. Despite this, MRI was considered superior to CT for its better discrimination of soft tissue. MRI also uses non-ionising radiation, unlike CT[86]. The superconducting magnets involved in MR imaging now operate at intense magnetic fields, measured in Tesla. The magnetic field of the Earth is calculated at 0.00005T. By comparison, a 1.5T MRI scanner has a field strength some 30,000 times greater than that of the Earth[86].

MR angiography (MRA) is a set of image sequences that are designed for the visualisation of vascular anatomy by forfeiting contrast from non-vascular tissue. Time-of-flight (TOF) MRA image generation is performed by supplying repetitive suppressive pulses to tissue in the image volume, so the static tissue is saturated. This

generates a high contrast image between the unsuppressed signal from blood in the arteries and the dark suppressed background tissue. Venous flow signal that lies adjacent to arteries i.e., the internal jugular vein may obscure the arterial signal. Combatting this requires the selective suppression of signal by applying a saturation band to the venous plane adjacent to the image slice, nulling venous signal. TOF techniques are subject to flow-related changes which may affect the image gradient. In planes where there is a high flow velocity, the blood appears hyperintense to the background image as the blood is free of the excitation (saturation) pulse. However, slower flow velocity, tortuous vessels or retrograde filling results in the blood becoming saturated by the pulse, causing limited/complex visualisation[85]. Therefore, stenosis estimation is affected by the wash-in efficiency of the unsaturated hydrogen ion spins within the blood.

TOF imaging can be used in 2D/3D planes. Either 2D or 3D TOF imaging may be used for the evaluation of the carotid arteries. In 2D TOF angiography, the images are acquired perpendicular to the plane. 3D TOF imaging often has multiple overlapping slab acquisition, which allows for a fully rendered image volume that is less susceptible to image saturation[85].

Due to the speed of acquisition, TOF MRA is often performed alongside brain MRI in the treatment of stroke/TIA. The high contrast imaging provided by TOF allows for the evaluation of vessel stenosis; maximum intensity projection (MIP) images are sometimes used for their appearance similar to CTA. As TOF does not require a contrast injection, it is not impeded by separating high intensity images from calcification and bone[85]. However, TOF can only provide information regarding the vessel lumen i.e., luminal stenosis. Evaluating the vessel wall requires additional pulse sequences.

A typical non-contrast enhanced imaging protocol includes TOF MRA, T1-weighted, T2-weighted and proton density (PD) weighted imaging. Their specific techniques in the visualisation of certain tissue classes allows for the discrimination of different atherosclerotic plaque components. T1-, T2-, and PD-weighted imaging may be collectively described as black-blood imaging, as fluid signal in these sequences is null.

Contrast-enhanced MR angiography (CE-MRA) requires the use of a paramagnetic contrast agent to increase T1 contrast in arteries. CE-MRA often utilises a gadolinium tracer to shorten T1-weighted relaxation time, providing high contrast imaging, without being as dependent upon inflow of blood into the image space. By using a fast gradient echo sequence, the images can be developed in time with the passing of the tracer through the arteries. However, image acquisition using contrast requires specific temporal precision, else arterial signal is obscured by the venous washout. Additionally, recent safety concerns have been announced over the use of a gadolinium tracer in patients with kidney disease. If the estimated glomerular filtration rate (eGFR) is <30 ml/min, this may cause renal toxicity, thus CE-MRA is contraindicated for patients with impaired renal function. Moreover, whilst CE-MRA may be more accurate in visualising blood vessels than 2D TOF, it does not offer an advantage over non-contrast imaging in categorising stenotic patients eligible for surgical intervention[85].

Digital subtraction angiography is considered a gold-standard technique in vascular imaging. Based around fluoroscopy, DSA involves a catheterisation to deliver an iodine contrast agent, followed by a series of X-rays to evaluate contrast flow through the arterial tree. DSA resolution is higher than that of MRA or CTA techniques; terminating branches distal to the catheter are viewed with much more accuracy and contrast than TOF. The rate of contrast flow through the arteries may be indicative of haemodynamic compromise, impairing transport through the imaged volume. Image assessment using DSA is mostly qualitative, unlike other modalities. Despite the superior visualisation of smaller arteries, DSA image acquisition is challenging. 2D DSA may be prone to overlap of vessels within the X-ray plane and tortuous vessels outside the plane, causing image artefact that impedes visualisation. Furthermore, 3D imaging is required to assess wall shear stress, an important marker in vascular health. Both 3D DSA and 4D (3D plus time series analysis) have been developed to overcome some of these issues[85].

2.4 Uric Acid, Stroke, and Carotid Artery Disease

The waste product uric acid (UA) is synthesised in many locations throughout the body, including the liver and vascular endothelia. Uric acid is produced resulting from

purine catabolism i.e., the breakdown of adenine triphosphate (ATP) (Figure 2.16), but also from the degradation of DNA in cell death[98,99]. Xanthine oxidase (XO) in an enzyme that metabolises hypoxanthine to xanthine, and xanthine to uric acid in the purine catabolism pathway (Figure 2.16).

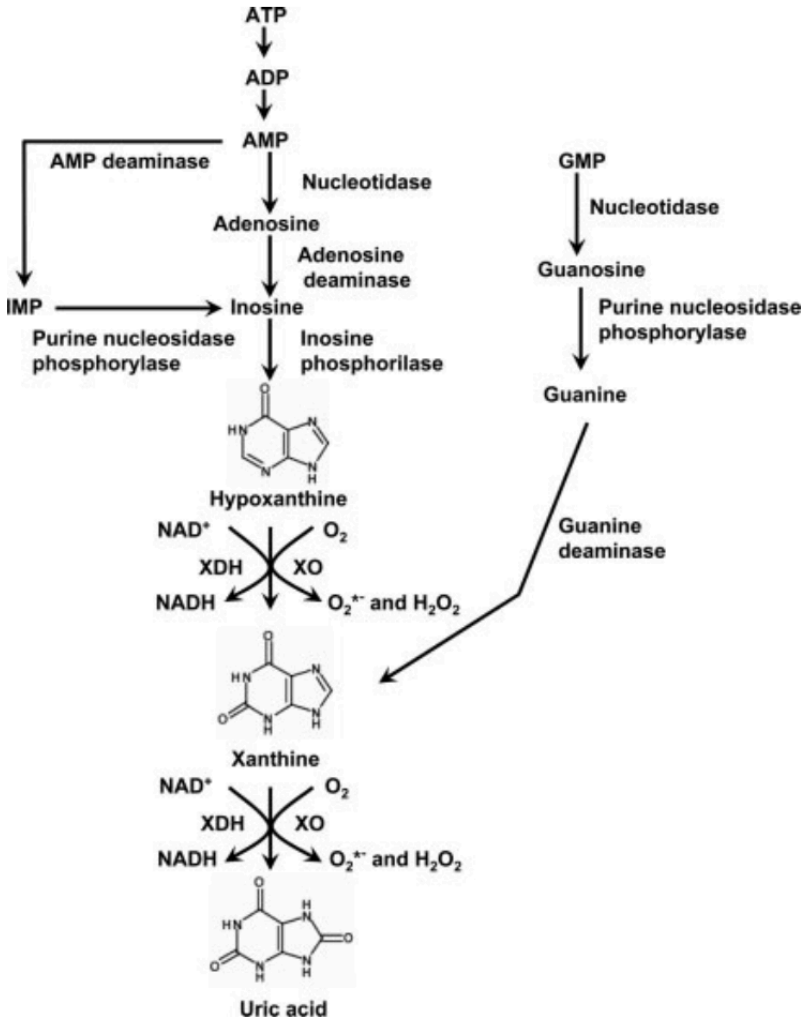

Figure 2.16: Schematic representation of the metabolic pathway for the creation of uric acid. The enzyme xanthine oxidase promotes the creation of xanthine from hypoxanthine, and uric acid from xanthine. Allopurinol, a xanthine oxidase (XO) inhibitor, decreases the creation of uric acid[99].

Elevated uric acid has been studied in ischaemic stroke patients. It has been found to associate with risk of first and recurrent stroke[100] poorer outcomes following stroke[101], and vascular cognitive impairment[102].

It is possible that higher concentrations of serum uric acid may be indicative of increased activity of xanthine oxidase and oxidative stress. Xanthine oxidase activity generates superoxide anions ($O_2^{*\cdot}$) and reactive oxygen species (ROS) like H_2O_2[99,103]. This enzymatic activity is a principal source of ROS within the vasculature. Superoxide anions can inactivate nitric oxide (NO), impeding vasorelaxation, promoting platelet aggregation and oxidising DNA and lipids, which all stimulate the development of atherosclerotic disease[103]. Furthermore, the production of ROS has been shown to increase following cerebral ischaemia and may reflect the extent of tissue damage. Oxidative stress is associated with increased lesion volume in stroke patients and worse neurological deficit[103].

Many meta-analytical studies have summarised links between either uric acid and ischaemia or allopurinol intervention and ischaemia. Hyperuricaemia, or elevated serum uric acid, is commonly seen in conditions including gout, but is considered a potential risk factor for ischaemic stroke[99,104]. In a meta-analysis, over 238,000 adults were assessed for relationships between uric acid and risk of stroke/stroke mortality. Hyperuricaemia was associated with both risk of stroke (RR 1.41, 95% CI 1.05-1.76) and stroke mortality (RR 1.36, 95% CI 1.03-1.69)[105]. Whilst hyperuricaemia in cardiovascular disease may reflect other risk factors such as hypertensive status, or diabetes[103], further analysis after standard adjustments for common risk factors (age, hypertension, diabetes, and high cholesterol) still demonstrated increased risk of incidence (RR 1.47, 95% CI 1.19-1.76) and mortality (RR 1.26, 95% CI 1.12-1.39)[105]. Additionally, analysis by Dawson et al. found elevated serum UA levels were independently associated with poorer outcomes following stroke (OR 1.57, 95% CI 1.02-2.42) in univariate analysis, though this association was missing in multivariate analysis[101].

However, xanthine oxidase inhibitors, which reduce the production of uric acid, have been shown to not significantly alter major adverse cardiovascular events (n = 10,684 patients, OR_P = 0.71, 95% CI 0.46-1.09) or death (n = 11,861 patients, OR_P 0.89, 95% CI 0.59-1.33) in a different meta-analysis[106]. It is important to note that these major adverse cardiovascular events contain “cardiovascular death, non-fatal myocardial infarction, unstable angina… or non-fatal stroke”, thus a heterogenous model of cardiovascular events

may override any effects seen in specific diseases. Upon further investigation of subgroups of these patients, a reduced risk of cardiovascular events was seen in individuals who presented with acute ischaemic stroke (OR_P 0.42, 95% CI 0.23-0.76, P = 0.004), which may suggest a benefit in inhibition of xanthine oxidase for secondary stroke prevention[106]. A comparison of the use of purine-like (allopurinol and oxypurinol) and non-purine like (febuxostat and topiroxostat) inhibitors found differing protective effects. Non-purine like inhibitors found no cardiovascular protective effects, but reductions in risk of cardiovascular events were seen in the analysis of purine-like interventions e.g., allopurinol and oxypurinol (OR_P 0.61, 95% CI 0.38-0.98, P = 0.042)[106].

In hyperuricaemic patients, a meta-analysis of cardiovascular morbidity found a reduced risk of morbidity (RR 0.65, 95% CI 0.46-0.91, P = 0.012) and reduced risk of heart attack (RR 0.47, 95% CI 0.27-0.80, P = 0.01) in treatment groups with allopurinol in comparison with controls. However, this analysis found that there was no significant effect of allopurinol intervention on risk of stroke. Cardiovascular benefits were only observed with sustained allopurinol dosing i.e., treatment >6 months, when administration was at a high enough level e.g., >300 mg/day, or when a reduction of <0.36 mmol/l of serum uric acid was noted[107]. This analysis differs to Bredemeier et al., which may be explained by the difference in population studied. Bredemeier et al. included patients with normal uric acid levels; reductions of normal uric acid levels due to allopurinol may demonstrate different effects to hyperuricaemic patients who have had strokes. These hyperuricaemic patients may never reach the protective levels found in Bredemeier et al. Moreover, very low urate concentrations may be indicative of vascular injury[106,107]. Combined, these data suggest that there is a medium range of serum uric acid that may contribute to protective antioxidant mechanisms in ischaemic stroke.

Since allopurinol inhibits xanthine oxidase activity, it can be described as having antioxidant effects. Oxidative stress and endothelial dysfunction in arteries are conditions that may be seen in patients with common cardiovascular risk factors such as heart failure, kidney disease and type 2 diabetes. A meta-analysis of allopurinol on endothelial activity found that allopurinol treatment exhibits statistically significant benefits to endothelial function in both heart failure (Hedges' g = 0.776, 95% CI 0.43-1.12, P <0.001) and chronic kidney disease groups (Hedge's g = 0.35, 95% CI 0.01-0.69, P = 0.04) but not in the type 2

diabetes group (Hedges' g = 1.33, 95% CI -0.78-3.44, P = 0.22). Only 12 studies were included in this analysis, totalling 550 participants, therefore links between endothelial function and these risk factors needs further investigation[108].

In an ApoE$^{-/-}$ mouse model, XO expression has been found to increase in macrophages in atherosclerotic plaques. XO activity was found to significantly increase in the serum of ApoE$^{-/-}$ mice treated with vehicle (mean$\pm$SEM 87.4$\pm$1.9 mU/mL) than with a XO inhibitor (mean$\pm$SEM 54.9$\pm$3.9 mU/mL, p< 0.0001). Furthermore, this activity was mirrored within aortic and hepatic atherosclerotic plaques[109].

The role of xanthine oxidase in carotid artery disease has been compared between symptomatic stroke patients and asymptomatic patients receiving carotid endarterectomy. Using immunohistochemical staining, the protein expression of xanthine oxidase and a macrophage marker (CD68) from carotid plaques was compared. The atherosclerotic plaques in the symptomatic cohort exhibited significantly higher XO expression in comparison to the asymptomatic group (median [interquartile range]: 1.24 [2.09] vs 0.16 [0.34], p<0.001). Furthermore, these participants displayed significantly higher serum uric acid levels (symptomatic mean (SD) 7.36(2.10) mg/dL; asymptomatic mean (SD) 5.37(1.79) mg/dL). The XO expression was directly associated with serum uric acid (p<0.001, r = 0.45). The proportion of macrophages expressing XO was greater in symptomatic plaques (median 93.37, IQR 21) compared with asymptomatic plaques (median 46.15, IQR 21, p<0.001)[110]. In a different study by Nardi et al., a similar relationship was identified with uric acid levels in carotid plaques. Following carotid endarterectomy, plaques from symptomatic and asymptomatic were immunohistochemically stained. UA was more frequently identified in symptomatic versus asymptomatic carotid plaques using Gomori methenamine silver staining (86.9% versus 22.2% respectively, p = 0.001) and immunohistochemistry (69.5% vs 11.1% respectively, p = 0.004). Additionally, the concentration of uric acid was higher in the symptomatic plaques (25.1 μg/g) than the asymptomatic plaques (17.9 μg/g, p = 0.021)[111].

Contrary evidence suggests that uric acid may have antioxidant activity and these increases in uric acid after stroke may be a neuroprotective mechanism. Previously, data

has been published that determined serum uric acid as an independent predictor of a favourable outcome at hospital discharge. In these 881 patients, serum uric acid was increased in admission in patients that had a good outcome, and increasing the levels of this uric acid was associated with favourable outcome as well (OR 1.12, 95% CI 1.00-1.25)[112].

2.5 Summary

Stroke is a major health burden across the globe. The paired carotid arteries are vital in providing the brain with oxygenated blood for normal functioning. However, these arteries are prone to atherosclerotic disease e.g., stenosis, that impairs blood flow leading to ischaemic stroke. Serum uric acid is elevated in ischaemic stroke and contributes to oxidative stress. Through xanthine oxidase inhibition, allopurinol reduces serum uric acid and oxidative stress This mechanism may reduce risk of recurrent stroke or carotid artery disease.

This programme of research aimed to delineate the relationships between carotid artery disease, brain structure and post-stroke cognition. Chapter 3 will describe a systematic review on carotid artery disease, brain structure and cognitive function in ischaemic stroke patients. Chapter 4 will illustrate the methods used in this work, including angiographic image analysis and validation of these techniques. Chapter 5 aims to clarify associations between carotid artery disease and common vascular risk factors. Chapter 6 will assess associations between carotid artery disease, brain structure and cognitive function in baseline data. Chapter 7 investigates the possible treatment effects of 2-year allopurinol treatment on carotid artery disease and brain structure in ischaemic stroke patients. Chapter 8 seeks to describe a structural equation modelling framework for carotid-brain interactions. Chapter 9 summarises these data and provides insight into future directions of the research.

3 A systematic review of carotid artery disease, brain imaging findings and cognitive function in ischaemic stroke patients

3.1 Introduction

Carotid artery disease is a major cause of first[113] and recurrent[114] ischaemic stroke. Carotid artery stenosis (CAS) has been attributed to more than 60% of extracranial large vessel strokes[113]. Stenosis and other features such as plaque characteristics may be related to risk of dementia and cerebral small vessel disease (SVD) findings such as white matter hyperintensities (WMH).

In asymptomatic subjects, the presence of CAS has been associated with grey matter atrophy in the middle temporal gyrus, and the superior, medial and middle frontal gyri and with more diffuse white matter atrophy[115]. Carotid plaque characteristics such as calcification, ulceration and fibrous components have been associated with the extent of WMH[116–118]. However, these relationships may be explained by a co-mediating factor such as age or hypertension[119].

Large population-based studies have investigated links between CAS and cognition in cohorts of people without stroke[120,121]. Higher grades of stenosis were associated with poorer memory performance in healthy individuals in one study[121], but not the other[120]. Studies using standardised tests of cognition (such as Mini-Mental State Examination (MMSE) and Montreal Cognitive Assessment (MoCA)) have demonstrated an association between degree of CAS and worse cognitive function[122] but not between vessel tortuosity and cognitive function[123].

3.2 Aims and Objectives

This chapter aims to systematically review the relationships between measures of carotid artery disease, brain imaging findings and cognitive function in people with ischaemic stroke. The objectives of this analysis are:

1. Identify studies that investigate carotid artery disease, brain structure and post-stroke cognition in ischaemic stroke participants.
2. Evaluate and summarise studies that describe the relationships between carotid artery disease, brain structure and cognition in ischaemic stroke participants.
3. If sufficient data is available, perform a meta-analysis of included data.

3.3 Methods

3.3.1 Data sources

I followed the "Preferred Reporting Items for Systematic reviews and Meta-Analyses (PRSIMA)" guidelines[124]. The review was registered with PROSPERO (CRD42019121845). From October 2018 – June 2019, I systematically searched MEDLINE, Embase and Cochrane databases. Additional publications not found in these searches were identified from hand searching of reference lists. Search terms for this review include derivatives of "ischaemic stroke", "carotid artery stenosis", "brain", "medical imaging" and "cognition". Keywords were adapted to best fit each database. The search strategy is found below (Table 3.1).

Table 3.1 Search strategy for the systematic review in MEDLINE database.

1	Ischaemic stroke OR ischaemic event OR ischaemic attack OR ischaemic accident OR ischaemic injury
2	Ischemic stroke OR ischemic event OR ischemic attack OR ischemic accident OR ischemic injury
3	Brain infarction OR cerebral infarction OR hypoxia-ischemia
4	Cerebrovascular disease OR CVD OR CVA
5	1 OR 2 OR 3 OR 4
6	Brain OR cerebrum OR cerebral matter OR brain tissue
7	5 AND 6
8	Carotid artery AND (disease OR stenosis OR narrowing OR thinning OR plaque OR occlusion OR obstruction)

9	Carotid bulb OR internal carotid artery OR external carotid artery OR common carotid artery
10	8 OR 9
11	7 AND 10
12	Magnetic resonance imaging OR MR imaging OR MRI
13	Cognition OR cognitive OR neuropsychology OR neuropsychological
14	12 OR 13
15	11 AND 14
FULL STRATEGY: 5 AND 6 AND 7 AND 10 AND 11 AND 14 AND 15	

3.3.2 Inclusion criteria

Studies were included if they enrolled an adult (aged >18 years) human population. Studies were considered eligible if they investigated: 1) a measure of carotid artery disease alongside either 2) a structural brain imaging measure (either using Magnetic Resonance Imaging (MRI) or Computed Tomography (CT) and/or 3) a measure of cognitive function in people with a history of ischaemic stroke. I did not include studies of healthy people or those with haemorrhagic stroke. There were no restrictions on the carotid imaging sequence or method used. There were no publication date restrictions. Publications were excluded if they did not contain any original research, though studies contributing to reviews were included if not found in our systematic search.

3.3.3 Study identification and selection

After completion of the search, titles and abstracts were reviewed to identify potentially eligible studies. These studies were then subject to full-text screening to allow a final decision.

3.3.4 Data extraction

A form was created for data extraction, performed by FNS. From the publications selected for review, data was sought on: 1) carotid imaging modality and sequences, 2) number of participants and clinical/demographic data, 3) carotid artery measurements, 4) brain imaging measurements and 5) cognitive tests performed. I extracted all relevant data as reported in the eligible manuscripts.

3.3.5 Quality assessment

I recorded whether eligible studies reported participant exclusion criteria and assessment blinding.

3.3.6 Data synthesis

Following data extraction, data were synthesised and summarised according to study characteristics, imaging methods used and cognitive assessments. I tabulated the prevalence of reported vascular risk factors and the completeness of their reporting. I recorded strengths and directions of associations between carotid artery measures, brain imaging findings, and cognition with test statistics, p-values and descriptive statistics, where available. The direction of associations was described as "positive", "neutral" or "negative". Studies that included adjustments for age, gender or other variables were noted in tables of results where applicable.

3.4 Results

I found 3656 articles, of which 48 were included[125–172] (Figure 3.1). Many studies used more than one method of imaging. Fifty-five percent of studies used MRI to evaluate the carotid arteries, ultrasound (35%), digital subtraction angiography (DSA) (31%), and CT (22%) were also used. MRI sequences used in brain imaging included diffusion weighted imaging (DWI) (61%), T2 (59%) and T1 (45%). Participant exclusions were

reported in 63% (Table 3.2). An adapted Newcastle-Ottawa scale for assessing quality of non-randomised studies is shown in Table 3.3. This reporting scale assesses the quality of the participant selection, comparability, and outcome assessments[173,174]. In this review, due to the nature of the included studies, there were no comparisons with control populations i.e., non-stroke populations were excluded.

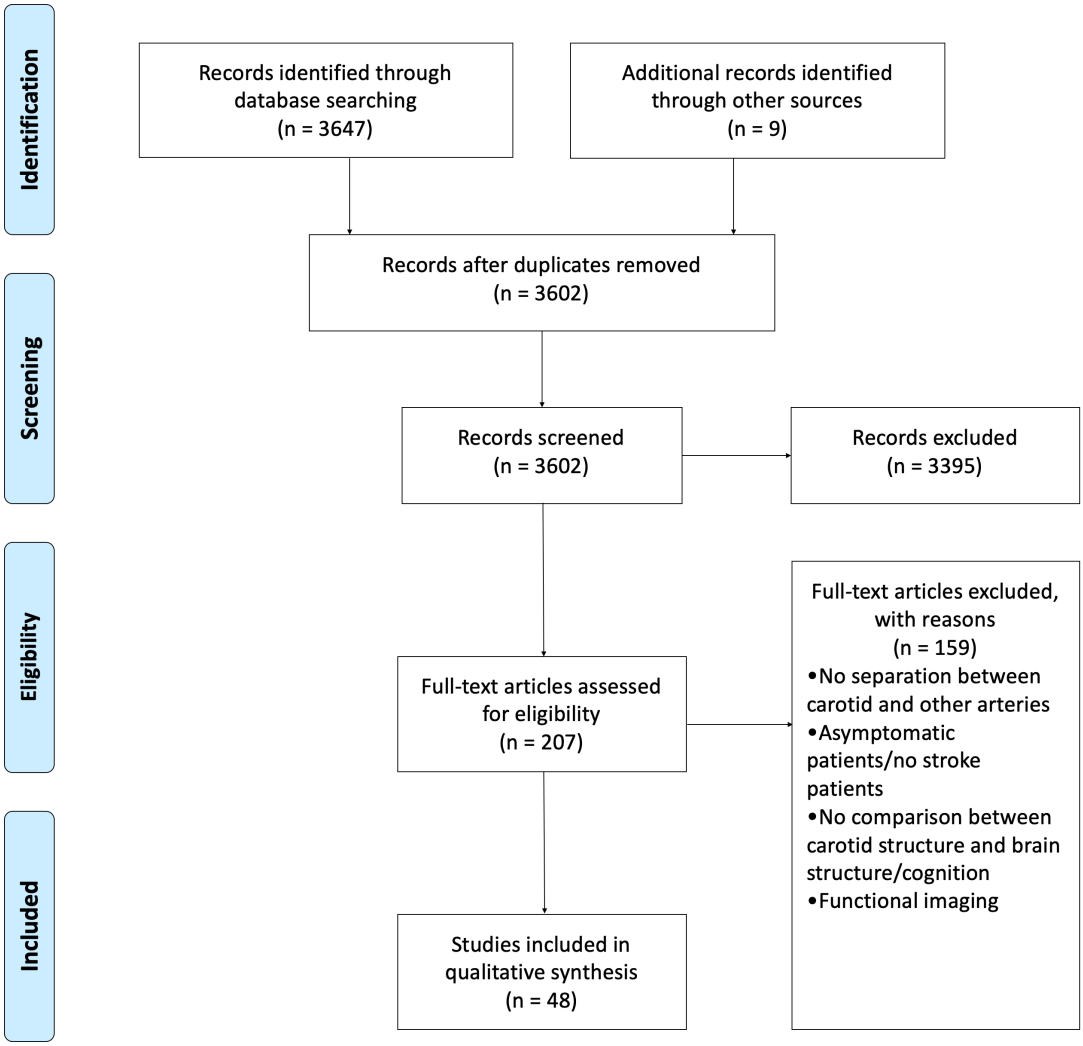

Figure 3.1: The PRISMA flow-diagram for the systematic review, which demonstrates the implementation of the search strategy to find relevant manuscripts. 48 manuscripts were included in the qualitative synthesis.

Table 3.2: The image modalities utilised within the included studies, as well as reporting of patient exclusions. CEMRA = contrast enhanced magnetic resonance angiography, CT = computed tomography, DSA = digital subtraction angiography, DWI = diffusion weighted imaging, FLAIR = fluid attenuated inversion recovery, MRI = magnetic resonance angiography, PCMRA = phase contrast magnetic resonance angiography, PD = proton density, PET = positron emission tomography, PWI = perfusion weighted imaging, SWI = susceptibility weighted imaging, TCD = transcranial doppler ultrasound, TOF = time of flight, US = ultrasound "." Denotes missing data.

	Carotid Image Modality	Field Strength (T)	Brain Image Modality	Exclusion
1	TOF	1.5	T2, FLAIR, DWI, PWI	Yes
2	US, TOF, T1, T2, PD	3	T2, FLAIR, DWI	Not reported
3	TOF, CEMRA	1.5	T2, FLAIR, DWI, PWI	Yes
4	DSA	1.5	T1, T2, PD	Not reported
5	DSA	1.5	T1, T2, PD	Yes
6	DSA	1.5	T1, T2	Not reported
7	US, CT, MRI	3	T1, T2, FLAIR, DWI	Yes
8	CT	1.5	T1, T2, FLAIR, DWI	Yes
9	MRI	7	T1, T2, FLAIR	Yes
10	TOF	1.5	T2, PWI, CT	Yes
11	TOF	1.5	T2, PWI, CT	Yes
12	US, MRI	1.5	DWI	No
13	TOF	1.5	T2	No
14	TOF	1.5	T2, DWI, PWI	Yes
15	US, CT, MRI, DSA	1.5	DWI	Not reported

16	TOF, T1, T2, PD	1.5	DWI	Yes
17	US, CT, MRI	.	T1, FLAIR, DWI	Yes
18	US	N/A	CT	Yes
19	DSA	1.5	T1, T2, DWI	Yes
20	US, CT	3	DWI, PWI, CT, PET	Not reported
21	CEMRA	.	DWI	Yes
22	T1	1.5 OR 3	DWI	Not reported
23	US, TOF	1.5	T1, T2, PD, DWI	Not reported
24	US, CT, MRI	1.5 OR 3	T1, T2, FLAIR, DWI, SWI	Yes
25	TOF	1.5	DWI	Not reported
26	DSA	.	DWI	Yes
27	US, TOF, CEMRA	1.5 OR 3	T1, T2, FLAIR	Not reported
28	US, CT, MRI, DSA	.	T1, T2, FLAIR, DWI	Not reported
29	US	.	MRI, CT	Yes
30	US	N/A	TCD	Yes
31	PCMRA	1.5	T1, T2, DWI, PWI	Yes
32	MRI	3	T1, FLAIR, DTI	Yes
33	US, DSA	N/A	CT	Yes
34	TOF, PCMRA	1.5	T1, T2, FLAIR, DWI, PWI	Yes
35	DSA	N/A	CT	Not reported
36	US	1.5	DWI, PWI, "conventional imaging"	Yes

37	CT, CEMRA, DSA	3	T2, FLAIR, DWI	Yes
38	CT, CEMRA, DSA	1.5	T1, T2, FLAIR, PD, DWI	Yes
39	CT, MRI, DSA	1.5	T1, T2, FLAIR, DWI	Yes
40	DSA	.	MRI, CT	Yes
41	DSA	N.A	CT	Not reported
42	US, MRI, DSA	1.5	T1, T2, DWI, PWI	Yes
43	CT	3	T1, T2, FLAIR, DWI, SWI	Not reported
44	PCMRA	1.5	T1, T2, DWI, PWI	Yes
45	US, MRI	1.5	T1, T2, FLAIR, DWI	Not reported
46	DSA	1.5	T1, T2, FLAIR	Yes
47	US	1.5	T1, T2, FLAIR, DWI	Not reported
48	MRI	1.5	T2, DWI	Not reported

Table 3.3: Newcastle-Ottawa Scale assessment of study quality. A star is given to each question; the total is given in the rating column as a product of the study quality.

	Q1 Are the cases adequately defined?	Q2 Are the cases representative of the population?	Q3 Are the cases compared with controls?	Q4 Are the results controlled for age?	Q5 Are the results controlled for other factors?	Q6 Is there a report of blinded assessment?	Q7 Are the statistics appropriate?	Rating
1	*	*				*	*	****
2	*	*				*	*	****
3	*	*					*	***
4	*	*				*	*	****
5	*	*					*	***
6	*	*					*	***
7	*	*		*	*	*	*	******
8	*	*		*	*		*	*****
9	*	*					*	***
10	*	*				*	*	****
11	*	*			*	*	*	*****
12	*	*					*	***
13	*	*					*	***
14	*	*				*	*	****
15	*	*					*	***
16	*	*		*	*	*	*	******
17	*	*				*	*	****
18	*	*				*	*	****
19	*	*					*	***

20	*	*				*	*	****
21	*	*				*	*	****
22	*	*					*	***
23	*	*				*	*	****
24	*	*	*	*			*	*****
25	*	*				*	*	****
26	*	*	*	*		*	*	******
27	*	*				*	*	****
28	*	*				*	*	****
29	*	*	*	*		*	*	******
30	*	*				*	*	****
31	*	*					*	***
32	*	*	*			*	*	*****
33	*	*				*	*	****
34	*	*				*	*	****
35	*	*					*	***
36	*	*					*	***
37	*	*					*	***
38	*	*				*	*	****
39	*	*				*	*	****
40	*	*	*	*		*	*	******
41	*	*				*	*	****
42	*	*					*	***
43	*	*	*	*		*	*	******
44	*	*					*	***
45	*	*	*	*		*	*	******

46	*	*	*	*	*	*	******
47	*	*	*	*		*	*****
48	*	*	*	*	*	*	******

There were 8758 participants across the 48 included studies (median n = 69; mean n = 182; range n = 19-2618), with a mean age of 66.7 years. Of these, 65% (n = 5656) were male and 35% (n = 2985) female; one study[159] did not report sex. Vascular risk factors included hypertension (67%), diabetes (27%), and smoking (49%) (Table 3.4). 19 studies (40%) did not report any risk factors.

Table 3.4: Vascular risk factors from included studies. The total n is the reviewed population per risk factor; reported n is the number of participants with recorded risk factor; weighted % is the recorded VRF/ population. The magnitude of reporting is the number of participants reported to have a VRF/total n (n = 8758).

Vascular Risk Factor	Total N per VRF	Number of Participants Reported	Weighted %	Magnitude (%)
Hypertension	8061	5375	67	61
Diabetes	8061	2138	37	24
Smoking	7961	3940	49	45
Hyperlipidaemia	6006	2470	41	28
Hypercholesterolaemia	1049	393	37	4
Coronary artery disease	2923	383	13	4
Peripheral artery disease	358	52	15	0.6
Atrial fibrillation	1465	257	18	3
Alcohol consumption	466	156	33	2

Standardised scales were used to quantify CAS in 18/48 (38%) studies[125,129,131–133,135,137,139,142,144,154,155,157,158,162,165,166,175]. The North American Symptomatic Carotid Endarterectomy Trial (NASCET) criteria was reported in 15/48 (31%) studies; European Carotid Surgery Trial (ECST) criteria was reported in 3/48 (6%) studies[132,133,165]; US Consensus criteria[131] and Thrombolysis in Myocardial Infarction (TIMI) criteria[142] were each reported once. An additional 2/48 (4%) studies described carotid plaque features[161,169]. The remaining 30 studies (62%) did not report the scale used for measuring stenosis[126–128,130,134,136,138,140,141,143,145–153,159–161,163,164,167–172].

Brain imaging findings were reported in 44/48 (92%) studies[125–135,138–144,146–148,150–155,157–172,175] and included stroke lesion volume, infarct location, and measures of SVD. Infarct location was described in 26/48 (54%) studies[125,128,129,132,133,135,138,140,141,146,150,152,157,159,160,162–168,170,172,176]; stroke lesion volume was reported in 12/48 (25%) studies[126,127,130,134,142,147,148,151,153,167,168,171]; SVD burden was described in 8/48 (17%) studies[141,144,154–156,161,169,176]. Cognition was reported in 4/48 (8%) studies[136,137,145,149]. No study investigated carotid stenosis, brain imaging and cognition together. Figure 3.2 shows the data describing the relationship of brain imaging or cognitive findings with carotid arteries and the directions of their associations.

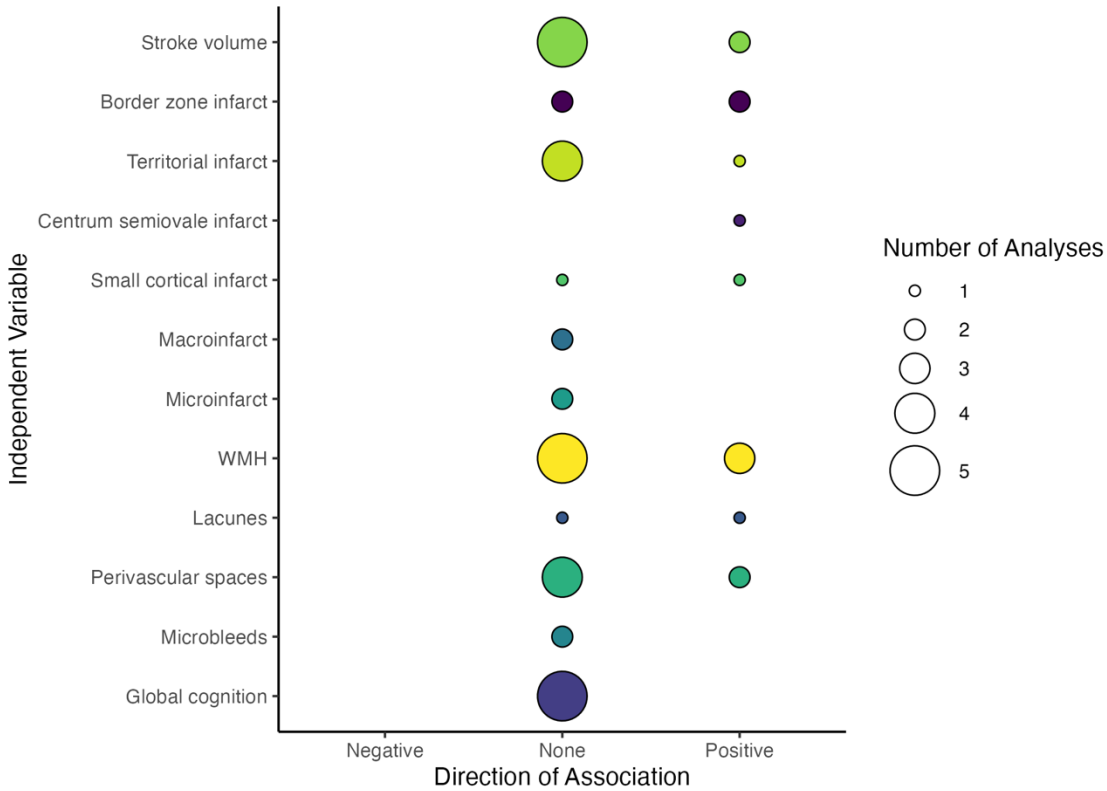

Figure 3.2: The direction of associations between carotid arteries and either brain imaging or cognitive testing. The radius of the bubbles describes the number of analyses extracted for each independent variable. Colours are used to clearly delineate between each independent variable.

3.4.1 Associations between carotid artery disease and brain imaging findings

Of the 26 studies that assessed infarct location, 10 (38%) assessed the relationship between carotid artery disease and infarct location[131,132,134,135,150,159,165,166,170,172]. Border zone infarction, centrum semiovale infarction and small cortical infarcts were typically associated with higher grades of CAS. There was a less clear relationship between CAS and territorial infarcts, macroinfarcts and microinfarcts (Table 3.5).

Table 3.5: Associations between carotid artery disease and lesion pattern. *macroinfarcts are classed as >3mm in cortical length, microinfarcts are classed as <3mm in cortical length. †adjusted for age, sex and % stenosis. ‡infarct patterns addressed are cortical, subcortical, lacunar, paraventricular and watershed (territorial). §adjustments unknown. | |adjusted for age, gender, diabetes, hypertension, hypercholesterolemia, smoking status, cardiac sources, and coagulopathy. ICA = internal carotid artery.

N	Description	Test	Value
117	Increase in internal border zone infarcts ipsilateral to ICA occlusion	Paired T-test	P=0.002
21	Correlation between stenosis grade and number of ipsilateral macroinfarcts*	Kendalls tau correlation test	τ=-0.18; P=0.29
	Correlation between stenosis grade and number of contralateral macroinfarcts*		τ=-0.19; P=0.33
	Correlation between stenosis grade and number of ipsilateral microinfarcts*		τ=-0.03; P=0.88
	Correlation between stenosis grade and number of contralateral microinfarcts*		τ=0.26; P=0.20
11	Comparison of territorial vs border zone infarcts between bilateral severe stenosis and occlusion	Fisher's exact test	P=0.856
65	Univariate analysis between IPH and border zone infarcts †	Fisher's exact test	P=0.20
142	Comparison between infarction pattern and degree of stenosis (0-49% vs 50-99%)	Fisher's exact	P>0.85
	Comparison between infarction pattern and degree of stenosis (0-49% vs occlusion)		P=0.036
	Comparison between infarction pattern and degree of stenosis (50-99% vs occlusion)‡		P=0.055
35	Comparison between territorial and border zone infarcts and degree of stenosis	Fisher's exact	P=0.80
38	Comparison between infarct type (pial and border zone) and ICA disease	Fisher's exact	P<0.001
40	Regression of ICA stenosis and centrum semiovale infarct pattern§	Fisher's exact	P=0.001
31	Comparison between small cortical infarct presence and degree of stenosis	Mann-Whitney U	P=0.56
	Regression of carotid disease and small cortical infarcts		P=0.002
120	Comparison between site of stenosis and border zone infarct type	χ^2	χ^2< 0.05

Of the 12 studies that assessed infarct volume, 4 (33%) studies investigated the relationship with carotid artery stenosis[142,148,153,168]. A positive association was found between ICA occlusion and internal border zone infarct volume in one study[168]. However, other studies found no relationship[142,148,153] (Table 3.6).

Of the 8 studies that reported a measure of SVD, 5 (63%) reported associations with carotid artery measurements[141,144,154,161,169]. There was a significant relationship between severe CAS and ipsilateral perivascular spaces[154]. A positive association between CAS and WMH was found[141,169]. Separate analyses found no association[141,144,161]. Microbleeds were not associated with carotid structure[141,161]. Lacunes were not found to relate to presence of ICA calcification in one study[161] (Table 3.7).

Table 3.6: Associations between carotid artery disease and infarct volume. DWI = diffusion weighted imaging, ICA = internal carotid artery, CAS = carotid artery stenosis.

N	Description	Test	Test Statistic
20	DWI lesion volume vs occlusion site	Paired T-Test	T= 0.415
68	Internal border zone infarct volume vs ICA occlusion	Kruskal-Wallis	H= 0.024
		Mann-Whitney U	U= 0.005
	External border zone infarct volume vs ICA occlusion	Kruskal-Wallis	H= >0.05
		Mann-Whitney U	U= >0.05
60	Infarct volume/pattern vs ICA occlusion	Chi-square test	χ^2= 0.077
9	Infarct volume vs presence of CAS	Kruskal-Wallis	P>0.05

Table 3.7: Associations between carotid artery disease and small vessel disease (SVD) burden. CAS = carotid artery stenosis, ICA = internal carotid artery, WMH = white matter hyperintensities. *β coefficients were missing in the manuscript.

N	Description	Test	Test Statistic
159	ICA calcification vs presence of periventricular WMH	Fisher's exact	P<0.001
	ICA calcification vs presence of deep WMH		P<0.001
587	ICA pulsatility vs lacunes	Linear regression*	P=0.001
	ICA pulsatility vs subcortical WMH		P=0.34
	ICA pulsatility vs periventricular WMH		P=0.012
	ICA pulsatility vs presence of perivascular spaces		P=0.86
	ICA pulsatility vs perivascular spaces (basal ganglia)		P=0.035
	ICA pulsatility vs perivascular spaces (centrum semiovale)		P=0.095
286	Severe CAS vs periventricular WMH	Chi-square test χ^2	χ^2=0.949
	Severe CAS vs deep WMH		χ^2=0.406
78	Correlation between ipsilateral perivascular space grade and increasing ICA stenosis	Spearman	ρ<0.05
	Correlation between contralateral perivascular space grade and increasing ICA stenosis		ρ >0.05
104	ICA calcification vs perivascular space score of 1	Chi-square χ^2 or Fisher's exact test	P=0.073
	ICA calcification vs perivascular space 2-4		P=0.382
	ICA calcification vs lacunes		P=0.373
	ICA calcification vs microbleeds		P=0.744
	ICA calcification vs WMH		P=0.718

3.4.2 Associations between carotid artery disease and cognition

Different cognitive tests were used in the 4 included studies[136,137,145,149]. The MoCA, MMSE, Alzheimer's Disease Assessment Scale (ADAS), Colour trail tests, category naming task of verbal fluency and Addenbrookes Cognitive Examination (ACE-R) were used (Table 3.8).

No associations between CAS and cognition were described in 2 studies[145,149]. There was no difference in MMSE score between severe and non-severe grades of stenosis[145]. One study[149] divided participants into "normal" and "abnormal" cognitive groups and found no statistically significant difference in stenosis between these groups (Table 3.8). Additional data were found in conference proceedings. These data were not included in our primary analysis but are found in Table 3.9.

Table 3.8: Associations between carotid artery stenosis (CAS) and cognition. MMSE = Mini-mental state examination, CAS = carotid artery stenosis.

N	Description	Test	Test Statistic
365	MMSE score vs degree of CAS (severe vs non-severe)	Unpaired T-test or Fisher's exact	P<0.1
108	Cognition score vs degree of ipsilateral CAS (>70%)	Fisher's exact	P=0.824
	Cognition score vs degree of ipsilateral CAS (>80%)		P=0.734
	Cognition score vs degree of contralateral CAS (>70%)		P=0.254
	Cognition score vs degree of contralateral CAS (>80%)		P=0.375

Table 3.9: Abstracts that may have investigated links between carotid artery stenosis and cognitive function. MMSE = Mini-mental State Examination, MoCA = Montreal Cognitive Assessment.

Ben Wee et al (2016). Neurology Conference. Vol. 86(16). Intracranial and extracranial stenosis interact with white matter disease in the pathogenesis of post stroke dementia.			
Number of participants	Age of participants	Stenosis %	Cognitive scores
317	61.24 (SD 12.24)	Described as significant	"Concomitant intracranial and extracranial stenosis scored lowest on MMSE… compared to patients without either stenosis."
Lees, R et al. International Journal of Stroke. Vol. 3. Vascular cognitive impairment/vascular dementia the pattern of cognitive impairment in stroke survivors with carotid stenosis.			
Number of participants	Age of participants	Stenosis %	Cognitive scores
33 (20M/13F)	70.4 (range 52-87)	>50%	Cognitive impairment "borderline". Used modified Hachinski 30-minute battery.
Mushba, A et al. Journal of the Neurological Sciences. Vol. 381. Cerebral hemodynamics and cognitive function in patients with atherosclerotic lesions of brachiocephalic arteries.			
Number of participants	Age of participants	Stenosis %	Cognitive scores
30 (19M/11F)	64.5 (SD 1.4)	<50%	MMSE 26.5+/-0.4; MoCA 27.5+/-0.4. No correlation between severity of stenosis and cognitive function.
Mushba, A et al. Journal of the Neurological Sciences. Vol. 1. Cerebral perfusion and cognitive status before and in early period after carotid endarterectomy for symptomatic internal carotid stenosis.			
Number of participants	Age of participants	Stenosis %	Cognitive scores
23 (20M/3F)	61.5 (SD 6.7)	Unknown	MMSE 26.1+/-2.4; MoCA +/- 27+/-2.
Mushba, A et al. European Stroke Journal Vol. 1. Cerebral perfusion and cognitive functions in patients after carotid endarterectomy for symptomatic carotid stenosis.			
Number of participants	Age of participants	Stenosis %	Cognitive scores
30	62.5 (SD 1.3)	Unknown	MMSE 25.1+/-0.5; MoCA 26.3+/-0.4.

Tan, CH et al. (2017). Neurology Conference. Vol. 88(16). Early cognitive decline in symptomatic carotid stenosis is related to plaque inflammation and concomitant intracranial stenosis.			
Number of participants	Age of participants	Stenosis %	Cognitive scores
39	Unknown	>50%	MMSE/MoCA scores unknown

3.5 Discussion

This systematic review formally demonstrates wide variation between studies that measured carotid artery disease, brain imaging measurements and cognition in ischaemic stroke. I found 44/48 studies that explored relationships between carotid atherosclerosis and brain imaging findings, and 4/48 studies investigated carotid stenosis and cognition. No study assessed all three, therefore results reported may not have adequately accounted for confounding between parameters. For example, WMH burden may mediate the association between carotid stenosis and cognition[177]. Due to insufficient data, no meta-analysis could be employed at this time.

NASCET and ECST scales are often used in quantifying CAS[178], though they differ in the valuation of internal CAS[179,180]. NASCET and ECST were the most used scales to assess CAS but most studies I found did not describe any methodology for measuring CAS. Further, NASCET and ECST may provide inconsistent measurements of CAS[179,180]. Carotid artery imaging studies may benefit from consistent, internationally defined standards similar to those developed for brain imaging studies[28].

Inclusion criteria varied between studies, particularly related to grades of stenosis, including people with more severe grades of CAS, limiting our understanding of how milder stenosis grades affect brain structure and cognition. Mild stenosis participants were underrepresented across studies, with some exclusion criteria including less severe gradings. There was limited vascular risk factor reporting in these studies; 40% did not report any vascular risk factors, and no study reported all stroke-relevant risk factors, as described in the INTERSTROKE study[181].

This review demonstrates the variability in associations between brain and carotid imaging findings. Regression statistics were employed in some studies and found that ICA stenosis was significantly related to either border zone infarcts or small cortical infarcts. However, this association was not seen in all studies. One study found a positive relationship was between internal border zone infarct volume and ICA occlusion, though

no such relationship with total stroke volume. Perivascular spaces, WMH and lacunes were significantly related to ICA calcification or severe stenosis. The relationship between calcification and SVD burden (perivascular space, lacunes, WMH or microbleeds) was no longer significant following adjustments in regression analysis. Hypertension in particular may override any relationship between CAS and SVD[119]. More research with rigorous adjustment for potential confounders is needed. I found no relationship between carotid artery measures and cognition but there was a limited number of studies. A relationship has been seen in some larger population-based studies.

The strengths of our review include the use of a systematic search strategy and the established PRIMSA review and reporting guidelines. The inclusion of any image modality for assessing carotid arteries in ischaemic stroke is another strength. I only included data from trials with novel interventions if pre-treatment data was available. I only included studies in people with stroke as I was interested in exploring whether carotid artery stenosis independently impacts cognition and features of SVD separate to the disease. Only data described in the manuscripts were included. Additional information from manuscript authors may have led to more detailed conclusions. I did not contact authors for more information. While I adopted a systematic strategy with extensive hand searching, it may be possible that I missed relevant publications not indexed in the repositories I searched.

3.6 Summary

This chapter presented a systematic review of medical imaging studies investigating relationships with carotid artery disease, brain structure and cognition in people with ischaemic stroke. I found substantial heterogeneity in reporting of carotid artery disease, brain imaging findings and cognitive function. This heterogeneity may have contributed to us finding no clear association between these measures. Further well-designed larger studies with standardised approaches to reporting of imaging measures are required to evaluate these associations. Chapter 4 will describe the image analysis methods employed in this thesis.

4 Methodology of the XILO-FIST trial and Image Analysis Validation

4.1 Introduction

This thesis uses data from the clinical trial "Xanthine oxidase inhibition for the improvement of long-term outcomes following ischaemic stroke and transient ischaemic attack (XILO-FIST)". This trial investigates the effect of allopurinol treatment on the progression of white matter hyperintensities and effect on blood pressure after stroke[182].

4.2 XILO-FIST study protocol

4.2.1 Ethical and regulatory approval

Ethical and regulatory approval was obtained for all sites participating within the XILO-FIST trial (REC number 14/WS/0113). The study was carried out in accordance with the World Medical Association Declaration of Helsinki (1964) and their amendments – Tokyo (1975), Venice (1983), Hong Kong (1989), South Africa (1996) and Edinburgh (2000). Trial participants were informed that they are free to withdraw consent from the study and treatment at any time. Participants were given information that described the nature of the study, and any side-effects/risks of participation. Trial participants gave written informed consent.

4.2.2 Participant population

The study population involved participants that are aged 50 years and over with an ischaemic stroke or transient ischaemic attack (TIA). The inclusion and exclusion criteria are described below (Table 4.1). Ischaemic stroke is diagnosed by a stroke specialist, defined as a focal neurological event lasting more than 24 hours. Symptoms of a TIA must last <24 hours, and a relevant lesion on diffusion weighted imaging or computed tomography must be found.

Table 4.1: the full inclusion and exclusion criteria for participants within the carotid sub-study of the XILO-FIST clinical trial. Significant hepatic impairment was classified as serum bilirubin, aspartate aminotransferase or alanine aminotransferase 3 times greater than the upper normal limit. IQCODE = Informant Questionnaire for Cognitive Decline in the Elderly, eGFR = estimated Glomerular Filtration Rate.

Inclusion Criteria
Age ≥ 50 years old
Ischaemic stroke / TIA with positive lesion on brain imaging
Carotid and brain MRI
Cognitive testing
Consent within 1 month of stroke onset
Exclusion Criteria
Modified Rankin scale score = 5
Dementia diagnosis, defined as a documented diagnosis or screening IQCODE score ≥ 3.6
Cognitive impairment deemed insufficient to give consent or comply with the protocol
Dependence on help for activities of daily living prior to ischaemic stroke
Co-morbidity or frailty likely to cause death within 24 months or make adherence to protocol challenging for participant
Contraindication to the administration of allopurinol or placebo ingredients
Concurrent azathioprine, 6-mercaptopurine therapy, cyclosporin, theophylline, didanosine or other cytotoxic therapy
Significant hepatic impairment
eGFR <30ml/min
Contraindication to MRI scanning
Women of childbearing potential
Prisoners
Active participation in another clinical trial within the past month
Korean, Han Chinese or Thai descent unless negative HLA-B*5801 status known

4.2.3 Visit schedule/treatment phase

The participants received oral allopurinol (300mg) or placebo twice daily for 104 weeks; a single daily dose of 300mg allopurinol/placebo was taken during the first 4 weeks. Then, participants underwent dose titration to twice daily treatment unless their eGFR was <60 ml/min. Dose reduction occurred in the event of side effects, and stopped if eGFR reached <30 ml/min. After 104 weeks, treatment stopped. Participants received MRI scanning and evaluation of cognitive function at weeks 4 and 104. A full participant schedule for the XILO-FIST trial can be found in Table 4.2. Stroke severity was assessed by the Modified Rankin Scale (mRS) and the National Institutes of Health Stroke Scale (NIHSS). These were performed during the run-in phase (Day 0).

Table 4.2: The schedule for XILO-FIST clinical trial. Participants are assessed for eligibility before brain and carotid MRI are performed. ECG = electrocardiogram, MRI = magnetic resonance imaging, ABPM = ambulatory blood pressure measurement, IMP = investigational medicinal product.

Activity	Run-in Phase		Treatment Phase						
	Day 0	Week 4	Week 0	Week 4	Week 13	Week 36	Week 52	Week 78	Week 104
Review Eligibility	✓	✓							
Informed Consent	✓								
Optimise Preventative Therapy	✓								
Clinical Evaluation	✓	✓		✓	✓	✓	✓		✓
Safety Blood Tests	✓	✓		✓	✓	✓	✓		✓
Blood for Uric Acid Level		✓							✓
Blood/Urine for Biobanking		✓							✓
ECG		✓							✓
Echocardiography		✓							
Determine Cardiac Sub-Study Eligibility		✓							
Carotid and Brain MRI		✓							✓
ABPM		✓		✓					✓
Cardiac MRI		✓							✓
Detailed Cognitive Function Evaluation		✓							✓
Assessment of run in Completion		✓							
Randomisation			✓						
Dispense			✓	✓	✓	✓	✓	✓	
Return/Count IMP				✓	✓	✓	✓	✓	✓
Adverse Event Review			✓	✓	✓	✓	✓	✓	✓

4.2.4 MRI protocol

MRI was performed at 3T across all included sites of the carotid sub-study. Study brain imaging sequences included T1-, T2-, diffusion (DWI) and susceptibility-weighted (SWI) imaging, fluid attenuation inversion recovery (FLAIR), diffusion tensor imaging (DTI) and arterial spin labelling (ASL). Carotid imaging sequences included time-of-flight angiography (TOF), T1- and T2-weighted imaging, and proton density (PD) imaging. All participants had brain MRI performed but carotid imaging was only performed at selected sites, based on hardware availability. Scanning sites for this study included Queen Elizabeth University Hospital, Glasgow, Ninewells Hospital, Dundee, and Aberdeen Royal Infirmary, Aberdeen. Sequence parameters can be found in Table 4.3.

Carotid and brain imaging were performed as baseline at week 4, and follow-up at week 104 of the treatment phase. The total scan time for carotid and brain imaging was approximately 55 minutes. All participants were scanned on the same scanner between baseline and follow up where possible. TOF imaging was acquired fully 3D with no gaps. T1, T2 and PD were all co-registered with each other during acquisition but remained thick axial slabs (3mm voxel size), with 3mm gaps between each axial slice.

Table 4.3: Sequence parameters for the brain and carotid MRI acquisition. TE = echo time, TR = repetition time, TI = inversion time, FOV = field of view, FLAIR = fluid attenuation inversion recovery, DWI = diffusion weighted imaging, SWI = susceptibility weighted imaging, DRI = diffusion tensor imaging, ASL = arterial spin labelling.

Scan	Sequence	Orientation	TE	TR	TI	Slice Thickness	Slice gap	Matrix	FOV	Slice number	Total time
Brain											
T1	TFL	SAG	1.85	2000	900	1.0	50%	256 × 100	255	176	4.4
T2	SPC	TRA	404	3000	–	0.9	–	256 × 100	230	176	5.32
FLAIR	SPCIR	SAG	397	5000	1800	1.0	–	256 × 100	255	160	4.02
DWI	RESOLVE	TRA	62	4100	–	4	30%	224 × 100	220	27	3.55
SWI	SWI_r	TRA	20	24	–	1.5	20%	256 × 95	230	96	4.45
DTI	EPSE	TRA	95	3600	–	4	30%	128 × 100	230	30	2.51
ASL	EPFID	TRA	11	3500	–	6	16%	64 × 100	255	20	6.06
Carotid											
TOF	FL_r	TRA	3.11	20	–	1.0	–	384 × 75	200	32/3 slabs	2.57
T1	tse	TRA	17	740	–	2.0	50–200%	256 × 100%	140	5 to 11	2.37
T2	tse	TRA	79	740	–	2.0	50–200%	192 × 100%	140	5–11	1.51
PD	tse	TRA	16	740	–	2.0	50–200%	192 × 100%	140	5–11	1.51

4.2.5 Cognitive testing protocol

All participants underwent a battery of neuropsychological tests to assess cognition and mood. These tests were performed as baseline at week 4, and follow-up at week 104 of the treatment phase. The battery of tests is listed in Table 4.4. The tests were performed in a standardised manner according to a neuropsychological workbook issued to each practitioner. The battery was scored to pre-specified marking sheets. If a participant was unable to complete the entire neuropsychological battery, the assessor prioritised the Montreal Cognitive Assessment (MoCA) and the Centre for Epidemiologic Studies – Depression Scale (CES-D).

Table 4.4: The full neuropsychological test battery performed on participants. *Neuropsychiatric Inventory Questionnaire Version (NIP-Q) was assessed only at the follow-up visit.

Neurocognitive Tests	Cognitive Process
Montreal Cognitive Assessment (MoCA)	Global cognition
Animal Naming	Semantic fluency
Controlled Oral Word Association Test (CoWAT)	Verbal fluency
Letter Digit Coding Test	Attention and visual perception
Hopkins Verbal Learning Test (HVLT)	Attention and short-term memory
Hopkins Verbal Learning Test Delay (HVLT Delay)	Attention and short-term memory
Trail Making Test	Visuospatial attention, processing speed
Quality of Life Questionnaires	
EQ-5D	
Stroke Impact Scale (SIS) Short Form	
Informant Interviews	
Informant Questionnaire for Cognitive Decline in the Elderly (IQCODE)	
Neuropsychiatric Inventory Questionnaire Version (NIP-Q)*	
Centre for Epidemiologic Studies – Depression Scale (CES-D)	

4.3 Angiographic image analysis methods

Anonymised images were visually reviewed for image quality by a trained adjudicator before analysis procedures. This was to ensure that all images were of sufficient quality for the primary endpoint data of the XILO-FIST trial to be gathered. A subset of XILO-FIST data was used as training data. This training data collected was not used in the final dataset, but all participants were included in the final dataset i.e., the training data remained fully independent of the XILO-FIST dataset.

4.3.1 Carotid artery stenosis

Carotid artery stenosis is a major risk factor for ischaemic stroke, thus is assessed using either Doppler ultrasound, CT angiography, or MR angiography as part of their radiological assessments. Our method of assessing stenosis follows the NASCET criteria, which aims to standardise image rating procedures[65]. Stenosis was assessed using Mango software[183] in the MRI TOF images for each patient (Figure 4.1).

A semi-automatic region growth mechanism was applied to create regions of interest (ROI) of each carotid artery for analysis. A random seed point was initiated, and a region growth mechanism relative to the seed was applied. A neighbouring voxel is added to the seed ROI assuming it falls into the range of intensity values within the growth algorithm. This process iterates continuously until no new neighbouring voxels are found within the range. The operator repeated this method starting a new seed until the whole vessel was estimated. Preservation of regions was employed where unconnected ROIs were generated. This would allow the isolation of the carotid artery, and remove any aberrant masks features outside the vascular anatomy i.e., the removal of hyperintense fatty tissue from the mask. Additionally, dilation and erosion of the masks may be performed to ensure the alignment of the ROI to the vasculature. Dilation and erosion are performed in a 3D symmetrical manner that may be manipulated i.e., 1x1x1mm. ROIs were stratified by location and vessel.

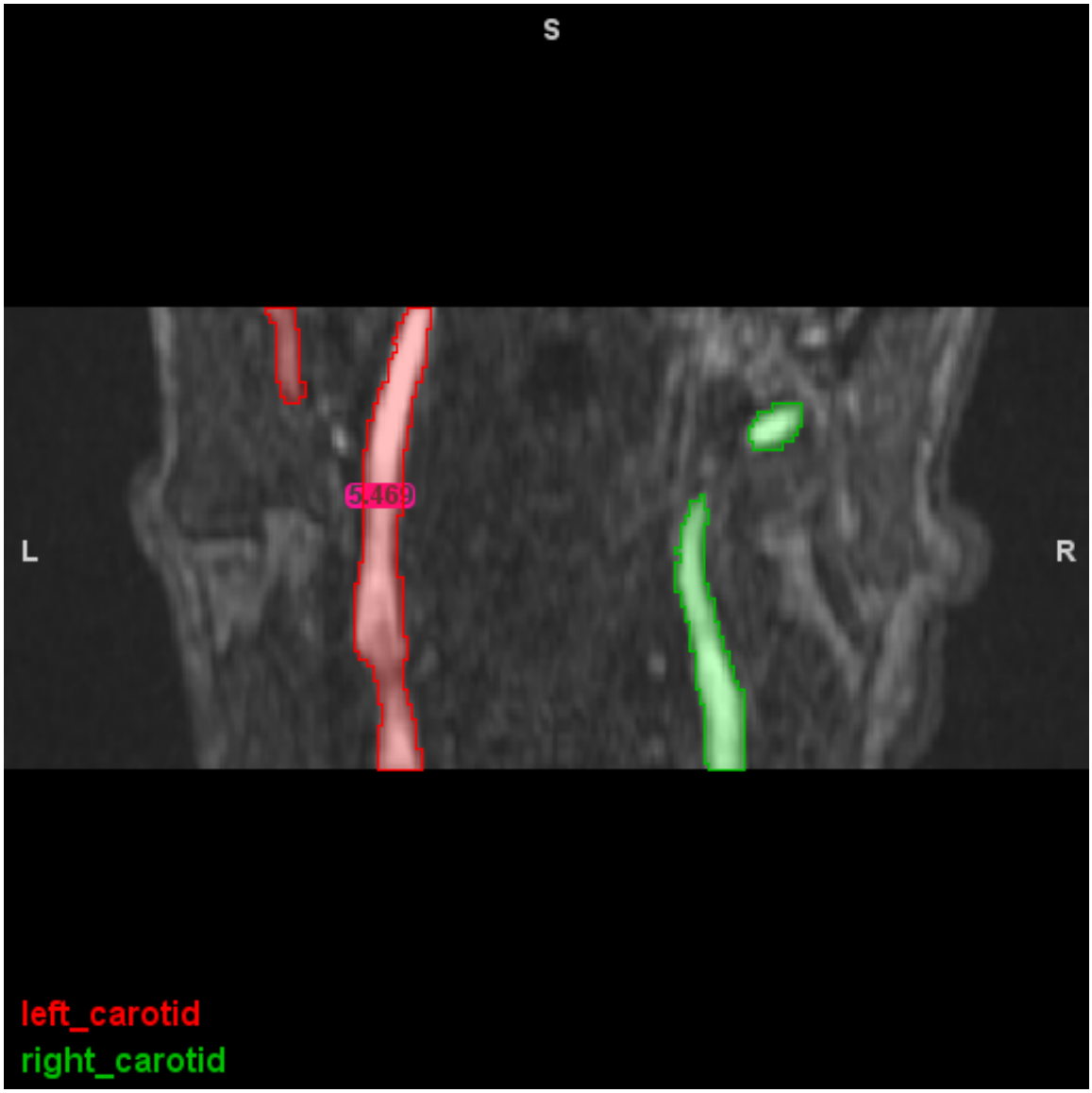

Figure 4.1: An example of the extraction of vessel diameter using a manual ruler tool within Mango on carotid artery masks. Regions of interest (ROI) are created using a growth mechanism. The vessel diameter is used to calculate stenosis based on the North American Symptomatic Carotid Endarterectomy Trial (NASCET) criteria.

Carotid artery stenosis measurements were compared with ground truth neuroradiologist CT/MR reports where available, which described % stenosis in terms relative to the NASCET criteria (mild, moderate, severe and occlusion), in both baseline and longitudinal datasets.

4.3.2 Carotid artery intima-media thickness

Carotid artery intima-media thickness (IMT) are measurements routinely assessed using carotid doppler ultrasound. Using sonography, IMT can be described as a parallel pattern consisting of the lumen-intima and media-externa boundaries. Moreover, carotid plaques can be identified using ultrasound. These plaques are described as local structures that invade the arterial lumen of ~50% IMT value or thickening >1.5mm. Arterial wall assessment in ultrasound involves the common carotid artery, but more superior segments i.e., carotid bulb/internal carotid artery assessments are dependent upon the skill of the sonographer and anatomical topography of the patient[184].

Carotid IMT was assessed in both the common carotid artery (CCA) and the internal carotid artery (ICA) manually, from PD weighted imaging (Figure 4.2). These images were assessed using Mango software[183]. Slices that correspond to CCA and ICA were selected, based on visual inspection in the axial view. Slices were chosen if the edges of the CCA or ICA could be clearly defined. Slices were chosen independently of participant side e.g., 1 axial slice may be chosen for left CCA, and a different axial slice for the right CCA. This is to account for variation in location of the carotid bifurcation. Slices were chosen to be as close to the carotid bifurcation as possible, as this is often the location of maximal plaque burden[58,61].

A tracing tool was used to manually draw around the entire axial view of the vessel, where the vessel wall appeared as isointense/ hyperintense to the background tissue, and around the lumen, often appearing as hypointense to the background. In participants where vessel wall is indiscriminate from the background tissue, image intensity values were temporarily manipulated within Mango to improve visualisation where possible. If manual alteration did not provide sufficient contrast between vessel wall and background image, this vessel was not assessed. Additionally, if carotid occlusion made the vessel lumen indiscriminate from the vessel wall, this artery would not be assessed, but occlusion noted.

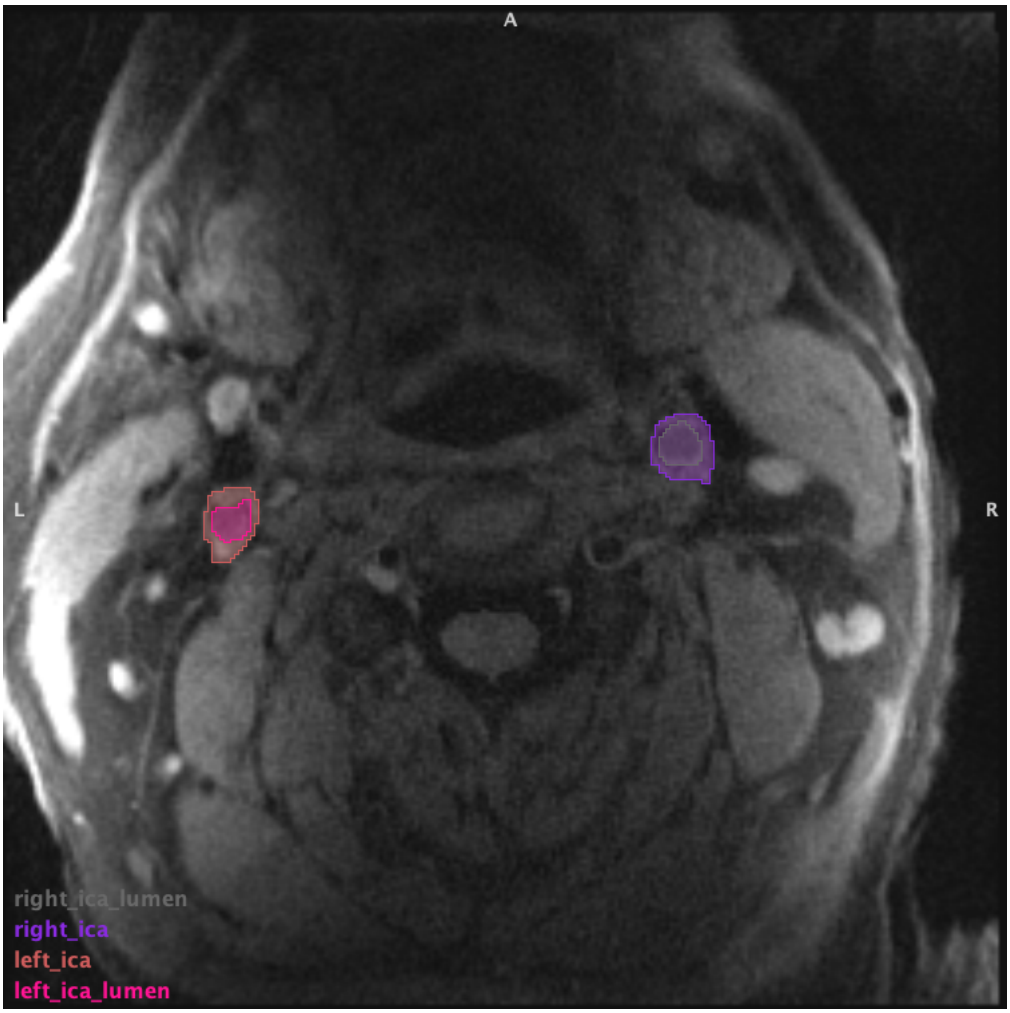

Figure 4.2 An example of intima-media thickness (IMT) assessment performed on PD-weighted imaging using Mango software. Regions of interest are created and basic subtraction of luminal area from total ROI area are performed.

Summary statistics of each ROI are given within Mango, including size (mm3). Following manual segmentation of whole axial view of carotid arteries and lumen, IMT was calculated by subtracting area of the lumen from the total carotid area.

Equation 1: Calculation of area of intima-media thickness in proton-weighted imaging

$$A_W = A_T - A_L$$

Where A_W is area of the wall, A_T is total area of the vessel in the axial slice, and A_L is area of the lumen.

The manual assessments of carotid IMT were validated by comparison between 2 of 3 observers independent of each other. Each observer evaluated a random assortment of 30 patient images, for a total of 60 participants assessed by 2 different image analysts. These data were compared for their spatial overlap and union using Dice Coefficients and Jaccard Indices within MATLAB, using a full mask of each axial slice assessed as a total volume measurement, and the first observer's data as an assumed ground truth. Numerical difference between observer measurements was investigated using Bland-Altman plots.

4.3.3 Carotid artery tortuosity

Carotid artery tortuosity was assessed using the Vascular Modelling Toolkit (VMTK)[185]. VMTK is a collection of tools that uses a Python environment for 3D image reconstruction, geometric analysis and vessel surface analysis of different image modalities[185]. TOF images for each participant are manipulated using a level set image segmentation[186] procedure. A level set method is an active contour model which is often utilised in data that is prone to inhomogeneity in image intensity i.e., medical imaging[187]. These methods are favoured for flexibility, usability and ability to adapt to *a priori* information[187]. Level set methods for image processing are advantageous for assessing vasculature as these can perform on structures prone to curving without creating a rigid parametric surface[188]. Level set methods can be described as "region-based" or "edge-based", depending upon the specific image classification algorithms used (Figure 4.3)[187]

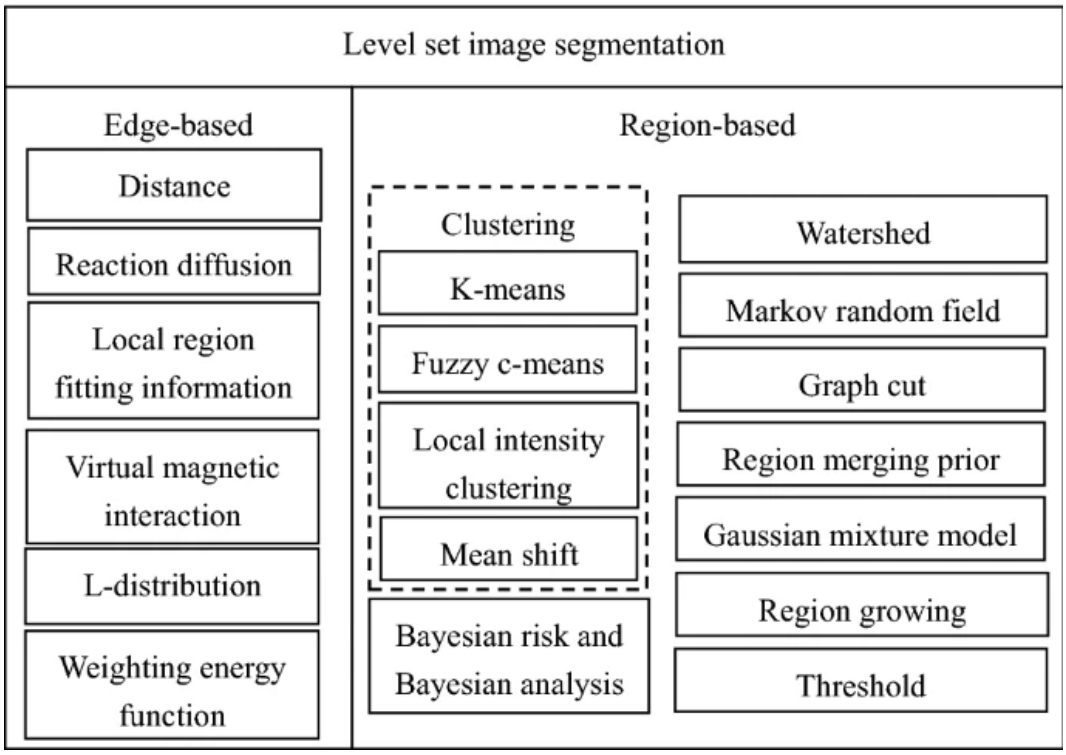

Figure 4.3: The classification of different level set image segmentation procedures into edge-or region-based methods.

Region-based level set methods are used in the VMTK framework for their ability to handle intensity inhomogeneity whilst not as heavily influenced by noise within the images[185,187].

Methods for the “Colliding Fronts” image segmentation procedure were replicated from previous work in geometric analysis of vasculature in cerebral aneurysms[186] and assessment of patient haemodynamics[189]. The Colliding Fronts segmentation is a region growing method that evaluates vascular structure by manually setting two seed points in the image, at either end of the carotid artery i.e., the most inferior and superior portions of the images. Two fronts are then propagated, proportional to the intensity of the image caused by the velocity of blood flow. The initial model is created from the collision of these two fronts[186,189]. The location of the seed sets around the superior and inferior points does not influence the segmentation procedure. The model conforms locally to the maximum change in image intensity across the vessel, whilst ignoring side branches[185,186,189].

Next, the procedure called for the setting of minimum and maximum threshold values to ensure accurate wave propagation for the segmentation procedure. This optional step can be utilised when a poor signal: noise (SNR) is evident in the data; this was not required in the TOF images, and thus set to null[185].

Once the initial deformable model was set, parameters of the segmentation may be altered, including number of iterations in the model, propagation scaling, curvature scaling and advection scaling[185,186,189]. The number of iterations of the model was set to a standard n = 300. Propagation scaling i.e., the weight of model inflation was set to 0 to prevent overestimation of the vessel wall. Curvature scaling i.e., weight of surface regularisation, was set to 0. Advection scaling i.e., the manipulation of the surface to the image gradient ridges, was set to 1.0. These parameters reliably led to segmented vessels that were close to the vessel wall. After the segmented vessel had been made, a polygonal surface was extracted from the mask using a "Marching Cubes" algorithm[185,190]. This algorithm created triangular vertices from a 3D isosurface using linear interpolation i.e., created a mesh of polygons from the segmented voxels.

Centerlines of the cervical carotid arteries were created automatically using a Voronoi diagram-based approach utilised in the VMTK framework[186,189]. The centerline, or medial axis of the vessel, is described as the locus of the centres of maximally inscribed spheres[189]. In contrast, the Voronoi diagram is a surface of polygons. The vertices of these polygons are associated with the radii of the maximally inscribed spheres (Figure 4.4), thus allowing the calculation of the difference between the medial axis and the vessel wall boundary.

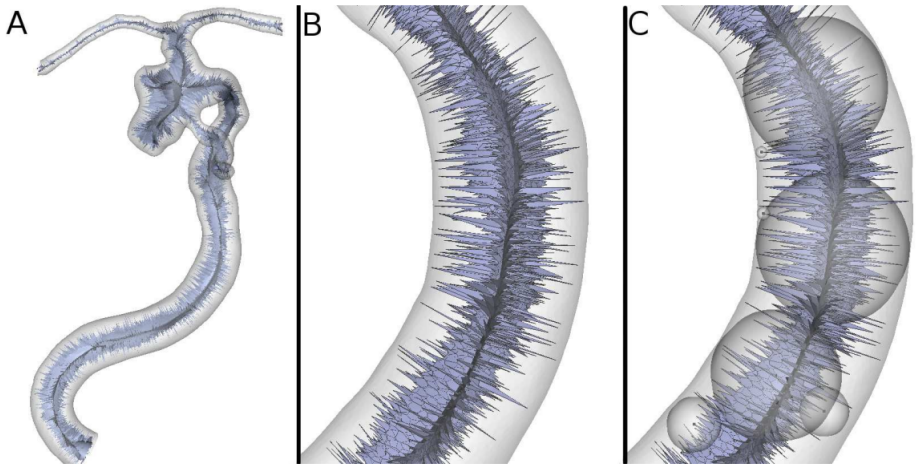

Figure 4.4: A schematic representation of carotid artery tortuosity assessment using the Vascular Modelling Toolkit (VMTK).A: Model of the internal carotid artery; B: The Voronoi diagram which stretches from the centerline to the vessel edge; C: The maximally inscribed spheres involved in the calculation of the vessel edge[186,189].

Once the centreline has been estimated within the polygonal surface model, values corresponding with curvature, torsion and tortuosity may be calculated. The vessel tortuosity is described as an index value, a scalar quantity between 0 and 1, using the simple calculation below:

Equation 2: Tortuosity Index formula for analysis of cervical carotid artery tortuosity.

$$\chi = \frac{L}{D} - 1$$

Where χ is the tortuosity index value, L is the length of the centreline path, and D is the minimum distance travelled.

4.4 Brain image analysis protocol

The brain image analysis protocol as part of the XILO-FIST trial was run on all 464 participants[182]. Only those with concurrent carotid MR angiography imaging were analysed in this work. STRIVE recommendations were followed during the MR image review[28] (Figure 2.2). Every scan was reviewed by assessors blinded to treatment allocation. Visualisation of WMH of presumed vascular origin is different across different MR modalities. WMH lesions are defined as hyperintense lesions on T2-weighted and FLAIR imaging, whilst appearing as isointense or hypointense on T1-weighted imaging, though not as hypointense as CSF.

Fazekas[191] and Scheltens[192] scores were assigned to both baseline and longitudinal imaging. The Rotterdam[193] and Schmidt's[194] progression scores were calculated by simultaneous review of the baseline and follow-up images. All visual rating scores were assigned by two trained observers independent of each other. A consensus score was applied to any image where the observers disagreed.

Fazekas score categorises WMH in periventricular and deep white matter regions dependent upon the size and confluence of the lesions. Periventricular lesions are defined as being contiguous with the lateral ventricle margins, whereas deep WMH lesions are separate to it. In some cases, WMH lesions may have coalesced. Irregular lesions and lesions >1cm from the ventricular margins are scored as deep white matter lesions[191]. Table 4.5 demonstrates the different lesion classifications according to the Fazekas score system.

Table 4.5: The Fazekas scoring system for white matter hyperintensities (WMH) of presumed vascular origin.

Score	Periventricular white matter lesions	Deep white matter lesions:
0	Absent	Absent
1	Caps/pencil-thin lining	Multiple focal lesions (>5 lesions)
2	Smooth halo around ventricles (6-10 mm range)	Small confluent areas
3	Irregular halo (>10mm range)	Large confluent areas

Comparatively, the Schelten's scale measures white matter abnormalities using 4 summed scores around distinct areas. These are the periventricular white matter and deep white matter mimicking Fazekas score but including hyperintense lesions around the basal ganglia and infratentorial foci. These areas are scored 0-84 in 16 regions (13 subcortical regions; 3 periventricular regions). Subcortical regions are scored 0-6; periventricular regions are scored 0-2. In the case of coalesced lesions, these were counted as deep white matter lesions. Table 4.6 demonstrates an exemplar scoring sheet for evaluating white matter hyperintensities using Schelten's scale.

Table 4.6: A rubric of Schelten's scale measurements to assess white matter hyperintensities (WMH) of presumed vascular origin.

Region	Scoring		Total Score
Periventricular lesions			
Occipital	0 (absent) 1 (≤ 5mm) 2 (> 5mm)		0 to 6
Frontal			
Bands of lateral ventricles			
Deep lesions			
Frontal	0 (absent) 1 (< 3mm, n ≤ 5) 2 (< 3mm, n > 6) 3 (4-10mm, n ≤ 5) 4 (4-10mm, n > 6) 5 (> 11mm, n >1) 6 (confluent)		0 to 24
Parietal			
Temporal			
Occipital			
Basal ganglia lesions			
Caudate nucleus	0 (absent) 1 (< 3mm, n ≤ 5) 2 (< 3mm, n > 6) 3 (4-10mm, n ≤ 5) 4 (4-10mm, n > 6) 5 (> 11mm, n >1) 6 (confluent)		0 to 30
Putamen			
Globus Pallidus			
Thalamus			
Internal Capsule			
Infratentorial lesions			
Cerebellum	0 (absent) 1 (< 3mm, n ≤ 5) 2 (< 3mm, n > 6) 3 (4-10mm, n ≤ 5) 4 (4-10mm, n > 6) 5 (> 11mm, n >1) 6 (confluent)		0 to 24
Mesencephalon			
Pons			
Medulla			

Volumetric assessment of WMH volume was performed in conjunction with the scoring systems. The assessments were performed both manually and using an automated extraction method. First, estimates of white matter area in each participant were calculated using atlas-based segmentation[195]. A probability map of white matter created from 313 adult volunteers (aged 18-96) was used[196], registered to each subject using non-linear co-registration, providing estimates of white matter in each subject[195]. Hyperintense outliers are presumed to be white matter hyperintensities. These are identified on T2 FLAIR imaging, and each voxel is transformed to a standardised z-score. A z-score ≥ 1.5 describes a WMH lesion within the white matter area. Once estimated, a 3D Gaussian smoothing kernel is applied to reduce noise, accounting for partial volumes that may be estimated around WMH edges. These automated estimates are visually checked by a trained observer following STRIVE guidelines[28]. Additionally, infarct lesions are masked by a trained image analyst.

Normal brain tissue i.e., grey matter (both cortical and sub-cortical), cerebral white matter and supratentorial CSF are segmented using population-specific probability maps of each tissue class, intra-subject T1 intensity data and adjoining voxel data[197,198]. These segmented masks are visually assessed by a trained observer in the same manner as the WMH.

4.5 Summary

This chapter describes the carotid artery imaging protocol, including the semi-automatic carotid artery stenosis estimation using TOF MRA, manual segmentation of the carotid vessel wall to derive carotid IMT, and the automated segmentation procedure for carotid artery tortuosity. Chapter 5 shall describe the different steps in validating these measurements before analysis.

5 Validation of the Carotid Image Analysis Protocol

5.1 Introduction

This thesis uses data from the clinical trial “Xanthine oxidase inhibition for the improvement of long-term outcomes following ischaemic stroke and transient ischaemic attack (XILO-FIST)”. This chapter describes the validation process undertaken to describe the efficacy of the methods employed in this PhD.

5.2 Aims and Objectives

This chapter aims to describe the steps employed in validating the combined carotid image analysis methods. The objectives of this chapter include:

1. Evaluate the interrater variability in ICA stenosis estimation using the Fleiss kappa statistical test on clinical labels.
2. Calculate the interrater variability in carotid IMT measurements using Dice coefficient and Jaccard indices on IMT image masks.
3. Assess the intrarater variability of automated carotid artery tortuosity measurements using intra-class correlation coefficients.

5.3 Methods

All carotid measurements were assessed in both baseline and follow-up imaging where available. All statistical analysis was performed in R (version 4.1.3) or IBM SPSS Statistics (version 28). The generation of Dice coefficients and Jaccard indices were created within MATLAB, using code provided elsewhere. Interrater differences of carotid artery stenosis measurements were validated using Fleiss kappa statistic. Interrater analysis of IMT area was performed using Dice Coefficient and Jaccard Indices with Bland-Altman plots created. The intrarater observability of cervical carotid tortuosity was assessed using intraclass correlation coefficients.

5.4 Results

5.4.1 Validation of carotid artery stenosis measurements

Carotid artery stenosis measurements in every patient were performed by one trained observer. I used NASCET criteria data from neuroradiologist MR or CT reports of each patient as a ground-truth measurement, where available. Agreement between qualitative clinical labels (non-significant stenosis, mild, moderate, severe, and occluded) was assessed by Fleiss kappa in a subset of 80 individuals within the XILO-FIST trial.

Table 5.1: Overall agreement of inter-rater observability in the evaluation of internal carotid artery stenosis. ICA = internal carotid artery.

	Overall Agreement (κ)	Standard Error	Z	Significance	95% Confidence Interval
Left ICA	0.751	0.86	8.775	<0.001	0.583-0.918
Right ICA	0.724	0.80	9.083	<0.001	0.568-0.881

Our data (Tables 5.1, 5.2) demonstrates that the inter-observer agreement between a trained observer and a cohort of radiologists is substantial. The overall agreement across all categories is estimated at $\kappa = 0.751$ (95% CI 0.583 – 0.918, $p < 0.001$) for the left ICA and $\kappa = 0.724$ (95% CI 0.568 – 0.881, $p < 0.001$) for the right ICA, respectively. Further analysis upon each NASCET category found varying results. Moderate stenosis in the left ICA i.e., 60-69% stenosis shows the lowest agreement; $\kappa = 0.378$ (95% CI 0.145 – 0.611, $p = 0.001$). Occluded arteries in the left ICA shows the highest agreement; $\kappa = 1.000$ (95% CI 0.767 – 1.233, $p < 0.001$).

Table 5.2: Individual Fleiss kappa agreement of inter-rater observability in the left and right internal carotid arteries, across all stenosis categories. ICA = internal carotid artery.

Artery	Category	Conditional Probability	Agreement (κ)	Standard Error	Z	Significance	95% Confidence Interval
Left ICA	<50%	0.965	0.822	0.119	6.927	<0.001	0.589-1.055
	50-59%	0.824	0.800	0.119	6.737	<0.001	0.567-1.032
	60-69%	0.400	0.378	0.119	3.186	0.001	0.145-0.611
	70-99%	0.500	0.486	0.119	4.091	<0.001	0.253-0.718
	Occlusion	1.000	1.000	0.119	8.426	<0.001	0.767-1.233
Right ICA	<50%	0.967	0.767	0.119	6.465	<0.001	0.535-1.000
	50-59%	0.667	0.644	0.119	5.427	<0.001	0.412-0.877
	60-69%	1.000	1.000	0.119	8.426	<0.001	0.767-1.233
	70-99%	0.000	-0.14	0.119	-0.12	0.904	-0.247-0.218
	Occlusion	0.800	0.793	0.119	6.679	<0.001	0.560-1.025

5.4.2 Validation of carotid artery intima-media thickness measurements

All carotid artery IMT measurements were assessed by one observer; two evaluators measured IMT in 60 participants total (30 participants evaluated by 2 raters; 30 participants evaluated by a different pair of raters). These data were validated by investigating inter-rater differences in the dual-rated scans. Participants were included randomly, but only participants where all four vessels were visible. Participants with occluded vessels were not included. This was to ensure maximum number of data points assessed. Spatial agreement was assessed using Dice coefficients and Jaccard indices in Matlab 2018; Bland-Altman plots were created to evaluate the numerical difference between these data.

Table 5.3: The level of agreement in carotid intima-media thickness (IMT between 2 of 3 trained observers. Group A are between raters 1 and 2; Group B are between raters 1 and 3.

	Group A	Group B
Dice Coefficient	0.89	0.91
Jaccard Index	0.81	0.84

These data (Figure 5.1, Table 5.3) show that between the 2 observers, there is a high level of agreement. Jaccard indices and Dice coefficients were averaged at 0.81 and 0.89 respectively for Group A. These values were averaged at 0.84 and 0.91 respectively, for Group B. Figure 5.1 shows the violin boxplots of the observer agreement. This graph demonstrates the assessed overlap between the observers in each participant on a case-by-case basis, as well as the density of the data spread. The Bland-Altman plots (Figures 5.2, 5.3) highlighted that almost all vessel estimates were clustered together within the bounds of confidence intervals.

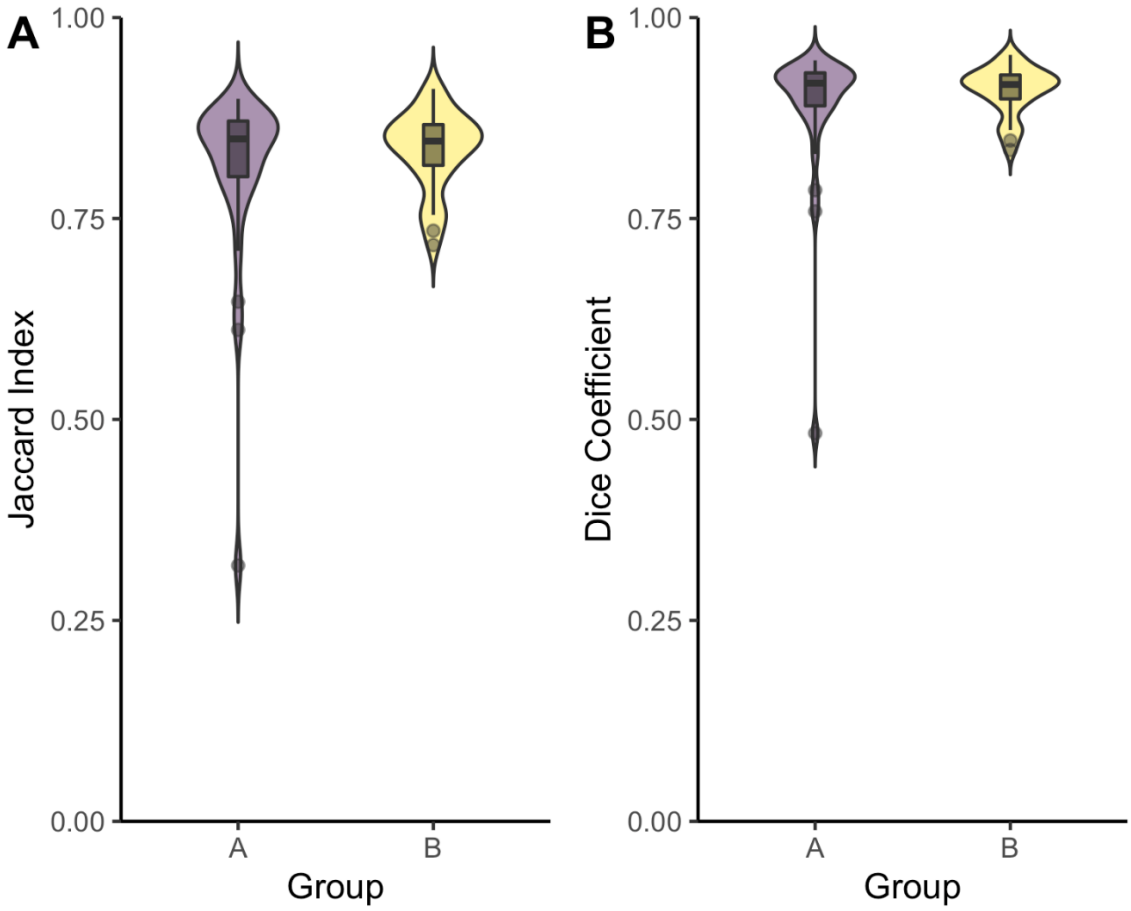

Figure 5.1: The violin boxplot graph of level of agreement between observers in 60 ischaemic stroke participants. Group A (purple) is between observers 1 and 2; Group B (yellow) is between observers 1 and 3. The observers analysed independently of each other, and both groups analysed different sets of participants. The boxplot demonstrates the mean and outliers of each group-level analysis; the violin plot demonstrates the density of the data spread. A: the Jaccard index of spatial agreement. B: the Dice coefficient of spatial agreement.

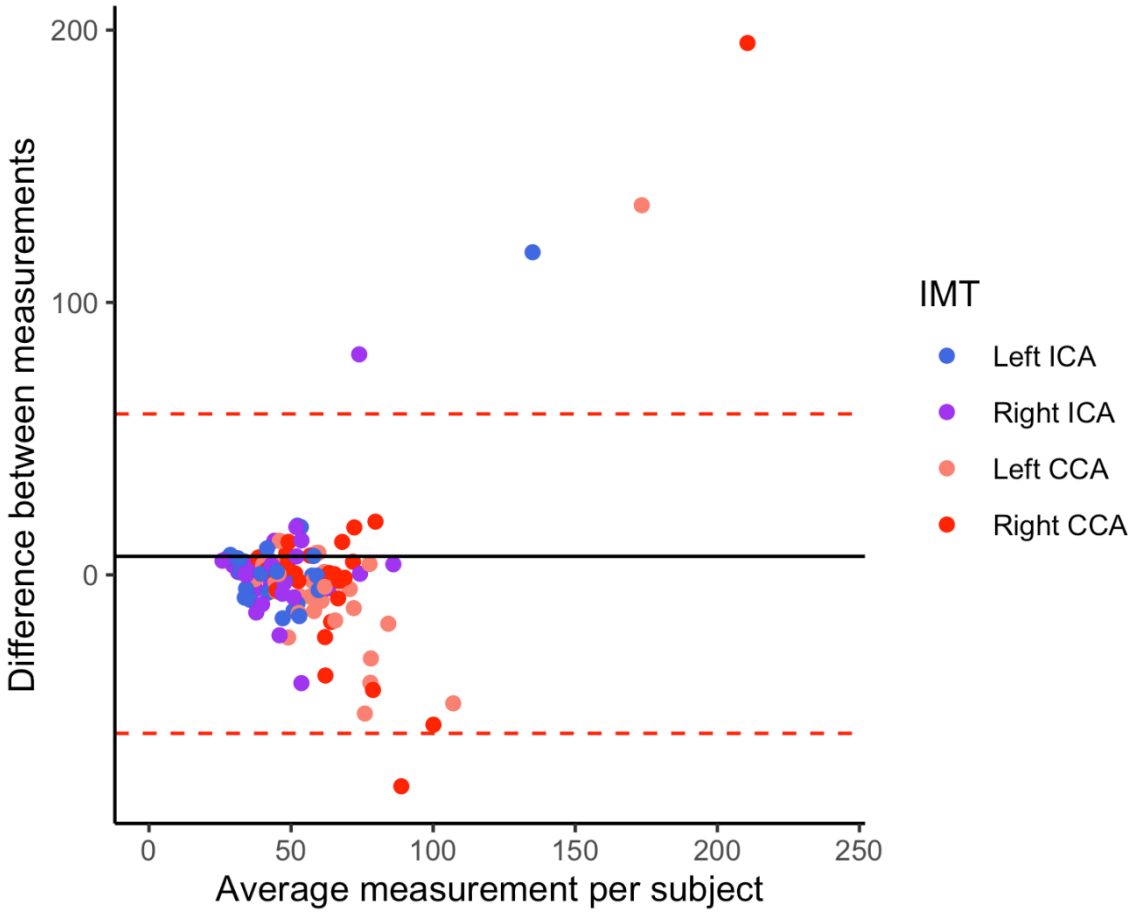

Figure 5.2: the Bland-Altman evaluation of numerical difference between Group A observers (analysts 1 and 2) on carotid intima-media thickness (IMT), stratified by artery assessed i.e., left common carotid artery (blue), right common carotid artery (purple), left internal carotid artery (peach) and right internal carotid artery (red). The dotted lines represent the 95% confidence intervals.

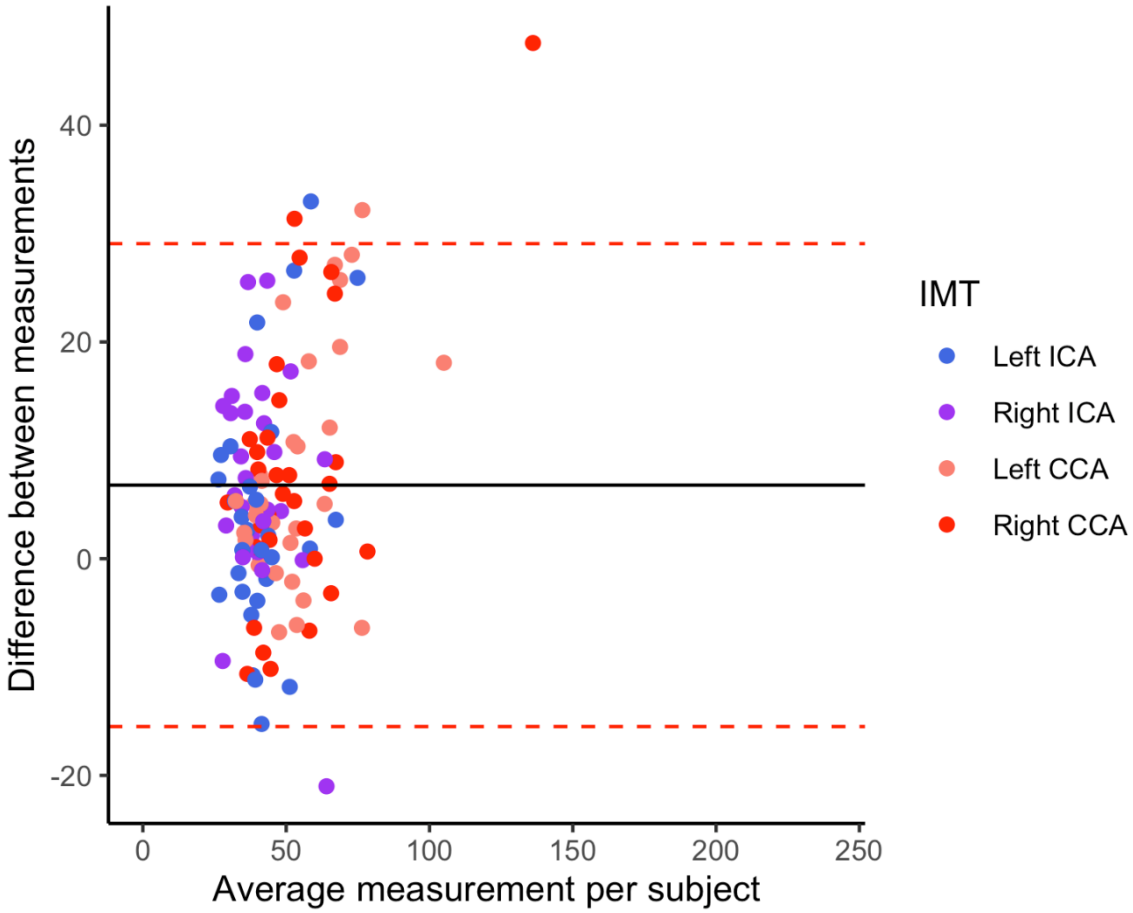

Figure 5.3: the Bland-Altman evaluation of numerical difference between Group B observers (analysts 1 and 3) on carotid intima-media thickness (IMT), stratified by artery assessed i.e., left common carotid artery (blue), right common carotid artery (purple), left internal carotid artery (peach) and right internal carotid artery (red). The dotted lines represent the 95% confidence intervals.

5.4.3 Validation of carotid artery tortuosity measurements

Carotid artery tortuosity measurements were assessed by one observer. These data were validated by the observer repeating the method at two different time points. 10 randomly assigned participants were utilised. Variance was observed using the intraclass correlation coefficient statistic (Table 5.4). Figure 5.4 describes the intra-observer variation between the tortuosity index values, separated by left and right carotid arteries.

Table 5.4: The intraclass correlation coefficient (ICC) of left and right carotid artery tortuosity indices.

			F Test with True Value 0			
Side of artery	ICC	95% Confidence Interval	Value	DF1	DF2	Significance
Left	0.999	0.996-1.000	2464.841	9	9	<0.001
Right	0.994	0.978-0.998	331.121	9	9	<0.001

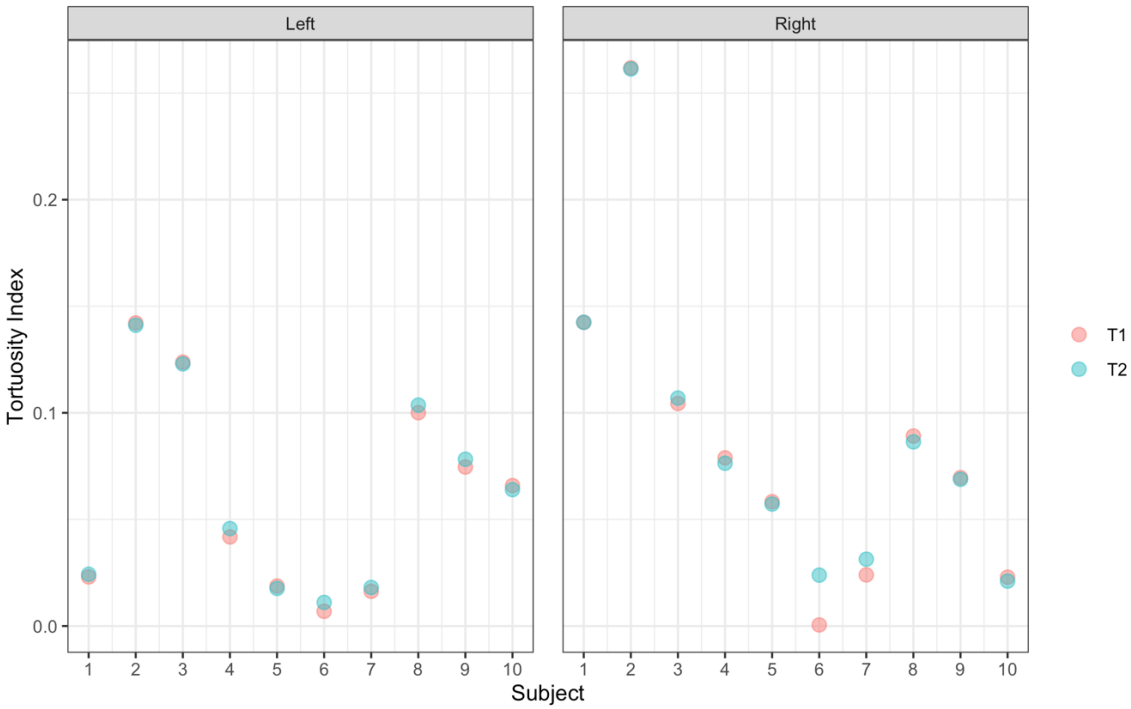

Figure 5.4: The tortuosity index values of 10 random participants assessed at baseline over different time points (T1 and T2), separated by the side of neck studied (left versus right).

These data (Table 5.4, Figure 5.4) demonstrate the intra-rater validity of the tortuosity measurement procedure. The intraclass correlation coefficient values were >0.99, suggesting excellent replicability. Figure 5.4 shows the individual differences in values between the two sets of measurements. The agreement within each subject varied extremely little, as evidenced by the overlap of the data points.

5.5 Discussion

Method validation across all three measurements (stenosis, intima-media thickness, and tortuosity) have performed well and can be considered reliable. Assessment of validation has been performed differently for each individual method, including Fleiss κ to assess qualitative clinical labelling of carotid artery stenosis, Dice coefficient and Jaccard indices to assess spatial agreement in our intima-media thickness measurements, and intraclass correlation coefficient to assess carotid artery tortuosity.

The agreement of carotid artery stenosis measurements arguably proved the lowest of all 3 parameters. Fleiss κ varied from 0.378 for moderate stenosis, to 0.822 for mild stenosis. It should be noted that vessel occlusion was expected to exhibit a perfect agreement ($\kappa = 1.000$), given a vessel occlusion upon TOF MRI will have no visible signal for the affected vessel. A negative kappa value was calculated for one measurement, right severe stenosis. This is because the severe stenosis category is missing in the sample data for the right internal carotid artery. This is further explained with a significance value $p = 0.904$. Many guidelines for the interpretation of kappa statistics exist. According to Dawson & Trapp (2004), a kappa agreement value of 0.751 and 0.724 for left and right ICA respectively lies within the boundary of good agreement[199]. Variation in the agreement between categorical labels may in part be due to the population assessed. The sample assessed show an overwhelming majority of participants with <50% stenosis. Furthermore, due to the unequal sharing of stenosis ranges within each category, this may further skew results. Values of 5% and 45% stenosis fall under the same category of non-significant stenosis which may explain part of the data skew. If our data included a larger range of participants using all clinical labels, variation between observer may increase. Furthermore, it is assumed that if % stenosis as a continuous variable, rather than an ordinal variable, was used to measure the agreement between the observer and ground-truth data from radiologists, the level of agreement may be lower.

Dice coefficient and Jaccard indices of carotid intima-media thickness were consistent in both observer groups. Groups A and B demonstrated Dice coefficients of 0.89 and 0.91, respectively. Jaccard indices were evaluated at 0.81 and 0.84 for Groups A and B, respectively. Manually rated imaging does not normally demonstrate such high levels of

agreement. Our intima-media thickness validation demonstrates that our method of analysis is repeatable as there is no significant difference between groups A and B, but some methodological limitations need to be considered beforehand. Firstly, MR data acquisition was only performed in non-isotropic 5 – 7 slices. If the data were acquired over a larger portion of the neck, it is assumed that more axial data points to choose from would relate in more difference between the observers. Additionally, I was only interested in small regions of the axial slices. Lumen regions appeared as hypointense to the background tissue, which are easily identified. If I included data from participants that featured an occluded vessel, agreement between observers may have decreased. This is due to differences in the visualisation of the blood vessel i.e., the vessel wall and lumen may both appear as hyperintense to the background, and therefore more difficult to distinguish between them. Accuracy of the IMT could not be measured as there was no ground truth measurement with which to compare.

Intraclass correlation coefficients of carotid artery tortuosity was >0.99, suggesting a near perfect agreement. The left carotid artery demonstrated an ICC of 0.999 (95% CI 0.996-1, p <0.001); the right carotid artery demonstrated an ICC of 0.994 (95% CI 0.978 – 0.998, p<0.001). According to Koo & Li et al., this suggests excellent reliability[200]. Additionally, some constraints should be addressed in our tortuosity validation. Firstly, the entire extracranial path of the carotid artery was assessed. If only the extracranial portion of the ICA was evaluated, this may yield different values. This would be due to variation in deciding where the ICA originates from in the raw images. Moreover, validity was assessed on the numerical output of the method. Frechet Distance metrics may be used to evaluate the spatial overlap between two sets of images, based on the polygonal surface extracted from each image. Due to a much-increased magnitude of data points assessed in spatial overlap versus ICC analysis, a greater range of individual differences between the two image sets may be found should these distance metrics be employed. Additionally, the accuracy of this data could not be tested due to no ground truth measurements.

5.6 Summary

Data presented throughout this thesis is extracted from the XILO-FIST trial, which investigates the effects of longitudinal allopurinol treatment in people with ischaemic stroke. The trial includes brain imaging and cognitive function tests at both baseline and 2-year follow-up in 464 participants. This thesis is concerned with the subgroup of participants that underwent additional angiographic imaging at baseline and 2-year follow-up. The angiographic images (TOF and black-blood imaging sequences) are used to assess ICA stenosis, carotid IMT within the CCA and ICA, and extracranial carotid tortuosity. This thesis uses NASCET criteria to evaluate ICA stenosis, a novel method to assess carotid IMT area, and a simple tortuosity index value to describe vessel tortuosity. All methods, though analysed differently, demonstrated good levels of reliability. ICA stenosis described a good reliability (average $\kappa > 0.72$); the reliability of the IMT method showed Dice >0.88. Lastly, the carotid tortuosity presented an ICC >0.99, a near perfect overlap. The next chapter assesses the relationships between these carotid measurements and common vascular risk factors for recurrent stroke.

6 Investigating the relationship between carotid artery disease and vascular risk factors in ischaemic stroke

6.1 Introduction

There have been many studies that aim to describe common vascular risk factors across stroke populations. Stroke risk factors are typically separated into non-modifiable risk factors e.g., age, sex, ethnicity, and modifiable risk factors such as hypertension and smoking status. Studies such as INTERSTROKE aimed at describing the common risk factors for stroke. INTERSTROKE described over 90% of variance seen in stroke risk, caused by common factors including current smoking, diagnosis of hypertension, diagnosis of diabetes, waist-to-hip ratio and other lifestyle factors such as alcohol consumption and regular physical activity[201]. Other risk factors include cardiac diseases such as angina[202], atrial fibrillation[203], and peripheral arterial disease[204]. Whilst risk factors independently increase the risk of stroke, multiple risk factors may interact with each other to increase the risk of stroke[203].

Due to the multiple interactions between these risk factors, cardiovascular scores such as ASSIGN[205] and Q-RISK[206] have been created to improve risk estimations. ASSIGN was developed to include a score of social deprivation with standard cardiovascular risk[205]. The ASSIGN score was determined from the Scottish Heart Health Extended Cohort, a group of 13,297 men and women aged between 30-74. This score strongly correlated with the Framingham 10-year cardiovascular risk score and improved upon risk data from the Scottish Heart Health Extended Cohort[207]. However, this measurement does not take atrial fibrillation into account, and has not been updated since 2007. Despite this drawback, ASSIGN has been determined to perform marginally better i.e., able to discriminate risk more accurately than the Framingham risk score and Q-RISK[208].

Despite these observations, in the systematic review (Chapter 3), I found a large portion of carotid imaging studies (%) do not describe common vascular risk factors in their study population. In this chapter, I aim to describe the relationship between the

structural carotid measurements (intima-media thickness, % stenosis and cervical tortuosity) and common stroke risk factors.

6.2 Aims and Objectives

This chapter aims to describe the baseline measurements of carotid artery disease. Additionally, this chapter will investigate relationships between these arterial measurements and common vascular risk factors for recurrent ischaemic stroke. The objectives of this chapter are:

1. Describe the baseline measurements of ICA stenosis, IMT of common and internal carotid arteries, and extracranial carotid artery tortuosity in ischaemic stroke participants.
2. Identify the distribution of these structural data to inform the types of statistical analyses to be employed e.g., parametric, or non-parametric statistical tests.
3. Determine the magnitude of associations between carotid artery disease and common vascular risk factors for recurrent stroke.

It is hypothesised that measurements of carotid artery disease will variably correlate with common vascular risk factors, though age will be a common risk factor of all baseline variables.

6.3 Methods

6.3.1 Participant selection

Participants which have carotid imaging at baseline were included in this analysis. Methods for structural carotid measurements (intima-media thickness, % stenosis and cervical tortuosity) have been described in the previous methods chapter (Chapter 4).

All participant demographic data were collected at trial induction. The cause of stroke was classified according to the Trial of Org 10172 in Acute Stroke Treatment (TOAST) criteria. Stroke severity was assessed using National Institute of Health Stroke Scale (NIHSS) and disability using the modified Rankin Scale (mRS).

6.3.2 Statistical analysis

Normality of the carotid artery disease variables was assessed using the Shapiro-Wilk test. Spearman-rank and Kendall-τ correlation statistics were used to identify the statistical significance of the dependent variables to common vascular risk factors. Mann-Whitney U test was used to assess any significant differences between the structural measurements across treatment groups. Independent sample T-test was used to evaluate any significant difference in demographic data between participants with and without carotid imaging. The standard p-value significance threshold of <0.05 was assumed for all analysis. Statistical analysis was performed using R (version 4.1.3).

6.4 Results

6.4.1 Participant population

A total of 538 participants consented to the run-in phase between May 2015 and November 2018. 464 participants were randomised to the treatment arms (232 per group). In this study, the participant population consists of participants from the XILO-FIST trial that have MR angiographic imaging at baseline, in concert with brain imaging and tests of cognitive function. Figure 6.1 shows the number of eligible participants included at baseline. Table 6.1 shows demographic data associated with these participants (n = 181). An independent sample T-test was used to evaluate any differences between the MRA-positive (n=181) and MRA-negative groups (n = 283).

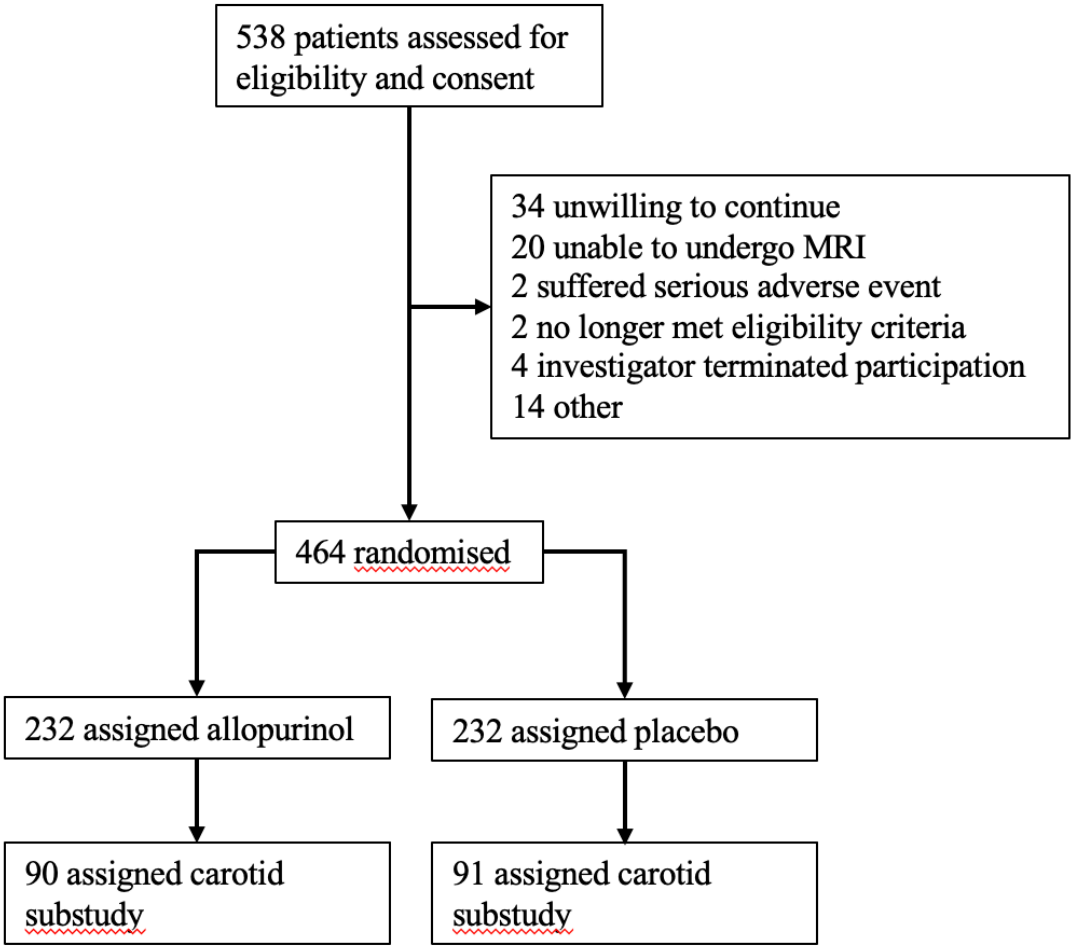

Figure 6.1: The trial profile detailing the inclusion of participants within the carotid substudy of the XILO-FIST trial. MRI = magnetic resonance imaging.

The entire XILO-FIST cohort (n = 466) exhibited differences between those that were included in the carotid sub-study (n = 181) i.e., are MRA-positive; and those that were not included (N = 283) i.e., are MRA-negative, seen in Table 6.1. The average age of the MRA+ group (64.37, SD 8.18) was significantly different to the MRA-group (66.56, SD 8.95) ($p=0.008$). Other risk factors exhibited a significant difference between these two groups. Current/former alcohol consumption was estimated in 141 (78%) participants with carotid imaging; 239 (85%) without ($p = 0.009$). Hypertension and dyslipidaemia both exhibited differences between groups. Hypertension was seen in 76 (42%) participants that took part in the carotid sub-study; 167 (59%) of the MRA negative cohort had a diagnosis of hypertension ($p<0.001$). Dyslipidaemia was diagnosed in 45 (25%) of the MRA positive cohort in comparison with 118 (42%) of the MRA negative cohort ($p<0.001$). Both scores of stroke severity (NIHSS and mRS) exhibited differences across the population. The mean NIHSS score in the carotid sub-study group is 1.06 (SD 1.34); with a mean score of 1.77 (SD 2.03) observed in the other group ($p<0.001$). The mean mRS score in the carotid sub-study group is 1.21 (SD 0.93) compared with a mean mRS score of 1.48 (SD 1.06) in the other group ($p = 0.005$).

Table 6.1: The demographic descriptions representative of the entire XILO-FIST dataset, separated by presence of angiographic imaging (MRA+) and absence of angiographic imaging (MRA-). The data was assessed using an independent sample T-test for continuous variables; Chi-square was used for binary variables e.g., presence/absence of disease. BMI = body mass index, TIA = transient ischaemic attack, NIHSS = National Institute of Health Stroke Scale, mRS = modified Rankin Scale.

	Group		
Variable	MRA + (n = 181)	MRA– (n = 283)	Sig.
Age (SD)	64.37 (8.18)	66.56 (8.95)	0.008
Sex (M/F)	130/51	189/94	0.253
Smoking history (current or former) (%)	96 (53.0)	152 (53.7)	0.751
Alcohol consumption (current or former) (%)	141 (77.9)	239 (84.5)	0.009
Systolic blood pressure (SD)	137.81 (16.88)	135.34 (17.75)	0.136
BMI (SD)	28.03 (4.88)	28.67 (5.20)	0.185
Angina (%)	16 (8.8)	30 (10.6)	0.536
Myocardial infarction (%)	16 (8.8)	25 (8.8)	0.998
Hypertension (%)	76 (42.0)	167 (59.0)	<0.001
Diabetes (%)	39 (21.5)	60 (21.2)	0.929
Dyslipidaemia (%)	45 (24.9)	118 (41.7)	<0.001
Peripheral artery disease (%)	8 (4.4)	19 (6.7)	0.303
Previous stroke (%)	11 (6.1)	30 (10.6)	0.094
Previous TIA (%)	17 (9.4)	29 (10.2)	0.764
NIHSS (SD)	1.06 (1.34)	1.77 (2.03)	<0.001
mRS (SD)	1.21 (0.93)	1.48 (1.06)	0.005

Structural measures of the carotid arteries include common carotid intima-media thickness, internal carotid artery intima-media thickness, internal carotid artery stenosis, evaluated according to NASCET criteria and extracranial carotid artery tortuosity.

Univariate normality test statistics are provided in Table 6.2 across all the vascular measurements. A significance value of <0.05 highlights that the variable is not normally distributed. Shapiro-Wilk test of normality was used.

Table 6.2: The normality test statistics provided for all carotid artery disease measurements extracted. CCA = common carotid artery, ICA = internal carotid artery, IMT = intima-media thickness. *stenosis measurements were calculated using NACSET criteria and reported in % for this level of analysis.

Variable	Shapiro-Wilk		
	Statistic	df	Sig.
Left CCA IMT	0.935	153	<0.001
Right CCA IMT	0.899	156	<0.001
Average CCA IMT	0.948	148	<0.001
Left ICA IMT	0.879	147	<0.001
Right ICA IMT	o.886	153	<0.001
Average ICA IMT	0.951	144	<0.001
Left ICA stenosis*	0.926	153	<0.001
Right ICA stenosis*	0.905	153	<0.001
Average ICA stenosis*	0.964	153	<0.001
Left carotid tortuosity	0.892	172	<0.001
Right carotid tortuosity	0.754	168	<0.001
Average carotid tortuosity	0.861	173	<0.001

All carotid variables are proven to be significantly not normally distributed. This was used to inform the types of statistical inferences performed i.e., non-parametric tests were used to assess relationships between dependent and independent variables.

6.4.2 Carotid artery measurements

Intima-media thickness was calculated at baseline from all patients with carotid black-blood imaging sequences. Table 6.3 presents the basic descriptive information for these data. As all carotid variables are do not follow normal distribution, data are described as median and interquartile range. The median CCA IMT values per artery were 55.03

mm^3 (IQR 28.51) and 54.83 mm^3 (IQR 24.42) respectively. Figure 6.2 provides a violin-boxplot of the data, highlighting the skewed data proportions.

Table 6.3: Descriptive statistics of the carotid variables measured. Due to non-normality, data provided are median and interquartile range. CCA = common carotid artery, ICA = internal carotid artery, IMT = intima-media thickness. Stenosis and tortuosity measurements were provided as % values for this level of analysis.

Variable	Side	
	Left	Right
CCA IMT mm^3	55.03 (28.51)	54.83 (24.42)
CCA IMT (%)	55.31 (9.17)	52.45 (10.15)
ICA IMT mm^3	38.41 (16.02)	39.21 (14.75)
ICA IMT (%)	56.99 (12.92)	57.04 (11.71)
ICA Stenosis (%)	31.99 (22.44)	31.40 (20.74)
Tortuosity Index (%)	5.24 (4.84)	5.64 (5.52)

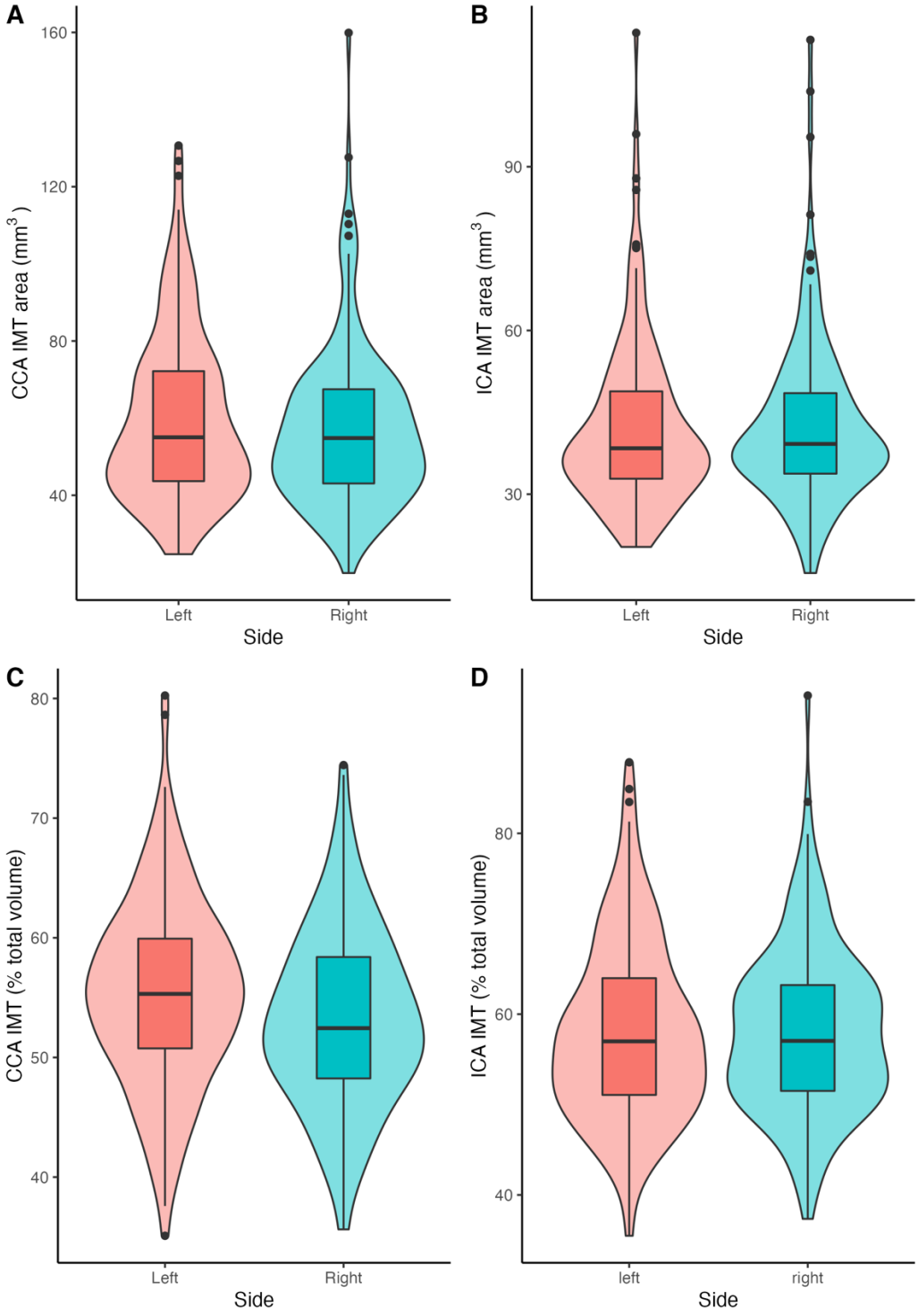

Figure 6.2: The intima-media thickness of all participants at baseline. The boxplot whiskers are set to 1.5x the inter-quartile range. Outliers are outside this range. The violin plot demonstrates the density of the data spread. A: Common carotid-intima media thickness, expressed in mm^3. B: Internal carotid intima-media thickness, expressed in mm^3. C: Common carotid artery intima-media thickness, expressed in % of total volume. D: Internal carotid artery intima-media thickness, expressed in % of total volume.

ICA stenosis % was calculated at baseline from all patients with an acceptable carotid TOF imaging sequence. 9 participants were not included due to significant artefact. The median stenosis values per artery are: left ICA = 32.50% (IQR 24.82) and right ICA = 31.77% (IQR 21.50) respectively. These values are within the non-significant stenosis range. Figure 6.3 presents this data using a violin-boxplot. Figure 6.4 provides a histogram of the stenosis values, classified into their respective clinical labels.

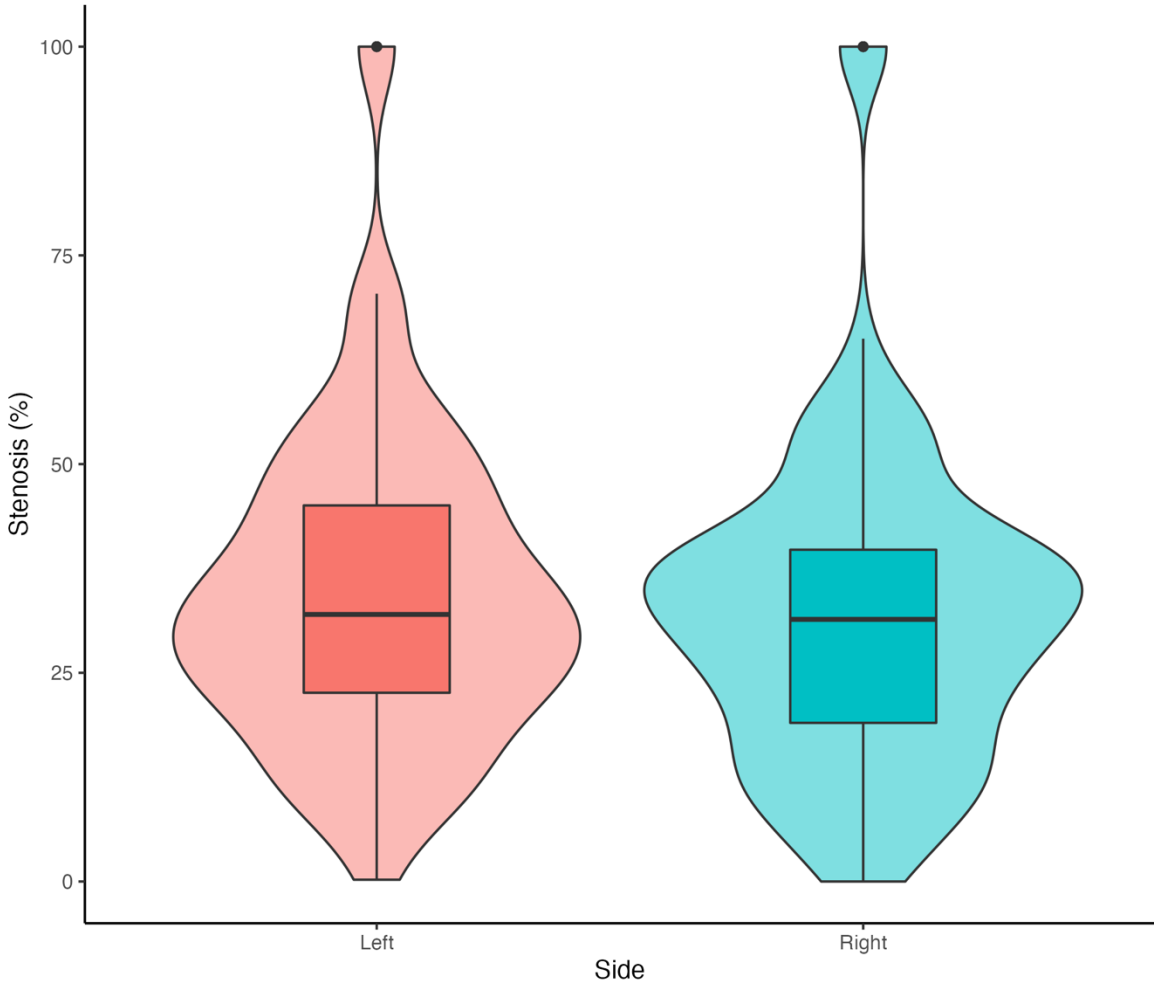

Figure 6.3: The internal carotid artery stenosis, expressed in percentage, at baseline. Boxplot whiskers are set to 1.5x the inter-quartile range. Outliers are outside this range. Violin plot represents the density of the data spread.

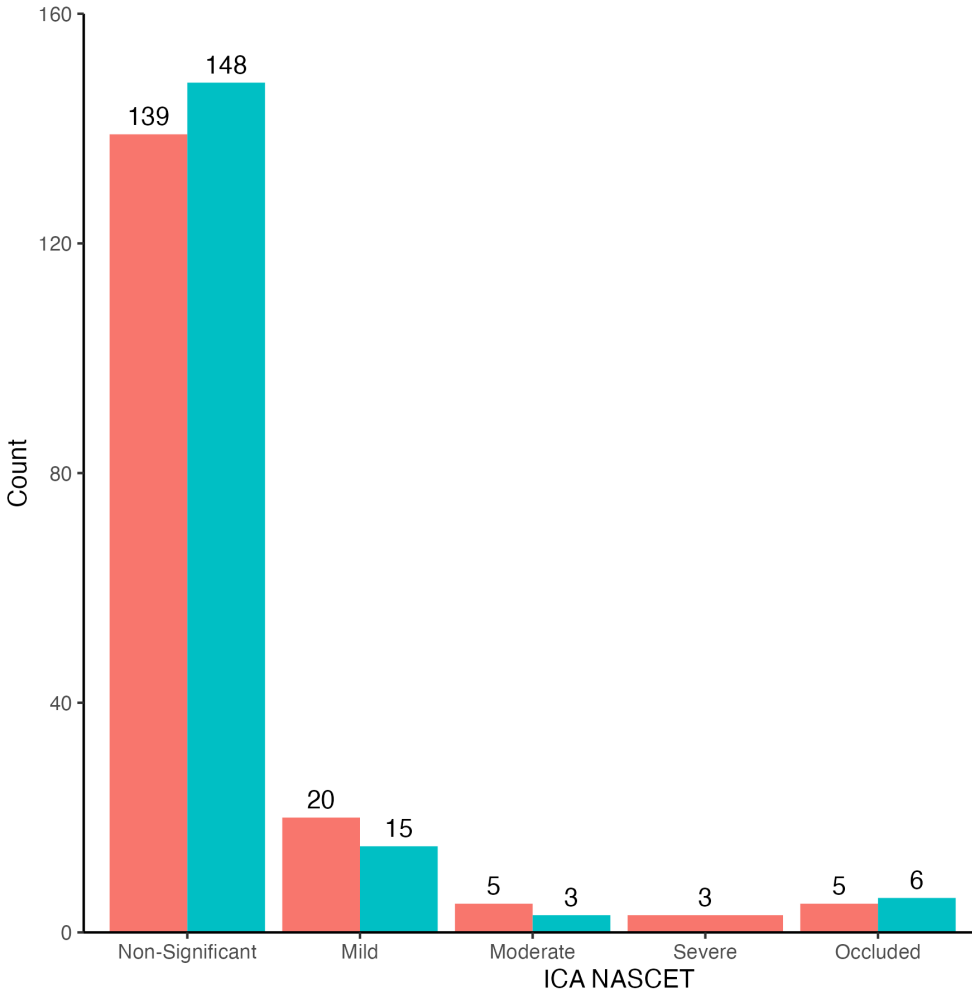

Figure 6.4: The North American Symptomatic Carotid Endarterectomy Trial (NASCET) descriptions of internal carotid artery stenosis, separated by side. Red = left ICA; blue = right ICA. Non-significant (<50%), mild (50-59%), moderate (60-69%), severe (70-99%), occluded (100%).

Carotid artery tortuosity was calculated at baseline for all participants with carotid TOF imaging sequence. In this assessment, 9 participants are missing data for the left carotid artery; 13 participant data points are missing in the right carotid artery. This is due to occlusion and insufficient image quality. The median tortuosity values were 5.24 (%) (IQR 4.84) for the left extracranial carotid artery, and 5.64 (%) (IQR 5.52) for the right extracranial carotid artery. Figure 6.5 provides these data in a violin-boxplot.

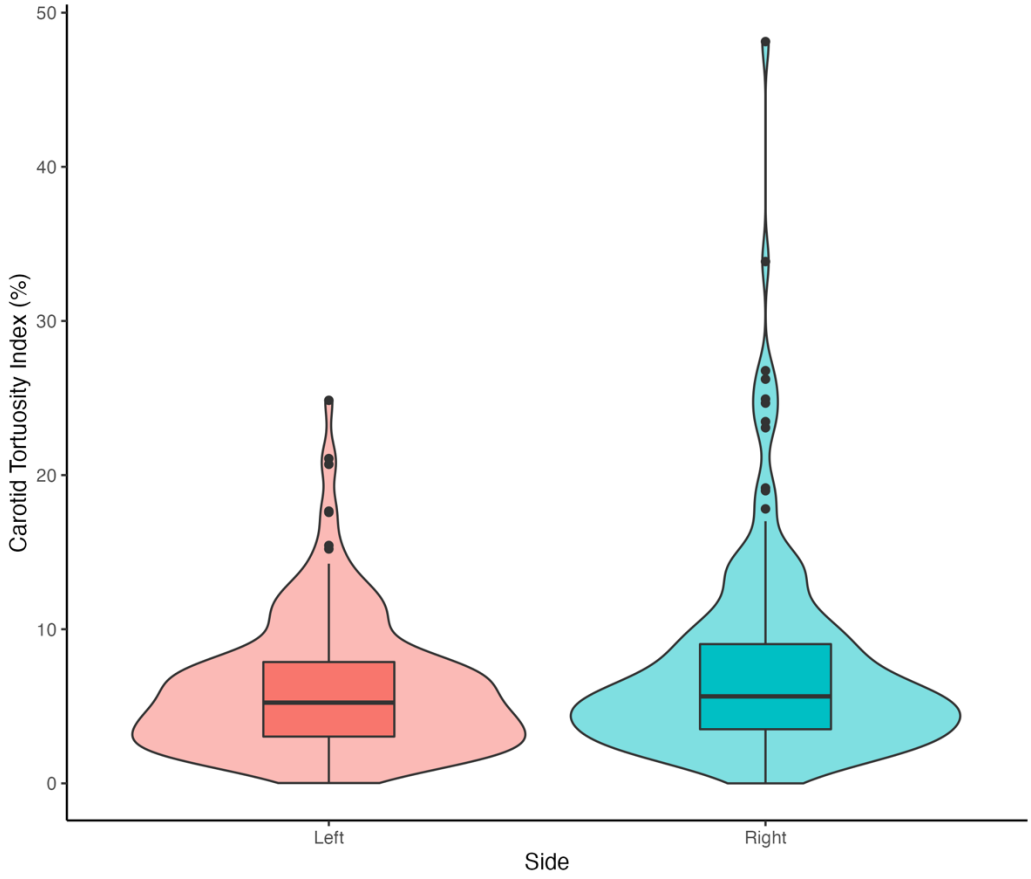

Figure 6.5: Cervical carotid tortuosity measurements at baseline across treatment groups, presented in percentage. The boxplot whiskers are set to 1.5x the inter-quartile range. Outliers are outside this range. The violin plot represents the density of the data spread.

6.4.3 Correlation between carotid artery disease and common vascular risk factors

Correlation coefficients were calculated between the structural measurements (CCA IMT, ICA IMT, ICA stenosis and cervical tortuosity), vascular risk factors, and stroke severity scores. Spearman's ρ correlation was calculated between two continuous variables; a Point-Biserial correlation was calculated between one continuous dependent variable and one binary independent variable. The data presented in Tables 6.4-6.6 and Figure 6.6 describes the correlation coefficients with associated p-values for each measurement.

Table 6.4: Univariate correlation coefficients of carotid variables versus vascular risk factors using Spearman's ρ. CCA = common carotid artery; IMT = intima-media thickness; ICA = internal carotid artery; BP = blood pressure; BMI = body mass index; ASSIGN = ASSIGN score. *p<0.05.

	Age		Systolic BP		BMI		ASSIGN		Sex		Smoking	
	ρ	sig	ρ	sig	ρ	sig	ρ	sig	ρ	sig	ρ	sig
Left CCA IMT	-0.036	0.907	0.173	0.272	0.151	0.351	0.004	0.998	-0.083	0.907	-0.033	0.907
Left ICA IMT	-0.042	0.995	0.215	0.153	0.131	0.557	0.003	0.995	-0.125	0.557	0.068	0.995
Right CCA IMT	0.055	0.933	0.072	0.795	0.035	0.976	0.101	0.694	-0.206	0.17	-0.099	0.694
Right ICA IMT	0.033	0.907	0.077	0.617	0.029	0.907	0.119	0.585	-0.102	0.585	-0.248*	0.034*
Average CCA IMT	0.043	0.828	0.140	0.510	0.100	0.772	0.077	0.825	-0.165	0.382	-0.104	0.772
Average ICA IMT	0.015	0.931	0.195	0.323	0.122	0.427	0.083	0.549	-0.153	0.357	-0.144	0.357
Left ICA Stenosis	0.064	0.871	0.020	0.871	-0.141	0.357	0.037	0.871	-0.013	0.871	-0.132	0.357
Right ICA Stenosis	-0.030	0.872	0.024	0.872	0.153	0.587	0.040	0.872	0.099	0.786	-0.036	0.872
Average ICA Stenosis	0.028	0.971	0.021	0.971	0.037	0.971	0.077	0.971	0.056	0.971	-0.105	0.971
Left Carotid Tortuosity	0.075	0.908	0.027	0.963	0.226	0.051	0.029	0.963	0.073	0.908	0.153	0.391
Right Carotid Tortuosity	0.225	0.051	0.083	0.568	0.045	0.865	0.124	0.472	0.080	0.568	0.153	0.400
Average Carotid Tortuosity	0.160	0.204	0.091	0.563	0.176	0.179	0.075	0.674	0.108	0.563	0.176	0.179

Table 6.5: Univariate correlation coefficients between carotid variables and vascular risk factors using Spearman's ρ. CCA = common carotid artery; IMT = intima-media thickness; ICA = internal carotid artery. MI = myocardial infarction *p<0.05

	Alcohol		Angina		MI		Hypertension		Diabetes		Dyslipidaemia	
	ρ	sig	ρ	sig	ρ	sig	ρ	sig	ρ	sig	ρ	sig
Left CCA IMT	0.012	0.998	-0.070	0.907	-0.062	0.907	-0.041	0.907	0.199	0.238	-0.029	0.907
Left ICA IMT	-0.082	0.995	-0.036	0.995	0.000	0.995	0.015	0.995	0.144	0.557	0.067	0.995
Right CCA IMT	-0.128	0.694	0.011	0.976	0.008	0.976	-0.014	0.976	0.094	0.694	0.010	0.976
Right ICA IMT	-0.069	0.617	-0.010	0.932	0.026	0.907	-0.007	0.932	0.099	0.585	-0.069	0.617
Average CCA IMT	-0.069	0.825	-0.008	0.928	-0.043	0.828	-0.040	0.828	0.185	0.382	-0.025	0.867
Average ICA IMT	-0.083	0.549	-0.026	0.931	0.007	0.931	-0.011	0.931	0.159	0.357	-0.010	0.931
Left ICA Stenosis	0.042	0.871	0.023	0.871	-0.018	0.871	0.036	0.871	0.044	0.871	0.214	0.136
Right ICA Stenosis	0.094	0.786	0.073	0.786	0.024	0.872	-0.039	0.872	-0.112	0.786	-0.025	0.872
Average ICA Stenosis	0.087	0.971	0.062	0.971	0.004	0.978	-0.002	0.978	-0.044	0.971	0.117	0.971
Left Carotid Tortuosity	0.071	0.908	0.074	0.908	0.052	0.946	0.000	0.997	0.022	0.963	-0.010	0.997
Right Carotid Tortuosity	0.015	0.899	0.085	0.568	0.124	0.472	0.015	0.899	0.020	0.899	0.078	0.568
Average Carotid Tortuosity	0.046	0.735	0.096	0.563	0.103	0.563	0.007	0.928	0.023	0.877	0.044	0.735

Table 6.6: Univariate correlation coefficients between carotid variables and vascular risk factors using Spearman's ρ. CCA = common carotid artery; IMT = intima-media thickness; ICA = internal carotid artery; PAD = peripheral artery disease; TIA = transient ischaemic attack; NIHSS = National Institute of Health Stroke Scale; mRS = modified Rankin Scale. *p<0.05.

	PAD		Prior Stroke		Prior TIA		NIHSS		mRS	
	ρ	sig	ρ	sig	ρ	sig	ρ	sig	ρ	sig
Left CCA IMT	-0.026	0.907	0.034	0.907	-0.059	0.907	0.076	0.907	0.000	0.998
Left ICA IMT	0.010	0.995	0.026	0.995	-0.040	0.995	0.012	0.995	0.002	0.995
Right CCA IMT	-0.116	0.694	0.075	0.795	-0.002	0.976	-0.008	0.976	0.022	0.976
Right ICA IMT	-0.107	0.585	-0.166	0.34	-0.095	0.585	-0.071	0.617	-0.020	0.915
Average CCA IMT	-0.083	0.825	0.058	0.825	-0.007	0.928	-0.060	0.825	0.026	0.867
Average ICA IMT	-0.096	0.531	-0.113	0.427	-0.116	0.427	-0.021	0.931	-0.049	0.864
Left ICA Stenosis	-0.124	0.357	0.029	0.871	-0.134	0.357	-0.179	0.23	-0.016	0.871
Right ICA Stenosis	0.079	0.786	0.083	0.786	0.148	0.587	0.012	0.902	0.010	0.902
Average ICA Stenosis	-0.027	0.971	0.071	0.971	0.012	0.978	-0.092	0.971	-0.029	0.971
Left Carotid Tortuosity	0.059	0.946	0.005	0.997	-0.020	0.963	0.068	0.908	-0.026	0.963
Right Carotid Tortuosity	0.025	0.899	0.095	0.568	0.075	0.568	0.001	0.989	-0.015	0.899
Average Carotid Tortuosity	0.062	0.705	0.070	0.674	0.046	0.735	0.011	0.928	-0.022	0.877

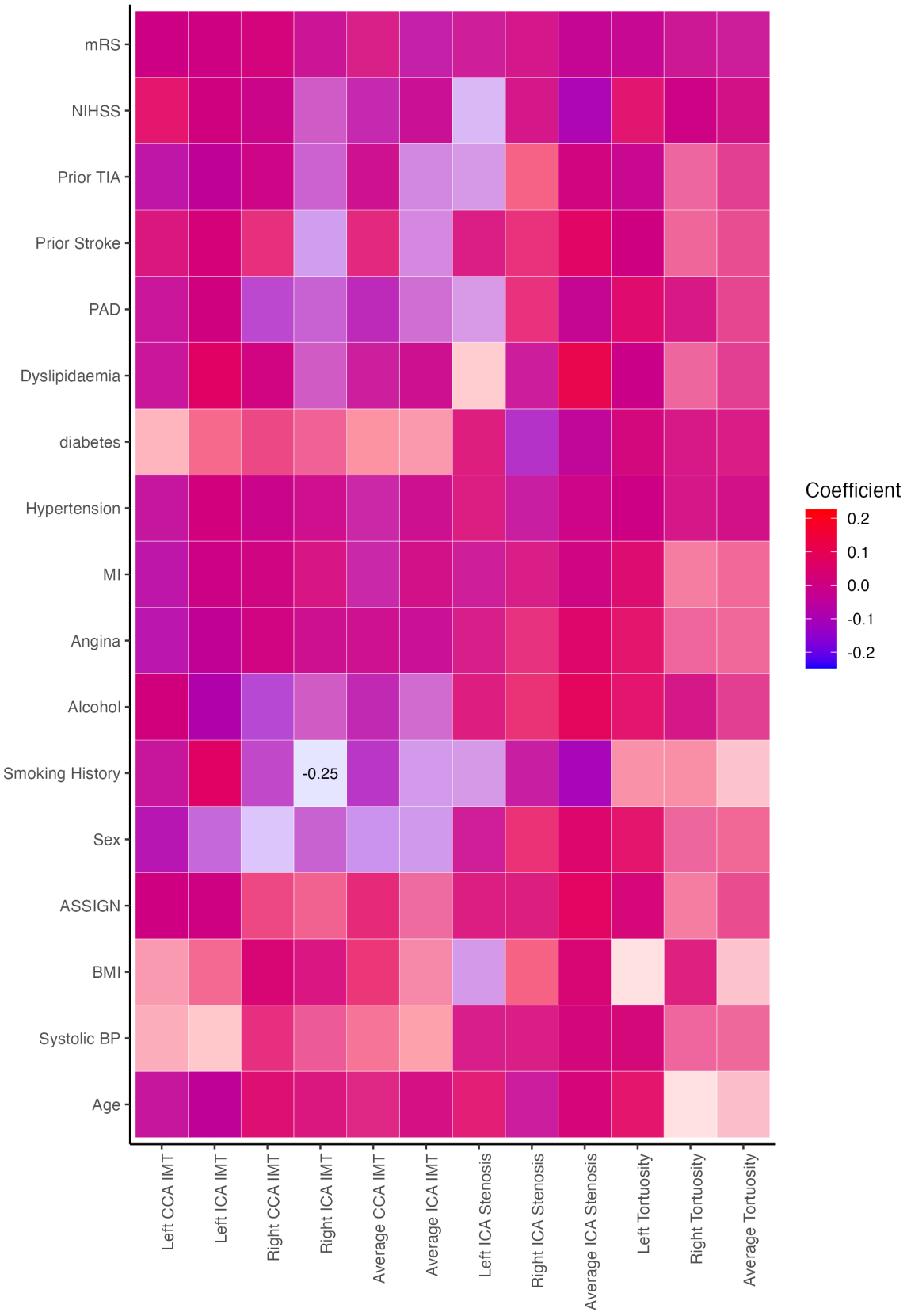

Figure 6.6: Correlation coefficient matrices of univariate relationships between dependent carotid variables and independent vascular risk factors and stroke severity scales. Colour represents the strength of the correlation. Correlations are either calculated using Spearman's rho or a Point-Biserial correlation, corrected by false

discovery rate (FDR). Values inside cells highlight the magnitude of the correlation if a significance threshold of $p<0.05$ is reached. BMI = body mass index, MI = myocardial infarction, PAD = peripheral artery disease, TIA = transient ischaemic attack, NIHSS = National Institute of Health Stroke Scale, mRS = modified Rankin Scale, CCA = external carotid artery, ICA = internal carotid artery, IMT = intima-media thickness. Stenosis was interpreted using % values.

6.5 Discussion

Results from this chapter highlights the relationships between carotid artery disease and ischaemic stroke. Initially, an investigation was employed to evaluate differences between those that were included in the study i.e., imaging positive, and those that were not, i.e., imaging negative. This analysis found some statistical differences between the two groups. Age, alcohol consumption, diagnosis of hypertension or dyslipidaemia, NIHSS and mRS scores were found to be significantly higher in the MRA-imaging negative cohort. These data may represent a source of disease spectrum bias. The low NIHSS and mRS scores indicate that the population recruited to the trial are minimally impaired. This may be reflective of the protocol requiring written consent from the affected individual, the length of the imaging and cognitive test protocols, and the frequency of ambulatory blood pressure management testing, all which may predispose to a less impaired cohort. However, these results are incidental findings, and do not reflect any clinical significance. The mean NIHSS scores of 1.06 and 1.77 both have standard deviation values greater than the mean (1.34 and 2.07, respectively). Whilst a significance value was reached in this analysis, as the scores have a minimum value of 0, I am confident that this analysis has occurred by chance and does not reflect any clinical significance.

Internal carotid artery stenosis measurements are routinely used in clinical practice to indicate treatment regimen. The data from this analysis demonstrates that the median vessel stenosis is approximately 33% across both left and right carotid arteries. According to the NASCET criteria, this is classified as non-significant stenosis, and not suitable for

surgical intervention. This gives additional evidence that the stroke cohort may be described as minimally impaired.

Spearman rank correlation coefficients or Point-Biserial coefficients were calculated between carotid variables and demographic data, corrected using the false discovery rate. Following correction for multiple comparisons, only smoking status correlated with the right carotid artery intima media thickness. No structural variable was correlated with all vascular risk factors. All correlations described in this analysis were within a -0.25 to 0.25 range; these relationships may be considered weak.

These data do not describe any relationships between IMT and vascular risk factors. Systolic blood pressure has been associated with increased IMT values in both hypertensive and normotensive people. This suggests that blood pressure may affect vessel wall thickening prior to hypertensive status[209]. The lack of relationship between IMT thickening and hypertensive status may be explained the use of anti-hypertensive medication, thus reducing the number of participants described as hypertensive at baseline. Whilst hypertension is commonly related to IMT measures[210,211], this would help explain why only systolic blood pressure would appear significantly related with an IMT measure. Participants with greater CCA IMT values were more likely to have a diagnosis of diabetes in our data, a common risk factor for stroke[201,203,204]. Our analysis did not consider differences between type 1 and type 2 diabetes. The results demonstrate that there are sex differences in the average common carotid IMT value. Men tended to have a greater IMT value than men. Men tend to have greater IMT values than women[212]; this may be representative of men of increased stature in comparison to women, though BMI was not related to any IMT measures. Our data demonstrates that prior stroke is correlated with increased internal carotid IMT. In the Rotterdam study, participants with greater common carotid IMT values were more likely to suffer from a stroke[76] .

The data in this chapter shows that after correction for multiple comparisons, decreasing cervical tortuosity was related with history of smoking. It is unknown why smoking status would only effect vessel tortuosity. Previous data has linked less tortuous retinal vessels with smoking status[213] A previous study has suggested that there are age-related changes in vessel tortuosity[214] which may reduce blood flow velocity. Age-related

changes in tortuosity may be a result of abnormal vascular elongation[79], including musculoskeletal changes caused by senescence or due to abnormal arteriogenesis as an embryo[215]. Additionally, hypertension or systolic blood pressure were not found to be significantly related to cervical tortuosity measures. However, carotid arteries are large, with lower flow resistance, potentially explaining why flow remodelling caused by hypertension does not cause a significant increase in cervical tortuosity[214]. It is posited that BMI may influence tortuosity via an increase in intra-abdominal hypertension. However, hypertension was not found to be significantly related to tortuosity, therefore BMI may influence tortuosity due to increased fatty tissue deposition around the arteries. Whilst this may affect hypertension, it may also influence shape of the carotid sheath, manipulating the direction of the carotid arteries[216]. This hypothesis is supported with previous observations of increased visceral fat contributing to aortic tortuosity in the thorax in stroke patients[217].

6.6 Summary

This chapter described the baseline measurements of carotid atherosclerosis, including ICA stenosis, CCA and ICA IMT, and extracranial carotid artery tortuosity. The mean stenosis value for this participant group was estimated at 33%, indicating a subclinical stenosis population. Few participants exhibited stenosed arteries above the 50% threshold for clinical intervention. Additionally, both CCA and ICA IMT values exhibited skewed data towards lesser IMT values. Carotid tortuosity was assessed at an average 0.068, or 6.8%. These data indicate that the extracranial carotid arteries are predominantly straight. Furthermore, this chapter aimed to evaluate the relationships between measurements of carotid artery disease and common vascular risk factors for recurrent ischaemic stroke. Data presented in this chapter showed that there are no risk factors that are associated with all vessel measurements. The risk factors assessed, including age, diagnosis of hypertension and smoking status, all described variable relationships with carotid artery disease. No more than 3 vascular risk factors were significantly associated with an arterial measurement. The next chapter will investigate the relationship between carotid artery disease and either small vessel disease or post-stroke cognition.

7 Investigating the relationship between carotid artery disease and white matter hyperintensities and between carotid artery disease and cognition in ischaemic stroke

7.1 Introduction

The results within the systematic review (Chapter 3) found that links between carotid artery disease and either small vessel disease or cognition in stroke are inconsistent. This is in part due to a lack of reporting standards for vascular risk factors or reporting of standard measurement protocols. Furthermore, insufficient statistics are often employed that fail to consider the role of vascular risk factors as confounding variables when determining the relationship between structural carotid artery measurements and brain findings/cognitive function.

Common reporting scales of white matter hyperintensities (WMH) include the Fazekas score and Schelten's scale[191,192]. These scores aim to determine the lesion burden of white matter beyond absolute volume and is determined upon the size and confluence of the lesions. Additionally, Fazekas score separates into periventricular and deep white matter lesions, as these are thought to have distinct aetiologies. Whilst deep WMH are related to chronic SVD, periventricular WMH may be related to a combination of physiological mechanisms including demyelination and SVD[191]. Conversely, the Schelten's scale is an analogous rating system to the Fazekas score. The scale is based around certain anatomical landmarks and aims to capture more lesion sites than the Fazekas score with the separate inclusion of basal ganglia and infratentorial lesions[192].

In Chapter 6, I found inconsistent univariate relationships between common vascular risk factors including age, dyslipidaemia and systolic BP and carotid artery disease. No one structural measurement correlated to any more than 3 vascular risk factors.

7.2 Aims and Objectives

This chapter aims to provide descriptions of the relationship between carotid artery disease, and either brain structure or cognitive function in ischaemic stroke, using data from the previous chapter to inform multivariate linear regression models. Objectives of this analysis are:

1. Describe the baseline measurements of brain volumes and small vessel diseases scores.
2. Calculate univariate correlations between the measurements of carotid artery disease (ICA stenosis, IMT of common and internal carotid arteries, and extracranial carotid artery tortuosity) and brain imaging metrics.
3. Estimate linear regression models between averaged measures of carotid artery disease and WMH, correcting for common vascular risk factors.
4. Define the baseline measurements of post-stroke cognitive function.
5. Assess univariate correlations between the measurements of carotid artery disease and tests of cognitive performance.
6. Estimate linear regression models between averaged measures of carotid artery disease and MoCA, as a score of global cognitive function, correcting for common vascular risk factors.

It is hypothesised that the measures of carotid artery disease will act as significant predictors of WMH burden or global cognitive function in univariate regression. In a multivariable model, % ICA stenosis will be the main predictor of WMH burden or global cognitive function.

7.3 Methods

7.3.1 Participant selection

The full participant selection was described in Chapter 4 but remains the same criteria for baseline and follow-up studies. All participants must have both carotid and brain imaging sequences and undergo a cognitive test battery.

7.3.2 Brain imaging measurements

All brain imaging measurements were evaluated elsewhere. Chapter 4 described the full brain image analysis protocol. Brain imaging measurements include volumetric analysis of tissues as well as the WMH scales.

7.3.3 Cognitive test protocol

The cognitive test protocol from XILO-FIST trial[182] is described fully in Chapter 4. Where the participant could not complete the neuropsychological battery, the MoCA and CESD-R were prioritised. Global cognition was assessed using two different methodologies. The MoCA was used as a test of global cognitive function.

7.3.4 Statistical analysis

Univariate correlations were evaluated using Spearman-rank correlation. For linear regression analysis, the R package finalfit() was used, displaying both univariable and multivariable linear regression. Log-transformed WMH was used for the linear regression analysis. All statistics were performed in R (version 4.1.3).

7.4 Results

7.4.1 Brain volumes and scores

The median (IQR) brain volumes and cerebral rating scales for the entire cohort can be found in Table 7.1. The median WMH volume was estimated at 12.62mm^3. A log transformation (previously applied_ estimated WMH volume at 2.54 (0.99) for the study population. Additionally, the WMH/ICV ratio was estimated at 0.009 (0.011).

Figures 7.1-7.5 represents the data spread of the WMH burden across the cohort, assessed by WMH volume (Figure 7.1) to Fazekas (Figures 7.2-7.3) and Schelten's scores (Figure 7.4-7.5). Most of the participants had minimal WMH burden, evidenced by the individual graphs with a positive skew.

Table 7.1: The brain imaging volumes and scores across treatment groups. Scores include the Fazekas score and Schelten's scales. WMH = white matter hyperintensities, ICV = intracranial volume, CSF = cerebrospinal fluid.

Variable	Median (IQR)
WMH volume (mm^3)	12.62 (13.98)
Log of WMH volume	2.54 (0.99)
Whole brain volume (mm^3)	1062.84 (124.84)
WMH/ICV ratio	0.009 (0.011)
Cortical grey matter volume (mm^3)	429.44 (53.52)
Subcortical grey matter volume (mm^3)	38.03 (6.30)
Cortical normal appearing white matter volume (mm^3)	424.25 (58.19)
CSF volume (mm^3)	309.39 (53.76)
Total Fazekas score	2 (1)
Periventricular Fazekas score	1 (1)
Deep white matter Fazekas score	1 (1)
Total Scheltens score	11 (10)
Periventricular Scheltens score	3 (1)
Deep white matter Scheltens score	6 (7)
Basal ganglia Scheltens score	0 (1)
Infratentorial Scheltens score	1 (2)

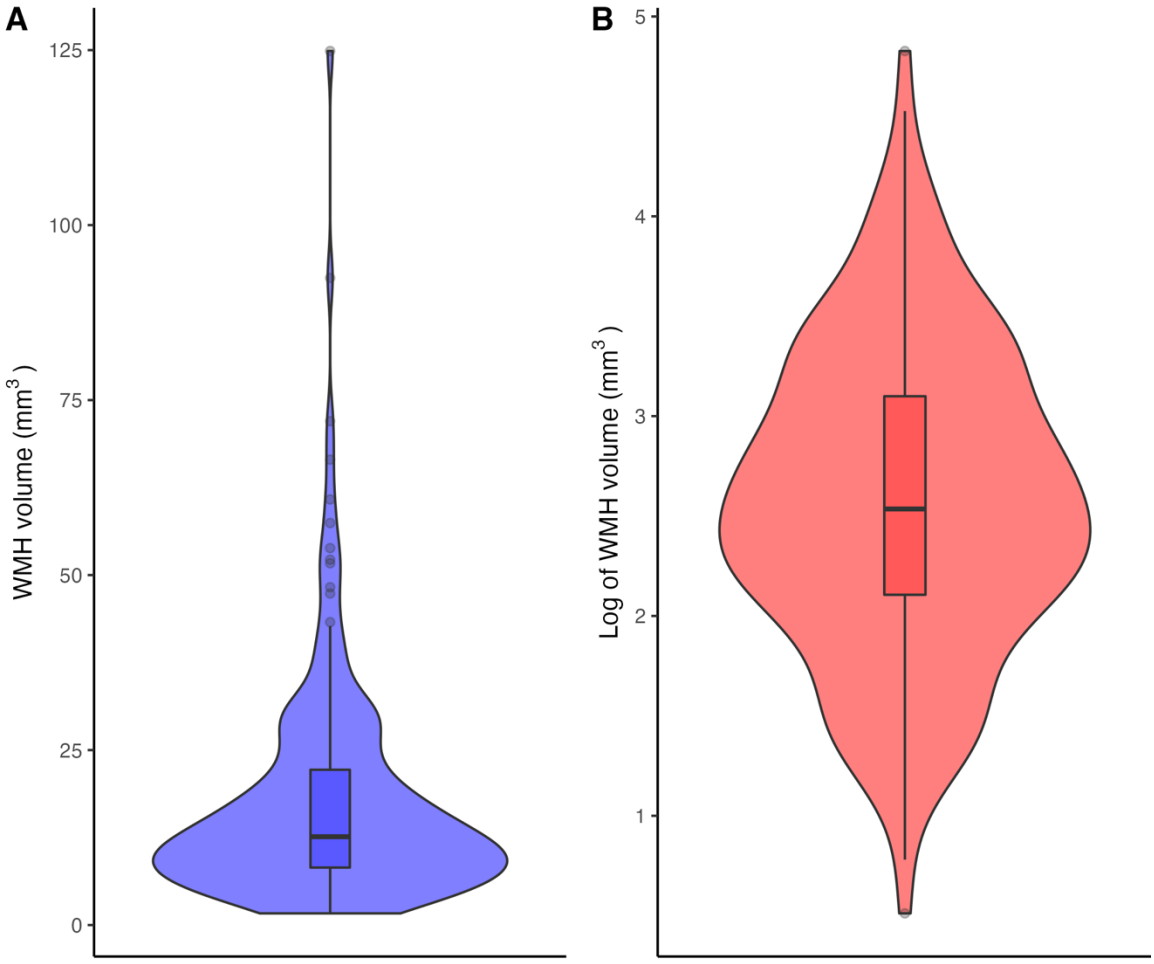

Figure 7.1: The white matter hyperintensity (WMH) volume (mm^3) in the XILO-FIST cohort. A: Absolute volumes of WMH; B: Log transformation of WMH volumes. The violin plot demonstrates the density of the data spread. The boxplot whiskers are set to 1.5x the interquartile range. Outliers are outside this range.

All Fazekas score values demonstrated a skew towards lesser WMH burden. The median total Fazekas score was 2; periventricular and deep white matter Fazekas scores exhibited a median score of 1 (Table 7.1, Figures 7.2 and 7.3).

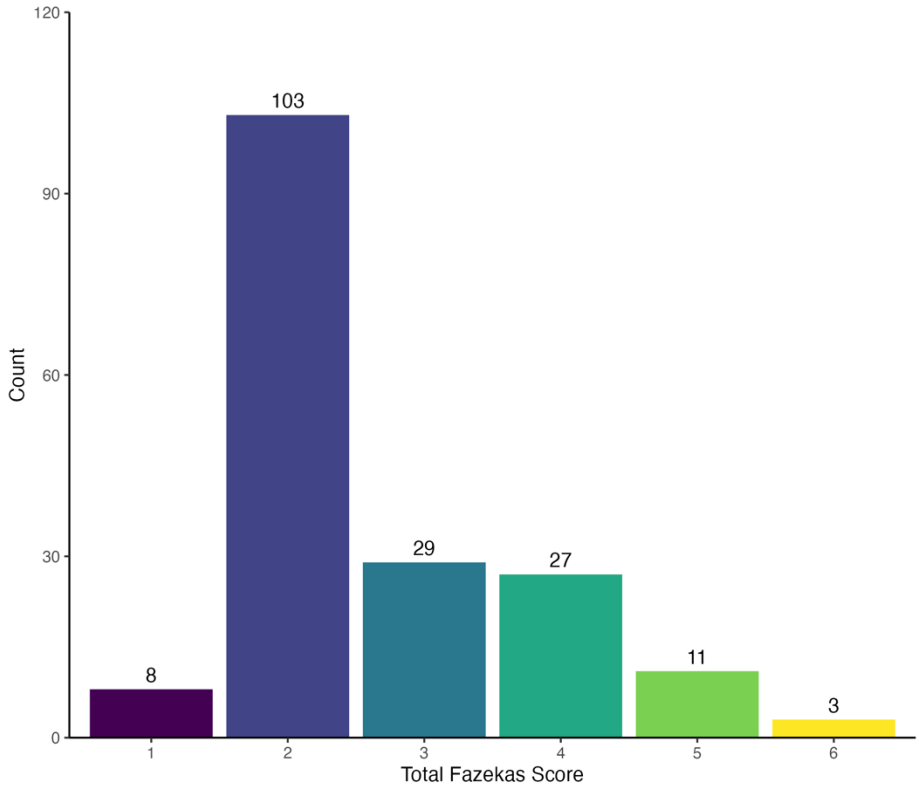

Figure 7.2: The total Fazekas score in the XILO-FIST cohort. The total score is the sum of the periventricular and deep white matter hyperintensity ratings.

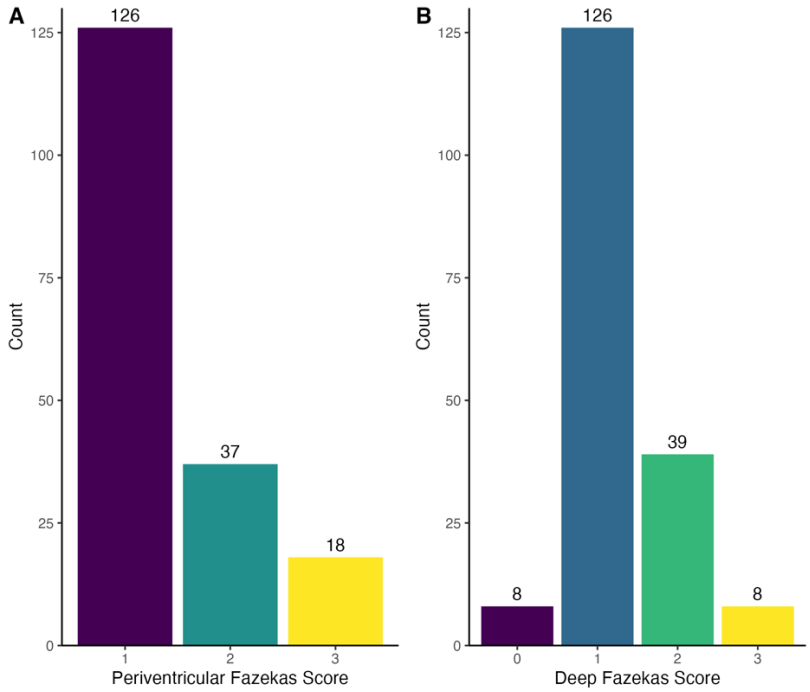

Figure 7.3: The Fazekas sub-scores in the XILO-FIST cohort. A: Periventricular white matter Fazekas score; B: Deep white matter Fazekas score.

Figures 7.4 and 7.5 demonstrate the spread of WMH burden summarised by the Schelten's scale. Like the Fazekas score, the Schelten's scale captured a positive skew of WMH burden, where the participants demonstrated lower scores across the four sub-regions of the scale. The median total Schelten's score is 11 (Table 7.1).

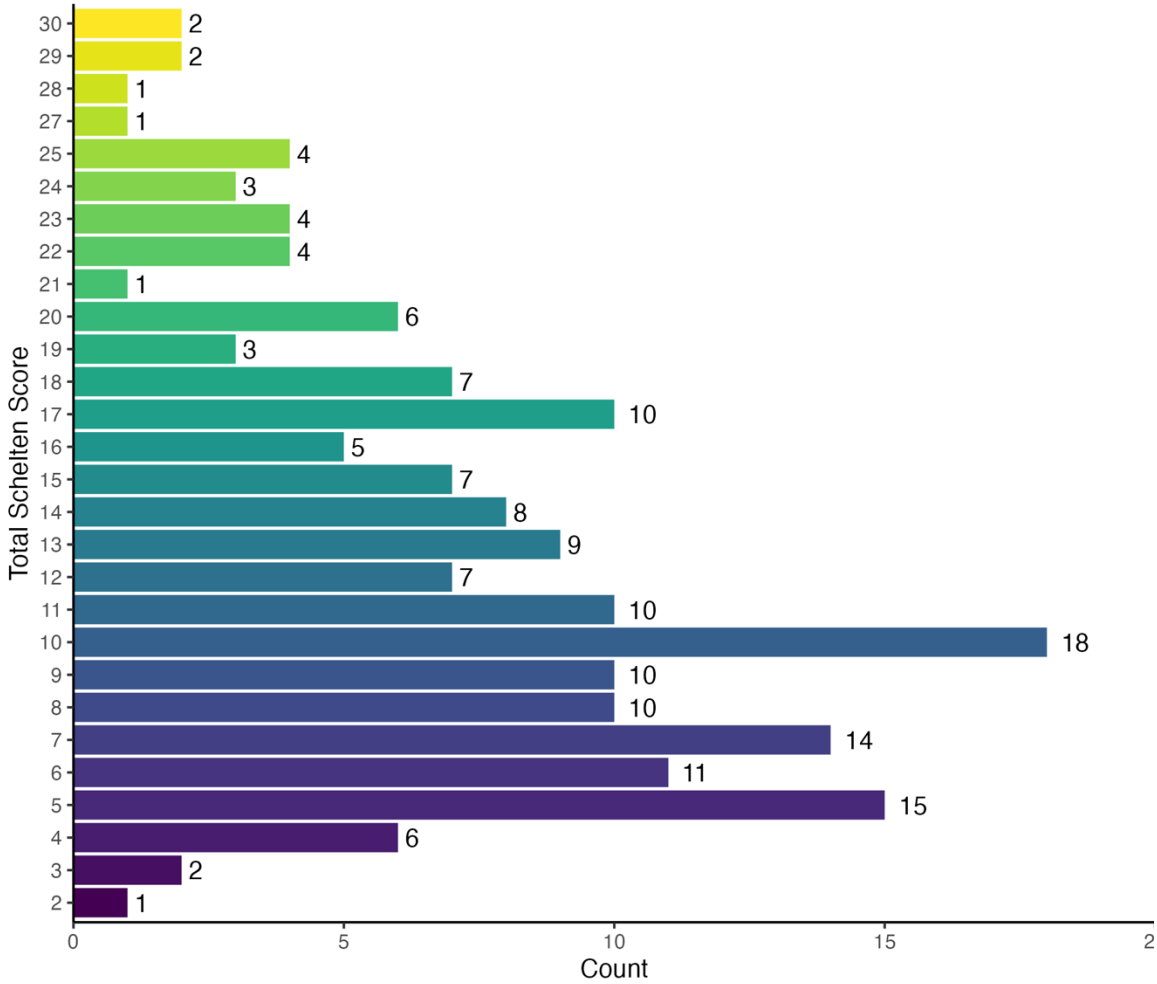

Figure 7.4: The total Schelten's scale scores in the study population. The total score is a summation of periventricular and deep white matter, and white matter around the basal ganglia and infratentorial regions.

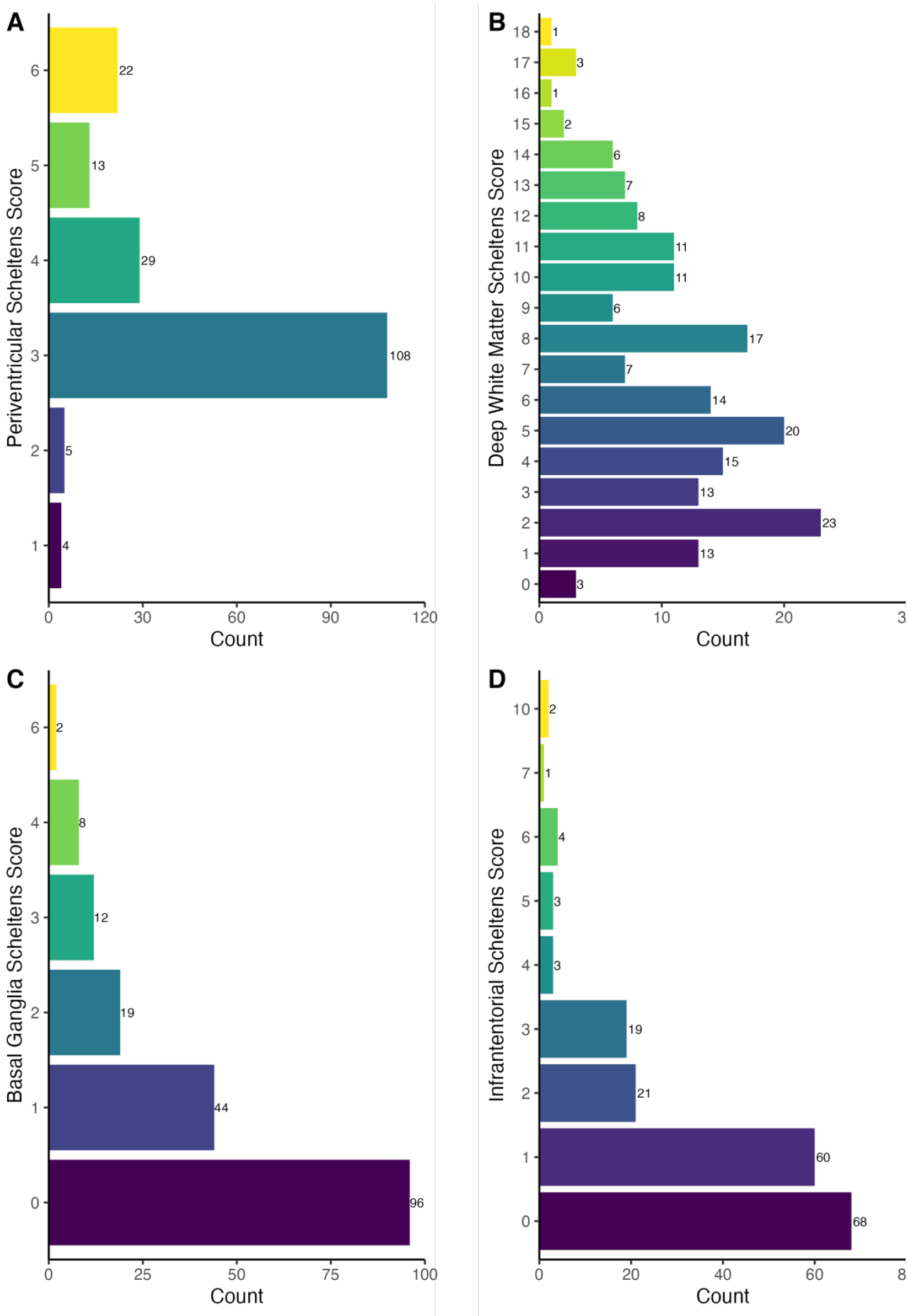

Figure 7.5: The Schelten's scale sub-scores in the XILO-FIST cohort. A: Score of periventricular white matter; B: Score of deep white matter; C: Score of white matter around the basal ganglia; D: Score of white matter in the infratentorial region.

7.4.2 Correlations between carotid artery disease and brain volumes/scores

Correlation coefficients were calculated using Spearman's rho, with adjusted p-values estimated by the false discovery rate (FDR). Data can be found in Tables 7.2-7.5, separated into univariate relationships between carotid structure and brain volumes or cerebral rating scales, respectively. Figure 7.6 describes these relationships, highlighting significance values where the probability is <0.05.

The right CCA IMT was found to significantly correlate with intracranial volume ($\rho = 0.303$, $p<0.001$), cortical grey matter ($\rho = 0.242$, $p = 0.005$), cortical normal appearing white matter ($\rho = 0.278$, $p<0.001$) and CSF ($\rho = 0.224$, $p = 0.009$); the average CCA IMT showed similar correlations with ICV ($\rho = 0.243$, $p = 0.021$), cortical grey matter ($\rho = 0.223$, $p = 0.024$) and cortical normal appearing white matter ($\rho = 0.205$, $p = 0.03$). No other correlations were found after post-hoc corrections.

Table 7.2: The univariate correlation coefficients of carotid variables versus white matter using Spearman ρ. CCA = common carotid artery, ICA = internal carotid artery, IMT = intima-media thickness, WMH = white matter hyperintensities, ICV = intracranial volume. *p<0.05, **p<0.001, corrected using False Discovery Rate (FDR).

	WMH		Log of WMH		Intracranial Volume		WMH/ICV Ratio	
	ρ	sig	ρ	sig	ρ	sig	ρ	sig
Left CCA IMT	0.131	0.210	0.131	0.210	0.146	0.210	0.117	0.210
Left ICA IMT	0.086	0.352	0.086	0.352	0.178	0.126	0.057	0.493
Right CCA IMT	0.132	0.118	0.132	0.118	0.303**	0.000**	0.093	0.250
Right ICA IMT	0.130	0.359	0.130	0.359	0.109	0.359	0.122	0.359
Average CCA IMT	0.161	0.088	0.161	0.088	0.243*	0.021*	0.132	0.153
Average ICA IMT	0.123	0.246	0.123	0.246	0.127	0.246	0.107	0.246
Left ICA Stenosis	-0.015	0.885	-0.015	0.885	0.048	0.885	-0.018	0.885
Right ICA Stenosis	-0.031	0.805	-0.031	0.805	0.109	0.390	-0.035	0.805
Average ICA Stenosis	-0.024	0.750	-0.024	0.750	0.086	0.647	-0.030	0.750
Left Carotid Tortuosity	0.104	0.672	0.104	0.672	0.064	0.827	0.100	0.672
Right Carotid Tortuosity	0.136	0.187	0.136	0.187	-0.051	0.595	0.136	0.187
Average Carotid Tortuosity	0.120	0.317	0.120	0.317	-0.026	0.816	0.120	0.317

Table 7.3: The univariate correlation coefficients of carotid variables versus other brain volume measurements using Spearman's ρ. CCA = common carotid artery; ICA = internal carotid artery; IMT = intima-media thickness; CSF = cerebrospinal fluid. *p<0.05 **p<0.001, corrected using False Discovery Rate (FDR).

	Cortical Grey Matter		Subcortical Grey Matter		Cortical Normal Appearing White Matter		CSF	
	ρ	sig	ρ	sig	ρ	sig	ρ	sig
Left CCA IMT	0.154	0.210	0.089	0.321	0.122	0.210	-0.030	0.718
Left ICA IMT	0.160	0.126	0.088	0.352	0.169	0.126	0.143	0.150
Right CCA IMT	0.242*	0.005*	0.140	0.115	0.278**	0.000**	0.224*	0.009*
Right ICA IMT	0.103	0.359	0.024	0.766	0.091	0.374	0.069	0.463
Average CCA IMT	0.223*	0.024*	0.104	0.226	0.205*	0.030*	0.101	0.226
Average ICA IMT	0.117	0.246	0.028	0.741	0.112	0.246	0.106	0.246
Left ICA Stenosis	0.011	0.885	-0.046	0.885	0.033	0.885	0.062	0.885
Right ICA Stenosis	0.105	0.390	0.196	0.070	0.093	0.390	0.007	0.925
Average ICA Stenosis	0.072	0.647	0.057	0.647	0.066	0.647	0.057	0.647
Left Carotid Tortuosity	0.025	0.827	-0.028	0.827	0.038	0.827	0.017	0.827
Right Carotid Tortuosity	-0.077	0.565	-0.140	0.187	-0.059	0.595	-0.007	0.933
Average Carotid Tortuosity	-0.056	0.810	-0.114	0.317	-0.034	0.816	-0.018	0.816

Table 7.4: The univariate correlation coefficients between carotid variables and Fazekas scores using Spearman's ρ. CCA = common carotid artery; ICA = internal carotid artery; IMT = intima-media thickness *p<0.05 **p<0.01, corrected using False Discovery Rate (FDR).

	Periventricular Fazekas Score		Deep Fazekas Score		Total Fazekas Score	
	ρ	sig	ρ	sig	ρ	sig
Left CCA IMT	0.055	0.502	0.129	0.333	0.090	0.407
Left ICA IMT	0.006	0.945	0.131	0.345	0.055	0.764
Right CCA IMT	-0.008	0.918	0.088	0.822	0.037	0.918
Right ICA IMT	0.015	0.854	0.110	0.525	0.065	0.640
Average CCA IMT	0.032	0.696	0.126	0.378	0.082	0.485
Average ICA IMT	-0.019	0.825	0.142	0.267	0.052	0.800
Left ICA Stenosis	-0.024	0.786	0.047	0.786	0.021	0.786
Right ICA Stenosis	0.013	0.862	-0.077	0.862	-0.042	0.862
Average ICA Stenosis	-0.030	0.870	-0.013	0.870	-0.018	0.870
Left Carotid Tortuosity	0.023	0.765	0.086	0.765	0.031	0.765
Right Carotid Tortuosity	0.083	0.287	0.127	0.264	0.105	0.264
Average Carotid Tortuosity	0.067	0.380	0.104	0.380	0.074	0.380

Table 7.5: The univariate correlation coefficients of carotid variables versus Scheltens score using Spearman's ρ. CCA = common carotid artery; ICA = internal carotid artery; IMT =intima-media thickness. * p<0.05 **p<0.01, corrected using False Discovery Rate (FDR).

	Periventricular Scheltens Score		White Matter Scheltens Score		Basal Ganglia Scheltens Score		Infratentorial Scheltens Score		Total Scheltens Score	
	ρ	sig	ρ	sig	ρ	sig	ρ	sig	ρ	sig
Left CCA IMT	0.106	0.238	0.086	0.289	0.142	0.238	0.111	0.238	0.120	0.238
Left ICA IMT	0.103	0.540	0.021	0.805	0.117	0.540	0.056	0.699	0.049	0.699
Right CCA IMT	0.058	0.498	0.060	0.498	0.176	0.140	0.055	0.498	0.083	0.498
Right ICA IMT	0.106	0.240	0.125	0.208	0.159	0.138	0.086	0.293	0.156	0.138
Average CCA IMT	0.092	0.268	0.099	0.268	0.140	0.268	0.104	0.268	0.125	0.268
Average ICA IMT	0.102	0.375	0.060	0.475	0.169	0.210	0.080	0.424	0.102	0.375
Left ICA Stenosis	0.000	1.000	-0.031	1.000	-0.014	1.000	0.026	1.000	-0.019	1.000
Right ICA Stenosis	-0.007	0.926	-0.026	0.926	0.019	0.926	0.033	0.926	-0.020	0.926
Average ICA Stenosis	-0.010	0.898	-0.035	0.898	-0.010	0.898	0.023	0.898	-0.028	0.898
Left Carotid Tortuosity	0.089	0.836	0.043	0.836	0.016	0.836	-0.041	0.836	0.021	0.836
Right Carotid Tortuosity	0.097	0.305	0.128	0.305	0.090	0.305	-0.003	0.971	0.114	0.305
Average Carotid Tortuosity	0.101	0.487	0.092	0.487	0.053	0.487	-0.055	0.487	0.064	0.487

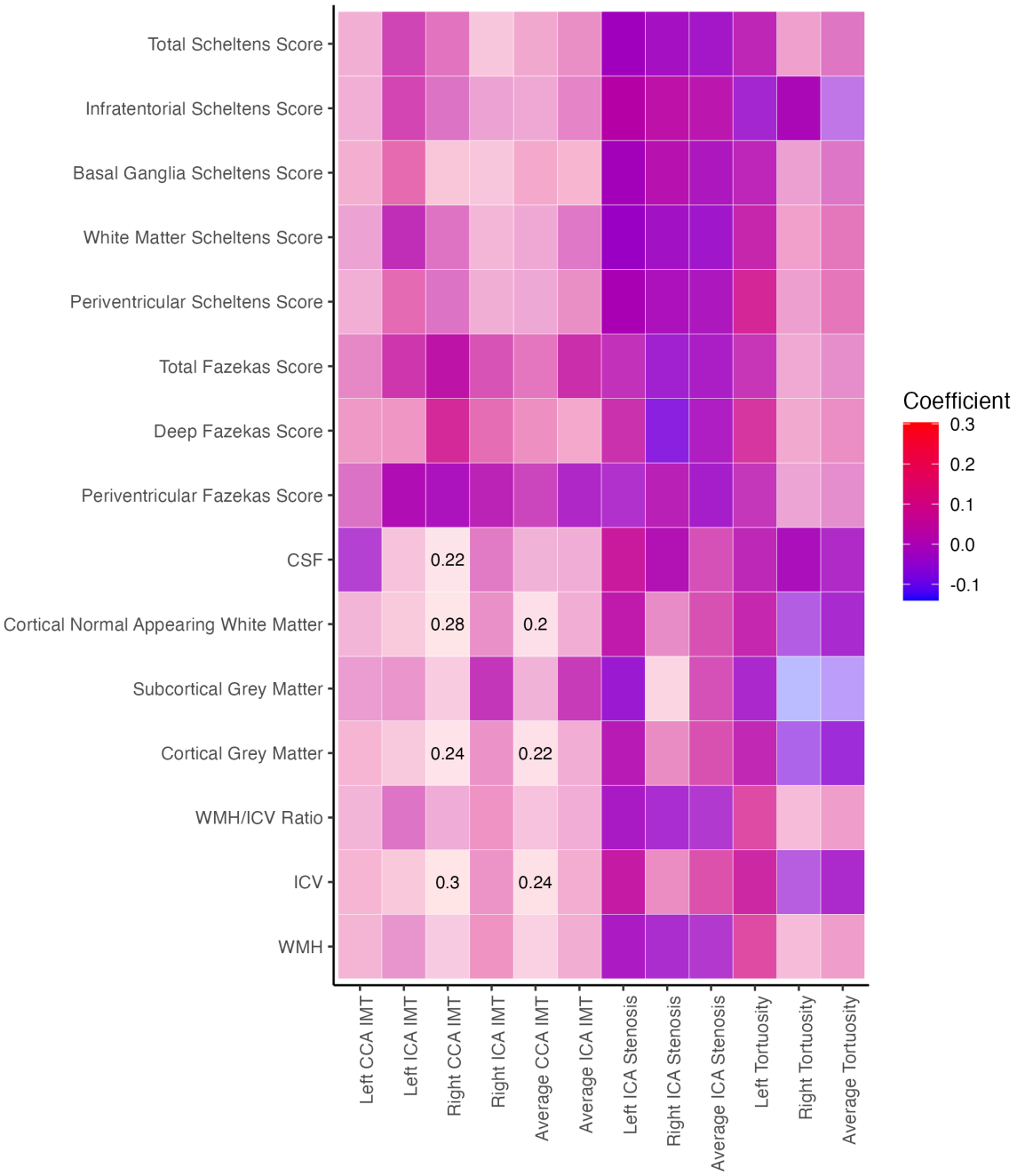

Figure 7.6: The correlation matrix of carotid variables versus brain volumes and scores. Colour gradation represents the direction and magnitude of the correlation coefficient. WMH: white matter hyperintensities, GM: grey matter, WM: white matter, ICV: intracranial volume, CSF: cerebrospinal fluid; PV: periventricular; BG: basal ganglia; IF: infratentorial; CCA: common carotid artery; ICA: internal carotid artery; IMT: intima-media thickness. Significant correlation coefficients are printed in their respective tiles.

7.4.3 General linear modelling of carotid artery disease and WMH

Univariable and multivariable models have been made for the following averaged carotid disease measurements: CCA IMT, ICA IMT, ICA stenosis and cervical carotid artery tortuosity with respect to the log-transformed WMH. Within the multivariable regression model, covariates of standard vascular risk factors were added. These risk factors are age, sex, smoking history, diagnoses of hypertension, diabetes, dyslipidaemia, and prior stroke/TIA. These data can be found in Table 7.6.

Table 7.6: Regression analysis exploring predictive factors in WMH burden in ischaemic stroke. Confidence intervals are reported in parentheses. CCA = common carotid artery, ICA = internal carotid artery, IMT = intima-media thickness * indicates significance $p<0.05$; ** indicates a significance $p<0.001$. β estimates are standardised.

Dependent: WMH Volume		Coefficient (Univariable)	Coefficient (Multivariable)
Average Tortuosity	[0.4,27.8]	0.80 (0.26 to 1.34, p=0.004)*	0.07 (-0.53 to 0.66, p=0.820)
Average ICA Stenosis	[0.1,85.2]	-0.04 (-0.20 to 0.12, p=0.625)	-0.06 (-0.22 to 0.11, p=0.495)
Average ICA IMT	[19.4,83.7]	0.06 (-0.17 to 0.29, p=0.595)	-0.10 (-0.35 to 0.15, p=0.423)
Average CCA IMT	[22.3,116.6]	0.08 (-0.05 to 0.20, p=0.215)	0.11 (-0.06 to 0.27, p=0.196)
Age	[50.1,87.5]	0.60 (0.32 to 0.88, p<0.001)*	0.58 (0.30 to 0.86, p<0.001)**
Sex	Female	-	-
	Male	-0.93 (-6.27 to 4.42, p=0.733)	-2.07 (-7.25 to 3.11, p=0.431)
Smoking History	Current	-	-
	Former	0.22 (-6.66 to 7.10, p=0.949)	-0.71 (-7.77 to 6.36, p=0.843)
	Never	-3.40 (-9.94 to 3.15, p=0.307)	-6.79 (-13.76 to 0.18, p=0.056)
Hypertension	No	-	-
	Yes	-2.21 (-7.07 to 2.65, p=0.371)	-0.58 (-5.75 to 4.59, p=0.824)
Diabetes	No	-	-
	Yes	1.18 (-4.66 to 7.03, p=0.690)	-1.78 (-8.07 to 4.51, p=0.576)
Dyslipidaemia	No	-	-
	Yes	0.24 (-5.32 to 5.80, p=0.932)	1.16 (-5.34 to 7.66, p=0.724)
Prior TIA	No	-	-
	Yes	10.95 (2.87 to 19.03, p=0.008)*	-1.48 (-10.61 to 7.64, p=0.748)
Prior Stroke	No	-	-
	Yes	0.86 (-9.21 to 10.92, p=0.867)	-2.96 (-13.12 to 7.20, p=0.565)

Log-likelihood = -508.47, AIC = 1046.9, $R^2 = 0.19$, Adjusted $R^2 = 0.1$

In the data described in Table 7.6, a maximum of 19% variance (adjusted 10%) was captured in a model including averaged measures of carotid artery disease and common vascular risk factors. Additionally, whilst average tortuosity was a significant factor in univariable analysis (coefficient 0.80 (0.26 to 1.34, p=0.004)), this disease measure was not included in the multivariable model. Only age was a significant risk factor in the multivariable model (0.58 (0.30 to 0.86, p<0.001)).

7.4.4 Cognitive test scores

Cognitive test scores are found in Table 7.7. The median MoCA score was 27 (IQR 4) for the whole cohort. Other scores are measured by number of correct responses. The score for the Trail Making Tests is measured in seconds. The Centre for Epidemologic Depression scale (CESD-R) is measured in a 5-point Likert scale.

Table 7.7: A summary of cognitive test scores recorded at baseline in all participants. Where a participant could not complete the full neuropsychological battery, the Montreal Cognitive Assessment was preferred.

Variable	Median (IQR)
MoCA	27 (4)
Animal Naming Test	18 (7)
Controlled Oral Word Association Test	35 (16)
Letter Digit Coding Test Total	32 (25)
Hopkins Verbal Learning Test	21 (8)
Hopkins Verbal Learning Test (Delayed recall)	8 (3)
Trail Making Test (Part A)	40 (24.25)
Trail Making Test (Part B)	70 (42)
Centre for Epidemiologic Depression Scale Revised	10 (14)

7.4.5 Correlations between carotid artery disease and cognitive test scores

Correlation coefficients were calculated using Spearman's ρ, with p-values adjusted using false discovery rate (FDR). Data can be found in Tables 7.8 and 7.9, separated into univariate relationships between carotid artery disease and various cognitive tests. Figure 7.7 demonstrates the correlation matrices. The only univariate correlation after post-hoc corrections was in the Animal Naming Test. This correlation was found with the right carotid artery tortuosity ($\rho = -0.219$, $p = 0.04$). No other correlations were found to be significant.

Table 7.8: The univariate correlation coefficients of carotid variables versus cognitive function tests using Spearman's ρ. CCA = common carotid artery, ICA = internal carotid artery, IMT = intima-media thickness. CESD-R = Centre for Epidemiologic Studies Depression Scale – Revised. *p<0.05, **p<0.01, corrected using False Discovery Rate (FDR).

	Montreal Cognitive Assessment		Animal Naming Test		Controlled Oral Word Association		Letter Digit Coding		CESD-R	
	ρ	sig	ρ	sig	ρ	sig	ρ	sig	ρ	sig
Left CCA IMT	0.119	0.552	0.031	0.976	-0.003	0.976	-0.081	0.729	0.108	0.552
Left ICA IMT	0.039	0.844	0.021	0.844	-0.070	0.844	0.063	0.844	0.026	0.844
Right CCA IMT	0.099	0.759	-0.001	0.989	0.065	0.801	-0.062	0.801	0.028	0.879
Right ICA IMT	0.083	0.549	0.180	0.261	-0.092	0.549	0.029	0.783	0.027	0.783
Average CCA IMT	0.110	0.606	0.021	0.979	0.036	0.979	-0.106	0.606	0.080	0.704
Average ICA IMT	0.073	0.686	0.122	0.492	-0.141	0.492	0.029	0.794	-0.022	0.794
Left ICA Stenosis	0.008	0.927	-0.021	0.927	-0.007	0.927	0.050	0.927	-0.048	0.927
Right ICA Stenosis	0.094	0.392	0.185	0.153	0.046	0.633	0.138	0.277	-0.121	0.277
Average ICA Stenosis	0.056	0.956	0.059	0.956	-0.010	0.956	0.080	0.956	-0.124	0.954
Left Carotid Tortuosity	0.054	0.843	-0.034	0.843	0.024	0.843	-0.039	0.843	-0.015	0.843
Right Carotid Tortuosity	-0.033	0.858	-0.219*	0.045	-0.111	0.265	-0.122	0.265	-0.018	0.921
Average Carotid Tortuosity	0.030	0.836	-0.155	0.423	-0.046	0.821	-0.088	0.587	0.011	0.888

Table 7.9: Further univariate correlation coefficients of carotid variables versus cognitive function tests using Spearman's ρ. CCA = common carotid artery, ICA = internal carotid artery, IMT = intima-media thickness, corrected using False Discovery Rate (FDR)

	Hopkins Verbal Learning		Hopkins Verbal Learning – Delayed Recall		Trail Making Test Part A		Trail Making Test Part B	
	ρ	sig	ρ	sig	ρ	sig	ρ	sig
Left CCA IMT	0.053	0.925	-0.010	0.976	-0.004	0.976	0.112	0.552
Left ICA IMT	0.037	0.844	-0.065	0.844	-0.055	0.844	-0.017	0.844
Right CCA IMT	-0.030	0.879	-0.106	0.759	0.023	0.879	0.093	0.759
Right ICA IMT	0.145	0.288	0.135	0.288	0.023	0.783	0.074	0.552
Average CCA IMT	0.002	0.979	-0.071	0.704	-0.008	0.979	0.139	0.606
Average ICA IMT	0.117	0.492	0.075	0.686	-0.036	0.794	0.033	0.794
Left ICA Stenosis	-0.035	0.927	-0.113	0.922	-0.073	0.927	0.098	0.922
Right ICA Stenosis	0.056	0.633	0.118	0.277	-0.026	0.732	-0.045	0.633
Average ICA Stenosis	0.016	0.956	0.004	0.956	-0.036	0.956	0.027	0.956
Left Carotid Tortuosity	-0.028	0.843	-0.036	0.843	0.050	0.843	0.019	0.843
Right Carotid Tortuosity	-0.113	0.265	-0.109	0.265	0.105	0.265	-0.005	0.949
Average Carotid Tortuosity	-0.075	0.587	-0.083	0.587	0.079	0.587	0.025	0.836

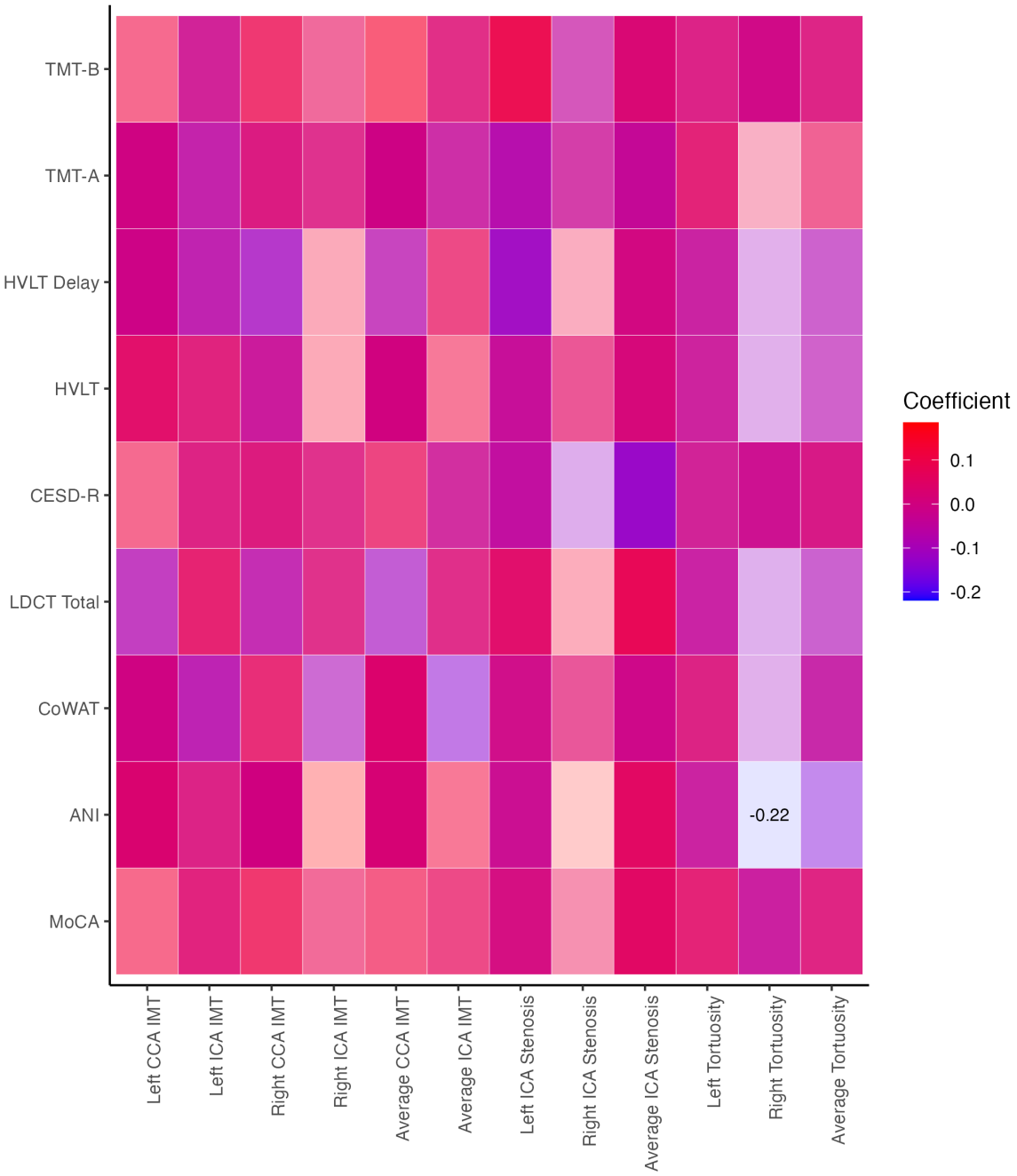

Figure 7.7: The correlation matrix of carotid variables versus cognitive function tests. Colour gradation represents the direction of the correlation coefficient. MoCA = Montreal Cognitive Assessment, ANI = Animal Naming Test, CoWAT = Controlled Word Association Test, LDCT = Letter Digit Coding Test, CESD-R = Centre for Epidemiologic Scale Depression – Revised, HVLT = Hopkins Verbal Learning Test, TMT = Trail Making Test. Significant correlation coefficients are printed in their respective tiles.

7.4.6 General linear modelling of carotid artery disease and cognition

Univariable and multivariable models have been made for the following averaged carotid disease measurements: CCA IMT, ICA IMT, ICA stenosis and cervical carotid artery tortuosity with respect to the MoCA as a measure of global cognitive function. Within the multivariable regression model, covariates of standard vascular risk factors were added. These risk factors are age, sex, smoking history, diagnoses of hypertension, diabetes, dyslipidaemia, and prior stroke/TIA. These data can be found in Table 7.10.

Table 7.10: Regression analysis exploring predictive factors in MoCA performance as a function of global cognition in ischaemic stroke. Confidence intervals are reported in parentheses. CCA = common carotid artery, ICA = internal carotid artery, IMT = intima-media thickness * indicates significance $p<0.05$; ** indicates a significance $p<0.001$. β estimates are standardised.

Dependent: MoCA		Coefficient (univariable)	Coefficient (multivariable)
Average Tortuosity	[0.4,27.8]	0.03 (-0.06 to 0.13, p=0.483)	0.13 (-0.00 to 0.26, p=0.051)
Average ICA Stenosis	[0.1,85.2]	0.01 (-0.02 to 0.04, p=0.366)	0.03 (-0.01 to 0.06, p=0.118)
Average ICA IMT	[19.4,83.7]	0.00 (-0.04 to 0.04, p=0.912)	-0.01 (-0.07 to 0.04, p=0.681)
Average CCA IMT	[22.3,116.6]	0.02 (-0.01 to 0.05, p=0.119)	0.01 (-0.02 to 0.05, p=0.465)
Age	[50.1,87.5]	-0.03 (-0.08 to 0.02, p=0.266)	-0.05 (-0.11 to 0.01, p=0.092)
Sex	Female	-	-
	Male	-0.24 (-1.16 to 0.68, p=0.613)	-0.45 (-1.58 to 0.67, p=0.427)
Smoking History	Current	-	-
	Former	0.53 (-0.66 to 1.71, p=0.382)	0.65 (-0.88 to 2.19, p=0.401)
	Never	0.80 (-0.33 to 1.93, p=0.163)	0.78 (-0.74 to 2.29, p=0.314)
Hypertension	No	-	-
	Yes	0.10 (-0.74 to 0.93, p=0.823)	0.09 (-1.04 to 1.21, p=0.880)
Diabetes	No	-	-
	Yes	0.18 (-0.82 to 1.19, p=0.720)	-0.04 (-1.41 to 1.33, p=0.951)
Dyslipidaemia	No	-	-
	Yes	0.26 (-0.70 to 1.21, p=0.600)	0.63 (-0.78 to 2.05, p=0.377)
Prior TIA	No	-	-
	Yes	-0.22 (-1.64 to 1.20, p=0.756)	1.13 (-0.86 to 3.12, p=0.262)
Prior Stroke	No	-	-
	Yes	-1.59 (-3.31 to 0.12, p=0.069)	-1.23 (-3.45 to 0.98, p=0.272)
Log-likelihood = -310.37, AIC = 650.7, R^2 = 0.11, Adjusted R^2 = 0.015			

In the data described in Table 7.10, a maximum of 11% variance (adjusted R^2 1.15%) was captured in a model including averaged measures of carotid artery disease and common vascular risk factors. Additionally, both univariable and multivariable regression failed to capture any relationship between a carotid structure measure and global cognitive function. No vascular risk factors contributed significantly to the models, which were all insignificant.

7.5 Discussion

These data demonstrate various and inconsistent relationships between carotid artery disease measurements and brain volumes and scores or cognitive function. Volumetric scores of WMH revealed small volumes of SVD burden. In previous studies, WMH volume has been shown to exhibit significant ranges[218,219], though the data presented here are in line with these other studies. The visual rating scores demonstrated that the WMH burden is diffuse. In Figure 7.3, the Fazekas scores of periventricular and deep white matter both demonstrate presence of WMH, where data was skewed to the lower scores, demonstrating small caps or multiple focal lesions respectively. Moreover, the Scheltens scores highlighted diffusivity in WMH location, evidenced by the variability across the different regions (Figure 7.5).

However, univariate associations for brain volumes and scores describe inconsistent relationships with structural carotid variables. Tables 7.2-7.5 and Figure 7.6 highlight that whilst most univariate correlations are insignificant, some relationships are found. These data describe weak positive relationships between CCA IMT values and brain volumes. This would suggest that greater intima-media thickness of the right CCA is correlated with larger volumes of cortical normal appearing white matter, intracranial volume, CSF and cortical grey matter. These relationships are unexpected and at odds with our understanding of effects of carotid atherosclerosis and brain volumes. In previous studies, increased IMT values were found to significantly relate with decreased brain volumes[220]. In a stroke-free cohort, larger intima-media thickness was associated with greater WMH volume ($\beta = 0.046$ per SD carotid IMT, $p = 0.04$) independent of demographic and vascular risk factor data. These data, much like the data presented here,

used log-transformed WMH volumes that were adjusted for head size[220] Moreover, higher carotid IMT was found to be significantly associated with both whole brain WMH volume ($\beta = 0.77$, $p = 0.01$) and periventricular white matter volume ($\beta = 0.80$, $p = 0.008$)[221]. Data in this chapter failed to demonstrate univariate linear regression between CCA or ICA IMT and WMH burden.

Differences between the data presented and the literature may be due to variation in methods used to measure intima-media thickness; the methods described in Chapter 4 are a method adapted to suit the TOF data, compared with more standard measurements from carotid Doppler ultrasound. Furthermore, our data separates the IMT into common carotid and internal carotid arteries; most studies only measure IMT around the common carotid arteries, close to the bifurcation. However, data from the CARDIA Brain study found that carotid IMT was not associated with white matter hyperintensities. It was found that greater IMT associated with decreased total cerebral blood flow ($\beta = -1.26$, $p = 0.04$) and cerebral blood flow in grey matter ($\beta = -1.36$, $p = 0.04$) after adjusting for age, sex, education, race and total brain volume[222].

The Spearman rank correlation data fails to describe any significant relationships with carotid artery disease and cerebral rating scales. No sub-scores were found to exhibit a significant relationship. This may reflect a weakness of using visual rating scales in the place of more quantitative methods. Single item scales, like Fazekas/Schelten's scales divide wide continuous variables into a few levels, representing thick bands of continuum in one score, which may reduce reliability[223].

Moreover, whilst there may be some unexpected relationships between carotid artery disease and brain volumes, no overarching relationships can be found with functional measures i.e., no relationship between carotid artery disease and global cognition measured by MoCA. Only the right carotid tortuosity negatively correlated with the Animal Naming Test; thus, that as tortuosity increased, the performance in this task would decrease (Table 7.8, Figure 7.7). Healthy population-based studies have found links between carotid stenosis and cognitive function. The Cardiovascular Healthy Study found in participants with no history of stroke, 32 participants with stenosis $\geq$ 75% in the left ICA

was associated with cognitive impairment, assessed by Mini-Mental State Examination (OR 6.7, CI = 2.4 – 18.1) when compared with no stenosis. Furthermore, IMT measurement of the left CCA was associated with cognitive impairment in univariate analysis, but failed after adjustment for common risk factors[224]. In the Tromsø study, carotid IMT and plaque features were analysed with cognitive function. In multivariable regression models, the presence of carotid plaques was associated with poorer performance in verbal memory ($p = 0.01$) and digit-symbol coding test ($p = 0.03$). Additional analysis found that the number of plaques and total area associated with poorer verbal memory performance. However, CCA IMT was not found to significantly relate to cognitive test scores[225]. Previous data from the Tromsø study found reduced performance in attention and memory in participants with asymptomatic carotid stenosis[226]. These data suggest that asymptomatic stenotic disease may be an independent risk factor for cognitive impairment. Our data may not demonstrate any relationship with cognitive function, potentially due to lower sample sizes. Population-based studies are often much larger than clinical trials. In the Cardiovascular Health Study, whilst only 32 participants with high grade stenosis were evaluated, this is higher than XILO-FIST, which only included 3 participants with high grade stenosis in the left ICA. Furthermore, my analysis here did not split participants into subgroups based on their stenotic range due to the skew of the population into subclinical range (<50%). The Tromsø study included over 4000 participants. This may suggest larger sample sizes are needed to find any significant relationships.

The linear regression models were generated separately for univariate and multivariate measurements. These were generated due to the lack of data supporting hypotheses of carotid structure measurements versus SVD features or cognitive functioning. Our data demonstrate that there may be a small, though significant relationships between carotid artery tortuosity and log of WMH (which was corrected for intracranial volume) in a univariate model; this relationship did not survive in the multivariate regression. These data captured 19% variance (assessed with R^2).

Carotid artery tortuosity demonstrated a significant relationship ($p = 0.004$) with log transformed WMH volume in the linear regression analysis. These data suggest that increasing carotid artery tortuosity is related with WMH volume. These data are in line with other publications, including Shang et. al. Relative to controls i.e., no history of

stroke, ischaemic stroke patients (classified as large artery atherosclerotic type by TOAST criteria) exhibited increased neck artery tortuosity at various segments (common carotid, internal carotid, extracranial internal carotid artery, and vertebral artery) in both paired arteries. Additionally, participants with higher tortuosity values in the carotid arteries were associated with increased WMH deposition (left extracranial ICA, $p = 0.07$; left carotid artery, $p = 0.005$; left CCA, $p = 0.003$)[227]. However, our data do not demonstrate such univariate relationships. In an earlier publication, linear regression modelling was performed on internal carotid artery tortuosity and WMH, finding significant associations between increased tortuosity and WMH burden in the left ICA ($\beta = 20.701$, $p<0.001$) and right ICA ($\beta = 11.223$, $p = 0.016$)[228]. These data differ significantly in the magnitude of the estimate. This is due to differences in the calculation of tortuosity. The data presented in this chapter calculated extracranial tortuosity i.e., including the common carotid artery and internal carotid artery across the entire image volume. This study investigated the intracranial portion of the internal carotid artery, which are more tortuous due to the cerebral anatomy and anastomosing with the Circle of Willis. Furthermore, in the linear regression reported in this chapter, the average tortuosity values were used i.e., mean of left and right carotid arteries for each participant.

The regression models were corrected for common risk factors for ischaemic stroke, including separate covariates for prior ischaemic stroke and TIA. No regression models of cognitive function were found to be effective. The low R^2 value in the regression statistics suggests either missing values that will account for greater variance, or the relationship between carotid and brain variables is too weak, and the inclusion of other model fit descriptors (log-likelihood, AIC) may provide further evidence of poor regression fit. However, these data make assumptions. The average values of all carotid variables were used, regardless of side (left or right). Some studies e.g., the Cardiovascular Health Study separate arteries based on the which side of the cervical spine[224]. I did not separate this data; this was due to lack of brain structure data separated by cerebral hemisphere. It was considered if this data was available, different relationships may be found.

7.6 Summary

This chapter aimed to determine the relationship between carotid artery disease and small vessel disease (evaluated as white matter hyperintensities of presumed vascular origin) or cognitive function in people with ischaemic stroke. Data presented here demonstrates that these relationships are inconsistent. Following the analyses in Chapter 6, the adjustment for common vascular risk factors in a linear regression model with WMH and cognition was performed for each averaged carotid variable. This analysis failed to find any significant relationship between carotid artery disease and WMH burden in the multivariable model. Only age was a significant covariate ($p < 0.001$), though this model demonstrated a poor R^2 value (adjusted $R^2 = 0.1$), The analysis here found no relationship with MoCA as a measure of global cognition. In the next chapter, I will analyse the longitudinal data from the XILO-FIST trial and investigate 2-year progression of carotid artery disease in these participants.

8 Evaluating the putative effects of long-term allopurinol treatment on carotid artery disease in people with ischaemic stroke

8.1 Introduction

Identified in the Introduction (Chapter 2), there are data describing the complex relationship between ischaemic stroke and increased serum uric acid concentration. Elevated serum UA is an indicator of impaired metabolic waste removal in the circulatory system. Serum UA levels are known to increase post-stroke and are found to exist after the acute phase. Elevated serum UA are associated with stroke risk (both first and recurrent), poorer outcomes following stroke and vascular cognitive impairment[100–102]. Allopurinol reduces serum UA, potentially reducing oxidative stress. In a meta-analysis, purine-like xanthine oxidase inhibitors e.g., allopurinol were found to have modest effects in preventing cardiovascular events. Furthermore, links between allopurinol and endothelial function have been investigated[108]. Allopurinol is suggested to have antioxidant properties that improve endothelial function. However, it is likely that the magnitude of the effect seen is influenced by the contribution of the xanthine oxidase pathway to oxidative stress. Furthermore, this study did not assess links between endothelial function and allopurinol treatment in ischaemic stroke[108].

The progression of carotid artery disease e.g., stenosis has been studied in ischaemic stroke patients, though there are no guidelines for the longitudinal assessment of carotid stenosis. Factors that may influence the progression of carotid artery stenosis include high blood pressure, diabetes, and male sex[229]. Carotid intima-media thickness progression has been linked to risk of ischaemic stroke, independent of vascular risk factors and medical therapy[230].

Many studies have reported mechanisms of action that my influence carotid artery disease. Oxidative stress may promote the aggregation of adhesive molecules to the vessel wall[58–60]. As allopurinol may act as an antioxidant, it is proposed by this mechanism that allopurinol induction may slow or halt the progression of carotid artery stenosis or the thickening of the intima-medial walls in the carotid arteries.

8.2 Aims and Objectives

This chapter aims to describe the change of carotid artery disease over 2-year follow-up and evaluate any differences between treatment groups and 10-year cardiovascular event risk, assessed using ASSIGN criteria. The objectives of these analyses are:

1. Describe the carotid artery disease measurements (ICA stenosis, IMT of common and internal carotid arteries, and extracranial internal carotid artery tortuosity) at the 2-year follow-up visit.
2. Calculate the progression rates of carotid artery disease and WMH volume.
3. Assess statistical differences between the treatment groups i.e., allopurinol and placebo for changes in progression rates of carotid artery disease, using non-parametric testing.
4. Assess for any statistical differences in the rates of carotid artery disease progression between participants labelled as low- and high-risk for future cardiovascular events, using non-parametric testing.

I hypothesise that participants who receive allopurinol will show a slower progression of carotid artery disease than the control group. Additionally, I hypothesise that participants who are high-risk for a cardiovascular event will show a faster progression of carotid artery disease than the low-risk group.

8.3 Methods

8.3.1 Participant selection

All participants that provided TOF and black-blood imaging were assessed for ICA stenosis, carotid artery IMT, and extracranial carotid artery tortuosity, in line with the

protocol described in Chapter 4. In this chapter, participants are separated into two groups: allopurinol vs placebo; ASSIGN high-risk and ASSIGN low-risk.

8.3.2 Carotid artery disease measurements

The methods used in this analysis have been described in Chapter 4. However, participants were unable to be co-registered between time points. To decrease potential bias, these measurements were performed independent of the results from baseline measurements. Once all tissue masks were generated/structural variables measured, change between datasets was assessed.

8.3.3 Measurements of white matter hyperintensity (WMH) progression

In addition to the volumetric change, WMH progression was assessed using the Rotterdam and Schmidt progression scales. The Rotterdam progression scale (RPS) evaluates the change in WMH within periventricular and subcortical regions. Disappearance of a lesion counted as a decrease in volume; appearance of a new lesion is counted as an increase in volume. Additionally, the scales have separate scores for periventricular white matter and deep white matter. Periventricular white matter is separated into 3 locations (frontal, lateral and occipital); deep white mater is separated into 4 locations (frontal, parietal, temporal and occipital). These methods result in a periventricular score range of -3 to +3 and a deep white matter change range of -4 to +4[193].

The Schmidt progression scale (SPS) is used to determine the longitudinal development of WMH change. This scale measures the progression of WMH as absent, mild, or marked, reliant upon the cross-sectional Fazekas scores for calculation. Mild WMH progression is described when the number of WMH lesions increases between 1-4. If the number of lesions is $\geq$ 5, or the Fazekas grade increases, this is known as "marked"[194].

8.3.4 Statistical analysis

Following from Chapters 6 and 7, non-parametric statistical analyses e.g., median and IQRs are reported in tabular form. Independent sample T-test or Chi-square was used to evaluate any significant difference in demographic data between participants who attended follow-up and those who did were lost to follow-up assessment. Mann-Whitney U test were performed to assess significant differences in the progression of carotid and brain structure between treatment groups. Additional analyses were performed by grouping participants into low- and high-risk categories, based on their ASSIGN scores. These analyses were performed to assess whether there was a difference in progression between participants at low and high risk of a future cardiovascular event. Stratification of these groups was performed in the whole cohort i.e., combined treatment groups. Scores <20 were categorised as low risk; scores of 20 or greater were categorised as high-risk for a cardiovascular event. All statistical analysis was performed in R 4.1.3.

8.4 Results

8.4.1 Participant selection

An updated diagram of the participant selection may be found below in Figure 8.1. From 181 participants studied at baseline, 32 participants did not return for follow-up imaging (16 from allopurinol and 16 from placebo), totalling 149 participants included. In the event of missing data, all available data were included i.e., if image quality or missing sequence prevented one vessel measurement, the participant was included in other measures where possible. The cohort was examined for significant differences between treatment groups (Table 8.1) and between those who attended follow-up/were lost over the longitudinal assessment (Table 8.2).

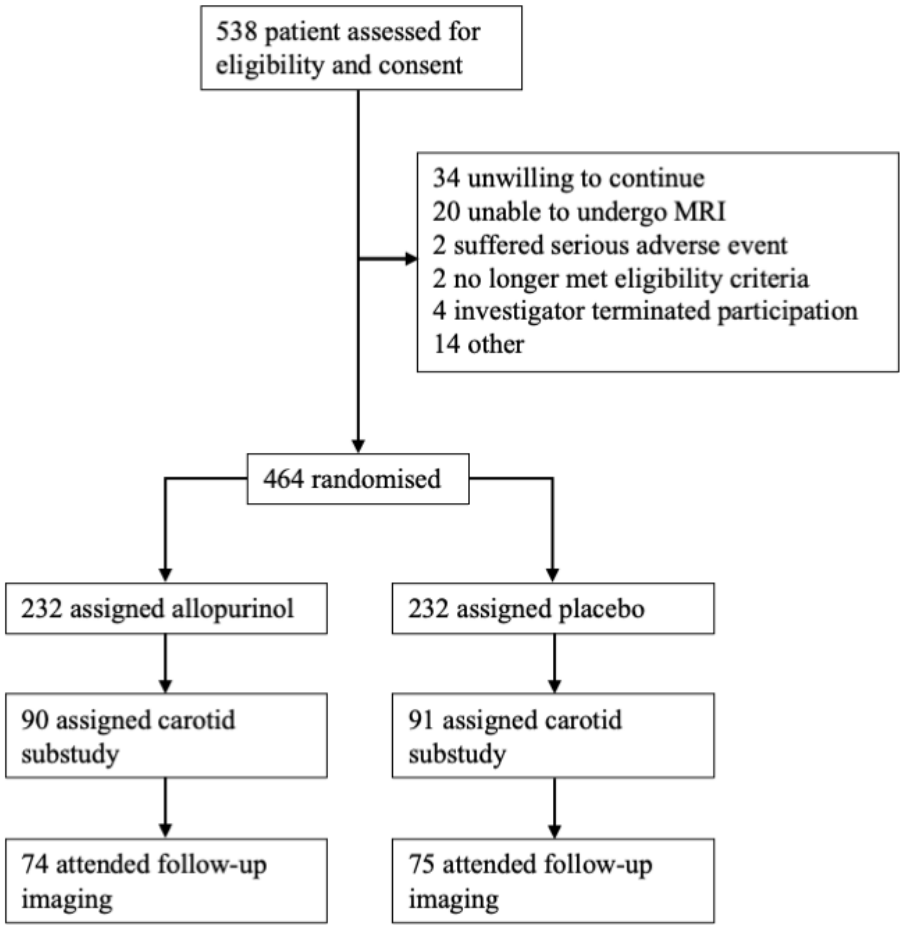

Figure 8.1: Trial profile of participants following longitudinal imaging visit. 149 participants were retained between baseline and follow-up. MRI = magnetic resonance imaging.

Table 8.1: The demographic descriptions representative of the carotid sub-study participants in the XILO-FIST trial, separated into treatment groups. Significance was calculated using the independent sample T-test for continuous variables; Chi-square was used for binary variables e.g., presence/absence of disease. Smoking history and alcohol consumption binarized as current/former or never. BMI = body mass index, TIA = transient ischaemic attack, NIHSS = National Institute of Health Stroke Scale, mRS = modified Rankin Scale.

	Group		
Variable	Allopurinol (n = 90)	Placebo (n = 91)	Sig.
Age at baseline (SD)	64.02 (7.55)	64.71 (8.78)	0.568
Sex (M/F)	66/24	64/27	0.653
Smoking history (current or former) (%)	49 (54.4)	47 (51.6)	0.728
Alcohol consumption (current or former) (%)	71 (78.9)	70 (76.9)	0.239
Systolic blood pressure (SD)	136.24(16.90)	139.37 (16.80)	0.213
BMI (SD)	28.23 (4.66)	27.83 (5.10)	0.578
Angina (%)	8 (8.9)	8 (8.8)	0.982
Myocardial infarction (%)	6 (6.6)	10 (11.0)	0.306
Hypertension (%)	43 (47.8)	33 (36.3)	0.117
Diabetes (%)	20 (22.2)	19 (20.9)	0.826
Dyslipidaemia (%)	24 (26.7)	21 (21.1)	0.576
Peripheral artery disease (%)	3 (3.3)	5 (5.5)	0.479
Previous stroke (%)	5 (5.6)	6 (6.6)	0.770
Previous TIA (%)	9 (10.0)	8 (8.8)	0.780
NIHSS (SD)	1.09 (1.25)	1.03 (1.43)	0.780
mRS (SD)	1.22 (0.85)	1.20 (1.00)	0.860

The carotid sub-study cohort (n = 181) from the XILO-FIST trial had an average age at baseline of 64.02 (SD 7.55) for the allopurinol group; the placebo control group had an average age of 64.71 (SD 8.78). 73% of participants in the treatment group were male compared with 71% in the control group. Stroke severity scale (NIHSS) and disability (mRS) were estimated at 1.09 (SD 1.25) and 1.22 (SD 0.85) for the allopurinol treatment group respectively. The control group had an estimated stroke severity of 1.03 (SD 1.43)

and 1.20 (SD 1.00) for NIHSS and mRS respectively. No statistical differences were found across the demographic variables described in the table.

Table 8.2: The demographic descriptions representative of the participants who attended or did not attend follow-up assessment. The data was assessed using an independent sample T-test for continuous variables; Chi-square was used for binary variables e.g., presence/absence of disease. BMI = body mass index, TIA = transient ischaemic attack, NIHSS = National Institute of Health Stroke Scale, mRS = modified Rankin Scale. Smoking history and alcohol consumption binarized as current/former or never. Significance of $p<0.05$ is noted with a *.

	Group		
Variable	Follow-Up (n = 149)	Lost to Follow-Up (n = 32)	Sig.
Age at follow-up (SD)	66.06 (7.96)	67.81 (9.10)	0.226
Sex (M/F)	115/34	15/17	0.001*
Smoking history (%)	78 (52.3)	18 (52.9)	0.915
Alcohol consumption (%)	100 (67.1)	24 (75.0)	0.556
Systolic blood pressure (SD)	137.94 (16.12)	137.22 (20.32)	0.592
BMI (SD)	27.78 (4.61)	29.18 (5.89)	0.142
Angina (%)	15 (10.1)	1 (3.1)	0.212
Myocardial infarction (%)	14 (9.4)	2 (6.3)	0.573
Hypertension (%)	60 (40.3)	16 (50.0)	0.314
Diabetes (%)	33 (22.1)	6 (18.8)	0.674
Dyslipidaemia (%)	37 (24.8)	8 (25)	0.986
Peripheral artery disease (%)	5 (3.4)	3 (9.4)	0.135
Previous stroke (%)	7 (4.7)	4 (12.5)	0.096
Previous TIA (%)	14 (9.4)	3 (9.4)	1.000
NIHSS (SD)	1.06 (1.35)	1.03 (1.33)	0.845
mRS (SD)	1.20 (0.89)	1.25 (1.08)	0.992

At 2-year follow-up assessment, the carotid sub-study cohort had a mean age of 66.06 (SD 7.96) compared with a mean age of 67.81 (SD 9.10) for the participants lost to assessment. The carotid sub-study cohort (n = 181) from the XILO-FIST trial had an

average age at baseline of 64.02 (SD 7.55) for the allopurinol group; the placebo control group had an average age of 64.71 (SD 8.78). 77% of participants included were male compared with 47% of participants excluded. Stroke severity scale (NIHSS) and disability (mRS) were estimated at 1.06 (SD 1.35) and 1.20 (SD 0.89) for the included group respectively. Participants lost to follow-up had an estimated stroke severity of 1.03 (SD 1.33) and 1.25 (SD 1.08) for NIHSS and mRS respectively. Sex was the only demographic variable to be significantly different between these groups ($p<0.001$).

8.4.2 Treatment effects of allopurinol induction on carotid artery intima-media thickness (IMT)

The intima-media thickness was calculated at follow-up from all available participants with carotid black-blood imaging sequences. The mean IMT area (mm^3) and % of total area can be found in Table 8.3 below, separated by treatment group and cardiovascular risk category. Statistical difference between treatment group and risk groups was performed using Mann-Whitney U test.

The median left CCA IMT across the whole cohort at follow-up is 57.49 mm^3 (IQR 31.27); 54.79% of total vessel area (IQR 11.68). The median right CCA IMT across the whole cohort is 51.31 mm^3 (IQR 22.46); 50.83 % of total vessel area (IQR 10.24). The median left ICA IMT across the whole cohort at follow-up is 36.42 mm^3 (IQR 16.15); 56.82% of total vessel area (IQR 12.28). The median right ICA IMT for the whole cohort at follow-up is 39.48 mm^3 (IQR 15.82); 56.96% (IQR 12.51) of total vessel area. These data, separated by treatment regimen and cardiovascular event risk are shown in Table 8.3. The median change in left CCA IMT between baseline and follow-up is 0.80 mm^3 (IQR 29.04); 0.11% increase in area (IQR 12.65). The median change in the right CCA IMT between baseline and follow-up is -4.12 mm^3 (IQR 20.99); -0.96% decrease in area (IQR 12.07). The median change in left ICA IMT between baseline and follow-up is -3.32 mm^3 (IQR 10.87). The median change in right ICA IMT is -2.07 mm^3 (IQR 16.46). Full data, separated by treatment group and cardiovascular event risk, are shown in Table 8.4. Figures 8.2-8.5 displays the IMT values (area and % of total area) for 2-year progression

stratified into treatment group and cardiovascular risk. All IMT progression values (mm^3 or %) across groups displayed non-significant differences.

Table 8.3: The median longitudinal follow-up values for carotid artery intima-media thickness, separated by both treatment group (allopurinol or placebo) and 10-year cardiovascular risk (low- or high-risk), assessed using ASSIGN methodology. The IMT % is based on the total vessel area. Statistical significance between groups was assessed using Mann-Whitney U test. IMT = intima media thickness, LCCA = left common carotid artery, LICA = left internal carotid artery, RCCA = right common carotid artery, RICA = right common carotid artery. * indicates $p<0.05$.

		Treatment				Risk Category			
IMT	Whole Cohort (IQR)	Allopurinol (IQR)	Placebo (IQR)	Sig.	CI	High (IQR)	Low (IQR)	Sig.	CI
LCCA (mm^3)	57.49 (31.27)	56.87 (25.49)	59.42 (31.90)	0.440	-9.704 – 3.954	59.81 (30.92)	56.36 (28.05)	0.365	-3.988 – 10.900
LCCA (%)	54.79 (11.68)	54.44 (9.95)	55.18 (12.87)	0.753	-3.408 – 2.322	57.47 (10.44)	54.35 (11.71)	0.230	-1.363 – 4.704
LICA (mm^3)	36.42 (16.15)	35.22 (16.90)	37.02 (15.42)	0.387	-5.850 – 2.127	38.35 (12.96)	35.22 (16.62)	0.178	-1.329 – 6.912
LICA (%)	56.82 (12.28)	56.45 (8.97)	57.27 (14.70)	0.511	-4.968 – 2.396	57.49 (18.13)	56.82 (10.91)	0.451	-2.543 – 5.818
RCCA (mm^3)	51.31 (22.46)	49.43 (23.93)	53.83 (19.94)	0.217	-9.304 – 2.392	55.83 (20.97)	49.59 (22.40)	0.070	-0.399 – 11.830
RCCA (%)	50.83 (10.24)	50.67 (8.90)	51.34 (10.38)	0.589	-3.376 – 1.873	53.63 (11.06)	50.40 (8.64)	0.091	-0.412 – 5.694
RICA (mm^3)	39.48 (15.82)	37.38 (17.69)	41.67 (15.68)	0.220	-6.794 – 1.371	41.07 (14.49)	37.83 (17.74)	0.084	-0.532 – 8.374
RICA(%)	56.96 (12.51)	56.30 (11.92)	59.94 (12.04)	0.625	-4.436 – 2.582	56.30 (16.22)	57.76 (9.89)	0.659	-4.785 – 3.093

Table 8.4: The median change between baseline and follow-up values for carotid artery intima-media thickness, separated by both treatment group (allopurinol or placebo) and 10-year cardiovascular risk (low- or high-risk), assessed using ASSIGN methodology. The IMT % is based on the total vessel area. Statistical significance between groups was assessed using Mann-Whitney U test. IMT = intima media thickness, LCCA = left common carotid artery, LICA = left internal carotid artery, RCCA = right common carotid artery, RICA = right common carotid artery. * indicates $p<0.05$.

		Treatment				Risk Category			
IMT	Whole Cohort (IQR)	Allopurinol (IQR)	Placebo (IQR)	Sig.	CI	High (IQR)	Low (IQR)	Sig.	CI
LCCA (mm^3)	0.80 (29.04)	0.80 (28.91)	0.93 (29.31)	0.950	-9.039 – 8.177	2.26 (34.11)	0.53 (27.18)	0.882	-10.406 – 9.235
LCCA (%)	0.11 (12.65)	1.68 (12.14)	-1.14 (13.15)	0.269	-1.781 – 5.454	3.57 (15.85)	-0.42 (10.24)	0.217	-1.733 – 6.569
LICA (mm^3)	-3.32 (10.87)	-2.86 (12.33)	-3.39 (9.57)	0.803	-3.190 – 4.918	-1.46 (13.16)	-4.73 (10.23)	0.077	-0.527 – 8.245
LICA (%)	0.40 (11.81)	0.51 (12.64)	0.30 (11.68)	0.832	-4.325 – 3.428	-0.18 (12.66)	0.56 (11.62)	0.929	-3.868 – 4.599
RCCA (mm^3)	-4.12 (20.99)	-2.92 (25.65)	-4.39 (16.62)	0.707	-5.318 – 7.914	0.68 (18.04)	-5.18 (22.46)	0.249	-3.057 – 10.899
RCCA (%)	-0.96 (12.07)	-1.56 (11.75)	-0.60 (12.55)	0.542	-4.264 – 2.258	-0.60 (12.59)	-1.49 (12.46)	0.249	-1.334 – 5.816
RICA (mm^3)	-2.07 (16.46)	-2.14 (16.75)	-1.99 (16.08)	0.390	-7.311 – 2.526	-3.46 (20.80)	-1.73 (13.96)	0.730	-5.849 – 4.386
RICA(%)	1.94 (11.96)	2.18 (12.26)	1.12 (11.54)	0.858	-3.460 – 2.786	-0.32 (12.99)	2.38 (11.37)	0.552	-4.691 – 2.502

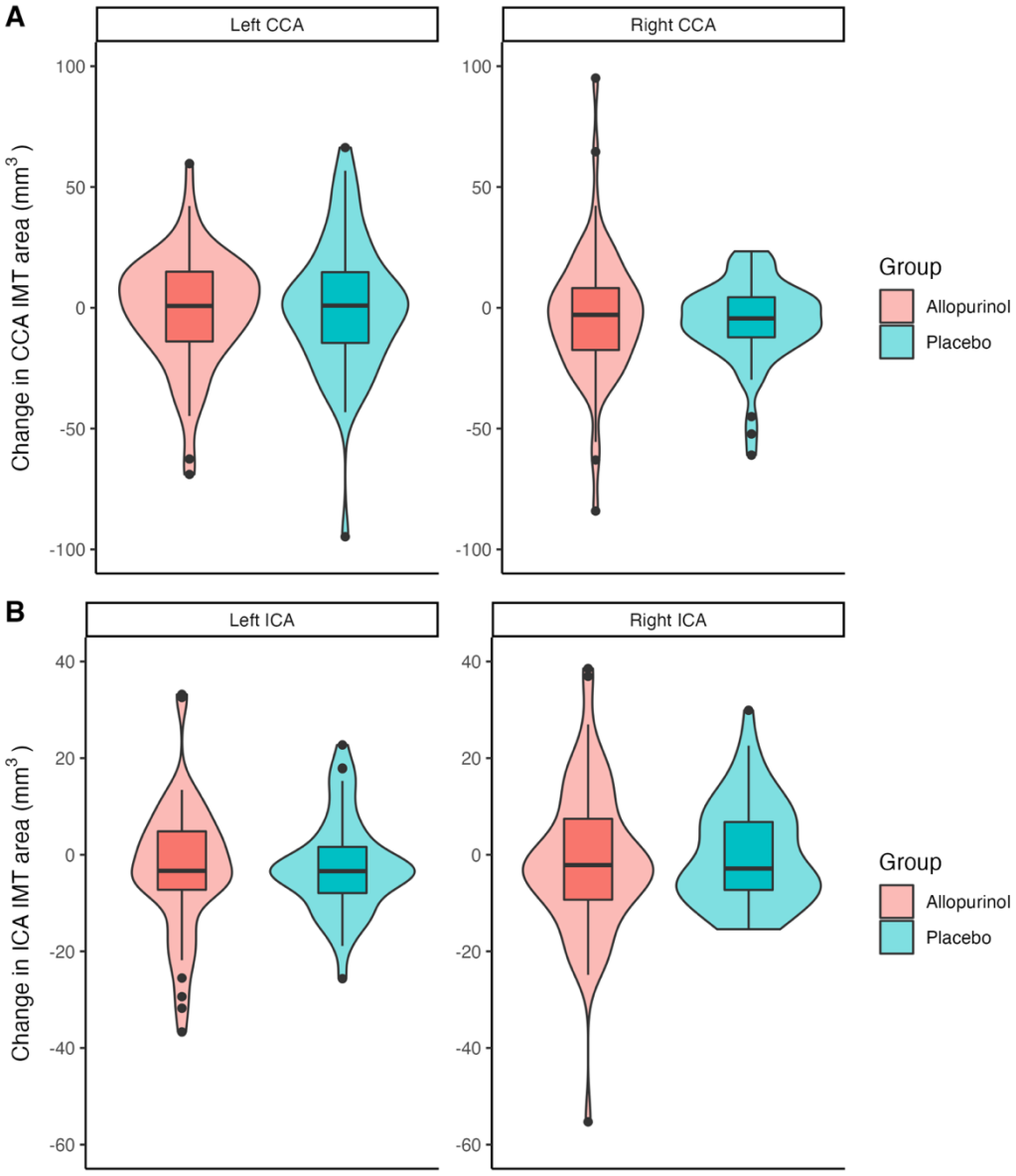

Figure 8.2: The intima-media thickness area (mm^3) change across treatment groups. The boxplot whiskers are set to 1.5x the inter-quartile range. Outliers are outside this range. The violin plot demonstrates the density of the data spread. A: Change in common carotid-intima media thickness, expressed in mm^3. B: Change in internal carotid artery intima-media thickness, expressed in mm^3.

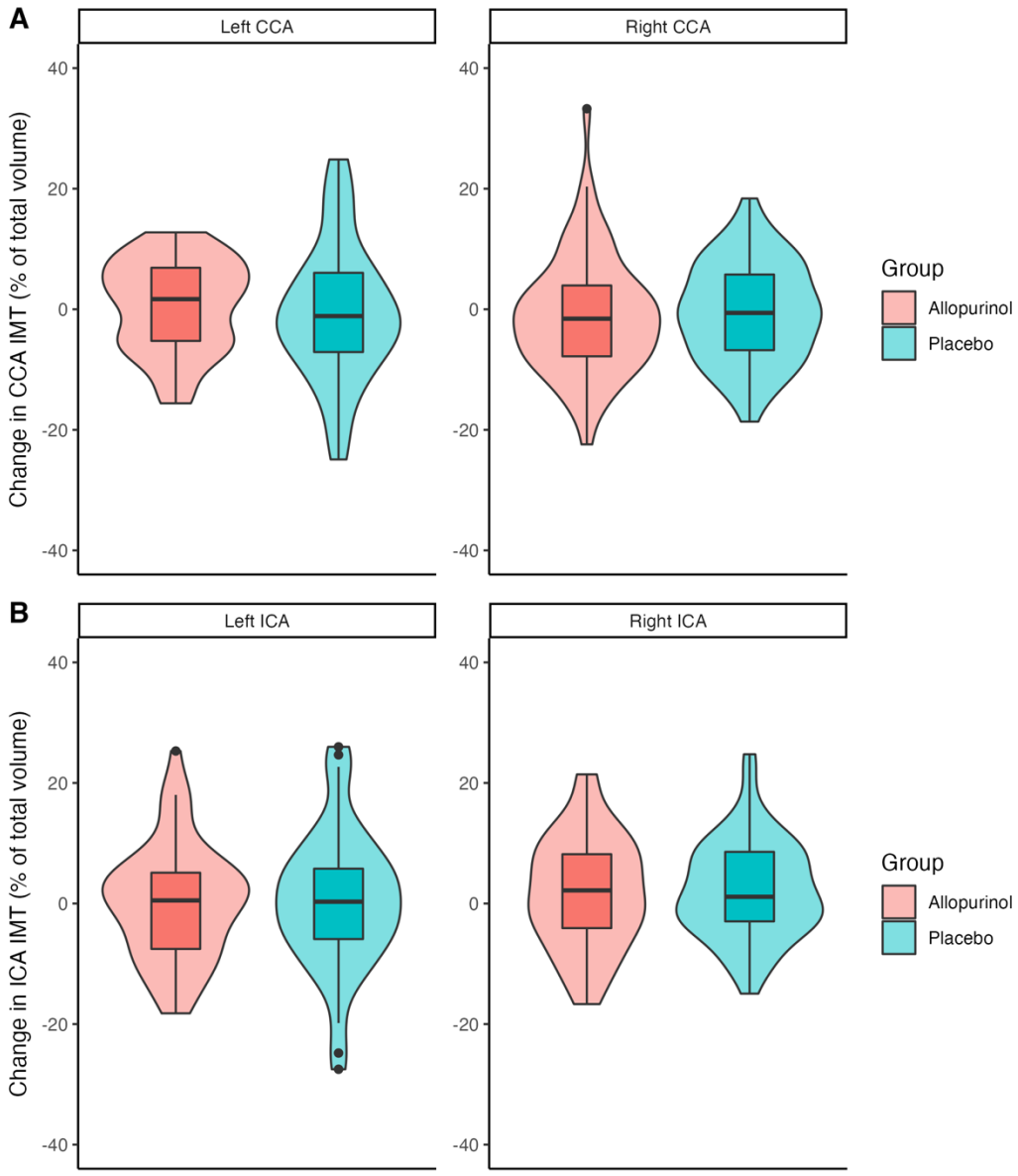

Figure 8.3: The intima-media thickness area (%) change across treatment groups. The boxplot whiskers are set to 1.5x the inter-quartile range. Outliers are outside this range. The violin plot demonstrates the density of the data spread. A: Change in common carotid-intima media thickness, expressed in %. B: Change in internal carotid artery intima-media thickness, expressed in %.

The change in intima-media thickness was stratified by cardiovascular risk (calculated by ASSIGN) in Table 8.4. Figures 8.4 and 8.5 demonstrate violin box-plot graphs of the average change in CCA and ICA IMT values in terms of absolute volume (mm^3) and % of total vessel area, grouped by low- and high-risk categories.

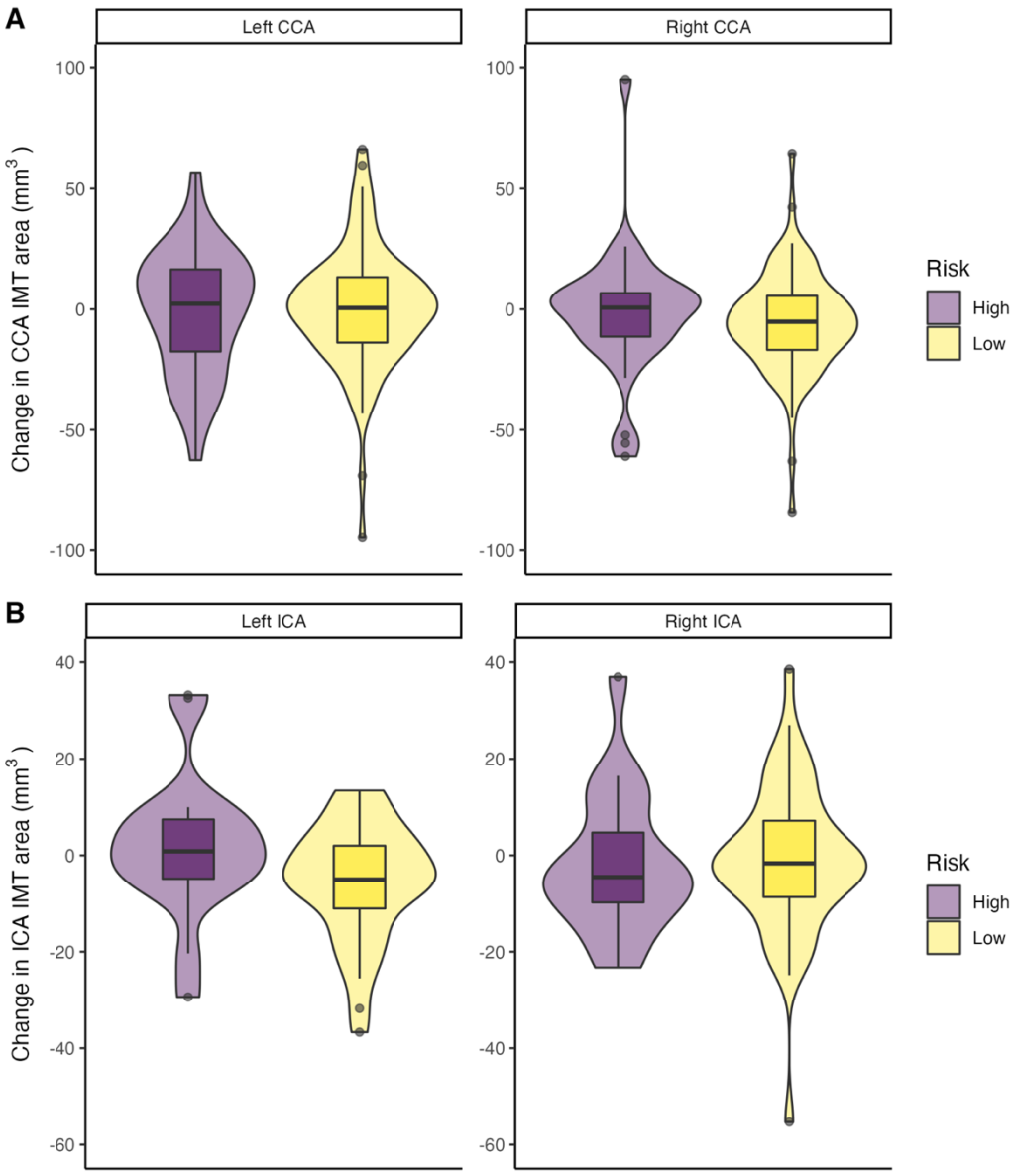

Figure 8.4: The average intima-media thickness area (mm^3) change across cardiovascular risk groups. The boxplot whiskers are set to 1.5x the inter-quartile range. Outliers are outside this range. The violin plot demonstrates the density of the data spread. A: Change in common carotid-intima media thickness, expressed in mm^3. B: Change in internal carotid artery intima-media thickness, expressed in mm^3.

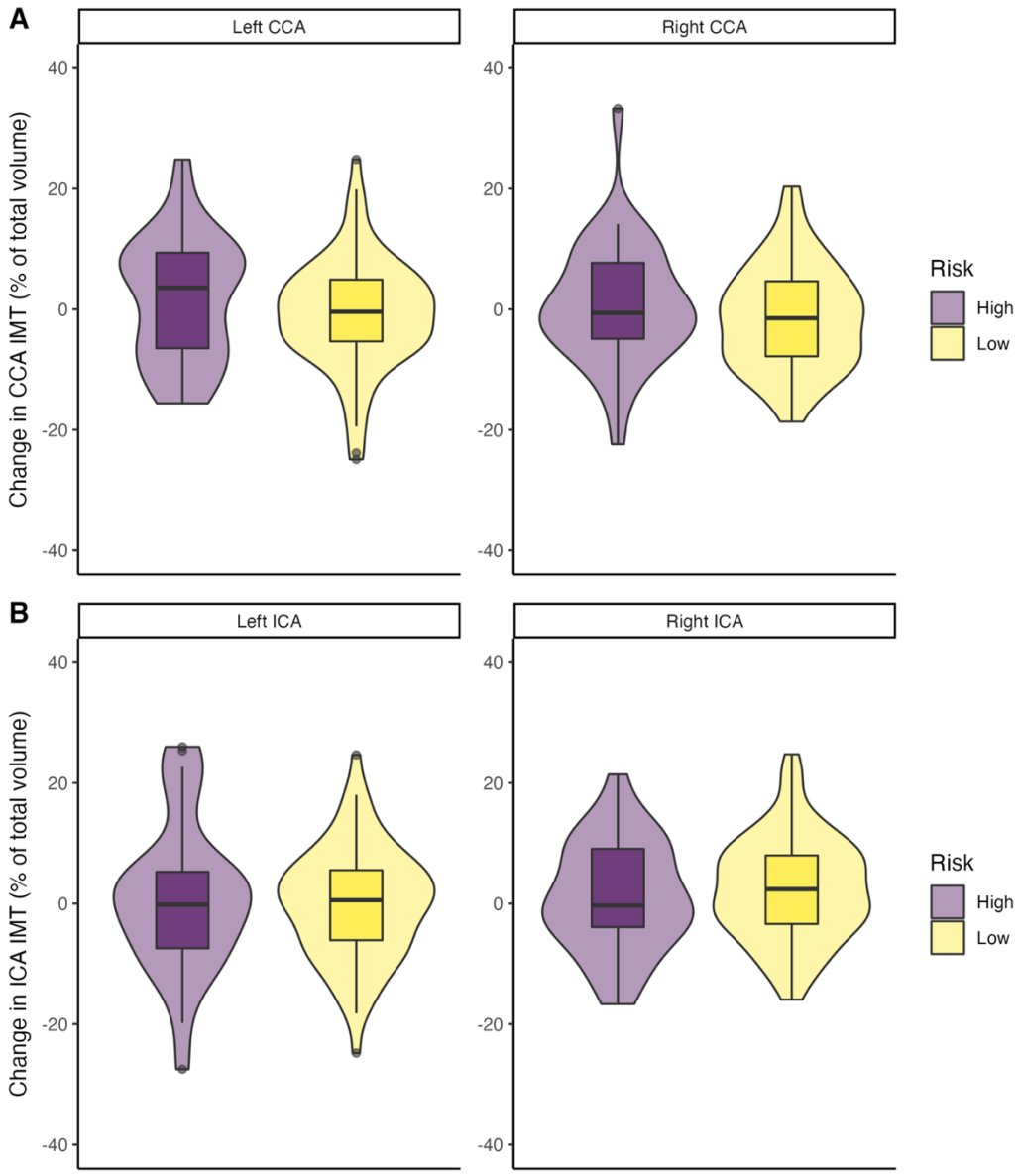

Figure 8.5: The average intima-media thickness area (%) change across cardiovascular risk groups. The boxplot whiskers are set to 1.5x the inter-quartile range. Outliers are outside this range. The violin plot demonstrates the density of the data spread. A: Change in common carotid-intima media thickness, expressed in %. B: Change in internal carotid artery intima-media thickness, expressed in %.

8.4.3 Treatment effects of allopurinol induction on carotid artery stenosis

Carotid artery stenosis was calculated at follow-up in all available participants with TOF MRA imaging. The median left ICA stenosis at follow-up is 37.00% (IQR 20.31); the median right ICA stenosis at follow-up is 38.13 % (IQR 20.32). The median 2-year

progression of left ICA stenosis is 3.12% (IQR 15.31); the median 2-year progression of right ICA stenosis is 4.08% (IQR 16.84). The follow-up data remains within the non-significant stenosis NASCET band i.e., <50%. Table 8.5 and Figures 8.6-8.7 provides data for the median stenosis values at longitudinal assessment and change between baseline and follow-up, stratified by both treatment group and 10-year cardiovascular risk. There are no significant differences seen in the change of ICA stenosis between groups.

Table 8.5: The median 2-year longitudinal assessment and change between baseline and follow-up values for carotid artery stenosis, assessed using NASCET criteria, separated by both treatment group (allopurinol or placebo) and 10-year cardiovascular risk (low- or high-risk), assessed using ASSIGN methodology. Statistical significance between groups was assessed using Mann-Whitney U test. LSTEN = left ICA stenosis (%), RSTEN = right ICA stenosis (%), CI = 95% confidence intervals. * indicates significance $p<0.05$.

Variable	Whole Cohort (IQR)	Treatment		Sig.	CI	Risk Category		Sig.	CI
		Allopurinol (IQR)	Placebo (IQR)			High (IQR)	Low (IQR)		
LSTEN	37.00 (20.31)	37.37 (18.90)	36.09 (22.25)	0.717	$-6.831e^{-5} – 2.228e^{-5}$	38.67 (17.12)	36.06 (21.64)	0.483	$-8.670e^{-5} – 1.163e^{-5}$
RSTEN	38.13 (20.32)	34.89 (16.13)	39.43 (24.78)	0.040*	$-1.834e^{-5} – 3.431e^{-6}$	39.64 (22.24)	35.75 (20.49)	0.297	$-7.881e^{-5} – 8.435e^{-5}$
LSTEN change	3.12 (15.31)	3.11 (13.67)	3.58 (15.08)	0.175	$-1.566e^{-5} – 3.721^{e}$-6	2.06 (15.26)	3.18 (15.96)	0.468	$-3.955e^{-6} – 1.755e^{-5}$
RSTEN change	4.08 (16.84)	2.19 (11.91)	4.97 (21.19)	0.229	$-5.453e^{-6} – 3.703e^{-5}$	5.63 (15.64)	2.31 (17.52)	0.611	$-3.086e^{-5} – 3.620e^{-5}$

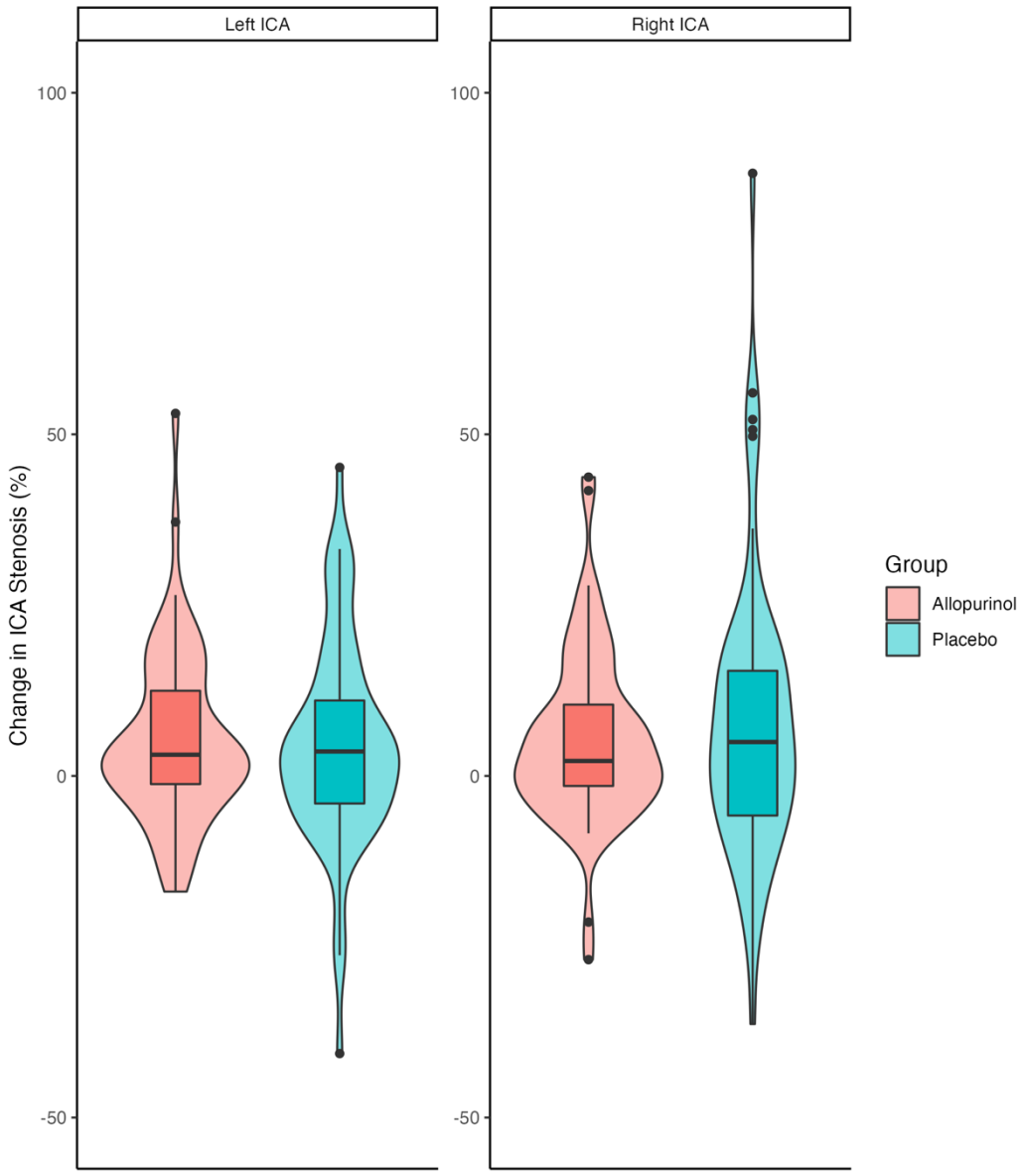

Figure 8.6 The internal carotid artery stenosis change, expressed in percentage (%) across treatment groups. Boxplot whiskers are set to 1.5x the inter-quartile range. Outliers are outside this range. Violin plot represents the density of the data spread.

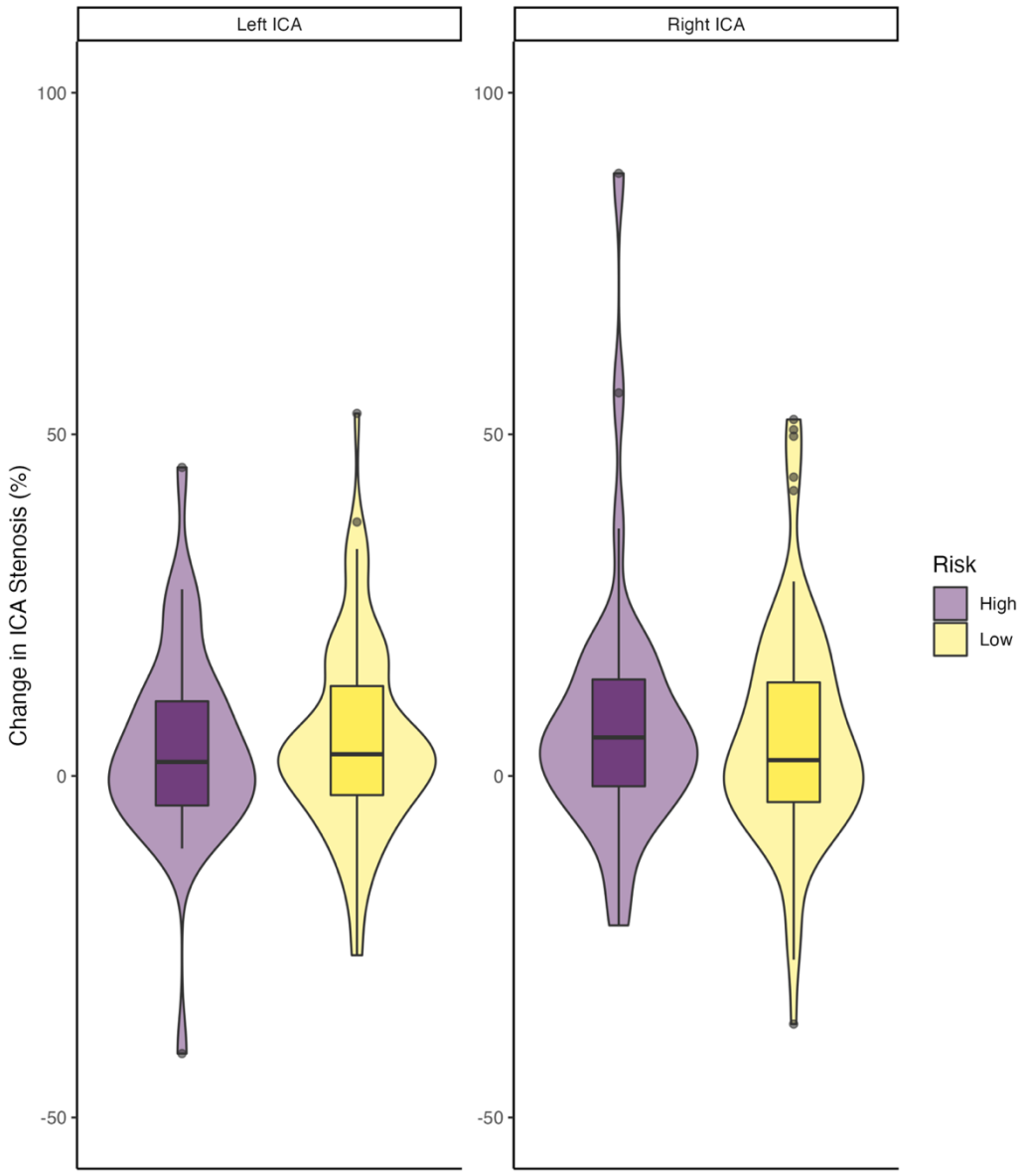

Figure 8.7: The internal carotid artery stenosis change, expressed in percentage (%) across cardiovascular risk groups. Boxplot whiskers are set to 1.5x the inter-quartile range. Outliers are outside this range. Violin plot represents the density of the data spread.

Figures 8.8 and 8.9 portray the change in ICA stenosis across the NASCET categories between treatment and cardiovascular risk groups, respectively. Change is represented by integer values i.e., a change of +1 means an increase from one category to the next; a change of -1 describes a decrease from a more stenosed to less stenosed category.

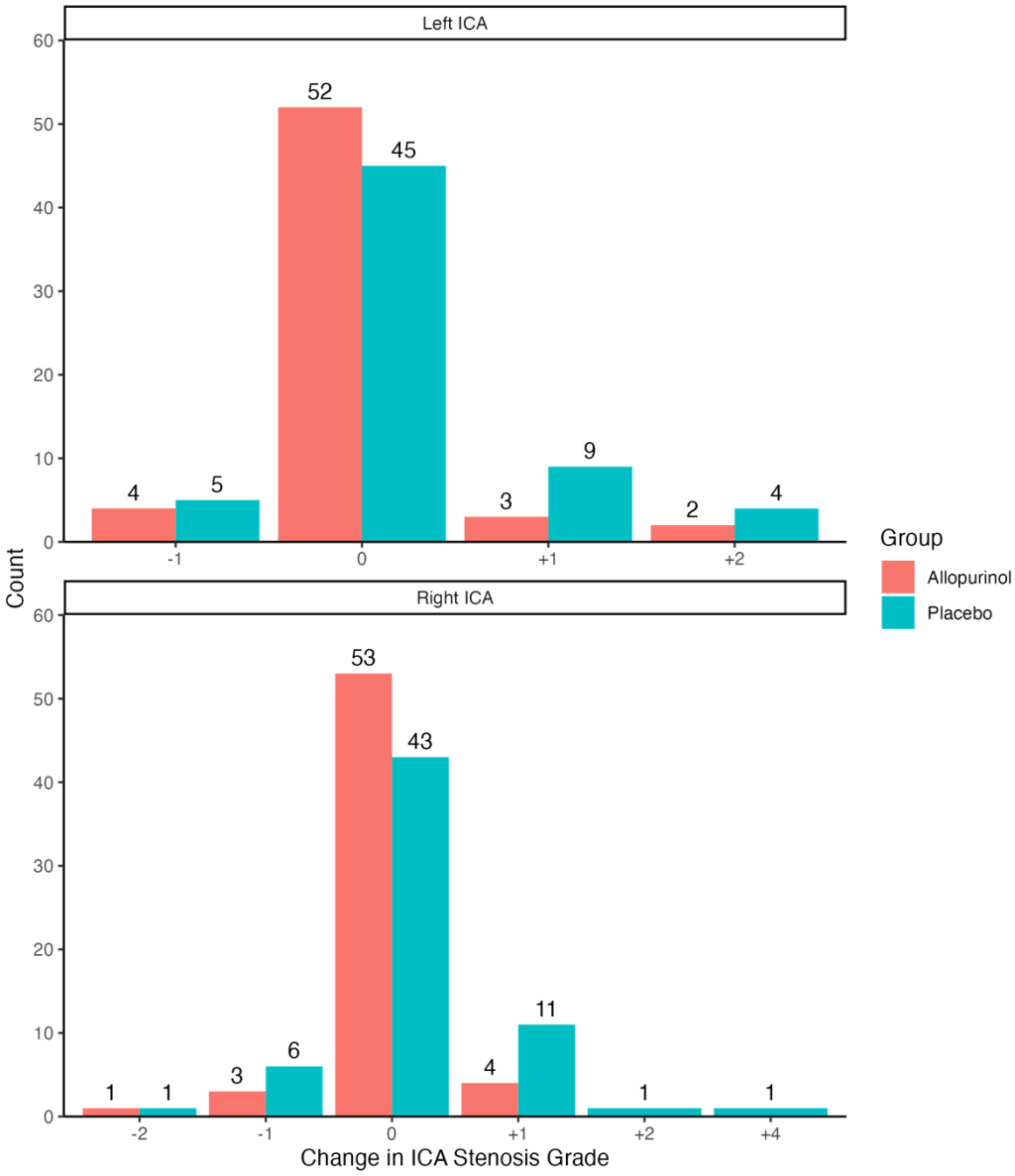

Figure 8.8: The change in ICA stenosis between baseline and 2-year follow-up, categorised into NASCET criteria of stenosis, and separated by treatment group. 0 represents no change, with positive integers showing the magnitude of an increase in stenotic grade; negative integers show the magnitude of decrease in stenotic grade.

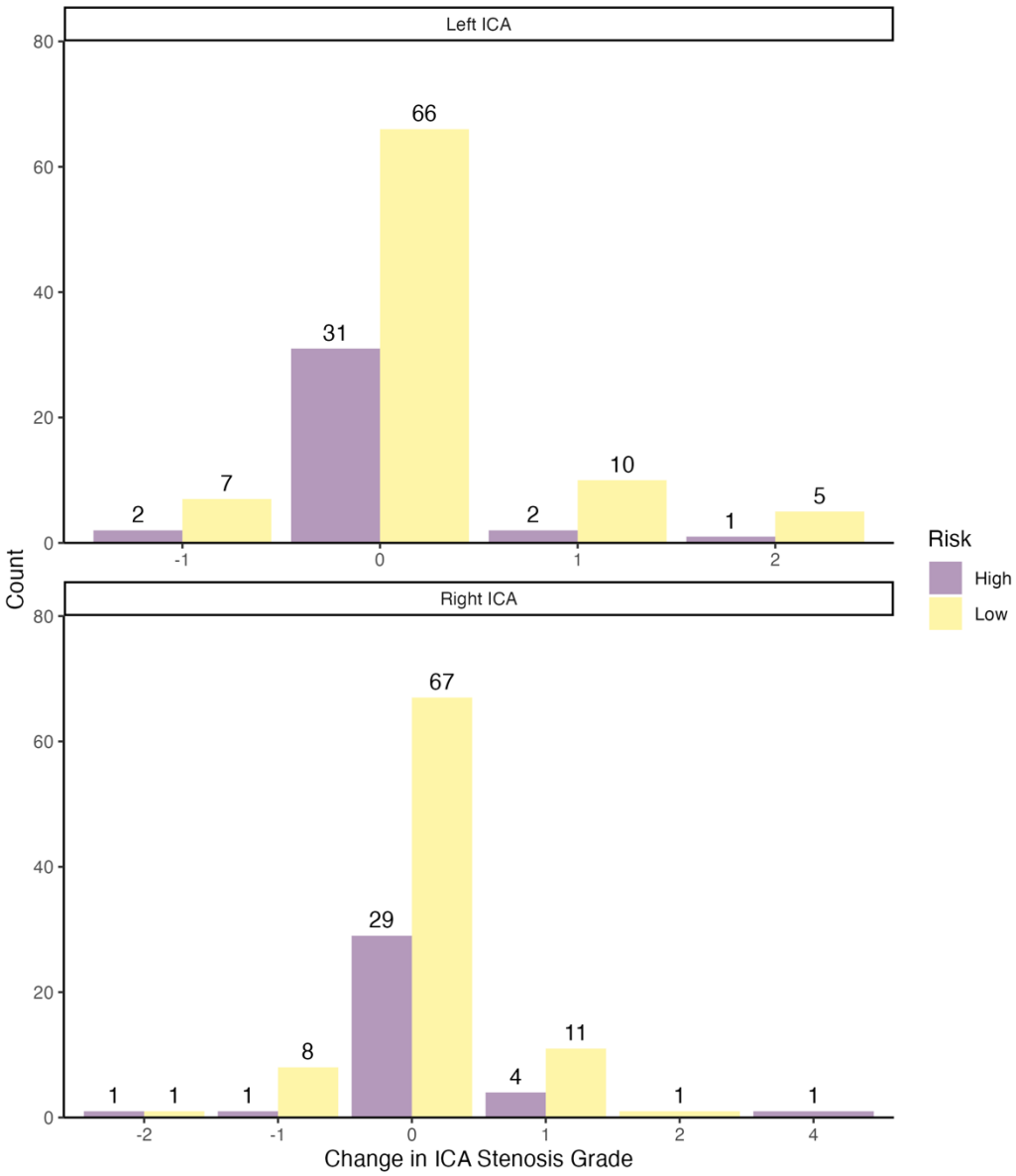

Figure 8.9: The change in ICA stenosis between baseline and 2-year follow-up, categorised into NASCET criteria of stenosis, and separated by ASSIGN risk group. 0 represents no change, with positive integers showing the magnitude of an increase in stenotic grade; negative integers show the magnitude of decrease in stenotic grade.

The Mann-Whitney U test was used to investigate significant differences between the ranked ordinal variables of the NASCET criteria across treatment groups and risk categories. In the left ICA, no significance was reached when comparing effects of treatment (allopurinol vs placebo, $p = 0.174$) or ASSIGN risk category (high vs low, $p = 0.604$). This lack of effect was replicated in the right ICA data (allopurinol vs placebo, $p = 0.227$; high vs low risk, $p = 0.695$).

8.4.4 Treatment effects of allopurinol induction on carotid artery tortuosity

The mean extracranial carotid artery tortuosity was assessed at 0.067 (SD 0.04) at 2-year follow-up. The mean change in extracranial carotid artery tortuosity was calculated at -0.002 (SD 0.05). Table 8.6 provides data demonstrating the change in carotid artery tortuosity; Figures 8.10 and 8.11 show the change in extracranial carotid artery tortuosity using violin-box plots, across treatment groups and cardiovascular risk, separately. Statistical differences between groups were assessed using Mann-Whitney U test. No significant differences were seen in the change between baseline and follow-up imaging.

Table 8.6: The median 2-year longitudinal assessment and change between baseline and follow-up values for extracranial carotid artery tortuosity, separated by both treatment group (allopurinol or placebo) and 10-year cardiovascular risk (low- or high-risk), assessed using ASSIGN methodology. Statistical significance between groups was assessed using Mann-Whitney U test. LTORT = left carotid tortuosity, RTORT = right carotid tortuosity CI = 95% confidence intervals. * indicates a significance $p<0.05$.

		Treatment				Risk Category			
Variable	Whole Cohort (IQR)	Allopurinol (IQR)	Placebo (IQR)	Sig.	CI	High (IQR)	Low (IQR)	Sig.	CI
LTORT	0.052 (0.05)	0.052 (0.05)	0.053 (0.05)	0.974	-0.010 – 0.010	0.039 (0.03)	0.055 (0.06)	0.088	-0.022 – 0.001
RTORT	0.055 (0.06)	0.048 (0.05)	0.065 (0.08)	0.030*	-0.029 –-0.001	0.061 (0.06)	0.055 (0.06)	0.578	-0.019 – 0.010
LTORT change	0.002 (0.03)	0.003 (0.03)	0.002 (0.03)	0.776	-0.008 – 0.011	0.000 (0.03)	0.003 (0.03)	0.528	-0.012 – 0.007
RTORT change	-0.001 (0.03)	-0.001 (0.04)	0.000 (0.03)	0.523	-0.016 – 0.007	-0.001 (0.03)	-0.001 (0.04)	0.918	-0.012 – 0.011

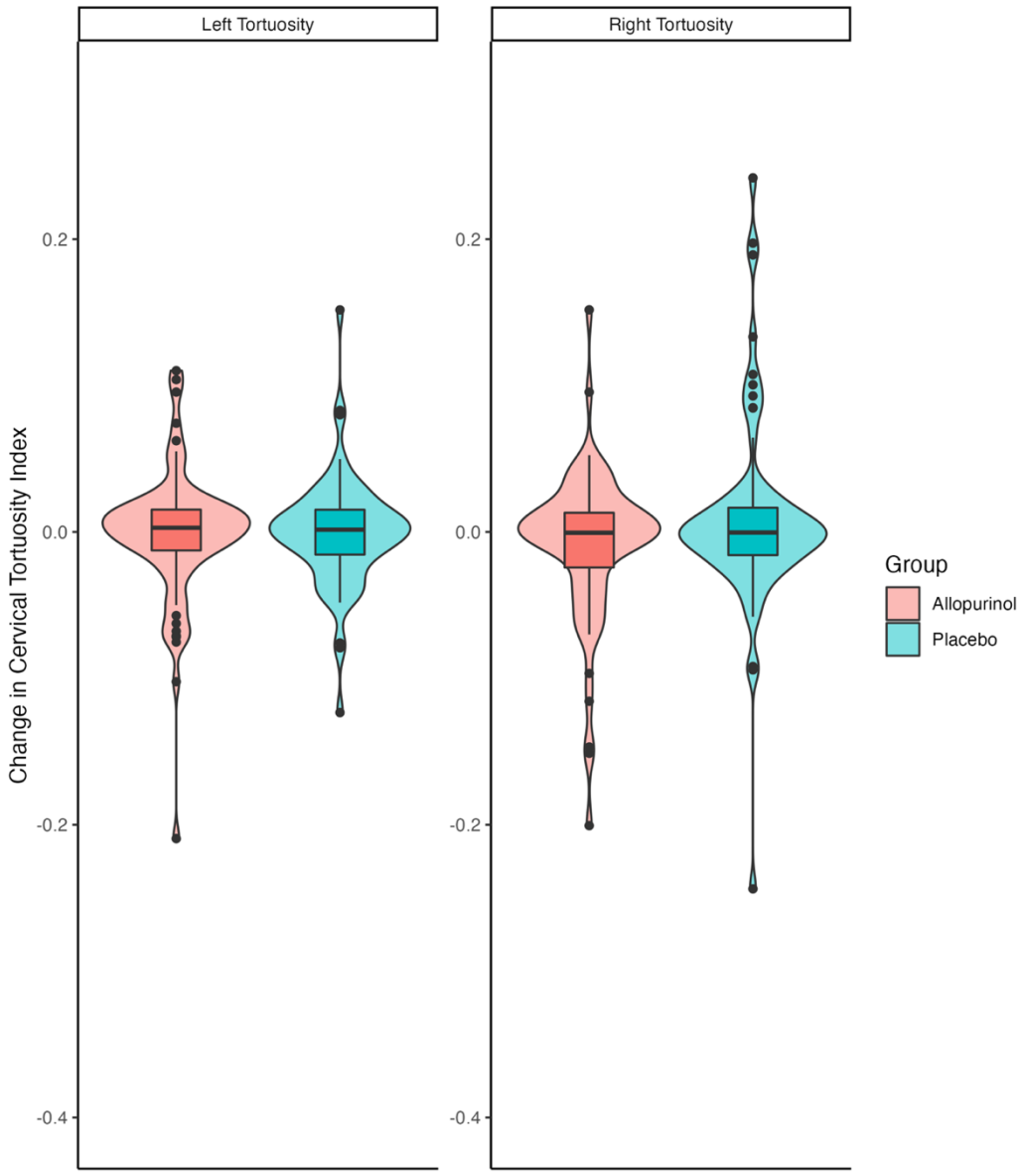

Figure 8.10: The change in extracranial carotid tortuosity measurements across treatment groups. The boxplot whiskers are set to 1.5x the inter-quartile range. Outliers are outside this range. The violin plot represents the density of the data spread.

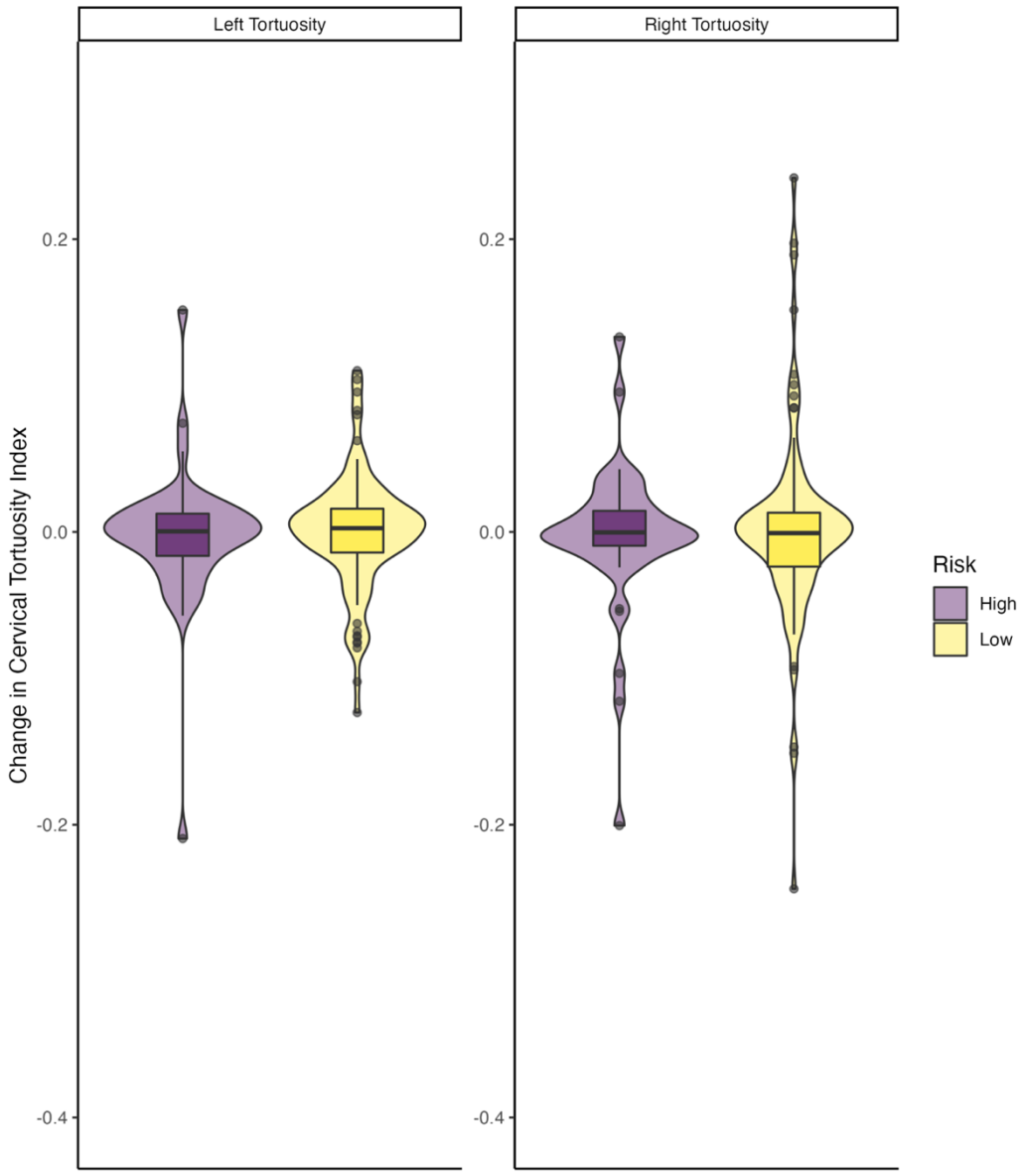

Figure 8.11: The change in extracranial carotid tortuosity measurements across cardiovascular risk groups. The boxplot whiskers are set to 1.5x the inter-quartile range. Outliers are outside this range. The violin plot represents the density of the data spread.

8.4.5 Treatment effects of allopurinol induction on white matter hyperintensity (WMH) progression

At the longitudinal assessment, the median WMH volume is calculated at 13.24 mm^3 (IQR 15.66). The median change in WMH volume is 0.90 mm^3 (IQR 3.81). Table 8.7 and Figures 8.12-8.13 highlight the WMH volume change across treatment group and cardiovascular event risk. The median Schmidt progression score is 1 (IQR 2); the median

Rotterdam progression score is 1 (IQR 2). Figures 8.14-8.15 display the distribution of these white matter progression scale. No significant differences in WMH progression, either volumetric or measured by visual scale, were seen between treatment groups or cardiovascular risk category.

Table 8.7: The median 2-year longitudinal assessment and change between baseline and follow-up values for white matter hyperintensity volume and scores, separated by both treatment group (allopurinol or placebo) and 10-year cardiovascular risk (low- or high-risk), assessed using ASSIGN methodology. Schmidt and Rotterdam scores are only created by evaluating change. Statistical significance between groups was assessed using Mann-Whitney U test. WMH = white matter hyperintensities, LWMH = log of white matter hyperintensity volume. * indicates significance $p<0.05$; ** indicates significance $p<0.001$.

		Treatment				Risk Category			
Variable	Whole Cohort (IQR)	Allopurinol (IQR)	Placebo (IQR)	Sig.	CI	High (IQR)	Low (IQR)	Sig.	CI
WMH (mm^3)	13.24 (15.66)	14.61 (15.67)	12.74 (14.85)	0.811	-2.840 – 3.555	18.19 (22.87)	12.50 (13.83)	<0.001**	2.546 – 10.386
LWMH	2.58 (1.07)	2.68 (1.02)	2.54 (1.04)	0.811	-0.236 – 0.280	2.90 (1.10)	2.53 (1.08)	<0.001**	0.197 – 0.720
WMH change (mm^3)	0.90 (3.81)	0.90 (3.88)	0.90 (0.07)	0.879	-0.960 – 0.903	0.85 (4.35)	0.96 (3.12)	0.622	-0.381 – 1.527
LWMH change	0.07 (0.25)	0.07 (0.26)	3.97 (0.22)	0.919	-0.061 – 0.074	0.04 (0.20)	0.07 (0.26)	0.757	-0.085 – 0.057
Schmidt progression	1 (1)	1 (1)	1 (1)	0.897	$-5.238e^{-6}$ – $6.229e^{-5}$	1 (1)	1 (1)	0.197	$-4.290e^{-5}$ – $2.699e^{-5}$
Rotterdam progression	1 (2)	1 (2)	1 (2)	0.228	-0.999 – $5.236e^{--5}$	1 (3)	1 (2)	0.209	$-2.540e^{-5}$ – 0.999

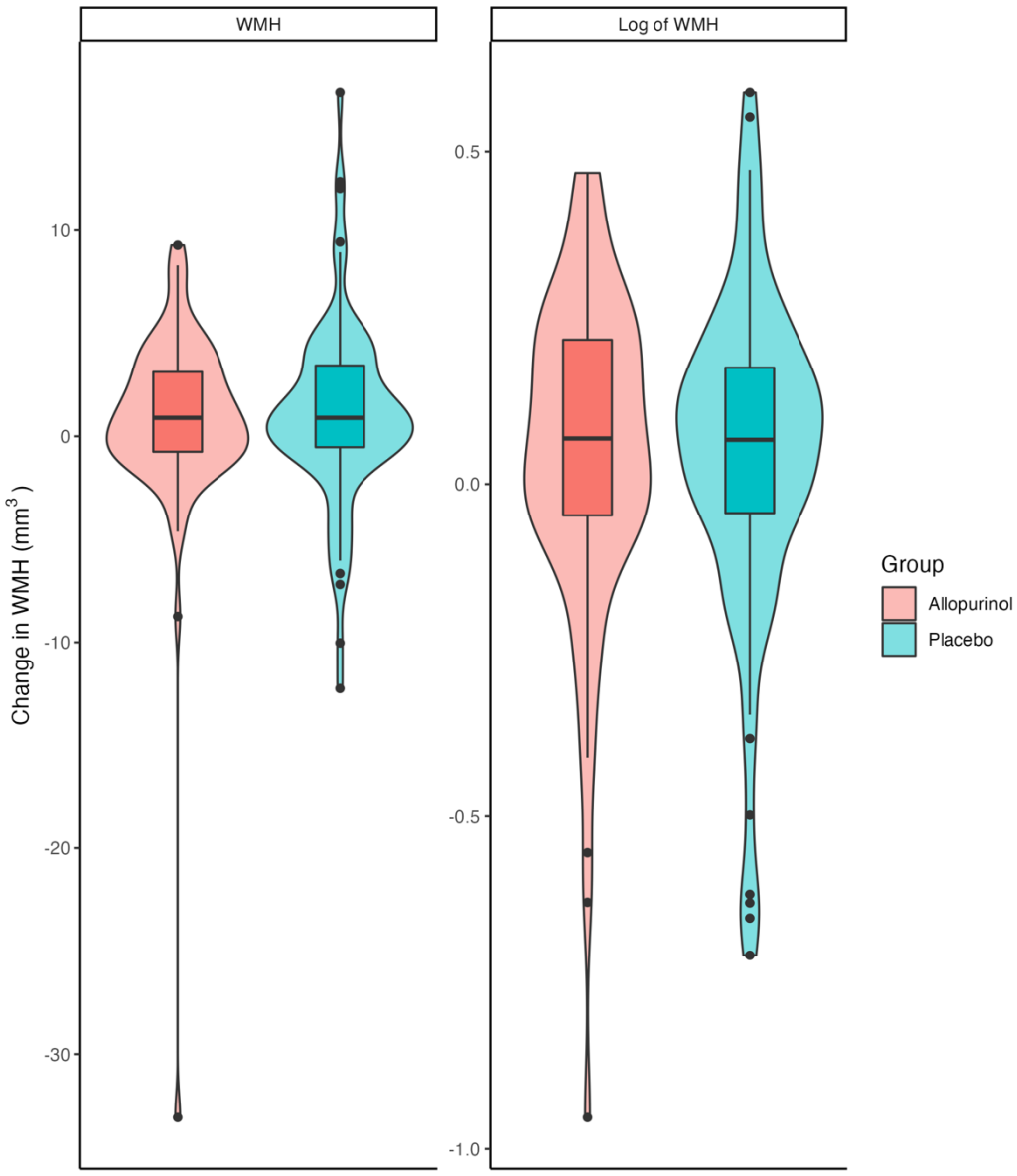

Figure 8.12: The change in WMH volume across treatment groups. The boxplot whiskers are set to 1.5x the inter-quartile range. Outliers are outside this range. The violin plot represents the density of the data spread.

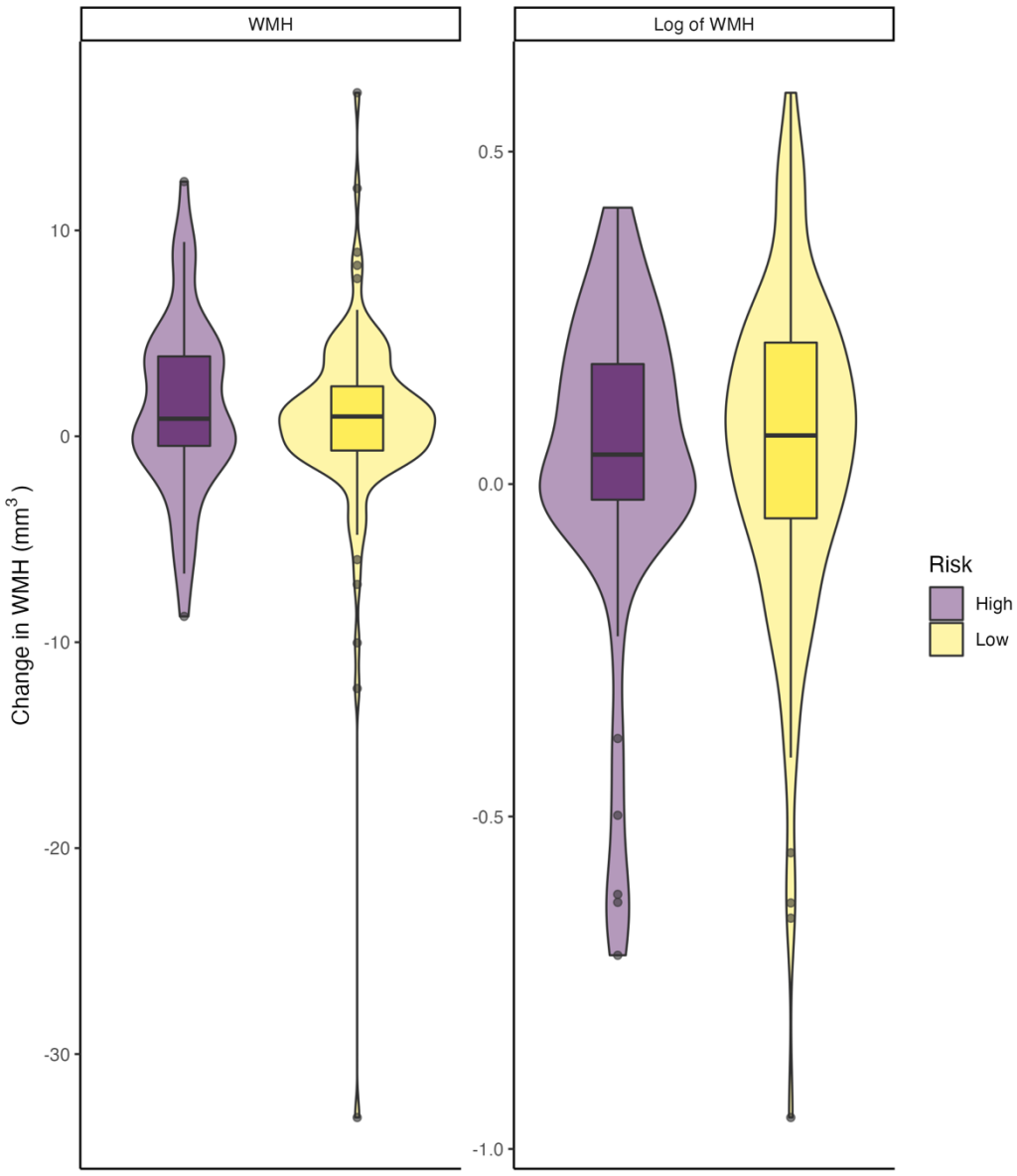

Figure 8.13: The change in WMH volume across cardiovascular risk groups. The boxplot whiskers are set to 1.5x the inter-quartile range. Outliers are outside this range. The violin plot represents the density of the data spread.

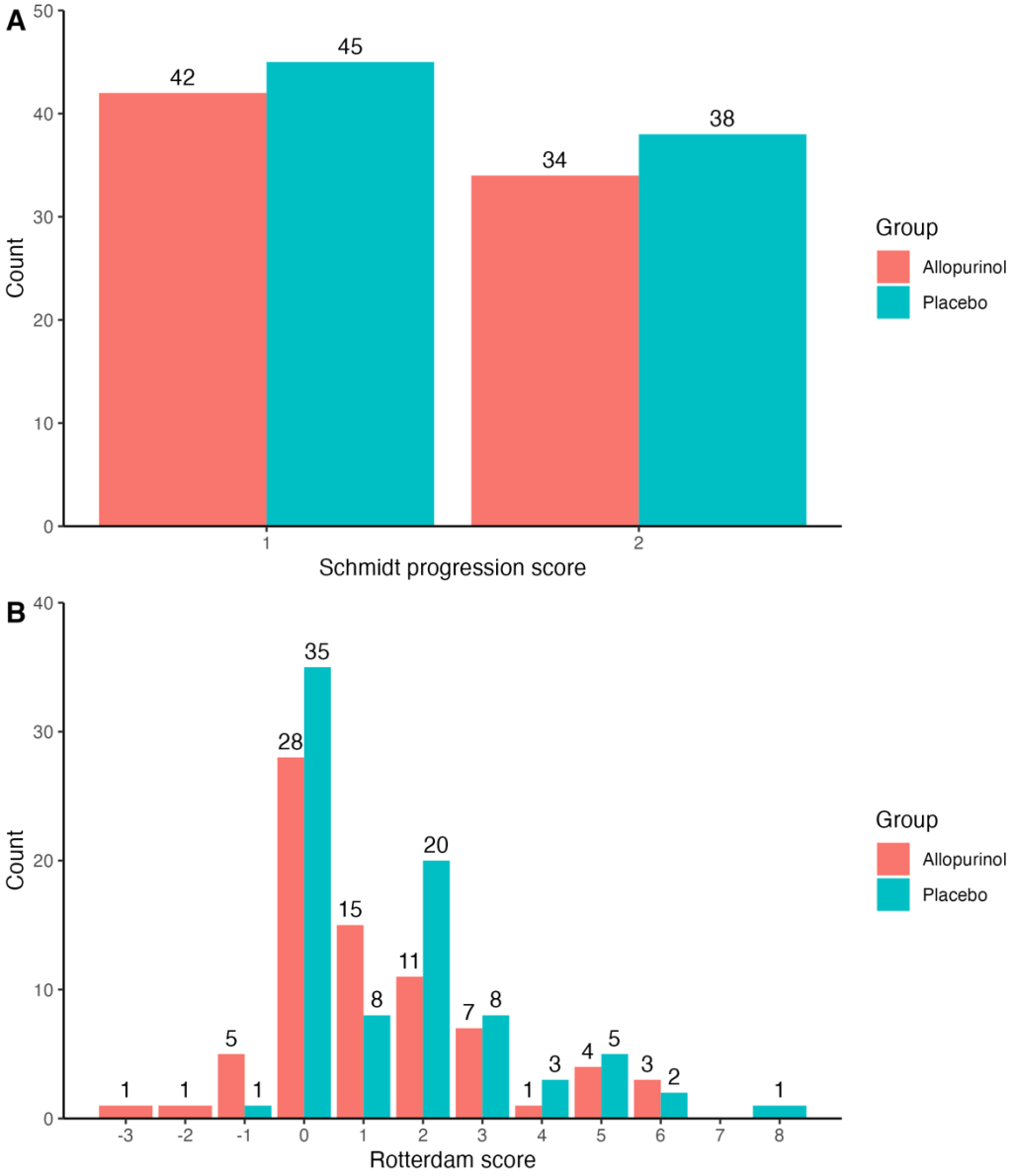

Figure 8.14: Visual WMH change assessed using Schmidt and Rotterdam progression scores across treatment groups.

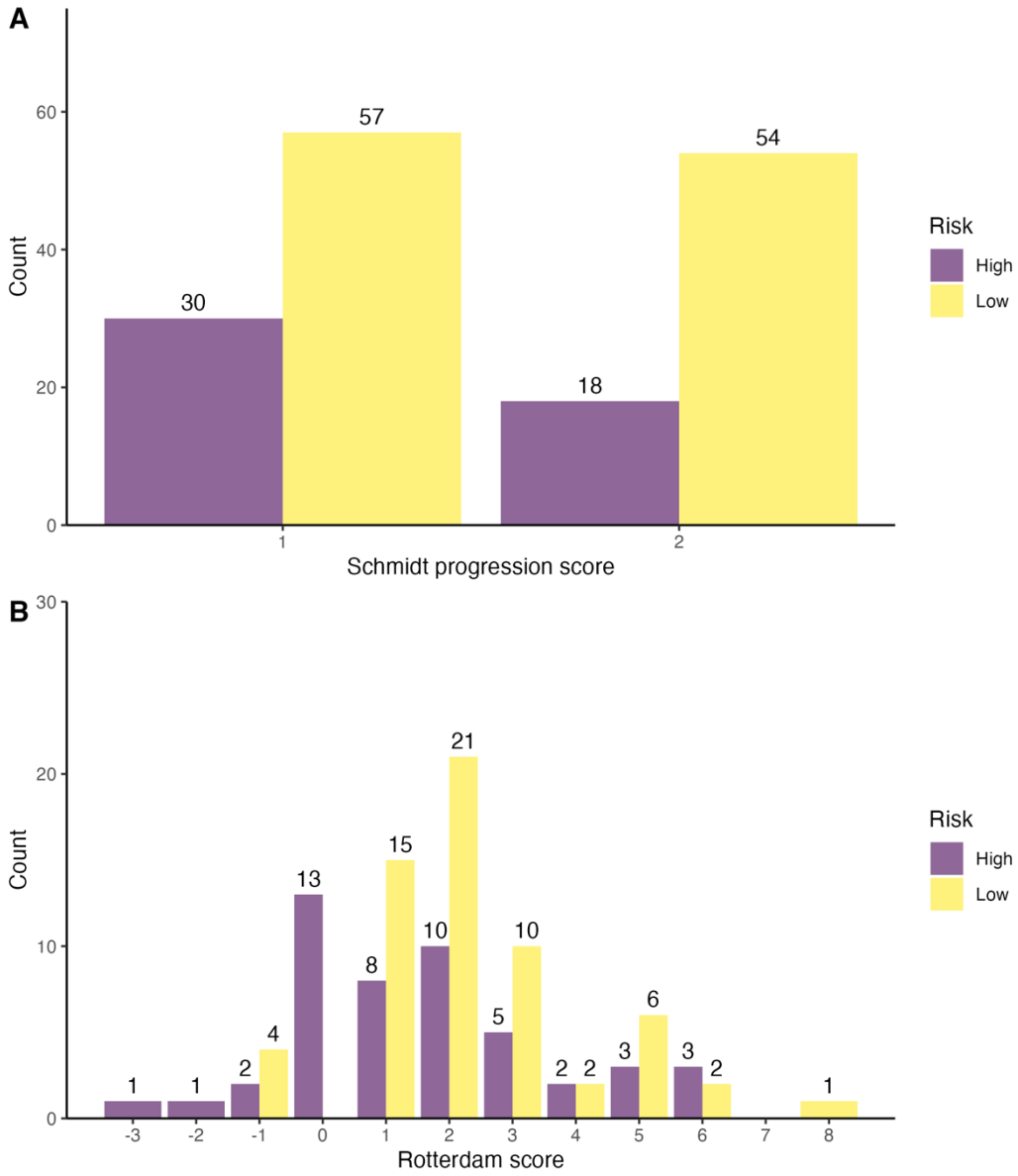

Figure 8.15: Visual WMH change assessed using Schmidt and Rotterdam progression scores by cardiovascular risk.

8.5 Discussion

The results aimed to describe the effects of allopurinol induction on carotid artery disease and white matter hyperintensity progression. The results described here demonstrate that there are no significant benefits of long-term treatment in stroke/TIA subjects aged >50. There was no significant difference between the treatment and control groups in managing carotid artery disease. There were no significant differences in the progression of ICA stenosis, CCA IMT or extracranial carotid artery tortuosity.

Furthermore, there were no significant differences in change when stratifying by the baseline 10-year cardiovascular risk score attributed by ASSIGN. In follow-up there were significant differences in the WMH volume when grouped by ASSIGN score and right carotid tortuosity at follow-up when grouped by treatment. Due to the small variation between these values, they are likely incidental findings and bare no clinical relevance.

In previous research, the progression of carotid IMT has been studied over a median 21.5 months. In 3482 stroke-free subjects with a mean age 64.1, various carotid IMT measures, including mean and maximum were studied. Between baseline and 15-month follow-up, all IMT measures showed a significant increase in volume. In these data, the mean CCA IMT at baseline was measured at 0.741mm (SD 0.138) and follow-up 0.747mm (SD 0.147), with a yearly progression 0.005mm (SD 0.058). The mean ICA IMT at baseline was measured at 0.869 (SD 0.350) and 0.882 (SD 0.351), with a yearly progression 0.013 (SD 0.116). Both measurements were assessed with a paired T-test on log-transformed variables, with significance values <0.001; non-parametric analysis using Mann-Whitney U test displayed significance values <0.001[230]. In comparison with data presented in this chapter, these data are markedly different. The data in this chapter are measured in volume i.e., 3D; the data referenced above are measured in 2D ultrasound. The data in this chapter demonstrated that the progression of carotid IMT is not linear, and significant variation exists between participants, and between the paired arteries. This is made evident with the standard deviation values that are larger than the mean progression values in Table 8.2. Moreover, previous research modelled the progression of these IMT values through time-to-event analysis, adjusting for vascular risk factors. For participants with 3 or more common vascular risk factors, the IMT values significantly progressed between the baseline and 15-month follow-up, exhibiting different rates depending on the sample of risk factors studied. The participants demonstrated IMT progression independent of treatment using atherosclerotic drugs[230].

Additionally, the progression of carotid artery disease in ischaemic stroke has been studied. In 179 participants with a mean age 68 over a median 36 months, carotid artery stenosis was assessed using ultrasound. In these participants, 17.9% (64/358) vessels progressed to higher stenotic grades. Patients with subclinical stenotic grades i.e., <50% were at a reduced risk of stenotic progression. The adjusted odds ratio (in comparison to

patients with 0-29% stenosis) were OR 3.50 (p = 0.09, 95% CI 0.81 – 15.84) for mild stenosis (50-59%) and OR 6.61 (p = 0.03, 95% CI 1.01 – 39.61). Furthermore, a diagnosis of hypercholesterolaemia increased stenotic progression risk; OR 2.22 (p = 0.03, 95% CI 1.05 – 4.71)[229]. However, these data are limited to the progression of a stenotic category; and do not describe the change in stenosis as a continuous variable. However, stenosis grades are uneven in their weighting, with subclinical stenosis i.e., non-significant stenosis ranging between 0-49%. Thus, change over this category may go underrepresented. Furthermore, the median ICA stenosis in XILO-FIST are less than 33% at baseline (see Chapter 6) and are minimally impaired. Rates of ICA stenosis progression has been measured using hazard ratios, finding 10-year increase in age (HR 1.19, 95% CI 1.01-1.41, p = 0.044), male sex (HR 1.71, 95% CI 1.28-2.28, p = 0.001) and coronary artery disease (HR 1.36, 95% CI 1.04-1.78, p = 0.023) are significant predictors. However, in the same study, other factors have been assessed as predictors of stenosis regression including 10-year increase in age (HR 0.62, 95% CI 0.44-0.87, p = 0.006). These data suggests that age is a predictor of both progression and regression of ICA stenosis, though the regression HR is mild. It is likely that increasing age is associated with higher collagen content/calcified plaques within the arteries, and are therefore unlikely to regress[231].

To the best of our knowledge, these data are novel with respect to longitudinal assessments of tortuosity. Longitudinal changes in vessel tortuosity may be identified in studies that last longer than a 2-year follow-up period. Mechanisms for change in carotid vessel tortuosity have been proposed, including age-related degeneration and deposition of visceral fat around arteries, altering the angiographic course[79,214,217]. However, it is unlikely that this mechanism of action would exhibit significant alterations over 2 years. Our data did not measure change in BMI, which may associate with change in vessel tortuosity. Population-based studies which often have a much longer longitudinal observation protocol may be better suited to investigate age-related changes in tortuosity.

There are limited data on the progression of carotid artery disease and WMH in stroke trials greater than 1 year. In the full trial, the logarithmic WMH change was estimated at 0.1% (SD 0.3) in both groups, with a between group difference of 0.01 (95% CI -0.04 – 0.07, p = 0.61). Additionally, by 1 month after trial induction, systolic BP had reduced by 2.3mmHg (SD 12.9) in the allopurinol group; this effect was not seen in the

placebo group (95% CI -5.55 - -1.11, p = 0.003). However, this measurement did not decrease further after 2 years treatment[232]. It should be noted that ABPM was not measured in some subjects in lieu of Covid-19 protocols. As stated in the full study, WMH change is in-line with other stroke studies e.g., PROGRESS MRI. The PROGRESS MRI study highlighted a WMH volume change of 1.6cm^3 in subjects with BP lowering treatment; systolic BP had reduced by 11.2mmHg after 3 years[233].

However, WMH progression over time is contested. There are several studies that have identified WMH load does not consistently progress, and participants with WMH are known to regress at follow-up visits. Hyun-Cho et al. studied 100 participants over a mean period of 28 months. It was found that WMH progressed in 27 participants and regressed in 9. Additionally, there was a pattern of regression/progression in a further 5 subjects. Whilst it was noted that several factors were associated with WMH progression (increasing age, large vessel disease, male sex, and renal dysfunction), there were no distinct associations found with WMH regression[234]. Clancy et al. studied changing WMH volumes and effects on cognitive function in a 3-year period. They stated a mean volume difference in WMH 1.3ml (SD 8.68); maximum progression 29.1ml and maximum regression 31.9ml after 1-year (imaging was not performed at 3 years). However, there was no description of the ratio of participants that exhibited WMH progression or regression[235].

Previous pilot data suggested a significant difference in treating carotid IMT progression with allopurinol. The black-blood imaging data, though performed at 2 time points, were unable to be co-registered to each other. Co-registration is a common step in image analysis techniques to compare between different tome points of image modalities. The large slice gaps in the images prevent cross-excitation artefacts to improve image quality at the cost of missing potential pathology. Scans were localised at the point of image acquisition to the carotid bifurcation, a common site of plaque progression. Due to this localisation and small slice number, only a small portion of the neck is covered through imaging. Despite these localisation attempts to minimise discrepancies, effects of allopurinol induction on carotid intima-media thickness cannot be fully ascertained.

8.6 Summary

This chapter aimed to assess the progression of carotid artery disease, and the treatment effects of longitudinal allopurinol treatment in ischaemic stroke. Data analysed in this chapter included all participants categorised by treatment group i.e., allopurinol or placebo, and either low- or high-risk of future cardiovascular events, calculated by ASSIGN. This was to evaluate whether the rate of disease progression may be affected by risk of cardiovascular disease.

The data presented here showed a median increase of 3.12% in left ICA stenosis; 4.08% right ICA stenosis across the whole cohort. Right ICA stenosis % demonstrated a significant difference between treatment groups at follow-up, though this is an incidental finding. There were no significant differences between treatment groups or risk groups when change in ICA stenosis was assessed. This is also true for the IMT measures, which all demonstrated non-significant differences in both progression (median left CCA IMT 0.80mm^3; right CCA IMT 0.40mm^3) or regression (median left ICA IMT -4.12mm^3; median right ICA IMT -2.07mm^3). The extracranial carotid artery tortuosity index values exhibited a median change of 0.002 (left carotid) or -0.001 (right carotid) in the entire cohort. Furthermore, there was a non-significant progression in the WMH in the whole cohort; no significant differences were found in the longitudinal assessment across the treatment groups or risk categories.

The next chapter will provide a structural equation modelling framework which aims to evaluate the validity of a carotid-brain-cognition model in ischaemic stroke.

9 A structural equation modelling framework for assessing carotid-brain interactions in people with ischaemic stroke

9.1 Introduction

In Chapters 6 and 7, I aimed to describe the relationships between carotid structure and common vascular risk factors (Chapter 7) and either brain structure or cognition (Chapter 8). These data found weak associations with carotid artery disease features e.g., univariate correlations between smoking status and right cervical carotid tortuosity (Chapter 6); right CCA IMT or ICA IMT and intracranial volume, cortical grey matter, and cortical normal appearing white matter (Chapter 7), or right cervical carotid tortuosity and performance on the Animal Naming Test.

Further analyses in Chapter 7 involved the creation of univariable and multivariable linear regression models to evaluate predictors of WMH volume or MoCA performance as a measure of global cognition. In these analyses, I found that whilst average cervical tortuosity was a significant predictor of WMH burden in a univariable model, only age remained a significant predictor in the multivariable analysis. Furthermore, in the linear regression analysis of cognition, none of these proposed predictors (carotid artery disease measurements, age, sex, and common vascular risk factors) were found to be significant in either the univariable or multivariable models. However, these analyses employed ignored the assumptions that altered brain structure, such as increased WMH burden, would influence cognitive function. These data provided in this thesis do not reject my null hypotheses i.e., there is no indication that carotid artery disease influences small vessel disease in the brain, nor does it influence cognitive function. These analyses do not fully describe the complex interactions of carotid artery disease, brain structure, and cognitive function. Previous research has found that small vessel disease burden, including WMH correlates with poorer cognitive function in healthy ageing and other populations such as Alzheimer's disease and ischaemic stroke[236–238].

The models employed in this thesis: univariate correlations, univariable and multivariable regression have some important limitations. These limitations are: (1) the models are of a simple design; (2) all variables are observable, and (3) they assume that all

included variables are measured without error[239]. When creating the regression models in Chapter 7, it was assumed that a carotid artery disease variable leads to increased WMH burden or poorer cognitive function, and then corrected with multiple explanatory variables. This type of analysis does not assess the data simultaneously, which may hamper the estimation of a relationship[239]. Furthermore, it is possible that these data include a degree of measurement error, either systematic or random. In Chapter 5, a caveat of the IMT data described that whilst there was good interobserver reliability in the manual segmentation procedure, there was no ability to compare with "real world" data. This is one example where unknown measurement error may hamper these analyses. To overcome these limitations, this chapter will look at the use of a structural equation modelling framework to estimate the complex relationship of carotid-brain interactions in people with ischaemic stroke.

Structural equation modelling (SEM) is a series of statistical inferences that can measure the relationships between multiple dependent and independent variables. SEM variables can be observed or latent i.e., not directly observed variables. By evaluating these unobserved variables, an SEM framework can account for some measurement error in the raw variables. SEM integrates 3 main components: confirmatory factor analysis, path analysis, and estimation of model fit. It is not a hypothesis testing framework, but confirmatory. Instead, SEM is used to describe the plausibility of a model. It relies upon *a priori* information before the creation of an SEM. Different methods for SEM estimation exist: (1) covariance-based SEM or, (2) partial least-squares SEM. Covariance-based SEM (used in this chapter) confirms theories and hypotheses. The latter partial least-squares SEM is concerned with explaining variance in the dependent variables[239].

Structural equation modelling has been used more recently in psychological and medical research, including on data from the Lothian Birth Cohort and Mild Stroke Study[241,242]. Previous analysis of data from the Lothian Birth Cohort described a theoretical model between progressive cognitive decline and carotid artery disease. By using latent growth curves i.e., a form of SEM used for longitudinal analyses, associations between carotid measures (stenosis, velocity, pulsatility and resistivity indices) and cognitive function was measured. These data described that carotid stenosis (median 12.96%) was not associated with cognitive function, nor cognitive decline between ages 70-76[243].

Furthermore, analysis of retinal microvasculature and SVD burden found arteriolar fractal dimension (a measure of retinal vascular structure) predicted 4% variance of WMH volume in a community-dwelling cohort, confirmed with an SEM model[241]. It is from these analyses that this chapter is based upon.

9.2 Aims and Objectives

This chapter aims to describe an overarching relationship between carotid artery disease, brain structure and cognitive function in ischaemic stroke using structural equation modelling. The objectives of these planned analyses are:

1. Perform structural equation modelling to confirm whether, given the data supplied, an overall relationship between carotid artery disease, brain structure and post-stroke cognitive function can be assumed.
2. Identify the strengths and weakness of the structural equation models that are created through this analysis.

9.3 Methods

9.3.1 Data source

The data used in this chapter is from the XILO-FIST carotid sub-study. The participant data has been previously described in depth in Chapters 6 and 7. Baseline data was used to assess the proposed carotid-brain interactions. In the case of missing data, the participant was excluded from the SEM. Only participants with fully complete structural and cognitive data were included in this analysis (n = 118).

9.3.2 Model estimation

Structural equation modelling was run using the package “lavaan” in R (version 4.1.3. Model estimation was performed using a variation of maximum likelihood

estimation. The ML estimation includes robust standard errors and Satorra-Bentler test statistic, to be used when data are non-parametric. The data in this thesis have consistently been described using non-parametric indices (Chapter 6). The model estimation involves the refinement of parameter estimates until the achievement of best fit. Initial values for these parameters are assumed before the model's equations generate predicted values from the observed variables. The predictions are compared with the "true" data, and differences measured. This process iterates successively based on the difference between the predicted and observed variables until a minimum is reached. A proposed model is shown in Figure 9.1 below; this includes measures of carotid artery disease, brain structure, and cognitive function.

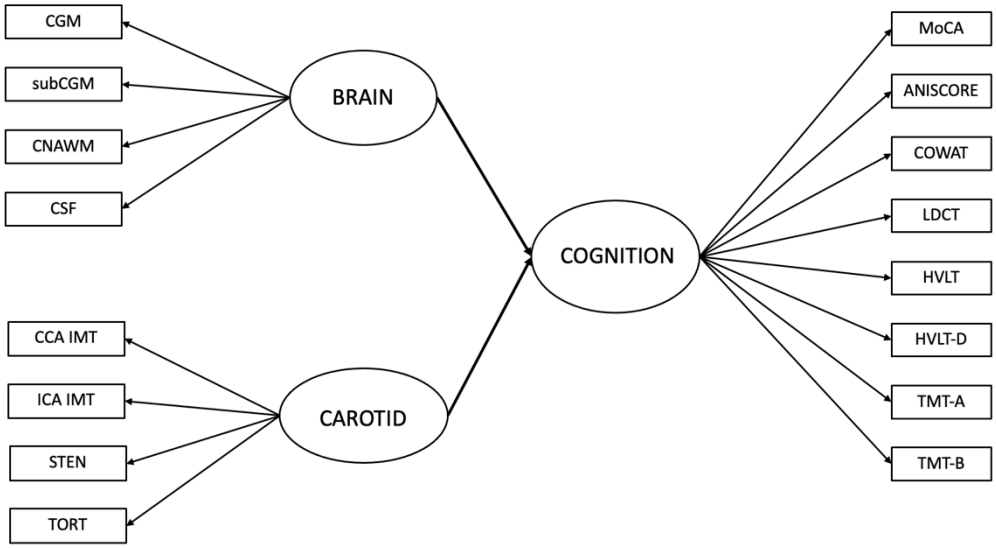

Figure 9.1: The proposed structural equation model for a relationship between carotid structure, brain structure and cognitive function, using baseline data from the XILO-FIST trial. CGM = cortical grey matter, subCGM = subcortical grey matter, CNAWM = cortical normal appearing white matter, CSF = cerebrospinal fluid, CCA = common carotid artery, ICA = internal carotid artery, IMT = intima-media thickness. MoCA = Montreal Cognitive Assessment, CoWAT = Controlled Oral Word Association Test, ANI = Animal Naming Score, LDCT = Letter Digit Coding Test, HVLT = Hopkins Verbal Learning Test, HVLT-D = Hopkins Verbal Learning Test Delay, TMT-A = Trail Making Test Part A, TMT-B = Trail Making Test Part B.

9.3.3 Model evaluation

The goodness of fit can be determined through many indices, set between 0 and 1. Typically, a combination of these indices is used when evaluating SEM fit. This chapter uses the Comparative Fit Index (CFI), Root Mean Square Error of Approximation (RMSEA) and Standardised Root Mean Square Residual (SRMR) parameters.

The CFI is the comparison between the model of interest and a restricted baseline model. As a ratio, it compares the difference between the implied model's covariance matrix with the covariance matrix of the restricted model and the difference between the observed covariance matrix i.e., the covariance of the raw data and the baseline covariance matrix. The CFI is less sensitive to sample size than other goodness-of-fit indices e.g., χ^2-test; thus, it is more suitable for a range of samples. The assumption of goodness-of-fit with CFI suggests a perfect fit = 1; CFIs >0.95 are considered acceptable[244].

The RMSEA estimates variance unaccounted for by the model. It is based on the discrepancy between the covariance matrices of the observed data and the implied model and adjusted for model complexity. To prevent overfitting, the RMSEA adjusts for the number of model parameters and the model's degrees of freedom. This adjustment provides an assessment that considers both model fit and parsimony. The assumption of goodness-of-fit with RMSEA should demonstrate low residual values (close to 0). An RMSEA = 0 would suggest all variance is accounted for in the model. In practise, an RMSEA value <0.06 is an acceptable fit[244].

The SRMR demonstrates the overall value of the model fit by assessing the model residuals. The SRMR is the square root of the averaged (squared) standardised model's residual variances and covariances[245]. As this goodness-of-fit index is based on standardised values, the SRMR is less sensitive to differences in variable scales and can be compared across different models and datasets. An SRMR <0.08 is considered an acceptable fit[244]. With these analyses, goodness-of-fit can be accurately described.

9.4 Results

9.4.1 Model 1: Estimation and Evaluation

In Model 1, latent factors were described as “vessel”, “brain” and “cognition. These factors contained observed variables measured throughout the XILO-FIST trial. The vessel factor contains the averaged measurements of carotid artery disease i.e., CCA IMT, ICA IMT, ICA stenosis and cervical carotid tortuosity. The “brain” factor contained 4 variables for cortical grey matter, subcortical grey matter, cortical appearing white matter, and CSF. These variables describe the main tissue types of the brain. The cognition factor includes all the cognitive tests assessed (see Chapter 4 for the complete cognitive battery). This was due to the assumption that any there may not be a complete overlap of cognitive domains assessed by either the MoCA or the other cognitive tests. Figure 9.2 presents the first SEM model. Goodness-of-fit for all equations can be found in Table 9.1. The regression esrimates can be found in Table 9.2. The complete outputs of the lavaan SEM analysis, including latent variables, regressions, covariances and variances can be found in the Appendix. All models were adjusted for age.

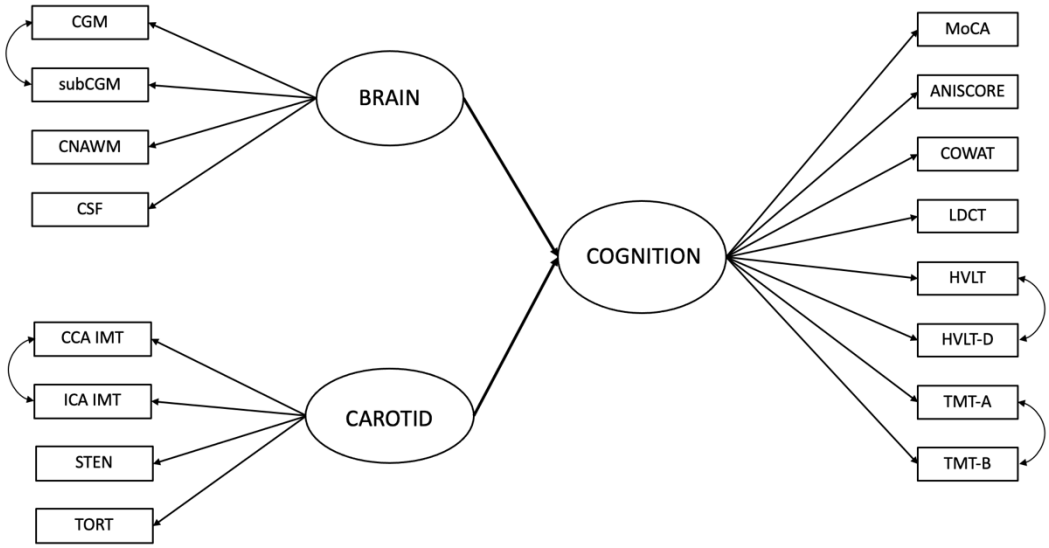

Figure 9.2: SEM Model 1 of carotid-brain interactions. CCA = common carotid artery, ICA = internal carotid artery, IMT = intima-media thickness, STEN = ICA stenosis, TORT = extracranial carotid artery tortuosity, CGM = cortical grey matter, subCGM = subcortical grey matter, CNAWM = cortical normal appear white matter,

CSF = cerebrospinal fluid, MoCA = Montreal Cognitive Assessment, ANI = Animal Naming Score, CoWAT = Controlled Oral Word Association Test, LDCT = Letter Digit Coding Test, HVLT = Hopkin's Verbal Learning Test, HVLT-D = Hopkins Verbal Learning Test Delayed Recall, TMT-A = Trail Making Test Part A, TMT-B = Trail Making Test Part B.

Table 9.1: Model parameters for the 3 equations generated. CFI = comparative fit index, RMSEA = root mean square error of approximation, SRMR = standardised root mean square residual, saBIC = sample-size adjusted Bayesian Information Criterion.

	χ^2	df	p	CFI	RMSEA	SRMR	saBIC
Model 1	232.377	112	<0.001	0.781	0.096	0.110	14299.247
Model 2	314.401	181	<0.001	0.779	0.079	0.104	18196.961
Model 3	366.827	201	<0.001	0.741	0.083	0.109	19156.730
Model 4	409.382	241	<0.001	0.805	0.077	0.106	20051.397

Table 9.2: Regression parameters of Models 2 and 3 assessing SEM of carotid structure, brain structure and cognition. Std. Err = standard error, Std.Weight= standardised regression weights of the latent variable.

		β	Std. Err	Z	Sig.	Std. Weight	Std.all
Model 1	Cognition ~						
	Vessel	0.000	0.006	0.059	0.005	0.005	0.005
	Brain	-0.005	0.006	-0.890	0.374	-0.124	-0.124
	Age	-0.055	0.017	-3.167	0.002	-0.037	-0.318
Model 2	Cognition ~						
	Vessel	0.001	0.014	0.082	0.935	0.010	0.010
	Brain	-0.006	0.007	-0.919	0.358	-0.134	-0.134
	Age	-0.055	0.017	-3.195	0.001	-0.037	-0.320
Model 3	Cognition ~						
	Vessel	0.001	0.014	0.082	0.935	0.010	0.010
	Brain	-0.006	0.007	-0.919	0.358	-0.134	-0.134
	Age	-0.055	0.017	-3.195	0.001	-0.037	-0.320
Model 4	Cognition ~						
	Vessel	0.003	0.016	0.171	0.865	0.022	0.022
	Brain	-0.008	0.007	-1.034	0.301	-0.163	-0.163
	SVD	-0.019	0.018	-1.302	0.302	-0.142	-0.142
	Age	-0.050	0.017	-2.853	0.004	-0.033	-0.288

Model 1 demonstrated a CFI = 0.781, RMSEA = 0.096, SRMR = 0.110, with the β_{vessel} 0.000, p = 0.005 when regressed on cognition. This suggested that the averaged values of carotid disease were inadequate in describing the model and had no influence in cognitive performance. Only age was a significant regressor in this model (β_{age} -0.055, p = 0.002).

9.4.2 Model 2: Estimation and Evaluation

In Model 2, latent factors were described as “vessel”, “brain” and “cognition”. The vessel factor contains more observed variables than in Model 1. The vessel factor contains carotid artery disease measurements i.e., CCA IMT, ICA IMT, ICA stenosis and cervical carotid tortuosity, separated by side of cervical spine. This totalled 8 observed variables within the first factor. The second “brain” factor and third “cognition” factor remain unchanged from Model 1. Figure 9.3 demonstrates the estimated SEM Model 2.

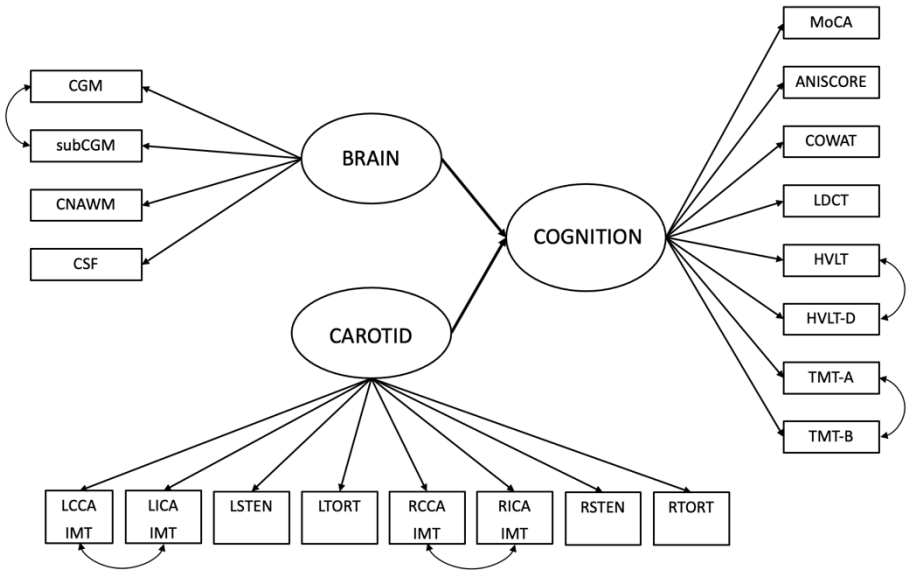

Figure 9.3: SEM Model 2 of carotid-brain interactions. LCCA = left common carotid artery, LICA = left internal carotid artery, RCCA = right common carotid artery, RICA = right internal carotid artery, IMT = intima-media thickness, STEN = ICA stenosis, TORT = extracranial carotid artery tortuosity, CGM = cortical grey matter, subCGM = subcortical grey matter, CNAWM = cortical normal appear white matter, CSF = cerebrospinal fluid, MoCA = Montreal Cognitive Assessment, ANI = Animal Naming Score, CoWAT = Controlled Oral Word Association Test, LDCT = Letter Digit Coding Test, HVLT = Hopkin’s Verbal Learning Test, HVLT-D = Hopkins Verbal Learning Test Delayed Recall, TMT-A = Trail Making Test Part A, TMT-B = Trail Making Test Part B

In the second model, the CFI = 0.779: RMSEA = 0.079, and SRMR = 0.104. Much like Model 1, these data suggest the model requires further fine tuning. With the reduced RMSEA and SRMR, this validates that averaged values of carotid artery disease variables are insufficient. In the regression estimates, only age is a significant predictor of cognitive function (β_{age} -0.055, p = 0.001). However, WMH has not been incorporated into the equation; this occurs in Model 3.

9.4.3 Model 3: Estimation and Evaluation

Like Models 1 and 2, the latent factors were described as "vessel", "brain", and "cognition". However, the latent factor "brain" is updated to include WMH volume. The latent factors "vessel" and "cognition" remain unchanged from Model 2. Figure 9.4 demonstrates the estimated SEM model.

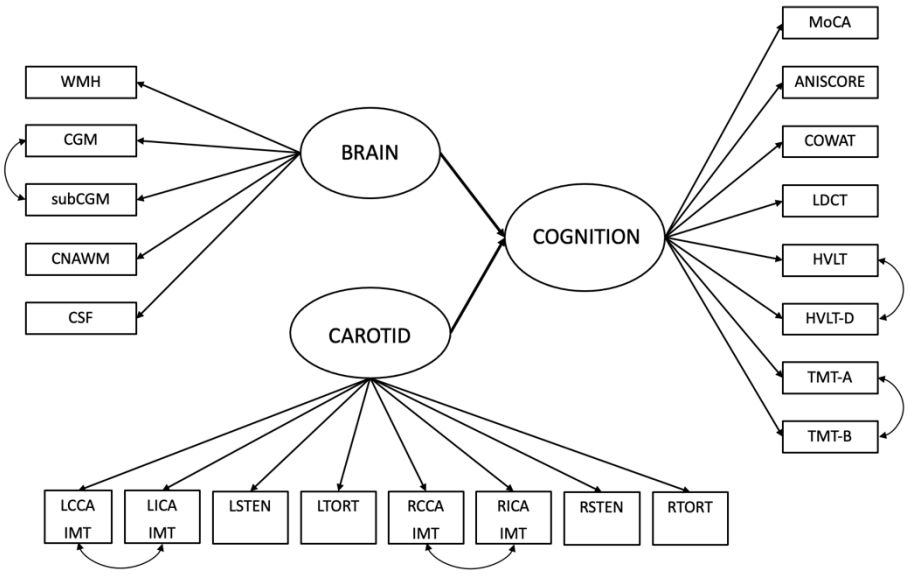

Figure 9.4: SEM Model 3 of carotid-brain interactions. LCCA = left common carotid artery, LICA = left internal carotid artery, RCCA = right common carotid artery, RICA = right internal carotid artery, IMT = intima-media thickness, STEN = ICA stenosis, TORT = extracranial carotid artery tortuosity, CGM = cortical grey matter, subCGM = subcortical grey matter, CNAWM = cortical normal appear white matter, CSF = cerebrospinal fluid, WMH = white matter hyperintensities, MoCA = Montreal

Cognitive Assessment, ANI = Animal Naming Score, CoWAT = Controlled Oral Word Association Test, LDCT = Letter Digit Coding Test, HVLT = Hopkin's Verbal Learning Test, HVLT-D = Hopkins Verbal Learning Test Delayed Recall, TMT-A = Trail Making Test Part A, TMT-B = Trail Making Test Part B

Model 3 now includes WMH has a measure of SVD burden. In this updated model, the CFI = 0.741, RMSEA = 0.083, SRMR = 0.109. The poorer model fit over Model 2 suggests that the SVD measure is not incorporated properly. Much like Models 1 and 2, only age is a significant predictor of cognitive performance (β_{age} -0.055, p = 0.001).

9.4.4 Model 4: Estimation and Evaluation

As per the previous frameworks, 3 latent factors were described as "vessel", "brain" and "cognition". However, "brain" no longer contains WMH volume. This is included in a fourth factor, "SVD", alongside total Fazekas score and total Schelten's scores. This inclusion of a fourth factor was used to describe a relationship between vessel structure and SVD that are independent of brain volume. Figure 9.4 demonstrates the estimated SEM Model 4.

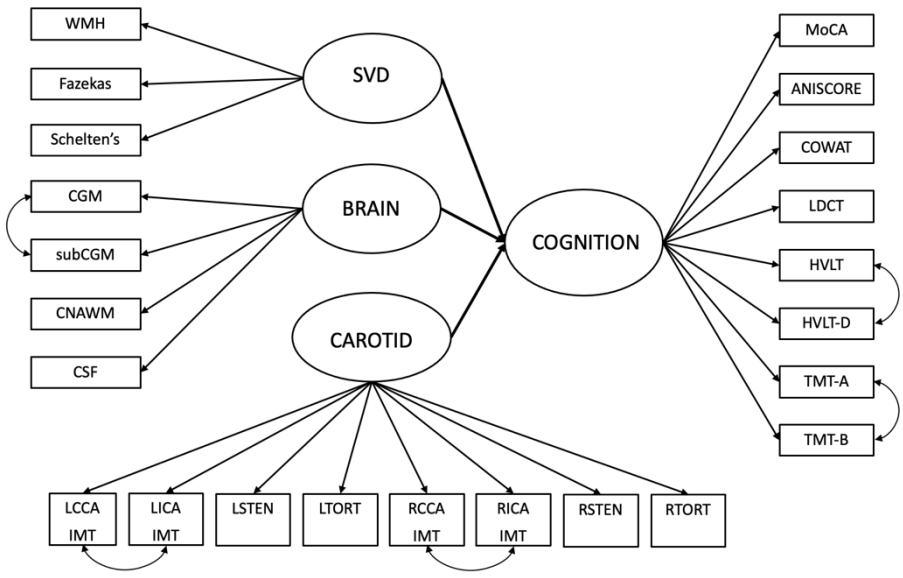

Figure 9.5: SEM Model 4 of carotid-brain interactions. LCCA = left common carotid artery, LICA = left internal carotid artery, RCCA = right common carotid artery, RICA = right internal carotid artery, IMT = intima-media thickness, STEN = ICA stenosis, TORT = extracranial carotid artery tortuosity, CGM = cortical grey matter, subCGM = subcortical grey matter, CNAWM = cortical normal appear white matter, CSF = cerebrospinal fluid, WMH = white matter hyperintensities, Fazekas = total Fazekas score, Schelten's = total Schelten's scale, MoCA = Montreal Cognitive Assessment, ANI = Animal Naming Score, CoWAT = Controlled Oral Word Association Test, LDCT = Letter Digit Coding Test, HVLT = Hopkin's Verbal Learning Test, HVLT-D = Hopkins Verbal Learning Test Delayed Recall, TMT-A = Trail Making Test Part A, TMT-B = Trail Making Test Part B

The fit of Model 4 is calculated as: CFI = 0.805, RMSEA = 0.077, SRMR = 0.106. The improvement in both CFI and RMSEA statistics suggests the likelihood of SVD as an independent latent variable to brain volume. Age was the only significant predictor of cognition in the regression estimates (β_{age} -0.050, p = 0.004).

9.5 Discussion

This chapter investigated a structural equation modelling framework to descript carotid-brain interactions in people with ischaemic stroke. Based on the theoretical understanding of carotid artery disease, brain structure and cognition in both this thesis and the wider literature, it was proposed that overarching variables used to describe the carotid arteries and brain structure may generate meaningful correlations with cognitive function.

These data describe all 4 models may not be satisfactory for describing carotid-brain interactions. In Model 1, I proposed the use of averaged values for carotid artery disease. In Chapter 3, I described some potential relationships between carotid artery disease and brain structure. Often, these relationships used one measure of disease e.g., stenosis. In this sense, an averaged measure of each disease biomarker would mimic the wider literature. Moreover, data from the multivariable regression in Chapter 7 suggested

that only age was a significant predictor of WMH volume. Whilst this relationship was not seen in the MoCA regression, using age as a covariate in this chapter was suggested, given its standard reporting in the wider literature. In Model 1, the CFI = 0.781, RMSEA = 0.096 and SRMR = 0.110. According to the guidelines proposed by Hu and Bentler, none of these statistics reached an acceptable goodness-of-fit standard[244]. In Models 2 and 3, by changing the definitions of the vessel and brain latent variables, neither of these models improved upon Model 1 (see Table 9.1). Model 4 incorporated SVD as an additional latent variable. Previous data provided in Chapter 3 and within the multivariable regression (Chapter 7) purported unreliable relationships between carotid artery disease and small vessel disease. By including SVD as a fourth latent variable, this model would suggest that SVD and carotid artery disease are independent predictors of cognitive function. In Model 4, the CFI = 0.805, RMSEA = 0.077, and SRMR = 0.106. This final model proved the best fit in this analysis. Despite this assertion, the goodness-of-fit is not sufficient to confirm the model accuracy.

The creation of latent (unobserved) variables only contain variance that is shared among the observed variables. This means that the latent variables are assumed to be free of measurement errors/other sources of variance that are specific to the individual observed variable. Subsequently, estimates that involve these latent variables are considered more reliable than single estimates between different manifest variables[240].

Testing the goodness-of-fit in SEM uses multiple statistical values, some of which are described above. These values (CFI, RMSEA, and SRMR) are often used in conjunction with each other. These statistics are used as a guide to infer the accuracy of the model generated. There are no fixed "cut-off" values that determines the model fit; rather an accurate model fit is at the discretion of the operator. Beran and Violata argue a CFI value $\geq$ 0.9, and an RMSEA <0.05 are considered adequate. However, Ullman suggests that an CFI > 0.95 is indicative of a good fit; RMSEA >0.10 indicates a poor fitting model[246,247]. Earlier in this chapter, I described values for a good model fit based on Hu and Bentler, which is more stringent in some measures[244]. Additionally, χ^2 values are often used in reporting the model accuracy. The χ^2 test is heavily influenced by sample size and is more often significant when evaluating models. Other factors should be considered when estimating the model including the sample size of the participants alongside the model

complexity and the research context. Nevertheless, no models reached the considered goodness-of-fit criteria according to any guidelines.

In the regression parameters (Table 9.2), the data suggests that increasing age significantly predicts poorer cognitive function. All 4 models displayed a modest β estimate (Models 1-3 $\beta = -0.055$, $p<0.005$; Model 4 $\beta = -0.05$, $p = 0.004$) with respect to age. Additionally, in Model 1, the averaged carotid artery disease markers had negligible effect on cognitive function ($\beta = 0.000$, $p = 0.005$). However, in Models 2-4, this relationship was not significant. These data suggest that cognitive function is not affected by carotid artery disease. Within asymptomatic (community-dwelling) individuals, carotid artery stenosis was not found to significantly alter cognitive function in an SEM model. In this analysis, carotid stenosis, blood flow velocity, pulsatility and resistivity were measured. The mean ICA stenosis was 12.96%, measured in 820 participants. Carotid stenosis was not a significant predictor of cognitive performance at baseline. The study measured a latent growth curve of cognitive change over 6 years. In the 4 latent variables of cognitive change, carotid stenosis did not significantly affect performance change when controlled for vascular risk factors. However, pulsatility and resistivity indices were significant predictors of crystallised cognition change ($\beta_{pulsatility} = -2.280$, $p = 0.008$; $\beta_{resistivity}$ -7.839, $p = 0.006$). This data would suggest that in place of structural markers of carotid artery disease, functional arterial measures may reliably predict cognitive performance[243].

The methods in this chapter were concerned with creating a model of ischaemic stroke at baseline. Latent growth curves are a method analogous to SEM used for longitudinal assessment. This chapter was not concerned with measuring longitudinal change due to the minimal progression of carotid artery disease and WMH load between baseline and the two-year follow-up (see Chapter 8). Furthermore, a 2-visit schedule for assessing cognitive performance change may not have been sufficient. Wardlaw et al., described change in cognitive performance over a 6-year (and 3 visit) schedule.

Whilst the SEM has proposed a complex relationship between carotid artery disease, brain structure and cognitive function, it is assumed that some variance has been

unaccounted for in this analysis. As previously mentioned, carotid plaque volume was not analysed in the black-blood imaging due to the thick slabs and large gaps between slices. Methods exist for describing plaque features across different MR sequences, based on the intensity of the pathology in relation to the background tissue. This could have given data describing the presence/absence of plaque features. However, it is thought that plaque volume would be a more robust measurement in place of a binary response variable. With data describing the influence of functional markers of carotid disease on cognitive performance, these data require further study. It is hoped that a framework of standardised carotid artery disease measurements, inclusive of both structural e.g., IMT, stenosis, tortuosity, plaque volume and functional measures e.g., pulsatility, blood flow velocity will greatly benefit the understanding of carotid artery disease in ischaemic stroke populations. Additionally, including total SVD burden (lacunes, WMH, perivascular spaces, microbleeds) may provide a more accurate model. It is possible that multiple imputation could have been used to bolster these data; however with n = 63 participants having missing data in some form, it was thought this may be unsuitable[248].

9.6 Summary

This chapter explored the use of structural equation modelling to confirm the hypothesis of an overarching relationship between carotid artery disease and brain structure, and their effect on cognitive function in ischaemic stroke. The data presented in this chapter, though significant, highlights that with some methodological advances, it is possible such a hypothesis may prove true. Future directions of studies into carotid artery disease and ischaemic stroke should take these additional measurements into account.

10 Conclusions

Stroke is a common illness that significantly impacts patients and society. It is assumed that stroke rates will increase in prevalence across the world, with low- and middle-income countries exhibiting the greatest increases. Carotid artery disease is a common risk factor for ischaemic stroke, with descriptions of disease including carotid artery stenosis and thickening of the intima-media thickness. This thesis has addressed several key areas by investigating relationships between carotid artery disease and small vessel disease in ischaemic stroke. This thesis found that small variations in carotid artery tortuosity are significantly related to white matter hyperintensity burden and found no evidence of reductions in carotid artery disease or small vessel disease by xanthine oxidase reduction.

This programme of work included a systematic review which described the lack of reporting standards in stroke/imaging studies, which may hamper conclusions from these trials. Vascular risk factors were often unreported in stroke studies, thus failing to describe common covariates that may explain previously significant associations between carotid structure and brain structure or cognition. It demonstrated that there are no studies that investigate links between carotid artery disease, brain structure and cognitive functioning in stroke patients.

In Chapter 5, the results obtained from method validation suggested that all image analysis techniques employed were valid in this work. The agreement of ICA stenosis between myself and radiologists varied greatly. However, the data analysed was stratified into the NASCET clinical labels. These labels of stenosis include non-significant (<50%), mild (50-59%), moderate (60-69%), severe (70-99%) and occluded (100%). The mean κ agreement values were sufficient for a description of "good" reliability; the variations are likely due to population skew towards the non-significant stenosis group, and the clinical labels which have uneven boundaries. Both the IMT and tortuosity assessments displayed excellent replicability.

In Chapter 6, the thesis highlighted that links between carotid artery disease and common risk factors for stroke are variable, with no more that 1 risk factor associated with any one carotid measurement. In Chapter 7, there were no significant relationships between ICA stenosis or with small vessel disease; and no relationships were seen between carotid artery disease and post-stroke cognitive functioning. This thesis demonstrated that upon accounting for common vascular risk factors in a multivariate regression model, carotid artery disease was not significantly related with small vessel disease burden. However, these data only demonstrated low R^2 values (0.19) which suggests most of the variance seen in WMH burden was still unaccounted for.

median increase of 3.12% in left ICA stenosis; 4.08% right ICA stenosis across the whole cohort. Right ICA stenosis % demonstrated a significant difference between treatment groups at follow-up, though this is an incidental finding. There were no significant differences between treatment groups or risk groups when change in ICA stenosis was assessed. This is also true for the IMT measures, which all demonstrated non-significant differences in both progression (median left CCA IMT 0.80mm^3; right CCA IMT 0.40mm^3) or regression (median left ICA IMT -4.12mm^3; median right ICA IMT -2.07mm^3). The extracranial carotid artery tortuosity index values exhibited a median change of 0.002 (left carotid) or -0.001 (right carotid) in the entire cohort. Furthermore, there was a non-significant progression in the WMH in the whole cohort; no significant differences were found in the longitudinal assessment across the treatment groups or risk categories.

Additionally, this thesis investigated the progression of carotid artery disease in a 2-year follow-up study. The progression of carotid artery stenosis was calculated as a median of 3.12% in the left ICA; 4.08% in the right ICA over 2 years. Intima-media thickness demonstrated both progression (median left CCA IMT 0.80mm^3; right CCA IMT 0.40mm^3) or regression (median left ICA IMT -4.12mm^3; median right ICA IMT -2.07mm^3). In these measurements, were no significant differences between treatment groups. This would suggest that allopurinol does not reduce carotid artery disease in an ischaemic stroke population. There were no significant alterations in extracranial carotid artery tortuosity; though a 2-year longitudinal assessment may fail to find significant differences in carotid tortuosity without sufficient lifestyle changes e.g., reduction in visceral fat deposition around arteries. Moreover, this thesis found that there are no significant differences between participants considered high-risk or low risk for

cardiovascular events in any carotid artery disease measures. The thesis studied the progression of carotid artery disease and small vessel disease finding no significant differences between the two groups. These data, in line with the full XILO-FIST study, demonstrates that allopurinol should not be a targeted therapy to reduce small vessel disease burden in ischaemic stroke.

In Chapter 9, various structural equation models were formed to confirm the hypothesis that there may be a relationship between carotid structure, brain structure and cognitive function. These data showed that the models failed to reach a significant valid threshold i.e., CFI was below 0.95 and RMSEA was above 0.05 in all 4 instances. However, these models did highlight that there may be an importance in creating a single carotid variable to assess vessel health. This would require additional imaging data e.g., carotid plaque to test this hypothesis. It also demonstrated that there was a small effect between carotid vessel structure and SVD independent of brain structure.

Future directions of this work point to evaluating carotid plaque formation in a mild stroke population. These missing data may have demonstrated other associations with brain structure and cognitive function. Plaque type and volume may help to understand the biological pathway that leads to carotid artery disease, and whether allopurinol would be a targeted medicine. Future work should aim to better describe SVD burden in ischaemic stroke. This thesis did not evaluate perivascular spaces, lacunes or microbleeds. Other research in this field aims to improve the assessment of these SVD measurements through automatic segmentation procedures. It is proposed that by replicating these methods, further analysis could be drawn between carotid structure and SVD burden. This may take the route of evaluating SVD using the Brain Health Index, an overall assessment of brain structure. The Brain Health Index requires only standard MR imaging sequences utilised in the XILO-FIST study; thus, this data could be readily available.

It is thought that with the additional vascular data, it may be possible to replicate previous work in the creation of the Brain Health Index and create a “Vascular Health Index” of similar function. Data like this would build upon the structural equation models previously described and create a singular value of vessel health.

Currently, both European Carotid Surgery Trial 2 (ECST-2) and Carotid Revascularization and Medical Management for Asymptomatic Carotid Stenosis Trial (CREST-2) are ongoing. These trials both investigate the medical management of carotid artery disease. Data from these trials may indicate preferred treatment options in carotid atherosclerosis. These data may aid the direction of future planned studies in carotid artery disease and ischaemic stroke.

11 References

1. Rajendran P, Rengarajan T, Thangavel J, et al. The vascular endothelium and human diseases. *Int J Biol Sci* 2013; 9: 1057–1069.

2. Longhorn M, Hughes S. Modern replication of Eratosthenes' measurement of the circumference of Earth. *Phys Educ* 2015; 50: 175–178.

3. Aird WC. Discovery of the cardiovascular system: from Galen to William Harvey. *J Thromb Haemost* 2011; 9: 118–129.

4. Ribatti D. William Harvey and the discovery of the circulation of the blood. *J Angiogenesis Res* 2009; 1: 3.

5. DeWeerdt S. How to map the brain. *Nature* 2019; 571: S6–S8.

6. Jain V, Langham MC, Wehrli FW. MRI estimation of global brain oxygen consumption rate. *J Cereb Blood Flow Metab* 2010; 30: 1598–1607.

7. Xing C-Y, Tarumi T, Liu J, et al. Distribution of cardiac output to the brain across the adult lifespan. *J Cereb Blood Flow Metab* 2017; 37: 2848–2856.

8. Jordan JD, Powers WJ. Cerebral autoregulation and acute ischemic stroke. *Am J Hypertens* 2012; 25: 946–950.

9. Warlow C, van Gijn J, Dennis MS, et al. *Stroke: Practical Management*. Oxford: Blackwell Publishing, 2008.

10. Sacco RL, Kasner SE, Broderick JP, et al. An Updated Definition of Stroke for the 21st Century. *Stroke* 2013; 44: 2064–2089.

11. Johnson W, Onuma O, Owolabi M, et al. Stroke: a global response is needed. *Bull World Health Organ* 2016; 94: 634.

12. Feigin VL, Forouzanfar MH, Krishnamurthi R, et al. Global and regional burden of stroke during 1990-2010: Findings from the Global Burden of Disease Study 2010. *The Lancet* 2014; 383: 245–255.

13. World Health Organization. The top 10 causes of death, https://www.who.int/news-room/fact-sheets/detail/the-top-10-causes-of-death (2014, accessed 1 October 2021).

14. Martínez-Vila E, Irimia P. The Cost of Stroke. *Cerebrovasc Dis* 2004; 17(suppl 1: 124–129.

15. National Audit Office. Department of Health: reducing brain damage : faster access to better stroke care. 2005; 2005: 60.

16. World Health Organisation. *The atlas of heart disease and stroke*. World Health Organisation, https://apps.who.int/iris/handle/10665/43007 (2004, accessed 5 July 2022).

17. Leeder S, Raymond S, Greenberg H, et al. *A Race Against Time: The Challenge of Cardiovascular Disease in Developing Countries*. The Trustees of Columbia University in the City of New York, 2004.

18. Wu Z, Yao C, Zhao D, et al. Sino-MONICA Project. *Circulation* 2001; 103: 462–468.

19. Mohan KM, Wolfe CDA, Rudd AG, et al. Risk and cumulative risk of stroke recurrence: A systematic review and meta-analysis. *Stroke* 2011; 42: 1489–1494.

20. Skajaa N, Adelborg K, Horváth-Puhó E, et al. Risks of Stroke Recurrence and Mortality After First and Recurrent Strokes in Denmark. *Neurology* 2022; 98: e329–e342.

21. Hill MD, Coutts SB. Preventing stroke after transient ischemic attack. *CMAJ Can Med Assoc J J Assoc Medicale Can* 2011; 183: 1127–1128.

22. Adams HP, Bendixen BH, Kappelle LJ, et al. Classification of subtype of acute ischemic stroke definitions for use in a multicenter clinical trial. *Stroke* 1993; 24: 35–41.

23. Venkataraman P, Tadi P, Lui F. Lacunar Syndromes. *StatPearls*, https://www.ncbi.nlm.nih.gov/books/NBK534206/ (2021, accessed 5 July 2022).

24. Bamford J, Sandercock P, Dennis M, et al. Classification and natural history of clinically identifiable subtypes of cerebral infarction. *The Lancet* 1991; 337: 1521–1526.

25. Stroke NI of ND and. *NIH Stroke Scale*. 2012. Epub ahead of print 2012. DOI: 10.1007/springerreference_184783.

26. Muir KW, Weir CJ, Murray GD, et al. Comparison of Neurological Scales and Scoring Systems for Acute Stroke Prognosis. *Stroke* 1996; 27: 1817–1820.

27. Wardlaw JM, Smith C, Dichgans M. Mechanisms of sporadic cerebral small vessel disease: insights from neuroimaging. *Lancet Neurol* 2013; 12: 483–497.

28. Wardlaw JM, Smith EE, Biessels GJ, et al. Neuroimaging standards for research into small vessel disease and its contribution to ageing and neurodegeneration. *Lancet Neurol* 2013; 12: 822–838.

29. Wardlaw JM, Smith C, Dichgans M. Small vessel disease: mechanisms and clinical implications. *Lancet Neurol* 2019; 18: 684–696.

30. Wardlaw JM, Benveniste H, Nedergaard M, et al. Perivascular spaces in the brain: anatomy, physiology and pathology. *Nat Rev Neurol* 2020; 16: 137–153.

31. Wardlaw JM, Valdés Hernández MC, Muñoz-Maniega S. What are White Matter Hyperintensities Made of? *J Am Heart Assoc Cardiovasc Cerebrovasc Dis* 2015; 4: e001140.

32. Debette S, Markus HS. The clinical importance of white matter hyperintensities on brain magnetic resonance imaging: systematic review and meta-analysis. *BMJ* 2010; 341: c3666–c3666.

33. Li Y, Li M, Zuo L, et al. Compromised Blood–Brain Barrier Integrity Is Associated With Total Magnetic Resonance Imaging Burden of Cerebral Small Vessel Disease. *Front Neurol* 2018; 9: 221.

34. Lau K-K, Li L, Lovelock CE, et al. Clinical Correlates, Ethnic Differences, and Prognostic Implications of Perivascular Spaces in Transient Ischemic Attack and Ischemic Stroke. *Stroke* 2017; 48: 1470–1477.

35. Wardlaw JM. What Is a Lacune? *Stroke* 2008; 39: 2921–2922.

36. Andersen SD, Skjøth F, Yavarian Y, et al. Multiple Silent Lacunes Are Associated with Recurrent Ischemic Stroke. *Cerebrovasc Dis* 2016; 42: 73–80.

37. Akoudad S, Wolters FJ, Viswanathan A, et al. Cerebral microbleeds are associated with cognitive decline and dementia: the Rotterdam Study. *JAMA Neurol* 2016; 73: 934–943.

38. Cerebral Microbleeds and Recurrent Stroke Risk | Stroke, https://www.ahajournals.org/doi/full/10.1161/strokeaha.111.000038 (accessed 28 April 2023).

39. Sun JH, Tan L, Yu JT. Post-stroke cognitive impairment: Epidemiology, mechanisms and management. *Ann Transl Med*; 2. Epub ahead of print 1 August 2014. DOI: 10.3978/j.issn.2305-5839.2014.08.05.

40. Douiri A, Rudd AG, Wolfe CDA. Prevalence of poststroke cognitive impairment: South London Stroke Register 1995-2010. *Stroke* 2013; 44: 138–145.

41. Rasquin S, Verhey F, van Oostenbrugge RJ, et al. Demographic and CT scan features related to cognitive impairment in the first year after stroke. *J Neurol Neurosurg Psychiatry* 2004; 75: 1562–1567.

42. Drozdowska BA, Elliott E, Taylor-Rowan M, et al. Cardiovascular risk factors indirectly affect acute post-stroke cognition through stroke severity and prior cognitive impairment: a moderated mediation analysis. *Alzheimers Res Ther* 2020; 12: 85.

43. Liang Y, Chen Y-K, Liu Y-L, et al. Cerebral Small Vessel Disease Burden Is Associated With Accelerated Poststroke Cognitive Decline: A 1-Year Follow-Up Study. *J Geriatr Psychiatry Neurol* 2019; 32: 336–343.

44. Arba F, Quinn T, Hankey GJ, et al. Cerebral small vessel disease, medial temporal lobe atrophy and cognitive status in patients with ischaemic stroke and transient ischaemic attack. *Eur J Neurol* 2017; 24: 276–282.

45. Jochems ACC, Muñoz Maniega S, Clancy U, et al. Associations of Peak-Width Skeletonized Mean Diffusivity and Post-Stroke Cognition. *Life* 2022; 12: 1362.

46. Allan PL, Wardlaw JM. Carotids, vertebrals and TCD (transcranial Doppler). In: *Clinical Ultrasound*. Elsevier Ltd, 2011, pp. 965–984.

47. Chengazi HU, Bhatt AA. Pathology of the carotid space. *Insights Imaging* 2019; 10: 1–16.

48. Garner DH, Kortz MW, Baker S. Anatomy, Head and Neck, Carotid Sheath. *StatPearls*, https://www.ncbi.nlm.nih.gov/books/NBK519577/ (2022, accessed 7 July 2022).

49. Anatomy, Head and Neck, Carotid Arteries - StatPearls - NCBI Bookshelf, https://www.ncbi.nlm.nih.gov/books/NBK545238/ (accessed 1 October 2021).

50. Uchino A, Saito N, Okada Y, et al. Variation of the origin of the left common carotid artery diagnosed by CT angiography. *Surg Radiol Anat SRA* 2013; 35: 339–342.

51. Harrigan MR, Deveikis JP. Essential Neurovascular Anatomy. In: Harrigan MR, Deveikis JP (eds) *Handbook of Cerebrovascular Disease and Neurointerventional Technique*. Totowa, NJ: Humana Press, pp. 3–98.

52. Bouthillier A, van Loveren HR, Keller JT. Segments of the Internal Carotid Artery: A New Classification. *Neurosurgery* 1996; 38: 425–433.

53. Lasjaunias P, Santoyo-Vazquez A. Segmental agenesis of the internal carotid artery: angiographic aspects with embryological discussion. *Anat Clin* 1984; 6: 133–141.

54. Leloup AJA, Van Hove CE, Heykers A, et al. Elastic and muscular arteries differ in structure, basal NO production and voltage-gated Ca2+-channels. *Front Physiol* 2015; 6: 375.

55. Mercadante AA, Raja A. Anatomy, Arteries. In: *StatPearls*. Treasure Island (FL): StatPearls Publishing, http://www.ncbi.nlm.nih.gov/books/NBK547743/ (2022, accessed 31 August 2022).

56. Pirahanchi Y, Bordoni B. Anatomy, Head and Neck, Carotid Baroreceptors. *StatPearls*, https://www.ncbi.nlm.nih.gov/books/NBK537223/ (2019, accessed 7 July 2022).

57. Andani R, Khan YS. Anatomy, Head and Neck, Carotid Sinus. *StatPearls*, https://www.ncbi.nlm.nih.gov/books/NBK554378/ (2021, accessed 7 July 2022).

58. Libby P, Ridker PM, Hansson GK. Progress and challenges in translating the biology of atherosclerosis. *Nature* 2011; 473: 317–325.

59. Bergheanu SC, Bodde MC, Jukema JW. Pathophysiology and treatment of atherosclerosis. *Neth Heart J* 2017; 25: 231–242.

60. Prasad K. Pathophysiology and Medical Treatment of Carotid Artery Stenosis. *Int J Angiol Off Publ Int Coll Angiol Inc* 2015; 24: 158–172.

61. Libby P, Ridker PM, Maseri A. Inflammation and Atherosclerosis. *Circulation* 2002; 105: 1135–1143.

62. Cunningham KS, Gotlieb AI. The role of shear stress in the pathogenesis of atherosclerosis. *Lab Invest* 2005; 85: 9–23.

63. Chiu J-J, Chien S. Effects of Disturbed Flow on Vascular Endothelium: Pathophysiological Basis and Clinical Perspectives. *Physiol Rev* 2011; 91: 10.1152/physrev.00047.2009.

64. Moore WS, Barnett H j. m., Beebe HG, et al. Guidelines for Carotid Endarterectomy. *Circulation* 1995; 91: 566–579.

65. Barnett HJM. North American Symptomatic Carotid Endarterectomy Trial. Methods, patient characteristics, and progress. *Stroke* 1991; 22: 711–720.

66. Barnett HJM, Taylor DW, Eliasziw M, et al. Benefit of Carotid Endarterectomy in Patients with Symptomatic Moderate or Severe Stenosis. *N Engl J Med* 1998; 339: 1415–1425.

67. Rothwell PM, Gutnikov SA, Warlow CP. Reanalysis of the Final Results of the European Carotid Surgery Trial. *Stroke* 2003; 34: 514–523.

68. O'Leary DH, Polak JF, Kronmal RA, et al. Distribution and correlates of sonographically detected carotid artery disease in the Cardiovascular Health Study. The CHS Collaborative Research Group. *Stroke* 1992; 23: 1752–1760.

69. de Weerd M, Greving JP, Hedblad B, et al. Prevalence of asymptomatic carotid artery stenosis in the general population: an individual participant data meta-analysis. *Stroke J Cereb Circ* 2010; 41: 1294–1297.

70. Stary HC, Chandler AB, Dinsmore RE, et al. A Definition of Advanced Types of Atherosclerotic Lesions and a Histological Classification of Atherosclerosis. *Circulation* 1995; 92: 1355–1374.

71. Gupta A, Baradaran H, Schweitzer AD, et al. Carotid plaque MRI and stroke risk: a systematic review and meta-analysis. *Stroke* 2013; 44: 3071–3077.

72. Howard DP, van Lammeren GW, Rothwell PM, et al. Symptomatic carotid atherosclerotic disease: correlations between plaque composition and ipsilateral stroke risk. *Stroke J Cereb Circ* 2015; 46: 182–189.

73. Simon A, Gariepy J, Chironi G, et al. Intima–media thickness: a new tool for diagnosis and treatment of cardiovascular risk. *J Hypertens* 2002; 20: 159–169.

74. Pignoli P, Tremoli E, Poli A, et al. Intimal plus medial thickness of the arterial wall: a direct measurement with ultrasound imaging. *Circulation* 1986; 74: 1399–1406.

75. Stein JH, Korcarz CE, Hurst RT, et al. Use of Carotid Ultrasound to Identify Subclinical Vascular Disease and Evaluate Cardiovascular Disease Risk: A Consensus Statement from the American Society of Echocardiography Carotid Intima-Media Thickness Task Force Endorsed by the Society for Vascular Medicine. *J Am Soc Echocardiogr* 2008; 21: 93–111.

76. Bots ML, Hoes AW, Koudstaal PJ, et al. Common Carotid Intima-Media Thickness and Risk of Stroke and Myocardial Infarction. *Circulation* 1997; 96: 1432–1437.

77. Lorenz MW, Markus HS, Bots ML, et al. Prediction of Clinical Cardiovascular Events With Carotid Intima-Media Thickness. *Circulation* 2007; 115: 459–467.

78. Lorenz MW, Polak JF, Kavousi M, et al. Carotid intima-media thickness progression to predict cardiovascular events in the general population (the PROG-IMT collaborative project): a meta-analysis of individual participant data. *Lancet* 2012; 379: 2053–2062.

79. Han H-C. Twisted Blood Vessels: Symptoms, Etiology and Biomechanical Mechanisms. *J Vasc Res* 2012; 49: 185–197.

80. Thomas JB, Antiga L, Che SL, et al. Variation in the carotid bifurcation geometry of young versus older adults: implications for geometric risk of atherosclerosis. *Stroke* 2005; 36: 2450–2456.

81. Del Corso L, Moruzzo D, Conte B, et al. Tortuosity, kinking, and coiling of the carotid artery: expression of atherosclerosis or aging? *Angiology* 1998; 49: 361–371.

82. Welby JP, Kim ST, Carr CM, et al. Carotid Artery Tortuosity Is Associated with Connective Tissue Diseases. *Am J Neuroradiol* 2019; 40: 1738–1743.

83. Saba L, Sanfilippo R, Suri JS, et al. Does Carotid Artery Tortuosity Play a Role in Stroke? *Can Assoc Radiol J* 2021; 0: 084653712199105.

84. AboElfetouh N, Khedr E, Aboloyoun H, et al. Prevalence of internal carotid artery morphological variations and its association with cerebrovascular ischemic stroke (hospital-based study). *Egypt J Neurol Psychiatry Neurosurg* 2020; 56: 90.

85. Settecase F, Rayz VL. Chapter 6 - Advanced vascular imaging techniques. In: Hetts SW, Cooke DL (eds) *Handbook of Clinical Neurology*. Elsevier, pp. 81–105.

86. Bradley WG. History of Medical Imaging. *Proc Am Philos Soc* 2008; 152: 349–361.

87. Wintermark M, Jawadi SS, Rapp JH, et al. High-resolution CT imaging of carotid artery atherosclerotic plaques. *AJNR Am J Neuroradiol* 2008; 29: 875–882.

88. Saba L, Caddeo G, Sanfilippo R, et al. Efficacy and Sensitivity of Axial Scans and Different Reconstruction Methods in the Study of the Ulcerated Carotid Plaque Using Multidetector-Row CT Angiography: Comparison with Surgical Results. *AJNR Am J Neuroradiol* 2007; 28: 716–723.

89. Link J, Brossmann J, Grabener M, et al. Spiral CT angiography and selective digital subtraction angiography of internal carotid artery stenosis. *AJNR Am J Neuroradiol* 1996; 17: 89–94.

90. Hasebroock KM, Serkova NJ. Toxicity of MRI and CT contrast agents. *Expert Opin Drug Metab Toxicol* 2009; 5: 403–416.

91. Reilly LM, Lusby RJ, Hughes L, et al. Carotid plaque histology using real-time ultrasonography. Clinical and therapeutic implications. *Am J Surg* 1983; 146: 188–193.

92. Park TH. Evaluation of Carotid Plaque Using Ultrasound Imaging. *J Cardiovasc Ultrasound* 2016; 24: 91–95.

93. Mathiesen EB, Bønaa KH, Joakimsen O. Echolucent Plaques Are Associated With High Risk of Ischemic Cerebrovascular Events in Carotid Stenosis. *Circulation* 2001; 103: 2171–2175.

94. Mitchell DG. Color Doppler imaging: principles, limitations, and artifacts. *Radiology* 1990; 177: 1–10.

95. Comerota AJ, Katz ML, White JV, et al. The preoperative diagnosis of the ulcerated carotid atheroma. *J Vasc Surg* 1990; 11: 505–510.

96. Sitzer M, Müller W, Rademacher J, et al. Color-flow Doppler-assisted duplex imaging fails to detect ulceration in high-grade internal carotid artery stenosis. *J Vasc Surg* 1996; 23: 461–465.

97. Saba L, Caddeo G, Sanfilippo R, et al. CT and Ultrasound in the Study of Ulcerated Carotid Plaque Compared with Surgical Results: Potentialities and Advantages of Multidetector Row CT Angiography. *AJNR Am J Neuroradiol* 2007; 28: 1061–1066.

98. El Ridi R, Tallima H. Physiological functions and pathogenic potential of uric acid: A review. *J Adv Res* 2017; 8: 487.

99. Pacher P, Nivorozhkin A, Szabó C. Therapeutic Effects of Xanthine Oxidase Inhibitors: Renaissance Half a Century after the Discovery of Allopurinol. *Pharmacol Rev* 2006; 58: 87.

100. Weir CJ, Muir SW, Walters MR, et al. Serum urate as an independent predictor of poor outcome and future vascular events after acute stroke. *Stroke* 2003; 34: 1951–1956.

101. Dawson J, Lees KR, Weir CJ, et al. Baseline serum urate and 90-day functional outcomes following acute ischemic stroke. *Cerebrovasc Dis Basel Switz* 2009; 28: 202–203.

102. Khan AA, Quinn TJ, Hewitt J, et al. Serum uric acid level and association with cognitive impairment and dementia: systematic review and meta-analysis. *Age Dordr Neth* 2016; 38: 16.

103. Dawson J, Walters M. Uric acid and xanthine oxidase: future therapeutic targets in the prevention of cardiovascular disease? *Br J Clin Pharmacol* 2006; 62: 633–644.

104. Dawson J, Quinn T, Walters M. Uric acid reduction: a new paradigm in the management of cardiovascular risk? *Curr Med Chem* 2007; 14: 1879–1886.

105. Seo YK, Guevara JP, Kyoung MK, et al. Hyperuricemia and Risk of Stroke: A Systematic Review and Meta-analysis. *Arthritis Rheum* 2009; 61: 885.

106. Bredemeier M, Lopes LM, Eisenreich MA, et al. Xanthine oxidase inhibitors for prevention of cardiovascular events: a systematic review and meta-analysis of randomized controlled trials. *BMC Cardiovasc Disord* 2018; 18: 24.

107. van der Pol KH, Wever KE, Verbakel M, et al. Allopurinol to reduce cardiovascular morbidity and mortality: A systematic review and meta-analysis. *PLoS ONE* 2021; 16: e0260844.

108. Alem MM. Allopurinol and endothelial function: A systematic review with meta-analysis of randomized controlled trials. *Cardiovasc Ther* 2018; 36: e12432.

109. Nomura J, Busso N, Ives A, et al. Xanthine Oxidase Inhibition by Febuxostat Attenuates Experimental Atherosclerosis in Mice. *Sci Rep* 2014; 4: 4554.

110. Ganji M, Nardi V, Prasad M, et al. Carotid Plaques From Symptomatic Patients Are Characterized by Local Increase in Xanthine Oxidase Expression. *Stroke* 2021; 52: 2792–2801.

111. Nardi V, Franchi F, Prasad M, et al. Uric Acid Expression in Carotid Atherosclerotic Plaque and Serum Uric Acid Are Associated With Cerebrovascular Events. *Hypertension* 2022; 79: 1814–1823.

112. Chamorro Á, Obach V, Cervera Á, et al. Prognostic Significance of Uric Acid Serum Concentration in Patients With Acute Ischemic Stroke. *Stroke* 2002; 33: 1048–1052.

113. Flaherty ML, Kissela B, Khoury JC, et al. Carotid artery stenosis as a cause of stroke. *Neuroepidemiology* 2013; 40: 36–41.

114. Inzitari D, Eliasziw M, Gates P, et al. The causes and risk of stroke in patients with asymptomatic internal-carotid-artery stenosis. North American Symptomatic Carotid Endarterectomy Trial Collaborators. *N Engl J Med* 2000; 342: 1693–1700.

115. Avelar WM, D'Abreu A, Coan AC, et al. Asymptomatic carotid stenosis is associated with gray and white matter damage. *Int J Stroke Off J Int Stroke Soc* 2015; 10: 1197–1203.

116. van den Bouwhuijsen QJA, Vernooij MW, Verhaaren BFJ, et al. Carotid Plaque Morphology and Ischemic Vascular Brain Disease on MRI. *Am J Neuroradiol* 2017; 38: 1776–1782.

117. Ammirati E, Moroni F, Magnoni M, et al. Relation between characteristics of carotid atherosclerotic plaques and brain white matter hyperintensities in asymptomatic patients. *Sci Rep* 2017; 7: 10559.

118. Lindsay AC, Biasiolli L, Lee JMS, et al. Plaque Features Associated With Increased Cerebral Infarction After Minor Stroke and TIA: A Prospective, Case-Control, 3-T Carotid Artery MR Imaging Study. *JACC Cardiovasc Imaging* 2012; 5: 388–396.

119. Potter GM, Doubal FN, Jackson CA, et al. Lack of association of white matter lesions with ipsilateral carotid artery stenosis. *Cerebrovasc Dis Basel Switz* 2012; 33: 378–384.

120. Romero JR, Beiser A, Seshadri S, et al. Carotid artery atherosclerosis, MRI indices of brain ischemia, aging, and cognitive impairment: the Framingham study. *Stroke* 2009; 40: 1590–1596.

121. Mathiesen EB, Waterloo K, Joakimsen O, et al. Reduced neuropsychological test performance in asymptomatic carotid stenosis: The Tromso Study. *Neurology* 2004; 62: 695–701.

122. Yue W, Wang A, Zhu R, et al. Association between Carotid Artery Stenosis and Cognitive Impairment in Stroke Patients: A Cross-Sectional Study. *PloS One* 2016; 11: e0146890.

123. Chen L, Huang J, Wang S, et al. Effect of Carotid Artery Morphological Variations on Cognitive Function. *Behav Neurol*; 2018. Epub ahead of print 2018. DOI: 10.1155/2018/7290431.

124. Moher D, Liberati A, Tetzlaff J, et al. Preferred Reporting Items for Systematic Reviews and Meta-Analyses: The PRISMA Statement. *PLOS Med* 2009; 6: e1000097.

125. Chen H, Hong H, Xing S, et al. Intracranial versus Extracranial Symptomatic Carotid Atherosclerosis in Chinese Patients: Risk Factors, Stroke Mechanisms, and Long-Term Prognosis. *J Stroke Cerebrovasc Dis Off J Natl Stroke Assoc* 2015; 24: 2632–2639.

126. Arenillas JF, Rovira A, Molina CA, et al. Prediction of early neurological deterioration using diffusion- and perfusion-weighted imaging in hyperacute middle cerebral artery ischemic stroke. *Stroke* 2002; 33: 2197–2203.

127. Derex L, Hermier M, Adeleine P, et al. Influence of the site of arterial occlusion on multiple baseline hemodynamic MRI parameters and post-thrombolytic recanalization in acute stroke. *Neuroradiology* 2004; 46: 883–887.

128. Guler S, Utku U, Aynaci O. Early clinical signs, lesion localization, and prognostic factors in unilateral symptomatic internal carotid artery occlusion. *J Stroke Cerebrovasc Dis Off J Natl Stroke Assoc* 2014; 23: 1908–1914.

129. Hendrikse J, Hartkamp MJ, Hillen B, et al. Collateral ability of the circle of Willis in patients with unilateral internal carotid artery occlusion: border zone infarcts and clinical symptoms. *Stroke* 2001; 32: 2768–2773.

130. Hermier M, Ibrahim AS, Wiart M, et al. The delayed perfusion sign at MRI. *J Neuroradiol J Neuroradiol* 2003; 30: 172–179.

131. Hong C-T, Chan H-F, Lee S-P, et al. Cerebral infarct in patients with bilateral high-grade internal carotid artery stenosis: analysis by diffusion-weighted imaging. *Eur Neurol* 2011; 65: 88–93.

132. Isabel C, Lecler A, Turc G, et al. Relationship between watershed infarcts and recent intra plaque haemorrhage in carotid atherosclerotic plaque. *PloS One* 2014; 9: e108712.

133. Joinlambert C, Saliou G, Flamand-Roze C, et al. Cortical border-zone infarcts: clinical features, causes and outcome. *J Neurol Neurosurg Ampamp Psychiatry* 2012; 83: 771 LP – 775.

134. Jongen C, Nederkoorn PJ, Niessen WJ, et al. Analysis of cerebral infarction pattern in computed tomography images of patients with internal carotid artery stenosis. *Invest Radiol* 2004; 39: 462–469.

135. Kang D-W, Chu K, Ko S-B, et al. Lesion patterns and mechanism of ischemia in internal carotid artery disease: a diffusion-weighted imaging study. *Arch Neurol* 2002; 59: 1577–1582.

136. Kao H-L, Lin M-S, Wu W-C, et al. Improvement of Cerebral Glucose Metabolism in Symptomatic Patients With Carotid Artery Stenosis After Stenting. *Clin Nucl Med* 2015; 40: 701–707.

137. Bayer-Karpinska A, Schwarz F, Wollenweber FA, et al. The carotid plaque imaging in acute stroke (CAPIAS) study: protocol and initial baseline data. *BMC Neurol* 2013; 13: 201.

138. Kim D-E, Lee K-B, Roh H, et al. Association of internal border zone infarction with middle cerebral artery steno-occlusion. *Eur Neurol* 2010; 64: 178–185.

139. Kotsugi M, Takayama K, Myouchin K, et al. Carotid Artery Stenting: Investigation of Plaque Protrusion Incidence and Prognosis. *JACC Cardiovasc Interv* 2017; 10: 824–831.

140. Kumral E, Bayulkem G, Sagcan A. Mechanisms of single and multiple borderzone infarct: transcranial Doppler ultrasound/magnetic resonance imaging correlates. *Cerebrovasc Dis Basel Switz* 2004; 17: 287–295.

141. Lau KK, Pego P, Mazzucco S, et al. Age and sex-specific associations of carotid pulsatility with small vessel disease burden in transient ischemic attack and ischemic stroke. *Int J Stroke Off J Int Stroke Soc* 2018; 13: 832–839.

142. Lee M, Saver JL, Hao Q, et al. Anterior choroidal artery ischaemic patterns predict outcome of carotid occlusion. *J Neurol Neurosurg Psychiatry* 2012; 83: 586–590.

143. Lee W-J, Jung K-H, Ryu YJ, et al. Progression of Cerebral White Matter Hyperintensities and the Associated Sonographic Index. *Radiology* 2017; 284: 824–833.

144. Li H, Xiong Y, Xu G, et al. The Circle of Willis and White Matter Lesions in Patients with Carotid Atherosclerosis. *J Stroke Cerebrovasc Dis Off J Natl Stroke Assoc* 2015; 24: 1749–1754.

145. Li X, Ma X, Lin J, et al. Severe carotid artery stenosis evaluated by ultrasound is associated with post stroke vascular cognitive impairment. *Brain Behav* 2017; 7: e00606.

146. Liberman AL, Zandieh A, Loomis C, et al. Symptomatic Carotid Occlusion Is Frequently Associated With Microembolization. *Stroke* 2017; 48: 394–399.

147. Liu Y, Karonen JO, Vanninen RL, et al. Acute ischemic stroke: predictive value of 2D phase-contrast MR angiography--serial study with combined diffusion and perfusion MR imaging. *Radiology* 2004; 231: 517–527.

148. Beck C, Cheng B, Krutzelmann A, et al. Outcome of MRI-based intravenous thrombolysis in carotid-T occlusion. *J Neurol* 2012; 259: 2141–2146.

149. Meng D, Hosseini AA, Simpson RJ, et al. Lesion Topography and Microscopic White Matter Tract Damage Contribute to Cognitive Impairment in Symptomatic Carotid Artery Disease. *Radiology* 2016; 282: 502–515.

150. Mounier-Vehier F, Leys D, Pruvo JP. Stroke patterns in unilateral atherothrombotic occlusion of the internal carotid artery. *Stroke* 1995; 26: 422–425.

151. Na DG, Ryoo JW, Lee KH, et al. Multiphasic perfusion computed tomography in hyperacute ischemic stroke: comparison with diffusion and perfusion magnetic resonance imaging. *J Comput Assist Tomogr* 2003; 27: 194–206.

152. Nakano S, Yokogami K, Ohta H, et al. CT-defined large subcortical infarcts: correlation of location with site of cerebrovascular occlusive disease. *AJNR Am J Neuroradiol* 1995; 16: 1581–1585.

153. Neumann-Haefelin T, Wittsack HJ, Fink GR, et al. Diffusion- and perfusion-weighted MRI: influence of severe carotid artery stenosis on the DWI/PWI mismatch in acute stroke. *Stroke* 2000; 31: 1311–1317.

154. Park AY, Chung T-S, Suh SH, et al. Asymmetric dilatation of virchow-robin space in unilateral internal carotid artery steno-occlusive disease. *J Comput Assist Tomogr* 2011; 35: 298–302.

155. Sahin N, Solak A, Genc B, et al. Dilatation of the Virchow-Robin spaces as an indicator of unilateral carotid artery stenosis: correlation with white matter lesions. *Acta Radiol Stockh Swed 1987* 2015; 56: 852–859.

156. Sahin N, Solak A, Genc B, et al. Brain diffusion changes in unilateral carotid artery stenosis with non-shunt endarterectomy: Correlation with white matter lesions. *Clin Neurol Neurosurg* 2015; 133: 24–29.

157. Streifler JY, Eliasziw M, Benavente OR, et al. Prognostic importance of leukoaraiosis in patients with symptomatic internal carotid artery stenosis. *Stroke* 2002; 33: 1651–1655.

158. Streifler JY, Eliasziw M, Benavente OR, et al. Lack of relationship between leukoaraiosis and carotid artery disease. The North American Symptomatic Carotid Endarterectomy Trial. *Arch Neurol* 1995; 52: 21–24.

159. Bisschops RHC, Klijn CJM, Kappelle LJ, et al. Prevalence and volume of internal border zone lesions in patients with impaired cerebral carbon dioxide vasomotor reactivity: a follow-up study. *Arch Neurol* 2003; 60: 1233–1236.

160. Szabo K, Kern R, Gass A, et al. Acute stroke patterns in patients with internal carotid artery disease: a diffusion-weighted magnetic resonance imaging study. *Stroke* 2001; 32: 1323–1329.

161. Tao X-X, Li G-F, Wu Y-L, et al. Relationship between intracranial internal carotid artery calcification and enlarged cerebral perivascular space. *Neuroradiology* 2017; 59: 577–586.

162. van der Grond J, van Everdingen KJ, Eikelboom BC, et al. Assessment of borderzone ischemia with a combined MR imaging-MR angiography-MR spectroscopy protocol. *J Magn Reson Imaging JMRI* 1999; 9: 1–9.

163. Wang Y, Wang J. Clinical and imaging features in different inner border-zone infarct patterns. *Int J Neurosci* 2015; 125: 208–212.

164. Yamauchi H, Kudoh T, Sugimoto K, et al. Pattern of collaterals, type of infarcts, and haemodynamic impairment in carotid artery occlusion. *J Neurol Neurosurg Psychiatry* 2004; 75: 1697–1701.

165. Yano C, Iwata M, Uchiyama S. Risk factors for small cortical infarction on diffusion-weighted magnetic resonance imaging in patients with acute ischemic stroke. *J Stroke Cerebrovasc Dis Off J Natl Stroke Assoc* 2011; 20: 68–74.

166. Yong SW, Bang OY, Lee PH, et al. Internal and cortical border-zone infarction: clinical and diffusion-weighted imaging features. *Stroke* 2006; 37: 841–846.

167. Bisschops RHC, Klijn CJM, Kappelle LJ, et al. Association between impaired carbon dioxide reactivity and ischemic lesions in arterial border zone territories in patients with unilateral internal carotid artery occlusion. *Arch Neurol* 2003; 60: 229–233.

168. Bisschops RHC, Klijn CJM, Kappelle LJ, et al. Collateral flow and ischemic brain lesions in patients with unilateral carotid artery occlusion. *Neurology* 2003; 60: 1435–1441.

169. Chung P-W, Park K-Y, Moon H-S, et al. Intracranial internal carotid artery calcification: a representative for cerebral artery calcification and association with white matter hyperintensities. *Cerebrovasc Dis Basel Switz* 2010; 30: 65–71.

170. de Rotte AAJ, Koning W, den Hartog AG, et al. 7.0 T MRI detection of cerebral microinfarcts in patients with a symptomatic high-grade carotid artery stenosis. *J Cereb Blood Flow Metab Off J Int Soc Cereb Blood Flow Metab* 2014; 34: 1715–1719.

171. Derex L, Nighoghossian N, Hermier M, et al. Influence of pretreatment MRI parameters on clinical outcome, recanalization and infarct size in 49 stroke patients treated by intravenous tissue plasminogen activator. *J Neurol Sci* 2004; 225: 3–9.

172. Lee DK, Kim JS, Kwon SU, et al. Lesion patterns and stroke mechanism in atherosclerotic middle cerebral artery disease: early diffusion-weighted imaging study. *Stroke* 2005; 36: 2583–2588.

173. Wells G, Shea B, O'Connell D, et al. The Newcastle-Ottawa Scale (NOS) for Assessing the Quality of Nonrandomized Studies in Meta- Analysis.

174. Ribeiro CM, Beserra BTS, Silva NG, et al. Exposure to endocrine-disrupting chemicals and anthropometric measures of obesity: a systematic review and meta-analysis. *BMJ Open* 2020; 10: e033509.

175. Sahin N, Solak A, Genc B, et al. Brain diffusion changes in unilateral carotid artery stenosis with non-shunt endarterectomy: Correlation with white matter lesions. *Clin Neurol Neurosurg* 2015; 133: 24–29.

176. Lee W-J, Jung K-H, Ryu YJ, et al. Progression of Cerebral White Matter Hyperintensities and the Associated Sonographic Index. *Radiology* 2017; 284: 824–833.

177. Ritchie SJ, Dickie DA, Cox SR, et al. Brain volumetric changes and cognitive ageing during the eighth decade of life. *Hum Brain Mapp* 2015; 36: 4910–4925.

178. Donnan GA, Davis SM, Chambers BR, et al. Surgery for prevention of stroke. *Lancet Lond Engl* 1998; 351: 1372–1373.

179. Van Damme H, Limet R. Lessons learnt from carotid artery trials. *Acta Chir Belg* 2006; 106: 489–499.

180. Staikov IN, Arnold M, Mattle HP, et al. Comparison of the ECST, CC, and NASCET grading methods and ultrasound for assessing carotid stenosis. European Carotid Surgery Trial. North American Symptomatic Carotid Endarterectomy Trial. *J Neurol* 2000; 247: 681–686.

181. O'Donnell MJ, Chin SL, Rangarajan S, et al. Global and regional effects of potentially modifiable risk factors associated with acute stroke in 32 countries (INTERSTROKE): a case-control study. *The Lancet* 2016; 388: 761–775.

182. Dawson J, Broomfield N, Dani K, et al. Xanthine oxidase inhibition for the improvement of long-term outcomes following ischaemic stroke and transient

ischaemic attack (XILO-FIST) - Protocol for a randomised double blind placebo-controlled clinical trial. *Eur Stroke J* 2018; 3: 281–290.

183. Habes M, Lancaster JL, Martinez MJ. Research Imaging Institute - Mango, http://mangoviewer.com/index.html (2006, accessed 9 June 2022).

184. Touboul P, Hennerici M, Meairs S, et al. Mannheim Carotid Intima-Media Thickness and Plaque Consensus (2004–2006–2011): An Update on Behalf of the Advisory Board of the 3rd and 4th Watching the Risk Symposium 13th and 15th European Stroke Conferences, Mannheim, Germany, 2004, and Brussels, Belgium, 2006. *Cerebrovasc Dis Basel Switz* 2012; 34: 290–296.

185. Antiga L. VMTK - The Vascular Modelling Toolkit. *OROBIX Srl*, http://www.vmtk.org/ (2015, accessed 8 June 2022).

186. Piccinelli M, Veneziani A, Steinman DA, et al. A framework for geometric analysis of vascular structures: Application to cerebral aneurysms. *IEEE Trans Med Imaging* 2009; 28: 1141–1155.

187. Wang Z, Ma B, Zhu Y. Review of Level Set in Image Segmentation. *Arch Comput Methods Eng* 2021; 28: 2429–2446.

188. Osher S, Sethian JA. Fronts propagating with curvature-dependent speed: Algorithms based on Hamilton-Jacobi formulations. *J Comput Phys* 1988; 79: 12–49.

189. Antiga L, Piccinelli M, Botti L, et al. An image-based modeling framework for patient-specific computational hemodynamics. *Med Biol Eng Comput* 2008; 46: 1097–1112.

190. Lorensen WE, Cline HE. Marching cubes: A high resolution 3D surface construction algorithm. In: *Proceedings of the 14th Annual Conference on Computer Graphics and Interactive Techniques, SIGGRAPH 1987*. 1987, pp. 163–169.

191. Fazekas F, Chawluk JB, Alavi A, et al. MR signal abnormalities at 1.5 T in Alzheimer's dementia and normal aging. *Am J Roentgenol* 1987; 149: 351–356.

192. Scheltens P, Barkhof F, Leys D, et al. A semiquantative rating scale for the assessment of signal hyperintensities on magnetic resonance imaging. *J Neurol Sci* 1993; 114: 7–12.

193. Prins ND, Van Straaten ECW, Van Dijk EJ, et al. Measuring progression of cerebral white matter lesions on MRI: Visual rating and volumetrics. *Neurology* 2004; 62: 1533–1539.

194. Schmidt R, Fazekas F, Kapeller P, et al. MRI white matter hyperintensities: Three-year follow-up of the Austrian Stroke Prevention Study. *Neurology* 1999; 53: 132–139.

195. Avants BB, Epstein CL, Grossman M, et al. Symmetric diffeomorphic image registration with cross-correlation: Evaluating automated labeling of elderly and neurodegenerative brain. *Med Image Anal* 2008; 12: 26–41.

196. Tustison NJ, Cook PA, Klein A, et al. Large-scale evaluation of ANTs and FreeSurfer cortical thickness measurements. *NeuroImage* 2014; 99: 166–179.

197. Avants BB, Tustison NJ, Wu J, et al. An open source multivariate framework for N-tissue segmentation with evaluation on public data. *Neuroinformatics* 2011; 9: 381–400.

198. Zhang Y, Brady M, Smith S. Segmentation of brain MR images through a hidden Markov random field model and the expectation-maximization algorithm. *IEEE Trans Med Imaging* 2001; 20: 45–57.

199. Dawson B, Trapp RG. *Basic & Clinical Biostatistics 4/E (EBOOK)*. McGraw Hill Professional, 2004.

200. Koo TK, Li MY. A Guideline of Selecting and Reporting Intraclass Correlation Coefficients for Reliability Research. *J Chiropr Med* 2016; 15: 155–163.

201. O'Donnell MJ, Chin SL, Rangarajan S, et al. Global and regional effects of potentially modifiable risk factors associated with acute stroke in 32 countries (INTERSTROKE): a case-control study. *The Lancet* 2016; 388: 761–775.

202. Tanne D, Shotan A, Goldbourt U, et al. Severity of Angina Pectoris and Risk of Ischemic Stroke. *Stroke* 2002; 33: 245–250.

203. null null, Sacco RL, Benjamin EJ, et al. Risk Factors. *Stroke* 1997; 28: 1507–1517.

204. Arboix A. Cardiovascular risk factors for acute stroke: Risk profiles in the different subtypes of ischemic stroke. *World J Clin Cases WJCC* 2015; 3: 418–429.

205. Woodward M, Brindle P, Tunstall-Pedoe H, et al. Adding social deprivation and family history to cardiovascular risk assessment: the ASSIGN score from the Scottish Heart Health Extended Cohort (SHHEC). *Heart* 2005; 93: 172–176.

206. Development and validation of QRISK3 risk prediction algorithms to estimate future risk of cardiovascular disease: prospective cohort study | The BMJ, https://www.bmj.com/content/357/bmj.j2099 (accessed 21 September 2022).

207. Woodward M, Brindle P, Tunstall-Pedoe H, et al. Adding social deprivation and family history to cardiovascular risk assessment: the ASSIGN score from the Scottish Heart Health Extended Cohort (SHHEC). *Heart Br Card Soc* 2007; 93: 172–176.

208. Tunstall-Pedoe H. Cardiovascular Risk and Risk Scores: ASSIGN, Framingham, QRISK and others: how to choose. *Heart* 2011; 97: 442–444.

209. Ferreira JP, Girerd N, Bozec E, et al. Intima–Media Thickness Is Linearly and Continuously Associated With Systolic Blood Pressure in a Population-Based Cohort (STANISLAS Cohort Study). *J Am Heart Assoc*; 5: e003529.

210. Ren L, Cai J, Liang J, et al. Impact of Cardiovascular Risk Factors on Carotid Intima-Media Thickness and Degree of Severity: A Cross-Sectional Study. *PLOS ONE* 2015; 10: e0144182.

211. Ren L, Shi M, Wu Y, et al. Correlation between hypertension and common carotid artery intima-media thickness in rural China: a population-based study. *J Hum Hypertens* 2018; 32: 548–554.

212. Łoboz-Rudnicka M, Jaroch J, Bociąga Z, et al. Impact of cardiovascular risk factors on carotid intima-media thickness: sex differences. *Clin Interv Aging* 2016; 11: 721–731.

213. Witt N, Wong TY, Hughes AD, et al. Abnormalities of Retinal Microvascular Structure and Risk of Mortality From Ischemic Heart Disease and Stroke. *Hypertension* 2006; 47: 975–981.

214. Sun Z, Jiang D, Liu P, et al. Age-Related Tortuosity of Carotid and Vertebral Arteries: Quantitative Evaluation With MR Angiography. *Front Neurol*; 13, https://www.frontiersin.org/articles/10.3389/fneur.2022.858805 (2022, accessed 21 September 2022).

215. Ciurică S, Lopez-Sublet M, Loeys BL, et al. Arterial Tortuosity. *Hypertension* 2019; 73: 951–960.

216. Wang H-F, Wang D-M, Wang J-J, et al. Extracranial Internal Carotid Artery Tortuosity and Body Mass Index. *Front Neurol* 2017; 8: 508.

217. Mochida M, Sakamoto H, Sawada Y, et al. Visceral Fat Obesity Contributes to the Tortuosity of the Thoracic Aorta on Chest Radiograph in Poststroke Japanese Patients. *Angiology* 2006; 57: 85–91.

218. Zerna C, Yu AYX, Hong ZM, et al. White Matter Hyperintensity Volume Influences Symptoms in Patients Presenting With Minor Neurological Deficits. *Stroke* 2020; 51: 409–415.

219. Wardlaw JM, Chappell FM, Valdés Hernández M del C, et al. White matter hyperintensity reduction and outcomes after minor stroke. *Neurology* 2017; 89: 1003–1010.

220. Della-Morte D, Dong C, Markert MS, et al. Carotid Intima-Media Thickness Is Associated With White Matter Hyperintensities: The Northern Manhattan Study. *Stroke* 2018; 49: 304–311.

221. Thurston RC, Wu M, Barinas-Mitchell E, et al. Carotid intima media thickness and white matter hyperintensity volume among midlife women. *Alzheimers Dement J Alzheimers Assoc*. Epub ahead of print 1 February 2023. DOI: 10.1002/alz.12951.

222. Cermakova P, Ding J, Meirelles O, et al. Carotid Intima–Media Thickness and Markers of Brain Health in a Biracial Middle-Aged Cohort: CARDIA Brain MRI Sub-study. *J Gerontol Ser A* 2020; 75: 380–386.

223. Hobart JC, Cano SJ, Zajicek JP, et al. Rating scales as outcome measures for clinical trials in neurology: problems, solutions, and recommendations. *Lancet Neurol* 2007; 6: 1094–1105.

224. Johnston SC, O'Meara ES, Manolio TA, et al. Cognitive impairment and decline are associated with carotid artery disease in patients without clinically evident cerebrovascular disease. *Ann Intern Med* 2004; 140: 237–247.

225. Arntzen KA, Schirmer H, Johnsen SH, et al. Carotid atherosclerosis predicts lower cognitive test results: a 7-year follow-up study of 4,371 stroke-free subjects - the Tromsø study. *Cerebrovasc Dis Basel Switz* 2012; 33: 159–165.

226. Mathiesen EB, Waterloo K, Joakimsen O, et al. Reduced neuropsychological test performance in asymptomatic carotid stenosis: The Tromso Study. *Neurology* 2004; 62: 695–701.

227. Shang K, Chen X, Cheng C, et al. Arterial Tortuosity and Its Correlation with White Matter Hyperintensities in Acute Ischemic Stroke. *Neural Plast* 2022; 2022: e4280410.

228. Liu J, Ke X, Lai Q. Increased tortuosity of bilateral distal internal carotid artery is associated with white matter hyperintensities. *Acta Radiol Stockh Swed 1987* 2021; 62: 515–523.

229. Ong C-T, Wong Y-S, Sung S-F, et al. Progression of Mild to Moderate Stenosis in the Internal Carotid Arteries of Patients With Ischemic Stroke. *Front Neurol* 2018; 9: 1043.

230. Baldassarre D, Veglia F, Hamsten A, et al. Progression of carotid intima-media thickness as predictor of vascular events: results from the IMPROVE study. *Arterioscler Thromb Vasc Biol* 2013; 33: 2273–2279.

231. Kakkos SK, Nicolaides AN, Charalambous I, et al. Predictors and clinical significance of progression or regression of asymptomatic carotid stenosis. *J Vasc Surg* 2014; 59: 956-967.e1.

232. Dawson J, Robertson M, Dickie DA, et al. Xanthine oxidase inhibition and white matter hyperintensity progression following ischaemic stroke and transient ischaemic attack (XILO-FIST): a multicentre, double-blinded, randomised, placebo-controlled trial. *eClinicalMedicine*; 57. Epub ahead of print 1 March 2023. DOI: 10.1016/j.eclinm.2023.101863.

233. Dufouil C, Chalmers J, Coskun O, et al. Effects of Blood Pressure Lowering on Cerebral White Matter Hyperintensities in Patients With Stroke. *Circulation* 2005; 112: 1644–1650.

234. Cho A-H, Kim H-R, Kim W, et al. White Matter Hyperintensity in Ischemic Stroke Patients: It May Regress Over Time. *J Stroke* 2015; 17: 60–66.

235. Clancy U, Makin SDJ, McHutchison CA, et al. Impact of Small Vessel Disease Progression on Long-term Cognitive and Functional Changes After Stroke. *Neurology* 2022; 98: e1459–e1469.

236. Hamilton OKL, Cox SR, Okely JA, et al. Cerebral small vessel disease burden and longitudinal cognitive decline from age 73 to 82: the Lothian Birth Cohort 1936. *Transl Psychiatry* 2021; 11: 1–12.

237. Kamal F, Morrison C, Maranzano J, et al. Topographical differences in white matter hyperintensity burden and cognition in aging, MCI, and AD. 2022; 2022.04.20.22274087.

238. Georgakis MK, Duering M, Wardlaw JM, et al. WMH and long-term outcomes in ischemic stroke: A systematic review and meta-analysis. *Neurology* 2019; 92: e1298–e1308.

239. An Introduction to Structural Equation Modeling | SpringerLink, https://link.springer.com/chapter/10.1007/978-3-030-80519-7_1 (accessed 25 February 2024).

240. Penke L, Deary IJ. Some guidelines for structural equation modelling in cognitive neuroscience: The case of Charlton et al.'s study on white matter integrity and cognitive ageing. *Neurobiol Aging* 2010; 31: 1656–1660.

241. McGrory S, Ballerini L, Doubal FN, et al. Retinal microvasculature and cerebral small vessel disease in the Lothian Birth Cohort 1936 and Mild Stroke Study. *Sci Rep* 2019; 9: 6320.

242. Hoffman P, Cox SR, Dykiert D, et al. Brain grey and white matter predictors of verbal ability traits in older age: The Lothian Birth Cohort 1936. *NeuroImage* 2017; 156: 394–402.

243. Wardlaw JM, Allerhand M, Eadie E, et al. Carotid disease at age 73 and cognitive change from age 70 to 76 years: A longitudinal cohort study. *J Cereb Blood Flow Metab* 2017; 37: 3042–3052.

244. Hu L, Bentler PM. Cutoff criteria for fit indexes in covariance structure analysis: Conventional criteria versus new alternatives. *Struct Equ Model Multidiscip J* 1999; 6: 1–55.

245. Pavlov G, Maydeu-Olivares A, Shi D. Using the Standardized Root Mean Squared Residual (SRMR) to Assess Exact Fit in Structural Equation Models. *Educ Psychol Meas* 2021; 81: 110–130.

246. Beran TN, Violato C. Structural equation modeling in medical research: a primer. *BMC Res Notes* 2010; 3: 267.

247. Ullman J. Structural Equation Modeling: Reviewing the Basics and Moving Forward. *J Pers Assess* 2006; 87: 35–50.

248. Jakobsen JC, Gluud C, Wetterslev J, et al. When and how should multiple imputation be used for handling missing data in randomised clinical trials – a practical guide with flowcharts. *BMC Med Res Methodol* 2017; 17: 162.

12 Appendix

12.1 Structural Equation Modelling Statistics

12.1.1 Model 1

```
lavaan 0.6-12 ended normally after 471 iterations

  Estimator                                         ML
  Optimization method                           NLMINB
  Number of model parameters                        40

  Number of observations                           118

Model Test User Model:
                                              Standard      Robust
  Test Statistic                               233.352     232.377
  Degrees of freedom                               112         112
  P-value (Chi-square)                           0.000       0.000
  Scaling correction factor                                  1.004
    Satorra-Bentler correction

Model Test Baseline Model:

  Test statistic                               693.781     666.621
  Degrees of freedom                               136         136
  P-value                                        0.000       0.000
  Scaling correction factor                                  1.041

User Model versus Baseline Model:

  Comparative Fit Index (CFI)                    0.782       0.773
  Tucker-Lewis Index (TLI)                       0.736       0.725

  Robust Comparative Fit Index (CFI)                         0.781
  Robust Tucker-Lewis Index (TLI)                            0.734

Loglikelihood and Information Criteria:

  Loglikelihood user model (H0)              -7117.435   -7117.435
  Loglikelihood unrestricted model (H1)      -7000.759   -7000.759

  Akaike (AIC)                               14314.869   14314.869
  Bayesian (BIC)                             14425.697   14425.697
  Sample-size adjusted Bayesian (BIC)        14299.247   14299.247

Root Mean Square Error of Approximation:

  RMSEA                                          0.096       0.095
  90 Percent confidence interval - lower         0.078       0.078
  90 Percent confidence interval - upper         0.113       0.113
  P-value RMSEA <= 0.05                          0.000       0.000

  Robust RMSEA                                               0.096
  90 Percent confidence interval - lower                     0.078
```

```
  90 Percent confidence interval - upper                  0.113

Standardized Root Mean Square Residual:

  SRMR                                            0.110       0.110

Parameter Estimates:

  Standard errors                           Robust.sem
  Information                                 Expected
  Information saturated (h1) model          Structured

Latent Variables:
                   Estimate  Std.Err  z-value  P(>|z|)   Std.lv  Std.all
  vessel =~
    avgcca            1.000                              20.516    1.141
    avgica            0.436    0.147    2.977    0.003    8.950    0.796
    avgsten          -0.017    0.056   -0.295    0.768   -0.340   -0.026
    avgtort           0.037    0.063    0.586    0.558    0.753    0.180
  brain =~
    cgm               1.000                              33.826    0.809
    subcgm            0.086    0.010    8.989    0.000    2.920    0.655
    cnawm             1.284    0.178    7.232    0.000   43.425    0.938
    csf               0.483    0.116    4.153    0.000   16.350    0.379
  cog =~
    moca              1.000                               1.497    0.552
    aniscore          1.666    0.369    4.515    0.000    2.494    0.651
    cowattot          3.080    0.789    3.902    0.000    4.612    0.372
    ldcttot           7.002    1.732    4.042    0.000   10.483    0.527
    hvlt              2.304    0.543    4.243    0.000    3.449    0.644
    hvltdelay         1.262    0.291    4.332    0.000    1.889    0.725
    tmta             -5.462    1.257   -4.345    0.000   -8.178   -0.303
    tmtb             -9.370    3.104   -3.019    0.003  -14.029   -0.359

Regressions:
                   Estimate  Std.Err  z-value  P(>|z|)   Std.lv  Std.all
  cog ~
    vessel            0.000    0.006    0.059    0.953    0.005    0.005
    brain            -0.005    0.006   -0.890    0.374   -0.124   -0.124
    age              -0.055    0.017   -3.167    0.002   -0.037   -0.318

Covariances:
                   Estimate  Std.Err  z-value  P(>|z|)   Std.lv  Std.all
 .avgcca ~~
   .avgica          -72.843  298.399   -0.244    0.807  -72.843   -1.083
 .cgm ~~
   .subcgm           12.498   16.260    0.769    0.442   12.498    0.151
 .hvlt ~~
   .hvltdelay         3.877    1.121    3.457    0.001    3.877    0.527
 .tmta ~~
   .tmtb            159.828   81.522    1.961    0.050  159.828    0.170
  vessel ~~
    brain           165.734   54.420    3.045    0.002    0.239    0.239

Variances:
                   Estimate  Std.Err  z-value  P(>|z|)   Std.lv  Std.all
   .avgcca          -97.636  674.077   -0.145    0.885  -97.636   -0.302
   .avgica           46.322  136.109    0.340    0.734   46.322    0.366
   .avgsten         173.583   19.523    8.891    0.000  173.583    0.999
   .avgtort          16.918    4.433    3.816    0.000   16.918    0.968
   .cgm             605.218  150.253    4.028    0.000  605.218    0.346
```

```
   .subcgm          11.341    2.189    5.181    0.000   11.341    0.571
   .cnawm          255.893  271.702    0.942    0.346  255.893    0.119
   .csf           1593.984  218.015    7.311    0.000 1593.984    0.856
   .moca             5.122    0.922    5.555    0.000    5.122    0.696
   .aniscore         8.474    1.467    5.776    0.000    8.474    0.577
   .cowattot       132.548   19.288    6.872    0.000  132.548    0.862
   .ldcttot        285.848   60.203    4.748    0.000  285.848    0.722
   .hvlt            16.755    3.006    5.574    0.000   16.755    0.585
   .hvltdelay        3.229    0.662    4.878    0.000    3.229    0.475
   .tmta           661.937  335.037    1.976    0.048  661.937    0.908
   .tmtb          1332.792  246.561    5.406    0.000 1332.792    0.871
    vessel         420.903  675.577    0.623    0.533    1.000    1.000
    brain         1144.198  238.238    4.803    0.000    1.000    1.000
   .cog              1.982    0.846    2.341    0.019    0.884    0.884

R-Square:
                Estimate
    avgcca            NA
    avgica         0.634
    avgsten        0.001
    avgtort        0.032
    cgm            0.654
    subcgm         0.429
    cnawm          0.881
    csf            0.144
    moca           0.304
    aniscore       0.423
    cowattot       0.138
    ldcttot        0.278
    hvlt           0.415
    hvltdelay      0.525
    tmta           0.092
    tmtb           0.129
    cog            0.116
```

12.1.2 Model 2

```
lavaan 0.6-12 ended normally after 664 iterations

  Estimator                                         ML
  Optimization method                           NLMINB
  Number of model parameters                        49

  Number of observations                           118

Model Test User Model:
                                              Standard      Robust
  Test Statistic                               311.881     314.401
  Degrees of freedom                           181         181
  P-value (Chi-square)                         0.000       0.000
  Scaling correction factor                                0.992
    Satorra-Bentler correction

Model Test Baseline Model:

  Test statistic                               811.143     799.224
  Degrees of freedom                           210         210
  P-value                                      0.000       0.000
  Scaling correction factor                                1.015

User Model versus Baseline Model:

  Comparative Fit Index (CFI)                  0.782       0.774
  Tucker-Lewis Index (TLI)                     0.747       0.737

  Robust Comparative Fit Index (CFI)                       0.779
  Robust Tucker-Lewis Index (TLI)                          0.743

Loglikelihood and Information Criteria:

  Loglikelihood user model (H0)            -9059.049   -9059.049
  Loglikelihood unrestricted model (H1)    -8903.109   -8903.109

  Akaike (AIC)                             18216.099   18216.099
  Bayesian (BIC)                           18351.862   18351.862
  Sample-size adjusted Bayesian (BIC)      18196.961   18196.961

Root Mean Square Error of Approximation:

  RMSEA                                        0.078       0.079
  90 Percent confidence interval - lower       0.063       0.064
  90 Percent confidence interval - upper       0.093       0.094
  P-value RMSEA <= 0.05                        0.001       0.001

  Robust RMSEA                                             0.079
  90 Percent confidence interval - lower                   0.064
  90 Percent confidence interval - upper                   0.093

Standardized Root Mean Square Residual:

  SRMR                                         0.104       0.104

Parameter Estimates:
```

```
  Standard errors                         Robust.sem
  Information                               Expected
  Information saturated (h1) model          Structured

Latent Variables:
                   Estimate  Std.Err  z-value  P(>|z|)   Std.lv  Std.all
  vessel =~
    lcca              1.000                              12.673    0.578
    lica              0.587    0.179    3.278    0.001    7.439    0.512
    rcca              1.182    0.312    3.791    0.000   14.977    0.719
    rica              0.404    0.180    2.244    0.025    5.121    0.351
    lsten            -0.036    0.140   -0.256    0.798   -0.455   -0.029
    rsten            -0.006    0.126   -0.048    0.961   -0.077   -0.005
    ltort             0.055    0.029    1.892    0.059    0.692    0.173
    rtort             0.108    0.071    1.516    0.129    1.373    0.215
  brain =~
    cgm               1.000                              33.193    0.794
    subcgm            0.087    0.010    9.028    0.000    2.891    0.648
    cnawm             1.332    0.189    7.052    0.000   44.202    0.955
    csf               0.485    0.116    4.186    0.000   16.113    0.378
  cog =~
    moca              1.000                               1.497    0.551
    aniscore          1.669    0.369    4.521    0.000    2.498    0.651
    cowattot          3.082    0.788    3.913    0.000    4.613    0.372
    ldcttot           7.006    1.731    4.047    0.000   10.487    0.527
    hvlt              2.311    0.543    4.256    0.000    3.459    0.646
    hvltdelay         1.265    0.291    4.346    0.000    1.893    0.726
    tmta             -5.446    1.254   -4.341    0.000   -8.152   -0.302
    tmtb             -9.346    3.098   -3.017    0.003  -13.990   -0.357

Regressions:
                   Estimate  Std.Err  z-value  P(>|z|)   Std.lv  Std.all
  cog ~
    vessel            0.001    0.014    0.082    0.935    0.010    0.010
    brain            -0.006    0.007   -0.919    0.358   -0.134   -0.134
    age              -0.055    0.017   -3.195    0.001   -0.037   -0.320

Covariances:
                   Estimate  Std.Err  z-value  P(>|z|)   Std.lv  Std.all
 .lcca ~~
   .lica             71.170   52.345    1.360    0.174   71.170    0.319
 .rcca ~~
   .rica             27.030   35.712    0.757    0.449   27.030    0.136
 .cgm ~~
   .subcgm           15.378   16.459    0.934    0.350   15.378    0.178
 .hvlt ~~
   .hvltdelay         3.860    1.120    3.448    0.001    3.860    0.526
 .tmta ~~
   .tmtb            164.070   81.530    2.012    0.044  164.070    0.174
 vessel ~~
   brain            149.161   53.835    2.771    0.006    0.355    0.355

Variances:
                   Estimate  Std.Err  z-value  P(>|z|)   Std.lv  Std.all
   .lcca            320.145   57.411    5.576    0.000  320.145    0.666
   .lica            155.432   62.045    2.505    0.012  155.432    0.737
   .rcca            209.866   82.258    2.551    0.011  209.866    0.483
   .rica            186.975   49.439    3.782    0.000  186.975    0.877
   .lsten           250.556   42.183    5.940    0.000  250.556    0.999
   .rsten           256.992   45.311    5.672    0.000  256.992    1.000
   .ltort            15.605    2.471    6.315    0.000   15.605    0.970
```

```
   .rtort            39.001   16.195    2.408    0.016   39.001    0.954
   .cgm             648.019  150.690    4.300    0.000  648.019    0.370
   .subcgm           11.516    2.205    5.222    0.000   11.516    0.579
   .cnawm           188.296  282.373    0.667    0.505  188.296    0.088
   .csf            1555.322  217.557    7.149    0.000 1555.322    0.857
   .moca              5.128    0.922    5.563    0.000    5.128    0.696
   .aniscore          8.465    1.465    5.778    0.000    8.465    0.576
   .cowattot        132.575   19.285    6.875    0.000  132.575    0.862
   .ldcttot         286.021   60.198    4.751    0.000  286.021    0.722
   .hvlt             16.716    3.002    5.567    0.000   16.716    0.583
   .hvltdelay         3.222    0.660    4.882    0.000    3.222    0.473
   .tmta            664.216  335.123    1.982    0.047  664.216    0.909
   .tmtb           1343.080  246.478    5.449    0.000 1343.080    0.873
    vessel          160.603   56.820    2.827    0.005    1.000    1.000
    brain          1101.767  235.887    4.671    0.000    1.000    1.000
   .cog               1.972    0.841    2.345    0.019    0.880    0.880

R-Square:
                 Estimate
    lcca            0.334
    lica            0.263
    rcca            0.517
    rica            0.123
    lsten           0.001
    rsten           0.000
    ltort           0.030
    rtort           0.046
    cgm             0.630
    subcgm          0.421
    cnawm           0.912
    csf             0.143
    moca            0.304
    aniscore        0.424
    cowattot        0.138
    ldcttot         0.278
    hvlt            0.417
    hvltdelay       0.527
    tmta            0.091
    tmtb            0.127
    cog             0.120
```

12.1.3 Model 3

```
lavaan 0.6-12 ended normally after 470 iterations

  Estimator                                         ML
  Optimization method                           NLMINB
  Number of model parameters                        51

  Number of observations                           118

Model Test User Model:
                                              Standard      Robust
  Test Statistic                               359.300     366.827
  Degrees of freedom                               201         201
  P-value (Chi-square)                           0.000       0.000
  Scaling correction factor                                  0.979
    Satorra-Bentler correction

Model Test Baseline Model:

  Test statistic                               858.562     853.842
  Degrees of freedom                               231         231
  P-value                                        0.000       0.000
  Scaling correction factor                                  1.006

User Model versus Baseline Model:

  Comparative Fit Index (CFI)                    0.748       0.734
  Tucker-Lewis Index (TLI)                       0.710       0.694

  Robust Comparative Fit Index (CFI)                         0.741
  Robust Tucker-Lewis Index (TLI)                            0.702

Loglikelihood and Information Criteria:

  Loglikelihood user model (H0)              -9537.324   -9537.324
  Loglikelihood unrestricted model (H1)      -9357.674   -9357.674

  Akaike (AIC)                               19176.649   19176.649
  Bayesian (BIC)                             19317.954   19317.954
  Sample-size adjusted Bayesian (BIC)        19156.730   19156.730

Root Mean Square Error of Approximation:

  RMSEA                                          0.082       0.084
  90 Percent confidence interval - lower         0.068       0.070
  90 Percent confidence interval - upper         0.095       0.097
  P-value RMSEA <= 0.05                          0.000       0.000

  Robust RMSEA                                               0.083
  90 Percent confidence interval - lower                     0.069
  90 Percent confidence interval - upper                     0.096

Standardized Root Mean Square Residual:

  SRMR                                           0.109       0.109

Parameter Estimates:
```

```
  Standard errors                           Robust.sem
  Information                                 Expected
  Information saturated (h1) model          Structured

Latent Variables:
                   Estimate  Std.Err  z-value  P(>|z|)   Std.lv  Std.all
  vessel =~
    lcca              1.000                               12.672    0.578
    lica              0.587    0.179    3.278    0.001    7.439    0.512
    rcca              1.182    0.312    3.791    0.000   14.977    0.719
    rica              0.404    0.180    2.244    0.025    5.121    0.351
    lsten            -0.036    0.140   -0.256    0.798   -0.455   -0.029
    rsten            -0.006    0.126   -0.048    0.961   -0.077   -0.005
    ltort             0.055    0.029    1.892    0.059    0.692    0.173
    rtort             0.108    0.071    1.516    0.129    1.373    0.215
  brain =~
    cgm               1.000                               33.191    0.793
    subcgm            0.087    0.010    9.029    0.000    2.891    0.648
    cnawm             1.332    0.189    7.054    0.000   44.204    0.955
    csf               0.485    0.116    4.186    0.000   16.111    0.378
    wmh              -0.000    0.037   -0.004    0.997   -0.005   -0.000
  cog =~
    moca              1.000                                1.497    0.551
    aniscore          1.669    0.369    4.521    0.000    2.498    0.651
    cowattot          3.082    0.788    3.913    0.000    4.613    0.372
    ldcttot           7.006    1.731    4.047    0.000   10.487    0.527
    hvlt              2.311    0.543    4.256    0.000    3.459    0.646
    hvltdelay         1.265    0.291    4.346    0.000    1.893    0.726
    tmta             -5.446    1.254   -4.341    0.000   -8.152   -0.302
    tmtb             -9.347    3.098   -3.017    0.003  -13.990   -0.357

Regressions:
                   Estimate  Std.Err  z-value  P(>|z|)   Std.lv  Std.all
  cog ~
    vessel            0.001    0.014    0.082    0.935    0.010    0.010
    brain            -0.006    0.007   -0.919    0.358   -0.134   -0.134
    age              -0.055    0.017   -3.195    0.001   -0.037   -0.320

Covariances:
                   Estimate  Std.Err  z-value  P(>|z|)   Std.lv  Std.all
 .lcca ~~
   .lica             71.175   52.344    1.360    0.174   71.175    0.319
 .rcca ~~
   .rica             27.026   35.713    0.757    0.449   27.026    0.136
 .cgm ~~
   .subcgm           15.387   16.456    0.935    0.350   15.387    0.178
 .hvlt ~~
   .hvltdelay         3.860    1.120    3.448    0.001    3.860    0.526
 .tmta ~~
   .tmtb            164.072   81.530    2.012    0.044  164.072    0.174
  vessel ~~
    brain           149.139   53.828    2.771    0.006    0.355    0.355

Variances:
                   Estimate  Std.Err  z-value  P(>|z|)   Std.lv  Std.all
   .lcca            320.156   57.413    5.576    0.000  320.156    0.666
   .lica            155.435   62.045    2.505    0.012  155.435    0.737
   .rcca            209.854   82.256    2.551    0.011  209.854    0.483
   .rica            186.974   49.439    3.782    0.000  186.974    0.877
   .lsten           250.556   42.183    5.940    0.000  250.556    0.999
   .rsten           256.992   45.311    5.672    0.000  256.992    1.000
```

```
   .ltort            15.605    2.471    6.315    0.000   15.605    0.970
   .rtort            39.001   16.195    2.408    0.016   39.001    0.954
   .cgm             648.155  150.649    4.302    0.000  648.155    0.370
   .subcgm           11.516    2.205    5.223    0.000   11.516    0.580
   .cnawm           188.073  282.328    0.666    0.505  188.073    0.088
   .csf            1555.375  217.560    7.149    0.000 1555.375    0.857
   .wmh             194.120   51.828    3.745    0.000  194.120    1.000
   .moca              5.128    0.922    5.563    0.000    5.128    0.696
   .aniscore          8.465    1.465    5.778    0.000    8.465    0.576
   .cowattot        132.575   19.285    6.875    0.000  132.575    0.862
   .ldcttot         286.021   60.198    4.751    0.000  286.021    0.722
   .hvlt             16.716    3.002    5.567    0.000   16.716    0.583
   .hvltdelay         3.222    0.660    4.882    0.000    3.222    0.473
   .tmta            664.217  335.124    1.982    0.047  664.217    0.909
   .tmtb           1343.080  246.477    5.449    0.000 1343.080    0.873
    vessel          160.592   56.818    2.826    0.005    1.000    1.000
    brain          1101.633  235.841    4.671    0.000    1.000    1.000
   .cog               1.972    0.841    2.345    0.019    0.880    0.880

R-Square:
                  Estimate
    lcca             0.334
    lica             0.263
    rcca             0.517
    rica             0.123
    lsten            0.001
    rsten            0.000
    ltort            0.030
    rtort            0.046
    cgm              0.630
    subcgm           0.420
    cnawm            0.912
    csf              0.143
    wmh              0.000
    moca             0.304
    aniscore         0.424
    cowattot         0.138
    ldcttot          0.278
    hvlt             0.417
    hvltdelay        0.527
    tmta             0.091
    tmtb             0.127
    cog              0.120
```

12.1.4 Model 4

```
lavaan 0.6-12 ended normally after 673 iterations

  Estimator                                         ML
  Optimization method                           NLMINB
  Number of model parameters                        58

  Number of observations                           118

Model Test User Model:
                                              Standard      Robust
  Test Statistic                               397.159     409.382
  Degrees of freedom                               241         241
  P-value (Chi-square)                           0.000       0.000
  Scaling correction factor                                  0.970
    Satorra-Bentler correction

Model Test Baseline Model:

  Test statistic                              1116.717    1108.846
  Degrees of freedom                               276         276
  P-value                                        0.000       0.000
  Scaling correction factor                                  1.007

User Model versus Baseline Model:

  Comparative Fit Index (CFI)                    0.814       0.798
  Tucker-Lewis Index (TLI)                       0.787       0.768

  Robust Comparative Fit Index (CFI)                         0.805
  Robust Tucker-Lewis Index (TLI)                            0.777

Loglikelihood and Information Criteria:

  Loglikelihood user model (H0)              -9979.025   -9979.025
  Loglikelihood unrestricted model (H1)      -9780.445   -9780.445

  Akaike (AIC)                               20074.050   20074.050
  Bayesian (BIC)                             20234.750   20234.750
  Sample-size adjusted Bayesian (BIC)        20051.397   20051.397

Root Mean Square Error of Approximation:

  RMSEA                                          0.074       0.077
  90 Percent confidence interval - lower         0.061       0.064
  90 Percent confidence interval - upper         0.087       0.090
  P-value RMSEA <= 0.05                          0.002       0.001

  Robust RMSEA                                               0.076
  90 Percent confidence interval - lower                     0.063
  90 Percent confidence interval - upper                     0.088

Standardized Root Mean Square Residual:

  SRMR                                           0.106       0.106

Parameter Estimates:
```

```
  Standard errors                           Robust.sem
  Information                                 Expected
  Information saturated (h1) model          Structured

Latent Variables:
                   Estimate  Std.Err  z-value  P(>|z|)   Std.lv  Std.all
  vessel =~
    lcca              1.000                               12.113    0.552
    lica              0.581    0.177    3.291    0.001    7.044    0.485
    rcca              1.301    0.319    4.077    0.000   15.764    0.757
    rica              0.434    0.186    2.336    0.020    5.261    0.360
    lsten            -0.037    0.141   -0.260    0.795   -0.445   -0.028
    rsten            -0.020    0.132   -0.155    0.877   -0.248   -0.015
    ltort             0.050    0.030    1.663    0.096    0.608    0.152
    rtort             0.112    0.072    1.562    0.118    1.363    0.213
  brain =~
    cgm               1.000                               31.800    0.760
    subcgm            0.089    0.010    9.079    0.000    2.830    0.635
    cnawm             1.444    0.184    7.837    0.000   45.925    0.992
    csf               0.477    0.116    4.111    0.000   15.160    0.356
  svd =~
    wmh               1.000                               11.471    0.823
    fazekastot        0.070    0.012    5.704    0.000    0.801    0.801
    scheltentot       0.518    0.045   11.550    0.000    5.937    0.943
  cog =~
    moca              1.000                                1.497    0.553
    aniscore          1.638    0.371    4.414    0.000    2.453    0.642
    cowattot          3.072    0.799    3.846    0.000    4.600    0.371
    ldcttot           7.083    1.768    4.007    0.000   10.606    0.535
    hvlt              2.258    0.542    4.164    0.000    3.381    0.634
    hvltdelay         1.230    0.287    4.284    0.000    1.842    0.710
    tmta             -5.453    1.288   -4.235    0.000   -8.165   -0.302
    tmtb             -9.424    3.216   -2.931    0.003  -14.112   -0.360

Regressions:
                   Estimate  Std.Err  z-value  P(>|z|)   Std.lv  Std.all
  cog ~
    vessel            0.003    0.016    0.171    0.865    0.022    0.022
    brain            -0.008    0.007   -1.034    0.301   -0.163   -0.163
    svd              -0.019    0.018   -1.032    0.302   -0.142   -0.142
    age              -0.050    0.017   -2.853    0.004   -0.033   -0.288

Covariances:
                   Estimate  Std.Err  z-value  P(>|z|)   Std.lv  Std.all
 .lcca ~~
   .lica            80.125   52.430    1.528    0.126   80.125    0.345
 .rcca ~~
   .rica            20.788   34.872    0.596    0.551   20.788    0.112
 .cgm ~~
   .subcgm          21.341   14.748    1.447    0.148   21.341    0.228
 .hvlt ~~
   .hvltdelay        4.042    1.133    3.568    0.000    4.042    0.537
 .tmta ~~
   .tmtb           160.460   82.027    1.956    0.050  160.460    0.171
  vessel ~~
    brain          132.345   48.441    2.732    0.006    0.344    0.344
    svd             21.805   20.390    1.069    0.285    0.157    0.157
  brain ~~
    svd            -57.334   32.818   -1.747    0.081   -0.157   -0.157

Variances:
```

```
                   Estimate  Std.Err  z-value  P(>|z|)   Std.lv  Std.all
   .lcca            334.013   59.814    5.584    0.000  334.013    0.695
   .lica            161.162   62.015    2.599    0.009  161.162    0.765
   .rcca            185.651   77.633    2.391    0.017  185.651    0.428
   .rica            185.521   50.016    3.709    0.000  185.521    0.870
   .lsten           250.565   42.227    5.934    0.000  250.565    0.999
   .rsten           256.936   45.304    5.671    0.000  256.936    1.000
   .ltort            15.715    2.475    6.349    0.000   15.715    0.977
   .rtort            39.030   16.205    2.409    0.016   39.030    0.955
   .cgm             738.539  138.364    5.338    0.000  738.539    0.422
   .subcgm           11.864    2.135    5.556    0.000   11.864    0.597
   .cnawm            33.000  256.775    0.129    0.898   33.000    0.015
   .csf            1585.122  221.058    7.171    0.000 1585.122    0.873
   .wmh              62.541   32.409    1.930    0.054   62.541    0.322
   .fazekastot        0.357    0.142    2.524    0.012    0.357    0.358
   .scheltentot       4.361    4.353    1.002    0.316    4.361    0.110
   .moca              5.078    0.914    5.554    0.000    5.078    0.694
   .aniscore          8.559    1.471    5.817    0.000    8.559    0.587
   .cowattot        132.244   19.240    6.873    0.000  132.244    0.862
   .ldcttot         281.156   59.778    4.703    0.000  281.156    0.714
   .hvlt             16.993    3.005    5.655    0.000   16.993    0.598
   .hvltdelay         3.338    0.667    5.007    0.000    3.338    0.496
   .tmta            662.586  335.526    1.975    0.048  662.586    0.909
   .tmtb           1335.479  243.868    5.476    0.000 1335.479    0.870
    vessel          146.734   52.751    2.782    0.005    1.000    1.000
    brain          1011.255  214.699    4.710    0.000    1.000    1.000
    svd             131.579   27.209    4.836    0.000    1.000    1.000
   .cog               1.975    0.840    2.352    0.019    0.881    0.881

R-Square:
                   Estimate
    lcca              0.305
    lica              0.235
    rcca              0.572
    rica              0.130
    lsten             0.001
    rsten             0.000
    ltort             0.023
    rtort             0.045
    cgm               0.578
    subcgm            0.403
    cnawm             0.985
    csf               0.127
    wmh               0.678
    fazekastot        0.642
    scheltentot       0.890
    moca              0.306
    aniscore          0.413
    cowattot          0.138
    ldcttot           0.286
    hvlt              0.402
    hvltdelay         0.504
    tmta              0.091
    tmtb              0.130
    cog               0.119
```